Techno-economic Assessment of a Hybrid Pipeline for the Synergetic Transmission of Liquid Hydrogen and Electrical Energy by High-temperature Superconductivity

Zur Erlangung des akademischen Grades eines

DOKTORS DER INGENIEURWISSENSCHAFTEN (Dr.-Ing.)

von der KIT-Fakultät für Elektrotechnik und Informationstechnik des
Karlsruher Instituts für Technologie (KIT)

angenommene

DISSERTATION

von

M.Sc. Juan Sebastian Palacios Vera

geboren in Bogotá, Kolumbien

Tag der mündlichen Prüfung:	20.07.2026
Hauptreferent:	Prof. Dr.-Ing. Mathias Noe
Korreferent:	Prof. Antonio Morandi, PhD

Abstract

To enable climate neutrality, the demand for both electrical energy and hydrogen is expected to increase substantially in Germany. Therefore, new transmission infrastructure is required for both energy vectors. A hybrid pipeline transmits both energy carriers efficiently, simultaneously, and compactly through the synergetic use of liquid hydrogen—serving as coolant and energy carrier—and high-temperature superconductors. Increasingly, multiple conceptual designs and a few prototypes have demonstrated the feasibility of combined energy transmission. However, a comprehensive techno-economic assessment of this technology is still not available. This dissertation investigates under which conditions can a hybrid pipeline be more cost-effective than conventional transmission alternatives.

An extensive literature review was carried out to identify a suitable case study, based on the future supply and demand for both energy carriers. A bottom-up design of the hybrid pipeline was developed for the selected regional case study. The design was used to estimate the investment costs of the hybrid pipeline. For the techno-economic assessment, system limits and a conventional transmission alternative were defined. To estimate the investment and operating costs of the components for both hybrid pipeline and conventional transmission alternatives, a comprehensive literature review was conducted. Sensitivity analyses were performed to evaluate the effect of varying underlying assumptions on the total costs.

The results indicate that the hybrid pipeline transmission system is significantly more cost-effective than the conventional alternative under a range of conditions. This finding is valid when 4.0 GW_e of electrical energy and 0.55–1.15 GW_t of imported liquid hydrogen are transported over distances up to at least 150 km, and when the conventional alternative comprises a gaseous hydrogen pipeline and an underground high-voltage direct-current (HVDC) cable system. The cost advantage holds for both liquid and gaseous hydrogen as the end-use product. For example, the 75 km long hybrid pipeline alternative reduces the total average yearly cost by 72% for liquid hydrogen delivery and by 28% for gaseous hydrogen supply compared with the conventional system. Additionally, the advantage also applies when the investment cost of underground HVDC cables is replaced by that of overhead HVDC lines. These outcomes provide a solid quantitative basis. It supports stakeholders and policy actors in deciding how to expand the electricity and hydrogen transmission infrastructure.

Kurzfassung

Um Klimaneutralität zu ermöglichen, wird die Strom- und Wasserstoffnachfrage in Deutschland voraussichtlich erheblich steigen. Daher benötigt das Land neue Übertragungsinfrastruktur für beide Energieträger. Eine hybride Pipeline überträgt beide Energievektoren effizient, gleichzeitig und platzsparend durch die synergetische Nutzung von flüssigem Wasserstoff – als Kühlmittel und Energieträger – sowie Hochtemperatur-Supraleitern. Zunehmend haben konzeptuelle Designs und einige Prototypen die Machbarkeit der kombinierten Energieübertragung bewiesen. Dennoch ist keine umfassende techno-ökonomische Bewertung dieser Technologie verfügbar. Diese Dissertation untersucht, unter welchen Bedingungen eine hybride Pipeline kostengünstiger als eine konventionelle Alternative sein kann.

Durch eine umfassende Literaturrecherche wurde eine geeignete Fallstudie zur künftigen Versorgung und Nachfrage beider Energieträger identifiziert. Für die regionale Fallstudie wurde ein Bottom-up-Design der hybriden Pipeline entwickelt. Das Design diente zur Abschätzung der Investitionskosten der hybriden Pipeline. Für die techno-ökonomische Bewertung wurden Systemgrenzen und eine konventionelle Alternative definiert. Die Investitions- und Betriebskosten der Komponenten für die Hybride-Pipeline- und Konventionelle-Alternative wurden auf Basis einer ausführlichen Literaturrecherche abgeschätzt. Sensitivitätsanalysen wurden erstellt, um den Einfluss von veränderten grundlegenden Annahmen zu bewerten.

Die Ergebnisse zeigen, dass das Hybride-Pipeline-System unter diversen Bedingungen maßgeblich günstiger als die konventionelle Alternative ist. Das Ergebnis trifft zu, wenn die hybride Pipeline 4,0 GW_e an Strom und 0,55–1,15 GW_t an importiertem Flüssigwasserstoff über Distanzen bis mindestens 150 km transportiert, und wenn die konventionelle Alternative eine gasförmige Wasserstoffpipeline und unterirdische Hochspannungs-Gleichstrom-Übertragungssysteme (HGÜ) umfasst. Der Kostenvorteil gilt für flüssigen und gasförmigen Wasserstoff als Endprodukt. Die 75-km-Hybride-Pipeline senkt z. B. die jährlichen Gesamtkosten im Mittel um 72% für Flüssigwasserstoff und um 28% für das gasförmige Produkt gegenüber dem koventionellen System. Der Vorteil bleibt gültig, wenn die Investitionskosten der unterirdischen HGÜ durch die der HGÜ-Freileitungen ersetzt werden. Diese Bilanz bietet eine robuste quantitative Grundlage. Sie unterstützt Stakeholder und politische Akteure bei der Entscheidungsfindung zum Ausbau der Strom- und Wasserstoff-Übertragungsnetze.

Resumen

Para posibilitar la neutralidad climática, se prevé que la demanda de energía eléctrica y de hidrógeno aumente sustancialmente en Alemania. Por ello, se requiere nueva infraestructura de transmisión para ambos vectores energéticos. Una tubería híbrida transmite ambos vectores de forma eficiente, simultánea y compacta mediante el uso sinérgico de hidrógeno líquido, que sirve como refrigerante y portador de energía, y superconductores de alta temperatura. Progresivamente, varios diseños conceptuales y algunos prototipos han demostrado la posibilidad de transmitir energía sinérgicamente. Sin embargo, aún no existe una evaluación tecno-económica integral de esta tecnología. Esta tesis doctoral investiga bajo qué condiciones una tubería híbrida puede ser más rentable que alternativas convencionales de transmisión.

Primero se realizó un amplio análisis bibliográfico para identificar un caso de estudio adecuado, basado en la futura oferta y demanda de ambos portadores de energía. Luego se diseñó la tubería híbrida para el caso regional seleccionado. El diseño se usó para estimar los costos de inversión de la tubería híbrida. Para la valoración tecno-económica, se definieron los límites del sistema y una alternativa convencional. Los costos de inversión y operación de los componentes para los sistemas de transmisión se estimaron con base en una revisión exhaustiva de la literatura. Además, se efectuaron análisis de sensibilidad para evaluar el efecto de variaciones en los supuestos subyacentes sobre el costo total.

Los resultados indican que el sistema de transmisión mediante la tubería híbrida es significativamente más económico que la alternativa convencional bajo un rango amplio de condiciones. Este hallazgo es válido cuando 4,0 GW_e de energía eléctrica y 0,55–1,15 GW_t de hidrógeno líquido importado se transportan en trayectos de hasta por lo menos 150 km, y cuando la alternativa convencional incluye una tubería de hidrógeno gaseoso y un cable subterráneo de corriente continua de alta tensión (HVDC). Por ejemplo, la alternativa de tubería híbrida de 75 km reduce el costo medio anual total en 72 % para la entrega de hidrógeno líquido y en 28 % para el suministro de hidrógeno gaseoso, en comparación con el sistema convencional. Además, la ventaja persiste cuando el costo de inversión de los cables subterráneos HVDC se reemplaza por el de líneas aéreas HVDC. Los resultados brindan una base cuantitativa robusta. Ésta apoya la toma de decisiones de las partes interesadas y de los responsables de políticas respecto a la expansión de la infraestructura de transmisión de electricidad e hidrógeno.

Acknowledgments

Firstly, I would like to express my sincere gratitude to Prof. Dr.-Ing. Mathias Noe for his reliable and continuous guidance throughout the creation of this work. His expertise and constructive feedback were essential for enhancing the quality of this dissertation. Beyond his academic mentorship, I value his genuine willingness to exchange ideas and spend time together at departmental events and international conferences.

I would like to thank Prof. Dr. Tabea Arndt for her professional assistance as a project and group leader. Her experience as an industrial physicist strengthened the basis of this work. I am truly grateful to Dr. Michael Wolf and Mira Wehr for their always-available open ear for discussing challenges and ideas. Michael was extremely helpful for the development of some Python-coded simulations. Mira provided me with invaluable support from day one. I also thank Dr. Wescley de Sousa for the insightful discussions regarding the cable design and my colleagues at the Institute of Technical Physics (ITEP) for their supplementary support.

My special thanks go to my industry and research consortium partners within *AppLHy!* for the enriching conversations related to liquid hydrogen and superconducting technologies. Especially, the exchange with Prof. Dr. Alexander Alekseev from Linde, Dr. Wolfgang Reiser from Vision Electric Super Conductors, and Dr. Paul Saß from SciDre was highly valuable for this work. My gratitude also goes to my colleagues within the *TransHyDE* project for clarifying consultations and for the enjoyable atmosphere during our meetings.

I am deeply thankful to life and to my family, especially my parents, for paving the path that formed the person I am today. Many thanks as well to my always-supportive friends, who unconditionally encouraged me in challenging times. Dear Christiane and Emma, thank you for your lovely company and immeasurable support, especially in the final stage of this project.

This work was funded by the German Federal Ministry of Research, Technology & Space and the European Union's NextGenerationEU (project *TransHyDE*, consortium *AppLHy!*, Ref. 03HY204A). I am responsible for the content and the consortium may not share this view.

Freiburg im Breisgau, June 2026
Sebastian Palacios

Contents

1 Introduction, Motivation, and Research Questions

This chapter introduces the framework of the dissertation and defines its underlying basis. It first provides the necessary general context, then outlines the motivation for the study, and finally formulates the research questions that guide the work.

1.1 Introduction

Energy derived from fossil fuels has enabled substantial economic growth over the past centuries. However, the extensive use of fossil fuels has caused significant greenhouse gas emissions, which are considered a serious and increasing threat to ecosystems, biodiversity, human well-being, and socio-economic systems [1]. In recent decades, interdisciplinary research and technological progress have made possible large-scale energy production from sustainable sources [2]. In response, many governments, companies, and organizations have adopted policies and targets aimed at achieving climate neutrality within the coming decades.

In Germany, the target of achieving climate neutrality by 2045 [3] is expected to significantly increase electrical energy demand and necessitate the import of chemical energy carriers, particularly hydrogen. Figure 1.1 illustrates both the current (2025) [4] and projected (2045) net electrical energy generation and hydrogen supply, based on several widely recognized studies in the German energy sector [5–7]. The hydrogen supply is differentiated into imports and domestic production via electrolysis, as well as others sources, such as fossil fuels (in 2025) and biomass (in 2045).

While the scenarios presented in these studies differ in quantitative estimates, they consistently indicate a common trend. On average, net electrical energy generation in Germany is projected to more than double by 2045 compared to 2025. In this work, all energy content comparisons are based on the lower heating value of hydrogen[1]. Based on this assumption, annual hydrogen supply is estimated to range between 213 TWh_t and 694 TWh_t. For comparison, Germany's net electrical energy generation in 2025 was 477 TWh_e, while hydrogen production reached only 37 TWh_t.

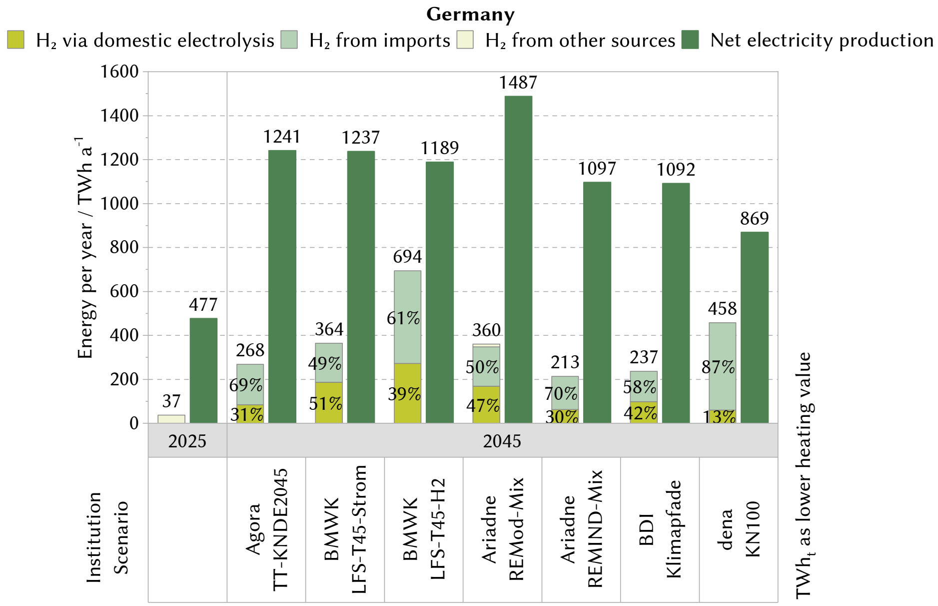

Figure 1.1: Net electrical energy production and hydrogen (H_2) supply in Germany for 2025 and projections for 2045, based on multiple studies commissioned by distinct German political entities. Hydrogen supply is differentiated into imports and domestic production via electrolysis and other sources, such as fossil fuels (2025) and biomass (2045). Own depiction based on [4–7].

Electrical energy and hydrogen are typically produced in regions where generation costs are lowest. This applies both to renewable energy imported from regions with particularly favorable wind and solar resources, and to energy produced domestically in Germany. However, energy demand is often geographically separated from production sites, and the spatial distribution of renewable energy differs significantly from that of conventional energy systems. Consequently, substantial expansion and adaptation of transmission infrastructure are required. This includes extensions of the electrical grid across all voltage levels [9], as well as the repurposing and modification of natural gas networks to enable hydrogen transport [10].

[1] The lower heating value, also known as the net heating value, is obtained by subtracting the latent heat of vaporization of the water formed during combustion from the gross heating value, which represents the total heat released during the complete combustion of a unit amount of fuel [8].

To accelerate the deployment of hydrogen technologies, the German government launched three flagship projects in 2021: *H_2Giga*, focusing on scaling up large-scale electrolyzer technologies; *H_2Mare*, addressing offshore hydrogen and Power-to-X production; and *TransHyDE*, within which this work is situated [11]. The *TransHyDE* project aimed to investigate and develop technologies for the transport and storage of gaseous hydrogen, liquid hydrogen, ammonia, and liquid organic hydrogen carriers (LOHC) [12]. One of its five research consortia, *AppLHy!*, brought together research and industry partners to analyze and implement technologies for the efficient production, storage, and transport of liquid hydrogen.

Within the *AppLHy!* consortium, researchers of the Institute for Technical Physics (ITEP) at the Karlsruhe Institute of Technology (KIT) explored synergies between cryogenic liquid hydrogen and electrical components. This synergy arises when a cryogenic coolant cools a superconducting material below its critical temperature. The superconductor is then able to transmit large amounts of electrical energy without resistance and using very low material amounts in comparison to copper.

Superconductivity was discovered in 1911 by the Dutch physicist Kamerlingh Onnes, using liquid helium to cool mercury below 4.2 K (−268.95 °C). In 1986, the German and Swiss physicists, Bednorz and Müller, discovered high-temperature superconductors (HTS) at around 30 K (−243.15 °C). Their finding led the Taiwanese-American physicist Chu to discover shortly after the yttrium barium copper oxide (YBCO) compound, which is a rare-earth barium copper oxide (REBCO) superconductor with critical temperature at 93 K (−181.15 °C) [13]. This critical temperature enabled the use of a less-expensive coolant—liquid nitrogen at about 77 K (−196.15 °C).

With the increasing adoption of liquid hydrogen as an energy carrier and given its cryogenic temperature of approximately 20 K (−253.15 °C), a hybrid pipeline offers synergetic transmission of liquid hydrogen and electrical energy by high-temperature superconductivity. The idea of combined energy transmission attracted growing attention in the early 2000s, when the founder of the U.S. American Electric Power Research Institute (EPRI), Starr, proposed a "SuperGrid" made of superconducting power transmission cables cooled with liquid hydrogen [14].

While a first basic design was presented in 2004–2005 [15, 16], more comprehensive concepts followed in 2006–2007 [17, 18] and 2008–2010 [19, 20], where case studies were proposed and more detailed engineering analyses were carried out. Between 2012 and 2015, researchers successfully built and tested the first prototype of a hybrid power transmission line cooled with liquid hydrogen in a corrugated pipe [21–26]. Their cable design was based on magnesium diboride (MgB_2), which is a superconducting material with lower critical temperature than YBCO (39 K [13]). Since then, several research groups have further refined, evaluated, and tested hybrid pipeline designs, as it will be later discussed. Within the *AppLHy!* consortium, ITEP is constructing a hydrogen integration platform to test a REBCO-based and smooth hybrid pipeline prototype at KIT [27, 28].

1.2 Motivation

Despite technological progress, a key challenge for hybrid energy pipelines remains achieving a cost advantage over conventional alternatives. Several conceptual designs and prototypes—including those by Trevisani [17], Yamada et al. [20], and Vysotsky et al. [26]—have demonstrated the technical feasibility of combined energy transmission that uses superconductivity with liquid hydrogen as both coolant and energy carrier. However, before this research project began in 2022, no study had evaluated the cost-effectiveness of hybrid pipelines.

In recent years, a number of studies have examined the cost-effectiveness of hybrid pipelines:

- Qi et al. (2024) proposed a superconducting energy pipeline connecting East Asia and North America across 12 time zones, with an estimated investment payback period of around 10 years. The study presents a high-level technical design with route planning and relay energy stations, but lacks detailed engineering analyses such as thermal-hydraulic modelling, cable layout, or benchmarking against conventional alternatives. Investment costs are derived from aggregated component-level estimates rather than a bottom-up design [29]. Consequently, the techno-economic results remain indicative because key cost components, including superconducting cables and cryogenic pipelines, depend strongly on project-specific design parameters and local conditions, limiting the transferability of per-unit-length cost estimates.
- Fu et al. (2024) presented a detailed technical design together with investment and operating cost estimates of a REBCO-based liquid hydrogen-electricity hybrid pipeline, including auxiliary components such as refueling stations, valve chambers, land, and installation. While their analysis is more comprehensive than the previous study, the concept is specifically developed for 1 km long railway applications. In addition, the system requires a liquid nitrogen shielding layer to thermally stabilize the liquid hydrogen and prevent boil off. The chemical transmission is relatively low at about 0.7 kg_{H2} s^{-1} [30].
- Cavallucci et al. (2025) performed a techno-economic optimization of a magnesium diboride (MgB_2) DC transmission line cooled with liquid hydrogen. The study minimizes total cable costs by jointly optimizing the electrical cable design and the cryogenic cooling system. Liquid hydrogen is treated as a coolant, although its potential role as an

energy carrier is only mentioned conceptually. The study did not include hydrogen delivery, matching of supply and demand, or an application use case [31].

- Mangiulli et al. (2026) analyzed auxiliary components for a 30 km MgB_2 hybrid superconducting cable transporting electrical energy and liquid hydrogen. The study focuses on the sizing of individual components and provides an investment cost breakdown for the cable system, storage tanks, current leads, pump, and grid connection. Results indicate that electrical infrastructure dominates overall costs, while cryogenic subsystems represent a small fraction. Operational expenditures, replacement cycles, and comprehensive techno-economic metrics are not addressed [32].

- Cais et al. (2026) provided a detailed system-level evaluation of MgB_2-based hybrid superconducting energy pipelines in Italy, using an optimization model to determine cost-effectiveness compared with conventional electricity and hydrogen transmission options across a 20-node network. The model captures interactions between electricity generation, hydrogen production, and transmission. Hydrogen demand is derived from national decarbonization pathways without explicit differentiation between gaseous and liquid hydrogen. For system-level modeling, a simplified investment cost of the hybrid pipeline is derived from Cavallucci et al. [31] and assumed to be approximately 1.1 MEUR km^{-1} [33]. However, this value appears to correspond primarily to the superconducting cable and may represent about 20–30% of the total cost, which in the source study includes the cryostat, cooling stations, project management, and installation. While fixed operating costs for the superconducting energy pipeline are represented as 2% of capital costs, variable cooling costs are not explicitly addressed. The reference study of Cavallucci et al. indicates that cooling requirements are of comparable maginitude to the capital costs. Cais et al. included electricity demand for hydrogen liquefaction, whereas they did not present the investment cost for the liquefier.

Existing approaches have not assessed the cost-effectiveness of a REBCO-based hybrid pipeline for long-distance energy transmission without intermediate cooling stations at the gigawatt scale. In particular, there is a lack of comprehensive assessments that integrate all relevant aspects. These include the derivation of investment costs from a bottom-up design, their evaluation within case studies reflecting liquid hydrogen demand, the performance of auxiliary components, sensitivity analyses, and relevant financial model parameters.

As a result, the economic viability of such systems remains uncertain, limiting their applicability for decision-making when considering the expansion of transmission infrastructure. This lack of robust cost assessment can lead to less effective investment decisions and hinders comparison of alternative system designs. Therefore, a systematic techno-economic assessment that address all significant aspects is required. To fill this gap, the present dissertation investigates the following research questions.

1.3 Research Questions

The central question of this dissertation is:

Main research question

Under which conditions can a hybrid pipeline be more cost-effective than conventional transmission alternatives?

The research question is formulated to explicitly account for the context-dependence of cost-effectiveness. The analysis focuses on identifying the conditions under which hybrid pipelines may achieve a cost advantage. A central objective of this work is to assess whether these conditions can exist and whether they are achievable in practice.

Based on the main research question, the study investigates three sub-questions. First, it examines where electrical energy and liquid hydrogen will increasingly be produced and consumed, as well as how they have been transmitted so far. Second, it analyzes how liquid hydrogen and electrical energy can be transported synergetically by means of superconductivity. Third, it evaluates how the underlying assumptions in a specific case study affect the cost-effectiveness of the hybrid pipeline.

The structure of the dissertation reflects these questions. Chapter 2 addresses the required background for combined energy transmission. Chapters 3 and 4 focus on the properties of the high-temperature superconducting tape and the conceptual design of the hybrid pipeline, respectively. Chapter 5 presents the techno-economic assessment of the two transmission alternatives: the hybrid pipeline alternative and the conventional alternative.

The availability of liquid hydrogen is essential for a hybrid pipeline. Consequently, liquid hydrogen must achieve sufficient market penetration for hybrid pipelines to become cost-effective. However, this dissertation does not provide a full levelized cost of energy, which includes production costs for electrical energy and liquid hydrogen. It either develops a business case based on revenue streams. Instead, it offers a comparative techno-economic assessment of the performance and costs of transmission technologies. Additionally, it reviews the techno-economic properties for importing liquid hydrogen and alternative carriers such as ammonia, and it examines the demand for liquid hydrogen to meet climate-neutrality targets.

This work concentrates on the large scale design and techno-economic assessment of a gigawatt class hybrid pipeline. Detailed technical implementation issues are therefore beyond the scope of the study. Nevertheless, collaborators in the *AppLHy!* consortium have investigated prototype components for the hybrid pipeline, including indirect liquid hydrogen cooling of the HTS cable to prevent undesirable material interactions with hydrogen [34], low resistive contact soldering [35], and reliable thermal coupling between the HTS and its support structure [36].

To compare the hybrid pipeline with conventional alternatives, this dissertation evaluates the auxiliary components required for transmitting both liquid hydrogen and electrical energy. The analysis focuses on the techno-economic properties of these components, not on their technical development. Within the *AppLHy!* consortium, partners have created several technologies for the liquid hydrogen supply chain, including a submersible multistage turbo pump, a cryopump with superconducting bearings, and a contact-less liquid hydrogen storage level measurement system [37]. Power electronics have been designed for the interface between the cryogenic hybrid pipeline and the electrical grid [38].

The dissertation assesses safety with varying levels of detail depending on the considered aspect. The focus lies on the safe operation of the hybrid pipeline at rated operating conditions and its behavior in the event of a short circuit. Potential hydrogen embrittlement is covered for some components, such as the pipe and the copper stabilizer. The study provides an overview of safety aspects related to the leakage of liquid hydrogen and its effect on the environment. However, a higher level of depth, for example regarding long-term exposure in liquid hydrogen [39], was investigated by other researchers within the *AppLHy!* consortium.

2 Background for Combined Energy Transmission

To evaluate the plausibility of a hybrid pipeline in Germany, the corresponding context in the energy sector, and the state of the art of transmission infrastructure must be known. This chapter presents the necessary background to integrate the concept of a hybrid pipeline in the German energy sector.

Given that the primary function of energy transmission infrastructure is to link producers with consumers, this chapter begins with an overview of the projected supply and demand of electrical energy and hydrogen in the future. As part of that, gaseous hydrogen, liquid hydrogen, and some hydrogen carriers are briefly compared as transport options for the hydrogen supply. The main focus of the chemical energy demand will be on the use of hydrogen in liquid state. However, the use of gaseous hydrogen is also mentioned, since liquid hydrogen can be regasified to supply gaseous hydrogen consumers.

Building on the previous insights, a specific regional case study is selected for the techno-economic assessment of the hybrid pipeline. The section names the reasons for the choice of Brunsbüttel and Hamburg, in northern Germany, as the case study. Since the techno-economic assessment aims to analyze the technical feasibility and economic viability of a relatively new technology, conventional technologies serve as a benchmark for evaluating the new system. Therefore, the state of the art of conventional transmission infrastructure for the separate transport of electrical energy and hydrogen in bulk will be introduced.

The chapter closes with the state of development of hybrid pipelines, presenting conceptual designs that have been proposed and prototypes that have been built to date.

2.1 Electrical Energy Supply

The German Electricity Network Development Plan, in German "*Netzentwicklungsplan Strom*", is the official document for planning the expansion and modernization of Germany's electrical energy sector. It considers the country's goals for climate neutrality, renewable energy integration, and grid reliability. According to the most recently approved German Network Development Plan 2037/2045 (2023), achieving climate neutrality by 2045 requires a minimum installed capacity of 70 GW_e of offshore wind energy, 160 GW_e of onshore wind energy, and 400 GW_e of photovoltaics [9]. By the end of 2025, the installed capacity amounted to 9.5 GW_e for offshore wind energy, 68.1 GW_e for onshore wind energy, and 117.0 GW_e for photovoltaics [40]. Other technologies, such as hydrogen, biomass, and hydroelectric power plants, are expected to contribute much less to the electrical energy supply [9].

Supplementary documents to the Network Development Plan 2037/2045 (2023) provide geographical specifications for the installed capacities of onshore wind energy, photovoltaics, and offshore wind energy. The level of detail and the methodology used for regionalization vary depending on each technology. For onshore wind energy and photovoltaics, capacities are defined at the postal code areas level [41]. In contrast, offshore wind energy is regionalized into designated zones within the North Sea and the Baltic Sea [42]. According to these documents, the highest installed capacity density for offshore and onshore wind energy is expected to be in the North Sea region. Conversely, the expansion of photovoltaics is more evenly distributed and decentralized across Germany.

The latest Network Development Plan 2037/2045 (2025) is under development, but has not been approved yet. In the new plan, the range of projected installed capacities in 2045 for offshore wind energy (60–70 GW_e), onshore wind energy (143.5–176.0 GW_e), and photovoltaics (315–440 GW_e) was lowered in comparison to the approved plan from 2023. This was justified by current trends in electrical energy consumption, which differ significantly from previous forecasts. The future regional distribution of renewable energy facilities remains similar to that expected in the plan from 2023 [43].

2.2 Hydrogen Supply

The German government set a Hydrogen Strategy to install 10 GW_e of electrolyzers by 2030 within the country [44]. By the end of 2024, the installed capacity amounted to 0.18 GW_e and a total of 7.2 GW_e was planned to be installed by 2030 [45]. Hydrogen from Germany is expected to have a higher cost than hydrogen from countries with lower costs for renewable energy sources. The lower costs are caused by higher full-load hours given by more favorable weather conditions. In chapter 1, figure 1.1 showed that 13% to 51% of Germany's green hydrogen demand is projected to be imported to enable climate neutrality. As a response, the German government launched an Import Strategy for Hydrogen and Hydrogen Derivates in 2024 to promote an international hydrogen economy [46].

In 2025, Odenweller et al. noted that there has been a notable delay between the global green hydrogen ambition and its implementation. From 190 hydrogen projects between 2021 and 2023, only seven percent were completed on schedule. This translates into 0.3 GW_e of accomplished projects, compared to 4.3 GW_e of planned installed capacity by companies and state-owned enterprises. For the authors of the study, three factors contributed to the low implementation outcome: an increase in electrolyzer and financing costs, insufficient purchase contracts, and lagging support policies, including the uncertainty about European and U.S. American production standards for green hydrogen [47].

The worldwide hydrogen production capacity with a final investment decision by 2024 is roughly one-third lower than the projected global hydrogen demand for 2030. However, the International Energy Agency (IEA) reported that the number of production projects attaining a final investment decision in 2024 was double that of 2023. The IEA estimated that the implementation of these projects will represent a fivefold increase in hydrogen production by 2030 compared to today's global output. The planned production is divided into 56% hydrogen production by electrolysis and 44% production from fossil fuels with carbon capture, utilization, and storage [48].

A graph suggesting that worldwide electrolyzer installed capacity is increasing more rapidly than that of photovoltaics, and electrolysis presently exhibits the highest growth rate among all energy technologies has been reported in a non-peer-reviewed source [49]. However, this finding has not been independently validated in this study and should therefore be interpreted with caution.

Hydrogen transport requires compression, liquefaction or conversion into hydrogen carriers at its production location to reduce the transporting volume. This is due to the fact that, at atmospheric conditions, the volumetric energy density of gaseous hydrogen is relatively small (2.7 Wh l^{-1} for normal-hydrogen at 298.15 K and 100 kPa). That is approximately one-third of that of gaseous methane under the same conditions (9.0 Wh l^{-1}) [50]. The most frequently discussed hydrogen transport methods are in the form of: compressed gaseous hydrogen, liquid hydrogen, ammonia, methanol, synthetic methane, LOHC, dimethyl ether, and Fischer-Tropsch products, such as kerosene and naphtha. The following sections will present some characteristics of the transport methods that are relevant for this work.

2.2.1 Imports of Gaseous Hydrogen by Pipeline

The IEA [48], the Joint Research Centre of the European Commission [51], Staiß et al. [52], and Wang et al. [53] concluded that the most cost-efficient hydrogen transport method would be the transmission of compressed gaseous hydrogen by pipeline. However, the results vary depending on the transport distance, diameter of the pipeline, and whether it is a new or a repurposed pipe. From the German perspective, for distances longer than 4 000 km, the transport by ship becomes more cost-efficient in comparison to newly constructed pipelines [52].

The German think-tank Agora Energiewende et al. [54], and the Fraunhofer Institute for Systems and Innovation Research et al. [55, 56] expected that most of the hydrogen supply for Germany will be coming from inside Europe. In comparison, Kigle et al. [57], Slowinski et al. [58], and the German National Academy of Science and Engineering (acatech) et al. [59] considered that most hydrogen imports will come from North Africa. According to these studies, countries that could deliver gaseous hydrogen by pipelines are those in the north with high wind speeds, such as Norway, Denmark, Finland, and the United Kingdom, and those in the south with high global solar radiation, such as Spain, Tunisia, Morocco, and Algeria.

The Hydrogen Infrastructure Map shows the current European hydrogen pipeline projects based on data from stakeholders, such as transmission and distribution system operators of gas (see figure 2.1) [60]. A notable point is that Norway is not connected by pipeline with Germany, because Norway announced that it would stop the project due to high costs and insufficient demand [61].

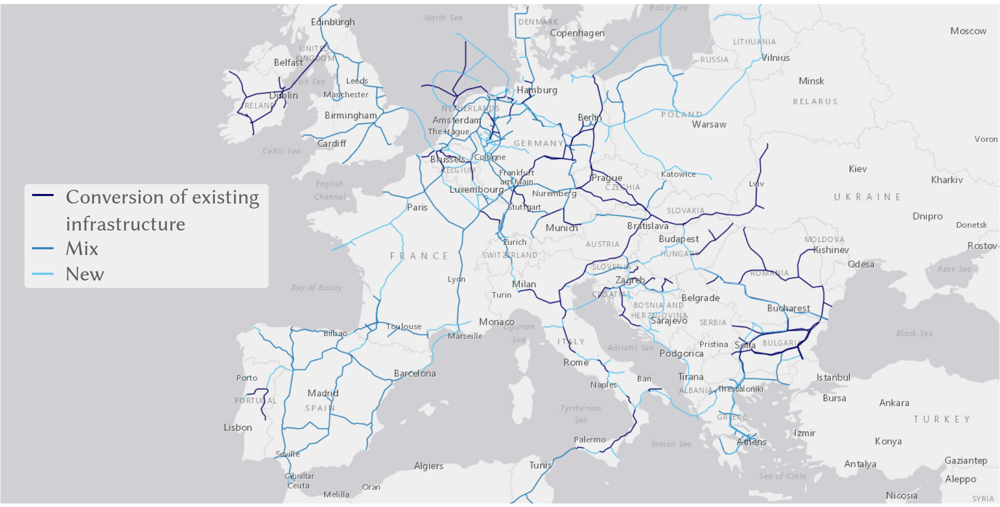

Figure 2.1: Current European hydrogen pipeline projects as of the end of 2025. Depiction without legend from H2inframap [60]; permission granted.

Worldwide, around 37 000 km of gaseous hydrogen pipeline projects are planned by 2035. This amount includes new pipelines and repurposed natural gas pipelines. However, less than 6% by length have obtained a final investment decision or are under construction. Most of the announced plans are concentrated in Europe, especially in Germany [62].

2.2.2 Imports of Liquid Hydrogen by Ships

The German Federal Network Agency believes that, because of the costs involved, it is more likely that most of the hydrogen imports will be transmitted via pipelines. However, the federal agency and German TSOs acknowledge that imports through terminals should remain possible for network development planning, in order to diversify the supply sources and guarantee security of supply. Consequently, the latest Approval of the Scenario Framework for the Natural Gas and Hydrogen Network Development Plan calls for a minimum of 4 $GWh_t\ h^{-1}$ of terminal imports using liquid hydrogen and other chemical energy carriers [63].

Hydrogen imports from distant overseas regions require the liquefaction or conversion of hydrogen to other chemical energy carriers and the use of ships. This is justified by the relatively small volumetric energy density of gaseous hydrogen (0.1 $kg_{H2}\ m^{-3}$ at 293.1 K and 100 kPa [50]) and the lack of long-distance intercontinental pipelines. This section briefly introduces the hydrogen liquefaction process—a key step in the liquid hydrogen supply chain—and some of the main characteristics of liquid hydrogen as an import medium compared with other chemical energy carriers.

Hydrogen Liquefaction

Hydrogen liquefaction involves condensing the gas to its liquid phase by reducing the temperature, e.g., from ambient conditions (293.15 K, 100 kPa) to typical storage conditions (20–23 K, 100-200 kPa) [64]. At room temperature and higher, diatomic hydrogen exists in two spin isomeric forms at a proportion of approximately 3 : 1. At a ratio of 75% to 25% and ambient temperature, the term normal-hydrogen is used [65]. The 75% share presents both proton nuclear spins aligned in parallel and is called ortho-hydrogen. The 25% share has the two proton spins aligned antiparallel in opposite directions and is known as para-hydrogen [66].

Lowering the temperature changes the share gradually in the direction of para-hydrogen. At 20 K, the proportion of ortho-hydrogen to para-hydrogen equals approximately 0.2 : 99.8 [65]. The ortho-para conversion is a substantial exothermic process, particularly at low temperatures. Today's industry standards specify that the liquid hydrogen product must exhibit a para-hydrogen content of at least 98% [67].

In comparison to the conversion of gaseous hydrogen to other chemical energy carriers, hydrogen liquefaction is an energy intensive process. Current industrial hydrogen liquefiers consume 10–15 MWh_e t^{-1}_{H2}, equivalent to 35–40% of hydrogen's lower heating value. The high energy demand is in part justified by relatively small capacities—up to 32 t^{-1}_{H2} d^{-1} per train—with a focus on lower investment costs than energy efficiency [64]. Long-term efficiency targets of 6.4 MWh_e t^{-1}_{H2} are reported to be feasible [68].

Energy Efficiency in the Import Supply Chain

The IEA [48], Staiß et al. [52], and Hank et al. [69] estimated the supply chain efficiency for importing several chemical energy carriers. All studies compared liquid hydrogen, ammonia, and LOHC. Staiß et al. additionally assessed methanol and Fischer-Tropsch products [52], whereas Hank et al. [69] additionally examined synthetic liquid methane and methanol.

For shipping, the IEA [48] and Staiß et al. [52] assumed a distance of 10 000 km. Hank et al. considered 4 000 km and presented a base case for 2020 and an optimistic case for $\sim$ 2030. Hank et al. assumed that the feed-in of carbon dioxide occurs by means of direct air capture in the case of synthetic liquid methane and methanol. This step can be supplied with or without heat integration from methanation or methanol synthesis, respectively [69].

Based on the results reported in these studies, figure 2.2 (a) presents the energy delivered in form of gaseous hydrogen (lower heating value) when using 100 kWh_e of electrical energy from renewable sources. The conversion step is equivalent to liquefaction (liquid hydrogen), synthesis (ammonia), and hydrogenation (LOHC). Reconversion to gaseous hydrogen requires regasification (liquid hydrogen), cracking (ammonia), and dehydrogenation (LOHC). The authors in all studies assumed that liquid hydrogen regasification does not represent energy losses [48, 52, 69]. In all works, the results indicate that the import of liquid hydrogen achieves the highest energy efficiency in comparison to ammonia and LOHC, when hydrogen is the final product.

When the importing medium is not reconverted to gaseous hydrogen, IEA [48] and Hank et al. [69] revealed that liquid hydrogen still exhibits the highest energy efficiency (see figure 2.2 (b)). Staiß et al. [52] estimated that importing ammonia has a higher energy efficiency when ammonia is the desired final product. The values for each step can be found in appendix A, tables A.1 and A.2.

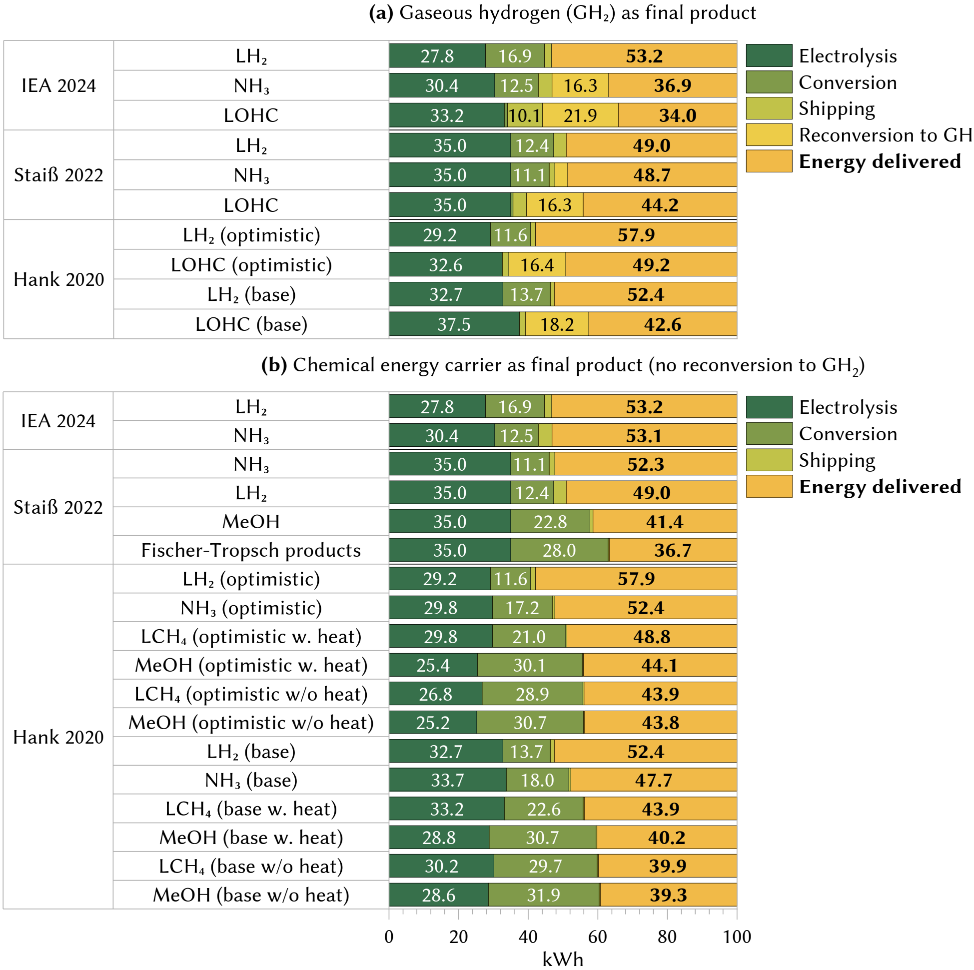

Figure 2.2: (a) Energy delivered in form of gaseous hydrogen (GH_2, lower heating value) after losses in the production and import chain of liquid hydrogen (LH_2), liquid organic carriers (LOHC), and ammonia (NH_3) when using 100 kWh of electrical energy from renewable sources. (b) Energy delivered in form of the corresponding chemical energy carrier when no reconversion to gaseous hydrogen is considered (lower heating value). Losses are included from the production and import chain of LH_2, NH_3, synthetic liquid methane (LCH_4), methanol (MeOH), and Fischer-Tropsch products when using 100 kWh of electrical energy from renewable sources. IEA and Staiß assume a distance of 10 000 km for shipping, while Hank considers 4 000 km. Hank considers a base case for 2020 and an optimistic case for $\sim$ 2030. Own depiction based on [48, 52, 69].

Environmental Effects

Liquid hydrogen is not toxic and it volatilizes fast [52, 67]. In contrast, Ammonia, LOHC, synthetic Fischer-Tropsch products, and methanol pose a very high hazard potential in the event of a leakage or an accident, owing to their respective chemical and physical properties [52, 70]. Therefore, liquid hydrogen demonstrates greater safety for wildlife in the case of leakages or accidents, in comparison to other chemical energy carriers [52].

Hydrogen has a relatively small indirect greenhouse-gas effect [52, 67]. Nevertheless, hydrogen leakages should be kept to the very least and hydrogen should be produced from renewable energy sources to reach the climatic advantages of transitioning to a hydrogen economy [71, 72]. The IEA estimated that the greenhouse gas emissions of the liquid hydrogen supply chain could be 40% lower than those of ammonia or LOHC, because improved energy efficiency leads to a higher yield of the final product and reduced specific emissions [48].

Safety

Motivated by the use of liquid hydrogen as a fuel in aerospace and as a source of high-purity gas, several decades of experience have been built for the safe production, transport, and storage of liquid hydrogen in large volumes. However, its transferability to emerging non-industrial applications is limited [67]. For example, in the field of mobile applications, such as aviation, road transport, railway transport, and the maritime sector, there is a notable absence of standardized procedures for liquid hydrogen technologies. This occurs particularly in safety-sensitive tasks, such as transferring liquid hydrogen from storage tanks in mobile systems operating in public environments [73].

However, recent projects, such as the liquid-hydrogen *GenH2* truck from Daimler 2023 [74], the *Hydrogen Energy Supply Chain (HESC)* between Australia and Japan 2022 [75], and the European Union (EU) project *Pre-normative REsearch for Safe use of Liquid HYdrogen (PRESLHY)* 2017–2021 [76] have delivered growing evidence that, when liquid hydrogen is managed professionally, and its unique properties are considered in system design and operation, it is not inherently more hazardous than other fuels.

For example, despite hydrogen's very high diffusivity and low minimum ignition energy, spontaneous ignition is extremely unlikely, while the combustible air-hydrogen cloud quickly dilutes. Although materials exposed to liquid hydrogen must withstand, e.g., embrittlement, and they must resist wide temperature ranges of approximately 20–293 K and broad pressure ranges, for example, between 100—1 200 kPa, multiple materials—such as metal alloys, fiber-reinforced composite materials, and laminated structures—have shown proper performance under such conditions of use [67]. A comparison with other hydrogen carriers has shown that, regarding humans in close proximity, non-directly involved parties, and material assets—such as buildings and technical facilities—liquid hydrogen offers a similar high safety level as that of methane [52].

Importing Costs

Previous studies reached differing conclusions on the most cost-effective medium for overseas hydrogen transport, variously identifying liquid hydrogen [51,77–79], ammonia [80,81], LOHC [82], or methanol [83] as the most cost-effective transport option. Some reasons for the different importing costs have been analyzed, for instance, in a meta-analysis of 30 studies that considered hydrogen imports to Europe. Genge et al. observed that numerous studies do not provide data on reconversion costs at the point of destination. Furthermore, large differences are given by individual assumptions on the weighted average costs of capital and on the capital expenditures. Assuming no reconversion process back to gaseous hydrogen owing to a lack of data, Genge et al. identified ammonia and LOHC as the most cost-effective energy carriers by 2030 and 2050, when only production and transportation costs are included [84].

The *LNG2Hydrogen* project, part of the flagship project *TransHyDE*, included the reconversion step to gaseous hydrogen at the import location. First, Ruske et al. evaluated the specific investment costs of import terminals for distinct chemical energy carriers. The results show that the specific investment cost for a liquid hydrogen terminal is three times lower than that for an ammonia terminal (see figure 2.3 (a)). This result is mainly justified by a lack of cracking or dehydrogenation requirements for liquid hydrogen imports, which increases the overall energy efficiency of the liquid hydrogen terminal (figure 2.3 (b)).

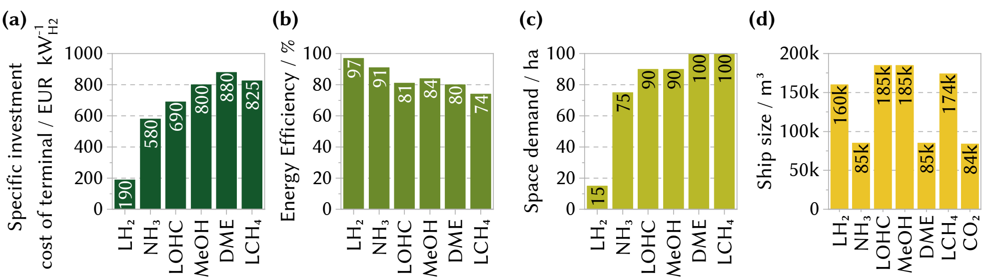

Figure 2.3: Techno-economic comparison of import terminals with a capacity of 100 $TWh_{t,H2}$ a^{-1} for: liquid hydrogen (LH_2), ammonia (NH_3), liquid organic carriers (LOHC), methanol (MEoH), dimethyl ether (DME), and synthetic liquid methane (LCH_4). (a) Specific investment costs; (b) Space demand; (c) Energy efficiency; (d) Ship size. Own depiction based on data from [85]; reproduced by permission.

The amount of space needed for a liquid hydrogen terminal is five times lower than that for an ammonia terminal (see figure 2.3 (c)). The costs for the acquisition of land are not included in the calculation of the specific investment costs of the terminals, since the analysis only considers the landing, storage, conversion, and feed-in [85]. It should be noted that the study reported noticeably lower technology readiness levels (TRL) for the components of liquid hydrogen import terminals than those of other chemical energy carriers (see appendix A, table A.3).

Ruske et al. compared the expected ship sizes for each energy vector (see figure 2.3 (d)) [85]. Dimethyl ether, methanol, and synthetic liquid methane would additionally require ships delivering carbon dioxide for the corresponding synthesis process at the export location. More information about liquid hydrogen carriers can be found in appendix C.

In a second step, Ruske et al. included three distinct cost scenarios (low, mid, and high) and compared seven potential importing countries to determine the levelized cost of hydrogen of each chemical energy carrier. The authors observed that the levelized cost of hydrogen is the lowest for liquid hydrogen and ammonia when the import terminal costs and reconversion are included (see figure 2.4 (a)). Synthetic liquid methane, methanol, and dimethyl ether have higher costs because of a required closed carbon dioxide loop and supplementary direct air capture. The results for LOHC are not included in the analysis owing to data-specific concerns of a project partner in the project [85]. For comparison, figures 2.4 (b) and (c) present the results observed by Genge et al. when reconversion to gaseous hydrogen is not included.

Figure 2.4: (a) Production, transport, and import terminal costs for importing liquid hydrogen (LH_2), ammonia (NH_3), synthetic liquid methane (LCH_4), methanol (MeOH), and dimethyl ether (DME) from selected countries—such as United Arab Emirates (UAE) and United States (USA)—to Germany, including reconversion to gaseous hydrogen (GH_2), shown for low, medium, and high cost scenarios. (b) 2030 and (c) 2050: Production and transport costs for importing LH_2, NH_3, LCH_4, MeOH, Fischer-Tropsch diesel (FTD), and liquid organic hydrogen carriers (LOHC) to Europe from 30 different studies. The costs exclude reconversion to GH_2. Own depiction based on data from [84, 85]; reproduced by permission.

In practice, most of the recent hydrogen trade projects use ammonia as the hydrogen carrier, with most of the ammonia projects originating in Saudi Arabia [48]. Genge et al. justified the selection of ammonia as the chemical energy carrier because it is suited for early adoption, owing to currently lower transportation costs and a presently high demand for fertilizer production. However, the authors acknowledged that the future utilization of each energy carrier continues to be uncertain, resulting in ongoing competition to define their respective roles and applications [84].

In summary, the literature review suggests that liquid hydrogen remains a competitive option for the transport of hydrogen overseas, due to its high energy efficiency, low importing costs, few environmental impacts, and comparable high safety level to other conventional fuels (see table 2.1). Some examples of ongoing liquid hydrogen export projects are between Oman and Europe [86, 87], Spain/Portugal/Scotland and Netherlands/Germany [88, 89], Australia and Japan [90, 91], and the assessment of liquid green hydrogen exports from Abu Dhabi to Europe [92].

Table 2.1: Characteristics of liquid hydrogen when importing it by ship.

Characteristic	Description	Sources
Energy efficiency	The import of liquid hydrogen presents the highest efficiency, compared to ammonia and LOHC, when reconversion to hydrogen is considered	[48, 52, 69]
Environmental effects	Liquid hydrogen has low risks for wildlife and climate because of non-toxicity, fast volatilizing, small indirect greenhouse gas effect, and low greenhouse gas emissions in the supply chain	[48, 52, 67]
Safety	Liquid hydrogen has a comparable high safety level as that of methane when managed professionally, but transferability to non-industrial applications is still limited	[52, 67, 76]
Importing costs	The levelized cost of hydrogen is the lowest for liquid hydrogen and ammonia, when the reconversion process back to hydrogen is included for the transport media at the import location	[85]

2.3 Electrical Energy Use

The future development of the electrical energy consumption has a decisive influence on the location and the amount of planned grid infrastructure. Figure 2.5 illustrates the net electrical energy consumption in 2024 and the projected net demand for 2045 according to the second draft of the Network Development Plan 2037/2045 (2025) under scenarios A, B, and C. In scenario A, the electrification level is low, hydrogen imports are high, and the expansion plans of renewable energy assets are delayed. Scenario B follows the legal expansion pathways for renewable energy and is closely aligned with the system development strategy. Scenario C is based on high electricity consumption and extensive power generation capacity [43].

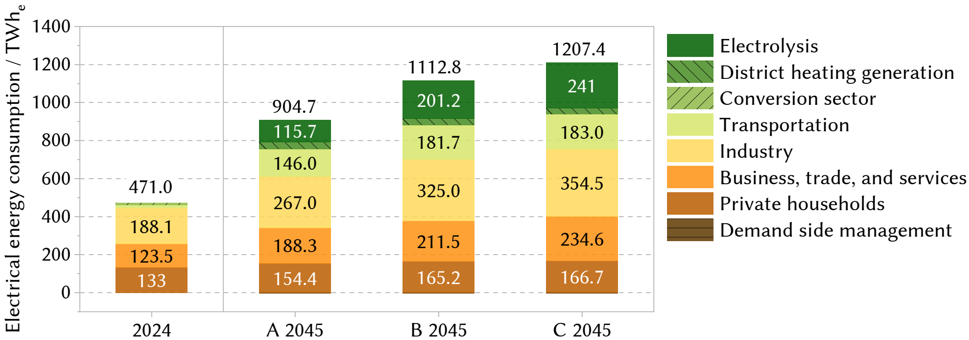

Figure 2.5: Net electrical energy consumption in Germany by sector or area of application. This figure does not take into account grid losses in the transmission grid. Own depiction based on the German Network Development Plan 2037/2045 (2025) [93].

The total electrical energy consumption can be broken down into the following sectors: industry, transportation, private households, and non-residential buildings, such as business, trade, and services [4]. Some applications are used by multiple sectors, for example, electrolysis or district heating generation. The second draft of the latest German Network Development Plan 2037/2045 (2025) projected that, by 2045, decarbonizing the energy system almost doubles the net electrical energy consumption in all sectors to 905 TWh$_e$ in scenario A, and raises it to 1 113 and 1 207 TWh$_e$ in scenarios B and C, respectively [93].

By 2045, electrical energy is expected to be directly used for many processes, which are today driven by fossil fuels. Examples are: heat pumps for private heating (69 to 82 TWh$_e$), heat pumps for non-residential heating (18 to 27 TWh$_e$), electric mobility for the transport sector (129 to 166 TWh$_e$), and the electrification of industrial processes (267 to 354 TWh$_e$). Additionally, the expected use of electrolyzers for the production of domestic hydrogen and the expansion of digitalization will also raise the electrical energy consumption [93].

The German transmission system operators (TSOs) expected that the geographical distribution of the electrical energy consumption by 2045 will be mostly concentrated in regions with high population density and where the manufacturing industry is located today. Regions such as the Ruhr area, and some parts of the metropolitan regions of Frankfurt, Hamburg, Stuttgart, Berlin, and Munich will have an electrical energy consumption density higher than 7 GWh$_e$ km^{-2} [93].

2.4 Liquid Hydrogen Use

Hydrogen liquefaction is not only convenient for the efficient transport of hydrogen by ship. Liquefying hydrogen also leads to three essential properties that are highly valuable for end users from various sectors:

1. high gravimetric energy density (LHV_{paraH2} = 32.9 $kWh_t\ kg^{-1}_{H2}$ for para-hydrogen at 20 K, 100 kPa) with significantly higher volumetric energy density (ρ_{paraH2} = 71.144 $kg_{H2}\ m^{-3}$) than that of gaseous normal-hydrogen[1] (0.1 $kg_{H2}\ m^{-3}$ at 293.15 K, 100 kPa) [50],
2. high purity ($\geq$ 99.995% by volume [94, 95]) and,
3. cryogenic temperature (approximately −253 °C or 20 K [50]).

The following sections present how each of these properties benefits a variety of applications, such as the long-range transport, parts of the manufacturing industry, and the transmission of electrical energy. Additionally, it is worth noting that liquid hydrogen can be regasified and flexibly employed for the decarbonization of hard-to-abate sectors with a large hydrogen demand, such as steel and chemical industries [44].

2.4.1 Aviation Sector

The gravimetric energy density of liquid hydrogen is the highest of all known substances [96]. This property is particularly advantageous for the aviation sector. Aircraft manufacturers, such as Airbus [97] and Boeing [98], trade associations, such as the Airport Council International [99] and the International Air Transport Association (IATA) [100], and political entities, such as the EU Clean Hydrogen Partnership [101] have recognized liquid hydrogen as a light and sustainable energy source to replace fossil fuels, at least in certain cases. Even when considering the weight of the cryogenic tanks, hydrogen is around 50% of the weight of jet fuel. In addition, the cryogenic temperature can be potentially used to improve energy efficiency by approximately 10% to 15% for long-haul flights in comparison to kerosene-fueled aircraft [102].

Academic and industrial research projects have demonstrated the viability of liquid hydrogen aircraft and propulsion technologies by 2050. A review of the literature and market developments suggests that the aviation industry is expected to undergo three progressive

[1] The gravimetric energy density of normal-hydrogen is LHV_{normH2} = 33.3 $kWh_t\ kg^{-1}_{H2}$ at 293.15 K and 100 kPa [50].

phases in the integration of hydrogen technologies: technical demonstration and certification (2025–2030), system-level optimization (2030–2040), and aircraft fleet deployment (2040–2050) [103].

Figure 2.6 shows the liquid hydrogen projects developed by airlines, airports, and lessors worldwide known by IATA. As of January 2025, at least 35 airlines have publicly declared their participation in diverse initiatives with the objective of developing hydrogen-powered aircraft. Companies such as International Airlines Group (e.g., British Airways and Iberia), United Airlines, and EasyJet have made direct investments in research and development efforts. Additionally, several pre-order agreements for hydrogen-fueled aircraft have been established, indicating growing commercial interest in this technology [100].

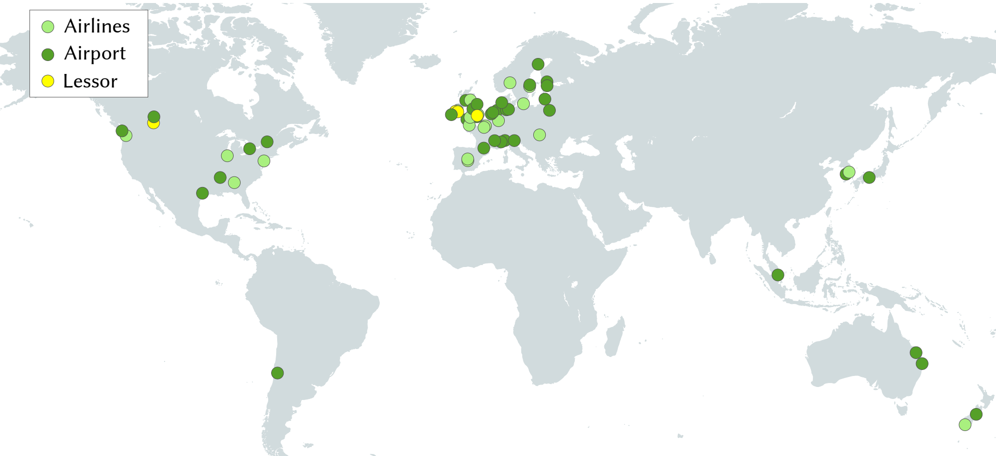

Figure 2.6: Liquid hydrogen projects developed by airlines, airports and lessors known by IATA as of January 2025. Own depiction based on [100]; reproduced by permission.

However, the Aviation Impact Accelerator convened by the University of Cambridge expected that the ongoing and publicly disclosed aircraft projects will contribute only 5% to 9% of emissions decrease by 2050 [102]. Therefore, the authors suggested launching large-scale hydrogen demonstrators in 2030, especially for medium-range and long-range aircraft. This measure could lower emissions levels by 15% to 20% in 2050, and 30% to 70% in 2060.

A key challenge associated with liquid hydrogen is its spatial requirement, which is approximately four times greater than that of the kerosene-type jet fuel A-1. This is because of a significantly lower volumetric energy density (2.3 $kWh_t\ l^{-1}$ for para-hydrogen at 20 K and 100 kPa [50] against 9.2 $kWh_t\ l^{-1}$ for jet fuel A-1 [104]). Therefore, new aircraft designs are necessary. For narrow-body aircraft, a 5–10 m longer fuselage could accommodate the fuel tanks [105]. When aircraft are retrofitted for hydrogen use, the space available for passengers decreases and the energy requirement per passenger grows. However, if aircraft are specifically designed for liquid hydrogen fuel, more passengers can be potentially carried than with an equivalent kerosene-powered aircraft [106].

Figure 2.7 shows the expected liquid hydrogen demand for direct use from aviation in Germany, based on the work from Busch et al. [107], and on the literature review by Oesingmann et al. [108] regarding the works from the European Hydrogen Backbone (EHB) [53], Grimme & Braun [109], Steer & the German Aerospace Center (DLR) [110], the Netherlands Aerospace Center (NLR) [111], and the consultancy Steer [112]. Indirect hydrogen use for the production of derivatives, such as Fischer-Tropsch jet fuel, is not considered. Since all authors assumed hydrogen in liquid and not in gaseous state, the conversion between million tons per year and GW_t has been carried out using the lower heating value of para-hydrogen and not of normal-hydrogen (see section 2.4).

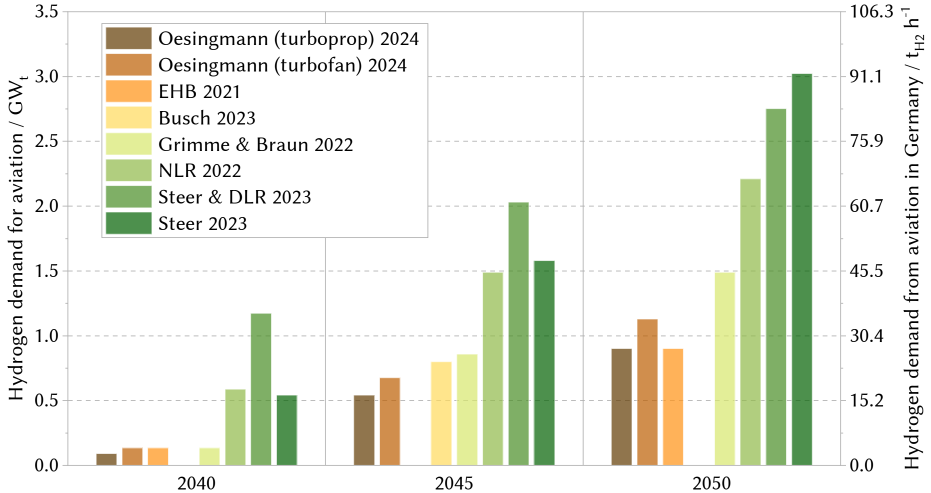

Figure 2.7: Liquid hydrogen demand in Germany for direct use in aviation. While only Busch et al. estimated the demand specifically for Germany, the European demand of the other studies was scaled down to 12% of the original, based on the number of departures and arrivals in Germany in 2024. Own depiction based on data from [107, 108, 113].

Oesingmann et al. proposed two scenarios: one with turboprop engines (more energy efficient), and another with turbofan engines [108]. Only Busch et al. calculated the hydrogen demand specifically for Germany [107]. All other studies estimated the hydrogen demand for

Europe[2] [53, 108–112]. Therefore, the European data was scaled down to 12% of the original to estimate the German demand share, based on the number of departures and arrivals in Germany in 2024, as given by Eurocontrol [113]. This rough approximation implicitly assumes that the fuel demand is proportional to the number of incoming and outgoing flights.

The literature comparison in figure 2.7 shows that the works from Oesingmann et al. [108], the EHB initiative [53], Busch et al. [107], and Grimme & Braun [109] tended to be more conservative than the works from NLR [111], Steer & DLR [110], and Steer [112]. The conservative works expected an annual liquid hydrogen demand between 0.9–1.5 GW_t in 2050, while the optimistic studies expected that the liquid hydrogen demand will range from 2.2 GW_t to 3.0 GW_t in the same year.

It remains to be seen which role liquid hydrogen will play when decarbonization in the aviation sector is achieved. However, it seems to be clear that liquid hydrogen alone will not be able to cover the energy demand for sustainable aviation. McKinsey & Company estimated liquid hydrogen as feasible but less cost-efficient for long-range aircraft designs, owing to larger airframes and a higher energy demand per passenger. This makes Fischer-Tropsch jet fuel together with biofuels likely the more cost-effective decarbonization solution in the long-range segment. McKinsey & Company expected that Fischer-Tropsch jet fuel and biofuels will supply approximately 60% of total aviation fuel by 2050, while liquid hydrogen will cover the remaining 40%. After 2050, the share of liquid hydrogen is projected to keep rising, especially for commuter, regional, short-range, and medium-range aircraft [101].

Dray et al. [114] and Ansell [115] agreed that decarbonizing the aviation sector by 2050 will require liquid hydrogen and Fischer-Tropsch jet fuel, with biofuels serving as an interim solution, owing to their near-future availability. Nevertheless, Dray et al. argued that the availability of biofuels is limited, thereby restricting its production capacity and driving up its costs [114]. In addition, biofuels have led to deforestation, biodiversity loss, peatland degradation, and higher greenhouse emissions [116]. Ansell noted that electric battery systems could become relevant in the long term, if disruptive improvements in their weight are produced. Today, Li-ion electric batteries are approximately 400 times heavier than liquid hydrogen (without storage system), when compared on a per-kilojoule basis [115].

[2] The works from Oesingmann et al. [108], EHB [53], Grimme & Braun [109], and Steer & DLR [110] considered the EU27 countries plus Switzerland, United Kingdom, Iceland, and Norway. The NLR study counted only the EU27 countries plus United Kingdom [111]. Steer took only into account intra-European flights [112].

2.4.2 Heavy-duty Long-distance Road Sector

Long-distance road transport could benefit from the high gravimetric energy of liquid hydrogen, which leads to long range, fast refueling time, and high payload capacity [117, 118]. In contrast to personal transport, where vehicles often remain parked during days or weeks, heavy-duty trucks are frequently used, consuming larger amounts of hydrogen and preventing vent losses caused by a pressure increase, owing to heat transfer from the environment [119]. In 2023, Daimler Truck demonstrated how one fill of 80 kg_{H2} was sufficient to cover a distance of 1 047 km with a fully loaded 40 tons fuel-cell truck [74]. Daimler Truck favors liquid hydrogen for the expansion of hydrogen-based drives, since cryogenic low-pressure tanks are more cost-efficient and significantly lighter compared to the carbon tanks used for compressed gaseous hydrogen [120].

However, it is yet to be determined which proportion of trucks will be fuel-cell versus battery-electric driven in the market of long distance road transport. The IEA reported that the lifecycle cost of a battery electric heavy-duty truck in China is, in 2025, already lower than that of a diesel equivalent in some cases. The same study expected that by 2030, battery electric trucks in Europe and the United States (USA) will achieve life-cycle cost equivalence with heavy-duty diesel trucks, maintaining total costs of ownership for battery electric trucks lower than for fuel cell trucks [121]. Other authors considered battery electric trucks to have an advantage because of a wider available recharging infrastructure compared to hydrogen refueling stations [122, 123] and owing to longer lifetimes than for fuel cell trucks [124]. However, the IEA recognizes that depending on the application and utilization profile of trucks, hydrogen-based drives may be more cost-efficient in certain cases [121].

A couple of recent studies have calculated the hydrogen demand from trucks in Germany by the middle of this century. Table 2.2 shows the approximations for Germany as given by Busch et al. [107] and Löfving et al. [125]. While Löfving et al. limited the use of hydrogen for long-haul trucks, Busch et al. did not specify which kind of trucks are hydrogen-driven. For comparability reasons, the lower heat value of para-hydrogen is used (see section 2.4) although Löfving et al. did not specify which state of matter was considered for hydrogen. Busch et al. calculated a large liquid hydrogen demand of 8.33 GW_t by 2045. In contrast, Löfving et al. estimated a hydrogen demand between 0.28 GW_t and 2.15 GW_t in 2050, depending on the assumed market diffusion of hydrogen trucks.

For comparison, table 2.2 presents the hydrogen demand from medium-haul trucks and long-haul trucks in the USA, as estimated by Elgowainy et al. [126]. The hydrogen demand calculation made for Germany by Busch et al. seems to be optimistic, as the amount of total truck kilometers in the USA is almost 15 times larger than in Germany [127].

Table 2.2: Hydrogen demand for direct use from trucks in Germany and the United States (USA).

Country	Source	Year	State of matter	Considered trucks	Diffusion of technology	Demand
Germany	Löfving 2025 [125]	2050	Hydrogen (unspecified)	Long-haul	5%	0.28 GW_t (8 t_{H2} h^{-1})
					15%	0.82 GW_t (25 t_{H2} h^{-1})
					25%	1.37 GW_t (42 t_{H2} h^{-1})
					35%	2.15 GW_t (58 t_{H2} h^{-1})
Germany	Busch 2023 [107]	2045	Liquid hydrogen	Unspecified	Unspecified	8.33 GW_t (253 t_{H2} h^{-1})
USA	Elgowainy 2020 [126]	2050	Hydrogen (unspecified)	Long-haul	22%	14.29 GW_t (434 t_{H2} h^{-1})
					35%	22.56 GW_t (685 t_{H2} h^{-1})
				Medium- & long-haul	22%	19.55 GW_t (594 t_{H2} h^{-1})
					35%	30.83 GW_t (936 t_{H2} h^{-1})

2.4.3 Maritime Sector

Green hydrogen has been identified by the IEA [128], the European Maritime Safety Agency [129], and academic research [130] as one of several potential fuels to decarbonize the maritime sector. The high energy density of hydrogen by weight enhances its suitability for maritime transportation [131], facilitating onboard storage in comparison to batteries and being a more favorable option for transport to refueling sites [132]. Hydrogen fuel cells function quietly and without strong vibrations, reducing significantly the impact of shipping on marine ecosystems in comparison to current shipping [130].

In 2020, Shell believed *"liquid hydrogen to be advantaged over other potential zero-emissions fuels for shipping, therefore giving a higher likelihood of success"* [133]. In 2021, many stakeholders view hydrogen as a feasible answer for coastal and short-sea shipping [132]. By 2022, over 20 maritime applications were powered by hydrogen fuel cell systems [134]. One recent example is from Norway's ferry company Norled, which proved the use of the first liquid hydrogen-fueled ferry with a capacity for 80 cars and almost 300 passengers, maintaining 99.9% uptime during the first year [135, 136].

Yet, challenges in the use of liquid hydrogen may lead the shipping industry to prefer other fuels. Balcombe et al. [130] and Gray et al. [137] argued that Fischer-Tropsch fuels, biofuels, and liquefied natural gas (LNG) can be dropped into existing motors without adjustments, while higher capital costs for hydrogen infrastructure may delay the adoption of hydrogen as a fuel. The authors in both studies considered that there is no single path to achieve decarbonization in the maritime sector, requiring a variety of "drop-in" fuels and zero-carbon energy carriers, such as hydrogen and ammonia.

According to expert interviews made in 2023 on behalf of Shell, there is a growing industry trust for bio- and synthetic liquid methane, methanol, ammonia and bio heavy fuel oil, while there is less interest in liquid hydrogen [138]. Urban et al. reported that fragments of the shipping industry are less willing to change, usually as a result of being less present for the public view, compared to aviation, and not necessitating a sustainable public profile, for instance, in the case of businesses managing oil tankers [139].

Only a few studies have quantified the expected hydrogen demand from the maritime sector by 2050, but none of them are specific to Germany. The results of these studies are shown in table 2.3. The International Renewable Energy Agency (IRENA) estimated that 4.6 million tons of liquid hydrogen will be employed mainly for short sailings by fuel cells or internal combustion engines in the international shipping sector. This amount is equivalent to 17.3 GW_t or 525 t_{H2} h^{-1}, and it accounts only for 10% of the total hydrogen demand from the maritime sector, because 73% are expected to be for the production of ammonia, and 17% for methanol synthesis [140].

Table 2.3: Hydrogen demand for direct use from the maritime sector. The countries considered along the European Atlantic coast are Portugal, Spain, France, Ireland, and the United Kingdom.

Region	Source	Year	State of matter	Considered vessels	Demand
Worldwide	IRENA 2021 [140]	2050	Liquid hydrogen	Short sailings, e.g., domestic navigation	17.3 GW_t (525 t_{H2} h^{-1})
European Atlantic coast	Ortiz-Imedio 2021 [141]	2050	Hydrogen (unspecified)	Passenger and freight transport	28.2 GW_t (856 t_{H2} h^{-1})

For comparison, Ortiz-Imedio et al. expected a hydrogen demand of 7.5 million t_{H2} for shipping on the Atlantic coast of Europe in 2050. The authors in this study considered the annual demand for marine passenger and freight transport from the coast regions of Portugal, Spain, France, Ireland, and the United Kingdom [141]. Ortiz-Imedio et al. did not specify the state of matter of hydrogen. Using the lower heat value of para-hydrogen, the resulting equivalent demand is 28.2 GW_t or 856 t_{H2} h^{-1}.

2.4.4 Semiconductor Industry and Power Generation

Hydrogen has the second-lowest boiling point among all elements, that is, 20.28 K, after that of helium at 4.22 K [142]. Through the cryogenic distillation method, the boiling point differences between hydrogen and impurities are used to purify hydrogen [143]. For the liquefaction process, hydrogen is cooled down further than for separation, reaching high-purity levels of at least 99.995% by volume [94, 95]. Therefore, liquid hydrogen provides a high degree of purity for applications with rigorous purity specifications.

Hydrogen is essential for the semiconductor industry owing to its ability to affect the electronic properties of semiconductors [144]. High-purity hydrogen is applied in its gaseous state, for instance in epitaxial growth, by the photovoltaics and semiconductor industries [145]. Impurities in hydrogen can reduce the manufacturing output of compound semiconductor devices, damage the production process guidance, or even lead to defective devices [146]. In addition, the purity level of hydrogen has a clear impact on the efficiency and lifespan of proton-exchange membrane (PEM) fuel cells for power generation, affecting directly their profitability [147]. For that reason, the International Organization for Standardization (ISO) issued ISO 14687 to specify the minimum standards of hydrogen purity for PEM fuel cells and internal combustion engines [148].

There are no known studies or reports that quantify the amount of high-purity hydrogen required by the semiconductor industry today or in the future. However, some recent projects present the hydrogen demand from single semiconductor facilities (see table 2.4). In Japan, a quartz glass manufacturer spends 1 900 tons of hydrogen per year for the production of components essential to the semiconductor industry [149]. In Austria, 290 tons of hydrogen covers the demand per year of a semiconductor production site [150]. Trapani et al. estimated that a silicon wafer factory has an annual hydrogen demand of 110 t_{H2} [151]. In none of these publications, the state of matter of the considered hydrogen has been specified. For comparability purposes, the lower heat value of para-hydrogen has been used to calculate the hydrogen demand in energy units.

Table 2.4: Hydrogen demand from single semiconductor facilities.

Region	Source	Year	State of matter	Considered facility	Demand
Japan	Siemens Energy 2025 [149]	2025	Hydrogen (unspecified)	Quartz glass manufacturer	7.1 MW_t (0.22 t_{H2} h^{-1})
Austria	Infineon 2025 [150]	2025	Hydrogen (unspecified)	Semiconductor production site	1.1 MW_t (0.03 t_{H2} h^{-1})
Unspecified	Trapani 2025 [151]	Unspecified	Hydrogen (unspecified)	Silicon wafer factory	0.4 MW_t (0.01 t_{H2} h^{-1})

2.4.5 Cryogenic Applications: Superconducting Cables, Motors, Generators and Others

The cryogenic temperature of liquid hydrogen is a valuable form of stored energy that can be used for several applications. At approximately 20 K, liquid hydrogen enables, for example, the use of high-temperature superconductors (HTSs). The steady increase in electrical energy demand, which is enhanced by the energy transition, can push existing electrical grids beyond their capacity limits. Superconducting cables can unload tensions in the existing grid [152], for instance, in high-population areas with restricted space. Two examples of superconducting cables are currently under development: the 15 km long HTS cable SuperLink in Munich, with a power transmission capacity of 500 MVA [153], and the two 60 m long 1.5 kV – 3.5 kA HTS direct current (DC) SuperRail cables for the railway network in Paris [154].

The "for-free" cooling of imported liquid hydrogen makes possible new concepts in electric machines [155]. The cooling provided by liquid hydrogen can be exploited for superconducting machines—for example, motors such as those developed for aircraft by Airbus [156], Rolls-Royce et al. [157], for ships by Siemens [158], and by Changwon National University of South Korea [159]—as well as for superconducting generators for wind turbines [160].

In addition, HTSs can reduce significantly the amount of copper for electrical energy transmission, and the quantity of critical materials that are usually needed in permanent magnets, for example, for the generation of strong magnetic fields [161]. The cryogenic temperature of liquid hydrogen can be employed for electrical energy generation by recuperating cold energy, for instance, when combining the Brayton and Rankine cycles [162], and potentially for preservation of food [163] and biological materials [164].

Overall, the published research suggests that liquid hydrogen's multiple properties will be required to enable partial decarbonization of several sectors. The energy density of liquid hydrogen is highly valuable for aviation, long-distance heavy-duty trucks, and vessels. The high-purity of liquid hydrogen serves the semiconductor industry and enhances the operation of PEM fuel cells. The cryogenic temperature of liquid hydrogen permits the use of HTSs—e.g., in efficient electrical energy transmission, motors, and generators—and also enables electrical energy generation through cold energy recovery or the preservation of organic materials.

2.5 Definition of the Case Study

The preceding sections outlined the expected supply of electrical energy and liquid hydrogen in Germany as well as the potential demand for both carriers. This information enables the identification of a region in Germany that can supply the hybrid pipeline with both energy vectors (upstream side) and a location that could require them (downstream side). Figure 2.8 presents a visual summary of the selected case study: Brunsbüttel–Hamburg. This section describes the reasons for the selection of this case study.

The coastal locations on the North Sea are highly suitable for the upstream side. This is because large amounts of offshore wind power are connected to the coast, and because imported liquid hydrogen will be brought to Germany by ships. Among those locations, Brunsbüttel is an important seaport that will develop into a main interconnection node for both electrical energy and liquid hydrogen. Multiple offshore wind farms will transmit a minimum of 3 GW_e to this area [165]. Additional electrical energy will be conducted through this region from Denmark [166] to the south of Germany [167,168]. In 2023, an LNG floating storage and regasification unit terminal was built in Brunsbüttel [169]. In 2027, a stationary terminal will start processing LNG and later hydrogen for the German energy supply [170]. This analysis indicates that Brunsbüttel is a suitable location for the upstream side of the hybrid pipeline.

For the downstream side, a region with a high concentration of liquid hydrogen demand and electrical energy consumers is ideal. Approximately 75 km away from Brunsbüttel is Hamburg, a big city with a broad range of sectors: manufacturing industry, maritime, aviation, and road transport hubs, private households, and non-residential buildings. In Hamburg, the largest German seaport [171], the biggest airport in northern Germany [172], and an extensive road logistic network [173] are located. Hamburg's manufacturing industry produces steel [174], aircraft [175, 176], chips [177], and chemical products [178]. Over five million people live in the metropolitan area [179]. Consequently, Hamburg has been selected for the downstream side of the hybrid pipeline. It will be assumed that the hybrid pipeline ends at a central location with a high demand for liquid hydrogen. From this place, other consumers with a lower hydrogen demand can be reached, for example by trailers.

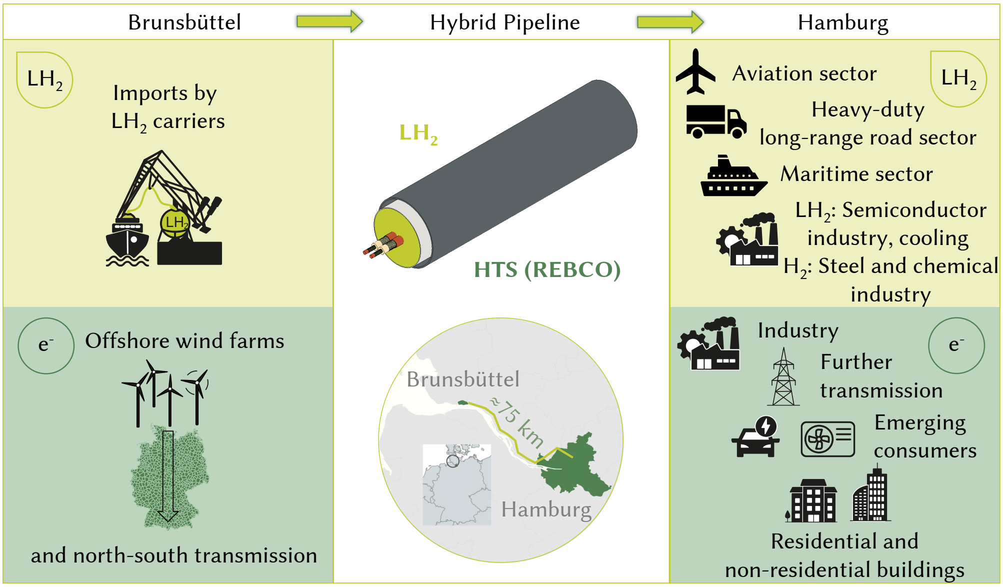

Figure 2.8: Visual summary of the supply, transmission and use of liquid hydrogen (LH_2) and electrical energy (e^-) when transmitted by a hybrid pipeline in the considered case study between Brunsbüttel and Hamburg. The high-temperature superconductor (HTS) in the cable is a rare-earth barium copper oxide (REBCO). Liquid hydrogen is principally used by the transport sector and segments of the manufacturing industry. Regasified liquid hydrogen (H_2) can be employed by large hydrogen consumers, such as the steel and chemical industries. Electrical energy is mainly utilized by the industry and emerging consumers, such as electric vehicles and heat pumps.

Table 2.5 presents the required specifications of the selected case study, Brunsbüttel–Hamburg. The electric rated power P_0 was assumed to be 4.0 GW_e based on the transmission power of current extra-high-voltage DC projects (see section 2.6.1) and owing to the large increase in electrical energy consumption until 2045 (see figure 2.5).

The Hamburg Ministry of Economic Affairs and Innovation interviewed relevant stakeholders in the city to approximate the total hydrogen demand in Hamburg in 2030. Their results led to an expected hydrogen import demand of 5.4 $TWh_t\ a^{-1}$ and a total hydrogen demand of 7.6 $TWh_t\ a^{-1}$ (0.62 and 0.87 GW_t, respectively) [180]. Assuming a hydrogen delivery in its liquid state, and therefore the lower heating value for para-hydrogen, this amount is equal to a constant mass flow rate from 5.20 to 7.32 $kg_{H2}\ s^{-1}$ (18.7 to 26.3 $t_{H2}\ h^{-1}$).

The German Economic Institute prognosticated for 2035 and 2045 a hydrogen demand in Hamburg of 14.4 TWh (1.64 GW_t, 13.86 kg_{H2} s^{-1} or 49.9 t_{H2} h^{-1}) and 32.7 TWh (3.73 GW_t, 31.48 kg_{H2} s^{-1} or 113.3 t_{H2} h^{-1}), respectively [181, 182]. As a conservative hypothesis, a hydrogen demand between 0.62 and 0.87 GW_t was assumed for the case study.

Table 2.5: Required specifications of the defined case study, Brunsbüttel–Hamburg.

Parameter	Symbol	Value
Length	ℓ	75 km
Electric rated power	P_0	4.0 GW_e
Hydrogen demand in Hamburg	–	From 0.62 GW_t (5.20 kg_{H2} s^{-1}) to 0.87 GW_t (7.32 kg_{H2} s^{-1})

2.6 State of the Art of Conventional Transmission Infrastructure

Conventional transmission infrastructure will be used as a benchmark for the techno-economic assessment of the hybrid pipeline. To date, the conventional method to transmit electrical energy and hydrogen in bulk is separately and without interconnections. High-voltage DC underground cables and gaseous hydrogen pipelines are commonly planned today in Germany for the transmission infrastructure. The next sections will introduce their technical aspects. Economical aspects will be treated in Chapter 5. Additionally, an overview of the state of the art of liquid hydrogen pipelines will be presented.

2.6.1 Extra-high-voltage Direct-current Underground Cables

In 2015, the German Federal Cabinet designated high-voltage direct-current (HVDC) underground cables as the preferred option over overhead lines to enhance the public acceptance and accelerate the expansion of the electrical network [183]. Consequently, new onshore HVDC links were required to use underground cables [184], and overhead HVDC lines were limited to exceptional cases, for example justified by environmental reasons [185].

In April 2026, the German Federal Cabinet adopted a mandate that new HVDC connections be built as overhead lines, aiming to reduce the overall cost of HVDC projects. Underground

HVDC cables may still be permitted in exceptional cases, for example when the route already contains an underground line, when technical constraints make an overhead solution infeasible, or when an underground option proves more cost-effective. The cabinet also stipulates that, upon request by the authority responsible for federal sector planning or project approval, specific sections may be required to be constructed, operated, or retrofitted as underground cables under the conditions outlined in the corresponding regulatory paragraph number 5 [186].

Because the majority of this work was carried out before the 2026 regulation took effect, the techno-economic assessment of transmission alternatives primarily assumes HVDC underground cables. Nevertheless, the sensitivity analysis in section 5.5.2 also explores the use of HVDC overhead lines.

Some of the main HDVC underground projects in Germany, such as SuedLink and SuedOstLink, will transmit the electrical energy from the north to the south of the country. SuedLink and SuedOstLink will operate at an extra-high voltage of ± 525 kV and will provide a total installed capacity of 4 GW_e each. Each project is composed of two independent 2 GW_e cable systems. Each system has two poles of 1 GW_e each. A pole transmits approximately 1.9 kA [187, 188].

The total width required for the operation of SuedLink is between 18 and 22 m, while during construction times 40 to 45 m of width are necessary [187]. According to an expert interview, the electrical topology of each cable system in SuedOstLink is a rigid bipole without a metallic return, divided into sleeve groups with grounding (see figure 2.9). For the connection of DC cables, such as SuedLink, to the existing alternating current (AC) grid, converters and inverters are necessary at the starting and ending nodes of the cable [189].

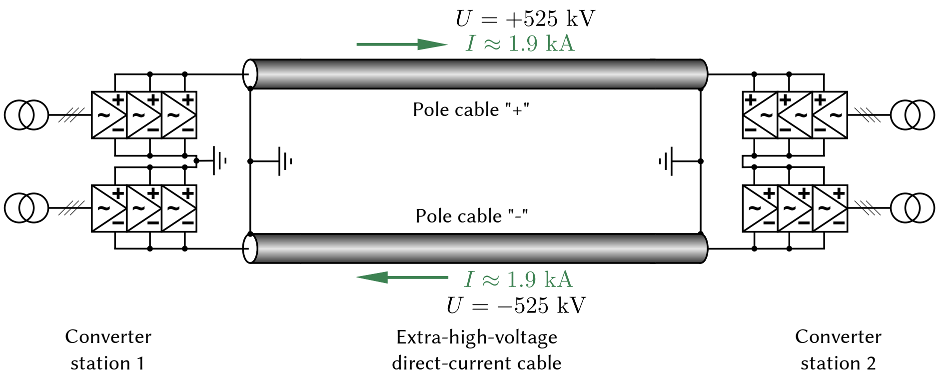

Figure 2.9: Electrical topology of SuedOstLink, a rigid bipolar HVDC system that operates without a metallic return conductor. Own depiction based on [190]; reproduced by permission.

2.6.2 Gaseous and Liquid Hydrogen Pipelines

Until now, there is no hydrogen transmission network in Germany. In 2024, the Federal Network Agency, in German *"Bundesnetzagentur"*, approved the application for a gaseous hydrogen core network from the gas TSOs with some changes [191]. The approved gaseous hydrogen core network for 2032 is presented in figure A.1, appendix A. It has a total extension of 9 040 km. For comparison, the existing natural gas transmission network in Germany has a length of approximately 40 000 km, as of January 2022, and is shown in figure A.2.

The current hydrogen network approval defines, for instance, the geographic location of the future infrastructure and the proportion of new to repurposed pipelines (44%/56%) [191]. Pipelines are repurposed when they were used to transmit natural gas and are modified for the transport of gaseous hydrogen. The approval refers to some pipe diameters of DN 300, DN 400, and DN 500, that is, approximately 30 cm, 40 cm, and 50 cm [192].

In 2020, a group of 33 European gas transmission operators proposed the concept of a European Hydrogen Backbone (EHB) for the transmission infrastructure of hydrogen. The initiative published novel techno-economic data for gaseous hydrogen infrastructure, which has been updated based on expert interviews in 2023 [58]. Within the initiative, three members are German transmission operators, which may give an indication of transferability to the German market. The report considers newly constructed onshore pipelines with diameters of 20", 36", and 48", or rather approximately 50 cm, 90 cm, and 120 cm. According to their report from 2021, the maximum corresponding transfer capacity of each pipeline size is 1.2 GW_t, 4.7 GW_t and 13 GW_t. The authors assumed an operating pressure for small pipelines of 50 bar and for large pipelines of 80 bar [53].

Liquid hydrogen transfer lines are a mature technology in industrial equipment [193]. However, it is not known that a liquid hydrogen pipeline has been built outside industrial facilities. A leading application has been the transfer of rocket fuel for the NASA space program [194]. Liquid hydrogen pipelines are available on the market, for example, from [195] and [196]. Their use for energy distribution has been demonstrated at pilot scale, e.g., by the *icefuel* project in 2010. The authors of the study expected transport distances up to 10 km without intermediate cryogenic cooling systems, considering a low mass flow rate of 10 MW_t, pipe diameter of approximately 20 mm, and thermal losses of less than 1 W m^{-1} [197]. Since large amounts of hydrogen are required to become climate-neutral, higher mass flows rates are expected today.

2.7 State of the Art of Hybrid Pipelines

The idea of simultaneous transmission of liquid hydrogen and electrical energy by high-temperature superconductivity dates back to the early 2000's, when the founder of EPRI, Starr, proposed the creation of a U.S. American "Continental SuperGrid" to be supplied from nuclear and supplementary power plants [14, 198]. Since then, multiple different conceptual designs have been proposed. Some prototypes have been built. The following review does not aim to provide a full survey of all prior research on the topic, but it offers a selective overview of studies relevant to the objectives of this work.

2.7.1 Conceptual Designs

Supporting the idea of a "Continental SuperGrid" and a hydrogen-based transportation economy, a U.S. American energy consultant, Grant, proposed in 2004–2005 the first basic design of a "SuperCable" for the dual delivery of hydrogen and electric power [15, 16]. A bipolar DC cable system was suggested to carry 1 GW_e of electrical energy, that is, 100 kA at ± 5 kV, using wires or tapes of high-temperature ceramic superconductors or magnesium diboride (MgB_2). Two cryostats, one for each monopole, should deliver in equal shares a total of 1.0 GW_t of liquid hydrogen with a diameter of 15 cm each, at a flow rate of 3.39 m s^{-1}. Liquid nitrogen was shortly discussed as an alternative coolant for the chemical transmission of cold gaseous hydrogen at 77 K and 12.8 MPa, or even as a coolant for the transmission of LNG instead of hydrogen, in the case that the impact of carbon dioxide on climate change is not *"scientifically and publicly accepted"* [16]. The scope of the design was limited to the transmission capacity, the general layout, and the cryostat diameter.

In 2006–2007, Trevisani et al., from the University of Bologna, presented a more complete design and simulation of a superconducting MgB_2/liquid hydrogen transmission line. Their focus was on the thermo-hydraulic design considering hydrogen as a compressible fluid [17, 18]. The aim of the combined system was to transmit electrical energy and excess renewable generation (with respect to grid demand) in form of liquefied hydrogen from North Africa to Europe through the Strait of Gibraltar. A system with two corrugated cryostats was assumed—one for sending and the other for returning liquid hydrogen. In this manner, the cooling function was planned to be independent from the transport function, so that the superconducting cable could function properly even when no actual amount of liquid hydrogen is transported but only recirculated. A maximum distance of 20 km was designated to be without cooling and pumping stations. The range of net transported liquid hydrogen mass flow was of 0–1 kg_{H2} s^{-1} (119 MW_t) through an inner diameter of 12 cm, with thermal losses of

2 W m^{-1}, and in an operating range between 15–25 K and 0.5–1.5 MPa. The DC cable should transmit 96 MW_e, that is, 12 kA at ± 4 kV.

Yamada et al., from Japan's National Institute for Fusion Science, proposed in 2008–2010 a hybrid energy transfer line of 1 000 km length with refrigeration stations every 10 km [19, 20]. The authors considered a case study in which electrical energy and hydrogen are simultaneously produced by a fusion reactor, where hydrogen is produced by electrolysis of water steamed by waste heat. The electrical transfer capacity was defined to be 1 GW_e, that is, 10 kA at ± 50 kV, and the total amount of liquid hydrogen to be transmitted was 137 MW_t (1.16 kg_{H2} s^{-1} or 100 t_{H2} d^{-1}). An MgB_2 wire was preferred as the prospective system owing to lower costs, but bismuth strontium calcium copper oxide (BSCCO) and yttrium barium copper oxide (YBCO) tapes were also seen as suitable alternatives.

Between 2012 and 2015, the first experimental results of a hybrid power transmission line were published by Kostyuk, Vysotsky et al. in Russia (see next section 2.7.2). In 2019–2022, Wang, Jin et al., from the Tianjin University, developed technical designs of a superconducting energy pipeline based on: a YBCO cable, liquid hydrogen as a coolant in the inner part of the pipeline, and LNG as a refrigerant for an outer superconducting electrical shield made of BSCCO. The cable was designed to transmit 1 GW_e by means of 10 kA at ± 50 kV. The hydrogen transmission power and length were respectively given as: 4 GW_t (33.73 kg_{H2} s^{-1} or 2 914 t_{H2} d^{-1}) and 100 km in [199], or as 1 m s^{-1} (2.4 GW_t, 19.86 kg_{H2} s^{-1} or 1 716 t_{H2} d^{-1}) and 10 km in [200]. The scholars focused on the avoidance of magnetic induction and direct heat exchange. No case study was formulated.

Since 2024, several researchers have published more detailed conceptual designs for a combined energy transmission by means of MgB_2 and liquid hydrogen. Savoldi et al., from the Polytechnic University of Turin, focused on the thermal-hydraulic design of a DC single-pole, single-coolant superconducting energy pipeline with a transmission power of 0.1 GW_e and > 0.1 GW_t. The scholars compared and proved the viability of corrugated pipeline lengths up to 120 km without intermediate cooling stations, inner diameters up to 19.8 cm, liquid hydrogen mass flow rates up to about 3.8 kg_{H2} s^{-1}, and inlet pressures between 2 MPa and 4 MPa [201].

Bracco et al., from the University of Genoa, designed a 30 km submarine single-pole corrugated hybrid pipeline that can transfer 0.3 GW_e and at least 60–70 MW_t from an offshore wind farm to the port of Ravenna, Italy. In addition to proposing a cable and pipeline layout, they performed a preliminary thermal-mechanical analysis to assess the effects of the coolant pressure on the pipe and the thermal contraction of the materials along the cable [202]. Savoldi et al. subsequently examined accidental transients in liquid-hydrogen flow (0.6–0.1 kg_{H2} s^{-1}, i.e., 0.07–0.12 GW_t) and cryostat to keep the MgB_2 cable superconducting. Their analysis considered three fault cases: loss of flow due to pump failure, loss of coolant caused by a cryostat crack, and loss of vacuum resulting from an outer-pipe rupture [203]. In a further study, Cavallucci et al. (University of Bologna) used a fully coupled model to assess how an electrical fault in the MgB_2 cable interacts with heat generation and the thermodynamic response of the liquid hydrogen coolant [204]. As part of the same project, Mangiulli et al. focused on the sizing of auxiliary components, such as tanks, current leads, pumps, and grid connection to evaluate their economic impact in the hybrid power cable. The findings indicated that the main cost driver are not the auxiliary cryogenic systems but the electrical infrastructure, such as the HVDC conversion [32].

For the European project *SCARLET (Superconducting CAbles foR sustainabLe Energy Transition)*, Bruzek et al., from ASG Superconductors and other research institutions, proposed the use of a medium-voltage DC cable at $\pm$ 25 kV and 20 kA. They aimed to transmit 1 GW_e in a bipolar system, composed of two 500 MW_e monopolar cables, which should be in a cryostat with a length up to 20 km that transmits liquid hydrogen without cooling stations. The hydrogen transmission power ranged from 0.2 t_{H2} h^{-1} to 10 t_{H2} h^{-1} (7 to 329 MW_t) under a heat load of less than 2 W m^{-1} at 20 K. The authors planned to analyze the behavior of the cable during a fault current of 58 kA during 10 ms. Both liquid hydrogen and electrical energy were expected to be consumed by a steelmaker (10 t_{H2} h^{-1}, 50–200 MW_e), ships (2–3 t_{H2} h^{-1}, 50–100 MW_e), 100–1 000 trucks (0.3–3.0 t_{H2} h^{-1}), and 100 electric vehicles (15 MW_e). The demand amounts were obtained through expert interviews [205]. In a follow-up publication, the researchers of *SCARLET* analyzed two monopoles in two liquid hydrogen pipes, being one monopole in each pipe. Mimmi et al., from the University of Bologna, simulated the current distribution during the energization ramp, and during a pole-to-pole fault, where the temperature increase was also calculated [206].

Recently, some techno-economic assessments of hybrid pipelines have been published. Qin et al., from the Xi'an Jiaotong University, suggested the use of superconducting energy pipelines to connect East Asia and North America across 12 time zones, recovering the investment within 10 years. The scholars dispensed with a technical design to focus on the investment costs, which are referenced from other projects that developed the components for other applications [29]. For railway transportation, Fu et al., from the Tongji University, presented a detailed technical design of a YBCO cable (1.5 kV/10 kA/0.15 GW_e) and a liquid hydrogen pipeline (0.7 kg_{H2} s^{-1} or 83 MW_t) with a liquid nitrogen cold shield. The scholars included the investment costs of the components and the operating costs owing to power consumption and maintenance. Varying the total length, electricity price, and discount rate, they estimated that the dynamic payback period for a 93 km pipeline would be within 20 years [30].

In 2025, Cavallucci et al. optimized a cost-minimized MgB_2 DC line cooled with liquid hydrogen, without analyzing hydrogen supply or demand. The optimization varied wire geometry, liquid hydrogen mass flow rate, annular flow gap thickness, and number of intermediate cooling stations. The simulations covered line lengths of 5–100 km, power ratings of 0.5–3.0 GW_e, and voltages of 50 kV, 110 kV, and 220 kV. Low liquid hydrogen mass flow rates of 0.15–0.26 kg_{H2} s^{-1} (0.02–0.03 GW_t) were examined, but no specific case study was defined. The results showed that a 10 km, 50 kV line needs only one cooling station, the lowest-cost configuration depends strongly on voltage and power (with 110 kV emerging as optimal above 1.0 GW_e) and unit-length cost decreases up to 23% when length increases from 5 km to 100 km [31].

Table 2.6 presents a review of the conceptual designs that have been discussed in this section.

Table 2.6: Review of conceptual designs for hybrid energy pipelines. *These authors presented some economical assessment.

Source	Total length	Length without cooling	Electric power	DC voltage	Chemical power (H_2)	HTS type	Coolant	Case study	Outer diameter
Grant 2004–2005 [15, 16]	> 100 km	10–20 km	1 GW_e	± 5 kV	1 GW_t	Cuprates or MgB_2	LH_2, H_2/LN_2, LNG/LN_2	-	25 cm
Trevisani 2006–2007 [17, 18]	20 km	20 km	0.1 GW_e	± 4 kV	< 0.12 GW_t	MgB_2	LH_2	Africa–Europe: Strait of Gibraltar	18 cm
Yamada 2008–2010 [19, 20]	1 000 km	10 km	1 GW_e	± 50 kV	0.14 GW_t	MgB_2, BSCCO or YBCO	LH_2	Fusion reactor	22 cm
Wang 2019 [199]	100 km	-	1 GW_e	± 50 kV	4 GW_t	YBCO/ BSCCO	LH_2/LNG	-	159 cm
Jin 2022 [200]	10 km	10 km	1 GW_e	± 50 kV	2.4 GW_t	YBCO/ BSCCO	LH_2/LNG	-	89 cm
Savoldi 2024 [201]	< 120 km	< 120 km	0.1 GW_e	10 kV	> 0.1 GW_t	MgB_2	LH_2	-	7–22 cm
Bruzek 2024 [205]	> 20 km	20 km	1 GW_e	± 25 kV	0.01–0.33 GW_t	MgB_2	LH_2	End user, e.g., steel foundry	16 cm
Qin* 2024 [29]	20 000 km	-	100 GW_e	400 kV	50 GW_t	HTS	LH_2	East Asia–North America	-
Fu* 2024 [30]	< 100 km	< 100 km	0.15 GW_e	1.5 kV	0.08 GW_t	YBCO	LH_2/ LN_2	Railway transportation	< 17 cm
Cavallucci* 2025 [31]	5–100 km	∼5 km	0.5–3.0 GW_e	50, 110, 220 kV	0.02–0.03 GW_t	MgB_2	LH_2	-	-
Mimmi 2025 [206]	10–100 km	-	1 GW_e	± 25 kV	0.33 GW_t	MgB_2	LH_2	Supply to a port, an industry and, a fleet of land vehicles	-
Bracco 2025 [202] Savoldi 2026 [203] Cavallucci 2026 [204] Mangiulli* 2026 [32]	30 km	30 km	0.3 GW_e	30 kV	0.06–0.12 GW_t	MgB_2	LH_2	Offshore wind farm–Ravenna	> 22 cm

2.7.2 Built Prototypes

Liquid hydrogen has been tested for cooling MgB_2 cables in corrugated flexible pipelines with lengths of 10 m and 30 m (see figure 2.10). Kostyuk, Vysotsky et al., from the Russian Academy of Sciences and the Russian Scientific R&D Cable Institute, respectively, experimented with liquid hydrogen mass flow rates of 70–450 g_{H2} s^{-1} (8–53 MW_t), and electrical transmission capacities of 50–75 MW_e [21–26]. In [26], the authors demonstrated the suitability of impregnated crepe insulation paper with liquid hydrogen at voltages up to 50 kV DC.

(a)

(b)

Figure 2.10: (a) 30 m prototype of hybrid energy transfer line as presented by V. Kostyuk, V. Vysotsky et al.; (b) Photograph of the superconducting cable. Reprinted from [22] with permission from Elsevier.

Recently, two prototypes of hybrid energy pipelines were built and tested with cables made of HTS tapes. However, these pipelines use LNG as a coolant and energy carrier instead of liquid hydrogen. Chen et al., from the University of Chinese Academy of Sciences, presented a 10 m long pipeline with a DC monopole cable made of BSCCO, which transmits 0.1 GW_e at 10 kV and $\geq$ 1 kA (see figure 2.11) [207]. Xiao, from the Chinese Academy of Sciences, presented a 0.2 GW_e cable design ($\pm$ 100 kV/1 kA) with a 30 m long pipeline [208]. Both prototypes used a cryogenic liquid dielectric, which is a mixture of liquid nitrogen and tetrafluoromethane (CF_4), the longest-lived greenhouse gas [209].

As part of the *AppLHy!* project in the flagship project *TransHyDE*, a 16 m long rigid hybrid pipeline is under construction at KIT, Germany [210]. For the superconducting cable of the prototype, it was decided to use REBCO tapes (see chapter 3). The cable is electrically insulated with Kapton® and is composed of two poles. Although each pole is designed for rated operating conditions of 10 kA and 1 kV (10 MW_e), the initial operation will be limited to 10 V because of limitations in the available source voltage. The two poles are immersed in liquid hydrogen, which will have a mass flow rate of approximately 5 g_{H2} s^{-1} (0.6 MW_t). Table 2.7 presents a summary of the discussed built prototypes.

Figure 2.11: Experimental prototype of the 10 m superconducting DC energy pipeline as presented by Chen et al. Reprinted from [207] with permission from Elsevier.

Table 2.7: Review of built prototypes of hybrid energy pipelines.

Source	Country	Length	Electric power	DC voltage	Chemical power (H_2)	HTS type	Coolant
Kostyuk/ Vysotsky 2012–2015 [21–26]	Russia	10 m, 30 m	50–75 MW_e	$\leq$ 50 kV	8–53 MW_t	MgB_2	LH_2
Chen 2020 [207]	China	10 m	100 MW_e	10 KV	-	BSCCO	LNG, LN_2, CH_4
Xiao 2023 [208]	China	30 m	200 MW_e	$\pm$ 100 kV	-	BSCCO	LNG, LN_2, CH_4
KIT 2025–today [27, 28, 210]	Germany	16 m	20 MW_e	$\pm$ 1 kV	0.6 MW_t	REBCO	LH_2

3 Properties of the High-temperature Superconducting Tape

This chapter justifies the selection of REBCO tapes as superconducting material. The properties of the selected HTS are introduced for the subsequent design of the cable.

The cryogenic temperature of liquid hydrogen enables the use of HTSs for large scale applications, such as REBCO and MgB_2 [211]. To date, MgB_2 is the only HTS that has been tested in a hybrid power transmission line cooled by liquid hydrogen (see section 2.7.2). The developers of the prototype justified the use of MgB_2 by the wide availability of its raw materials and comparatively low production costs [21, 25].

In comparison, REBCO materials provide a higher critical temperature (e.g., YBCO at 93 K versus MgB_2 at 39 K [13]) and larger current densities under similar conditions (e.g., [212]). Consequently, REBCO permits a larger temperature safety margin or lower superconducting-material requirements. Moreover, REBCO offers relatively widespread commercial availability, as will be discussed later. For these reasons, REBCO was selected as the superconducting material for this project.

The following sections will first present the composition and specific material parameters of the selected REBCO. Subsequently, the critical values of the superconducting state in a REBCO compound are briefly described. At the end of the chapter, the production capacity of some of the current REBCO manufacturers worldwide will be listed, including a short discussion about REBCO's present costs.

3.1 Composition of the REBCO Tape

To avoid layer defects that reduce the current transport, REBCO is epitaxially growth in thin layers limited to a few microns. Today, a flat tape geometry is standard in long-length REBCO production to maximize the surface on which the superconductor can be grown [211].

Figure 3.1 presents the layer composition and thickness of the selected REBCO tape for the cable design. The figure is based on the data sheet provided by the tape manufacturer, which is Fujikura Ltd. For the sake of simplicity, buffer layers, such as magnesium oxide, were neglected because they represent less than 0.7% of the materials. The total tape thickness of REBCO tapes is about 50–100 µm (0.05–0.1 mm). For the cable simulation, a thickness s_{tape} of approximately 100 µm was assumed.

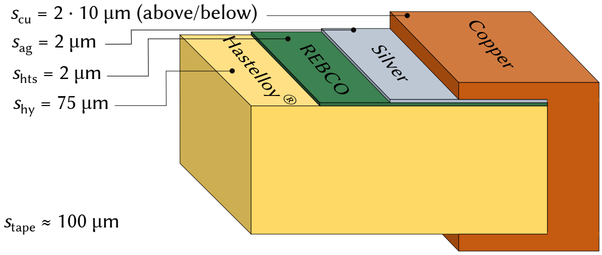

Figure 3.1: Layers in the REBCO tape and their corresponding thicknesses to scale.

The composition and thickness of the REBCO tape influence the cable behavior during a short circuit, whose simulation will be presented in section 4.2.4. For the simulation of the short circuit and the cable design, the resistivity, specific heat capacity, and mass densities of the materials in the REBCO tape can be found in appendix B.

3.2 Critical Values of Superconductivity

Three physical quantities characterize superconducting materials:

- critical temperature T_c,
- critical magnetic flux density $\vec{B}_c$, and
- critical current density $\vec{J}_c$.

The superconducting state exists while none of the critical thresholds are exceeded. In the Meissner phase, a superconducting material repels an applied magnetic field completely, behaving as a perfect diamagnet. The three physical quantities T_c, $\vec{B}_c$ and $\vec{J}_c$ are interdependent, which implies that each value varies depending on the others [213]. The critical temperature T_c and magnetic flux density $\vec{B}_c$ are thermodynamic properties specific to each superconducting material. The critical current density $\vec{J}_c$ is dependent on the metallurgical processing [214].

In a type I superconductor, such as mercury or aluminum, superconductivity ceases to exist abruptly at a critical magnetic flux density value B_c. In a type II superconductor, such as the considered REBCO material, there is a lower critical magnetic flux density B_{c1}, from which the magnetic repulsion gradually weakens in the so-called Shubnikov phase. At a higher critical magnetic flux density B_{c2}, superconductivity fully dissolves [13].

The subsequent sections describe the dependence of the critical current density $\vec{J}_c$ on the magnetic flux density $\vec{B}$ and on the temperature T for the selected REBCO tapes. The data were measured by the Robinson Research Institute in New Zealand, using 1 mm wide REBCO tape samples of the purchased product. The results show the critical current along the tape length per cm width. It is assumed that the REBCO material in the tapes is YBCO.

3.3 Field Angle Dependence of the Critical Current

Figure 3.2 shows the influence of the field angle on the critical current at different magnetic flux density values. The discrete data represent the measurements, which were all made at 30 K. Although the rated operation with liquid hydrogen occurs at temperatures close to 20 K, the design temperature T_{des} was selected to be 30 K to assure a safety margin in the case of higher operation temperatures.

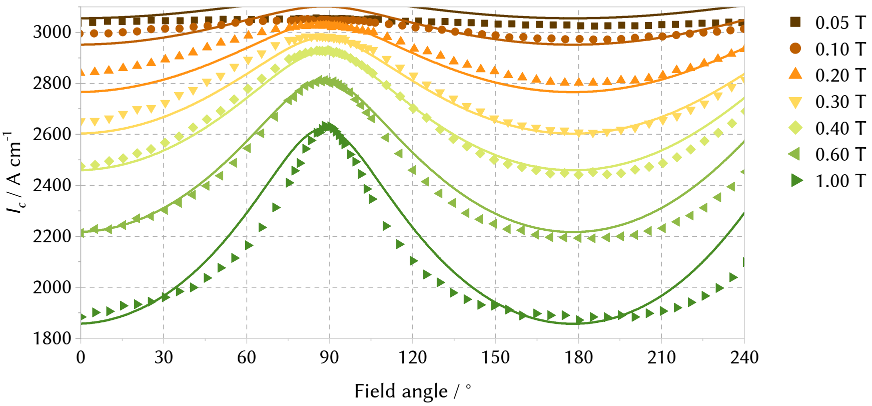

Figure 3.2: Field angle dependence of the critical current per cm width I_c for different magnetic flux density values at 30 K. The discrete data show the measurements on the selected REBCO tape, while the solid lines present the fitting function according to equation 3.1.

It can be seen that the highest critical currents occur when the field angle is parallel to the tape plane (90°). When the magnetic flux density is low (below 0.3 T), the critical current reaches values over 3 000 A cm^{-1}. The lowest measurements arise when the field angle is perpendicular to the tape plane (0° or 180°). For design purposes, the discrete measured data were linearly fitted using the following elliptical model from [215]:

$$I_c(\vec{B}) = I_{c,\text{ellip}} / \left(1 + \sqrt{k_{\text{ellip}}^2 \cdot B_{||}^2 + B_{\perp}^2} / B_{c,\text{ellip}}\right)^{\beta_{\text{ellip}}}, \tag{3.1}$$

where I_c is the critical current, $\vec{B}$ is an arbitrary magnetic flux density, and $I_{c,\text{ellip}}$, k_{ellip}, β_{ellip}, and $B_{c,\text{ellip}}$ are fitting parameters for the design temperature T_{des} of 30 K. In equation 3.1, the magnetic flux density $\vec{B}$ is split into a parallel component $B_{||}$ and a perpendicular component $B_{\perp}$. The fitting parameters were solved numerically and are shown in table 3.1. Figure 3.2 presents the resulting fitting functions in the form of solid curves.

Table 3.1: Elliptical model parameters to fit measured data of critical current dependence on the field angle.

Symbol	**Value (T_{des} = 30 K)**
$I_{c,\text{ellip}}$	316.6 A $\text{mm}_{\text{width}}^{-1}$
k_{ellip}	0.2871
β_{ellip}	0.89076
$B_{c,\text{ellip}}$	1.21901 T

3.4 Temperature and Magnetic Flux Density Dependence of the Critical Current

Figure 3.3 shows how the critical current varies with (a) temperature and (b) the magnitude of the magnetic flux density. The measurements shown in figure 3.3 (a) were made at magnetic flux densities between 0.05 T and 1.00 T. Figure 3.3 (b) presents multiple datasets for temperatures between 20 and 77 K. For all presented measurements, the field angle is the one with the lowest critical current at the corresponding temperature and magnetic flux density. This is a conservative assumption for a wider safety margin. As expected, increasing temperature or magnetic flux density lowers the critical current.

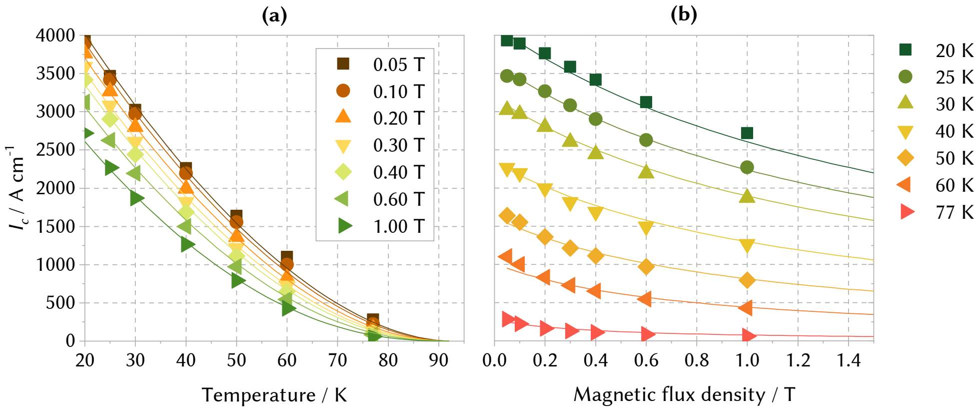

Figure 3.3: (a) Temperature dependence of the critical current per cm width I_c for different magnetic flux density magnitudes. (b) Magnetic flux density dependence of the critical current per cm width I_c for different temperature values. In both graphs, the field angle of each measurement is the one with the lowest critical current at the corresponding temperature and magnetic flux density magnitude. The discrete data show the measurements on the selected REBCO tape, while the solid lines present the fitting function according to equation 3.2.

The Kim model, introduced by Kuhnert [216], was used to calculate the critical current $I_{c,\mathrm{Kim}}$ at a temperature T and magnetic flux density magnitude B:

$$I_{c,\mathrm{Kim}}(B,T) = I_{c,\mathrm{Kim}}(0,0)\left(1-\frac{T}{T_c}\right)^{\beta_\mathrm{Kim}}\left[1+\frac{B}{B_\mathrm{Kim}\left(1-\frac{T}{T_c}\right)}\right]^{-1}. \tag{3.2}$$

Here, $I_{c,\mathrm{Kim}}(0,0)$, β_Kim, and B_Kim are fitting parameters that were calculated numerically. The parameter values are presented in table 3.2. A critical temperature T_c of 93 K was used, as it is defined by Iwasa for $YBa_2Cu_3O_{7\text{-x}}$ [214]. The fitting functions are presented as solid curves in figure 3.3.

Table 3.2: Parameters of the Kim model to fit the measured data of the critical current dependence on temperature and magnetic flux density.

Symbol	Value (T_c = 93 K)
$I_{c,\mathrm{Kim}}(0,0)$	6340.9 A $\mathrm{cm}^{-1}_{\mathrm{width}}$
B_Kim	2.18249 T
β_Kim	1.77127

3.5 Market Overview of REBCO Tapes

After the discovery of HTSs in 1986 by Bednorz and Müller [217], the production scale-up of REBCO tapes started around the mid-2000s [218, 219]. Since then, the commercial market has been in constant development. Table 3.3 shows seven consolidated manufacturers of REBCO tapes worldwide, their year of establishment, and their annual production capacity in certain years. In 2023, the worldwide 12 mm wide equivalent REBCO tape production was between 3 000–5 000 km per year and was expected to grow to 6 000–10 000 km per year in 2025 [220].

The cost of REBCO tapes is typically expressed in euros per kilo-ampere-meter (EUR kA^{-1} m^{-1}). This unit corresponds to the cost of one meter of tape that can conduct 1 kA of electrical energy, usually measured at 77 K in self-field (i.e., without an applied external magnetic field), but it can also be evaluated at any other temperature and magnetic-field condition. Today, costs for a 12 mm wide REBCO tape—with a critical current of 600–700 A at 77 K in self-field—are between 40–60 EUR m^{-1} [232]. This is approximately equivalent to 70–120 EUR kA^{-1} m^{-1}.

At 20 K, the approximate temperature of liquid hydrogen, the critical current density of a REBCO tape under self-field conditions is approximately 5 520 A mm^{-2} [233], 6 410 A mm^{-2} [234] or 9 190 A mm^{-2} [235], depending on the product and manufacturer. As a consequence, the costs of REBCO tapes used in liquid hydrogen are as low as 4–11 EUR kA^{-1} m^{-1}. For comparison, using a copper density of 8 940 kg m^{-3} [236] and price of 9.46 EUR kg^{-1} as of November 2025 [237], copper busbars for power distribution systems have a current density of 1–2 A mm^{-2} and costs of 85–42 EUR kA^{-1} m^{-1}, respectively.

One of the most widespread applications of superconductivity is in medical radiology, where it enables magnetic resonance imaging (MRI). A small 1.5 T MRI magnet for human extremities (e.g., the knee) with a magnet inner diameter of 242 mm needs approximately 5 km of REBCO tape [238]. Typical whole-body MRI magnets have an inner diameter of 600 to 700 mm [239]. Currently, the REBCO production capacity expansion is mostly driven by the development of commercial fusion devices, followed by power cables [220]. A single fusion power plant requires, for example, approximately 10 000 km of 4 mm wide tapes [240]. This development suggests that the REBCO production costs will continue to decline.

Table 3.3: Overview of manufacturers of REBCO tapes and their annual production capacity.

Name	Country	Founding year	Production year	Annual production capacity (tape width)
Faraday Factory	Japan	2011 [221]	2024	1 000 km (12 mm) [222] 3 000 km (4 mm) [222]
			2028: announced 2023	25 000 km (12 mm) [220]
Fujikura	Japan	1986 [223]	2024	1 200 km (? mm) [224]
Shanghai Creative Superconductors (SCSC)	China	2011 [225]	2023	400 km (4 mm) [220]
			2025: announced 2023	2 800 km (4 mm) [220]
Shanghai Superconductor Technology (SST)	China	2011 [226]	2023	2 000 km (12 mm) [227]
			2025	4 000 km (12 mm) [227]
SuNAM	South Korea	2004 [228]	2023	400 km (4 mm) [220]
			2025: announced 2023	1 000 km (4 mm) [220]
SuperPower/ Furukawa	USA/ Japan	2000 [218]	2022	200 km (4 mm) [229]
			2023	600 km (4 mm) [229]
			2025: announced 2023	1 200 km (4 mm) [220]
THEVA	Germany	1996 [230]	2023	100 km (12 mm) [231]
			2025-2027: announced 2023	2 500 km (12 mm) [231]

4 Conceptual Design of the Hybrid Pipeline

This chapter proposes the technical design of a hybrid pipeline for the case study Brunsbüttel–Hamburg, given the required specifications of 75 km length, 4.0 GW_e of rated electric power, and at least 0.62–0.87 GW_t of chemical power in the form of liquid hydrogen (see table 2.5). The conceptual design comprises the electrical design of the cable and the thermal-hydraulic design for liquid hydrogen transmission without intermediate cooling stations. The behavior of the cable is simulated in the case of a short circuit to assure safe operation even in the case of a fault.

Similar results have already been published in [241]. However, the results shown in this chapter improve those presented in [241] mainly because of the use of the phenomenological Kim model to fit the temperature and magnetic flux density dependence of the critical current (see section 3.4). In [241], a numerical fitting function was used instead.

4.1 Schematic Structure of the Hybrid Pipeline

Figure 4.1 shows the profile view of the hybrid pipeline. The following sections will explain the reasons for this schematic structure. The electrical energy is transmitted by a pair of DC coaxial monopoles. Copper layers with outer radii $r_{1,\mathrm{cu}}$ and $r_{2,\mathrm{cu}}$ in the inner and outer phases, respectively, stabilize the two cables mechanically and electrically. Commercially available REBCO tapes make electrical contact with the copper layers. In the inner phase, $r_{1,\mathrm{hts}}$ is the outer radius of the REBCO tape, while $r_{2,\mathrm{hts}}$ is the equivalent radius in the outer phase. The REBCO tapes transmit the electrical current within the rated operation range. An insulator with an outer radius $r_{1,\mathrm{ins}}$ presents an electrical barrier between the inner and outer phases. The selection of the insulating material will be discussed in section 4.2.2. The outer phase made of copper and REBCO tapes is grounded.

A double-walled, rigid, and smooth pipe transmits the liquid hydrogen with both cables inside. The inner pipe has an inner radius $r_{\mathrm{LH2,i}}$ and outer radius $r_{\mathrm{LH2,o}}$. It is made of Invar

(36% Ni-Fe) to reduce thermal contraction owing to large temperature variations. For comparison, the coefficient of thermal expansion of steel is approximately ten times greater than that of Invar [242]. Invar has been already used in pressure equipment, for example, for LNG pipes [243] and cryogenic tanks [244]. Research has indicated that Invar withstands hydrogen embrittlement, for example, in [245] and [246]. Between the inner and outer pipes, thermal insulation is produced combining multi-layer insulation (MLI) against thermal radiation—with outer radius $r_{\mathrm{MLI,o}}$—and vacuum against thermal conduction. The outer pipe is of carbon steel. It has inner and outer radii $r_{\mathrm{pipe,i}}$ and $r_{\mathrm{pipe,o}}$, respectively.

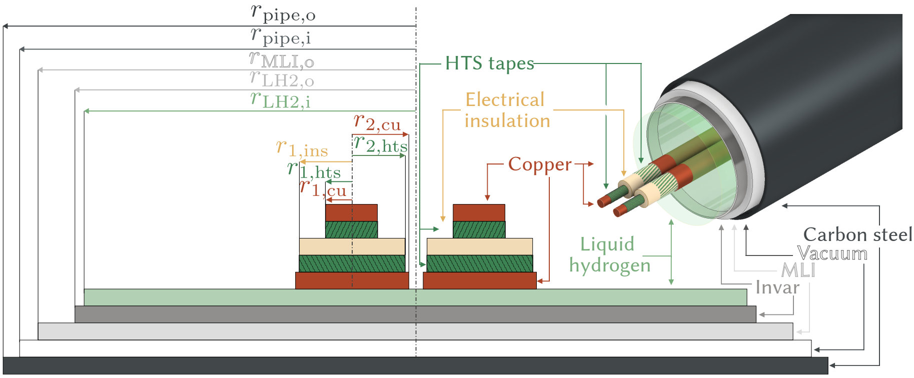

Figure 4.1: Profile view of the hybrid pipeline.

4.2 Electrical Cable Design

The electrical design includes choosing the topology, determining the cable layout while verifying the proper amount of superconductor, and simulating the cable in the case of a short circuit.

4.2.1 Selection of the Electrical Topology

Three topologies were compared for the transmission of electrical energy, as shown in figure 4.2. Initially, the topology of currently planned conventional underground extra-high-voltage DC cables was considered (see figure 2.9). The topology for a total of 4 $\mathrm{GW_e}$ includes two rigid bipoles without a metallic return. A single rigid bipole is composed of two cables. Figure 4.2 (a) shows that this topology leads to four cables, each of them transmitting 1 $\mathrm{GW_e}$.

In the inner phase, two cables operate at +50 kV, and the other two at −50 kV. Each cable conducts 20 kA and has an outer grounded shield. This topology significantly increases the space demand of the cables inside the pipeline. Additionally, the corresponding superconducting cable configuration induces a strong magnetic field outside each cable ($\approx$ 4 mT, applying the Biot–Savart law to a thin straight wire). Therefore, the critical current is reduced, mechanical effects are caused by Lorentz forces, and the configuration extends a fraction of the magnetic field to the immediate cable surroundings (at longer distances, the magnetic field is canceled owing to opposite current directions).

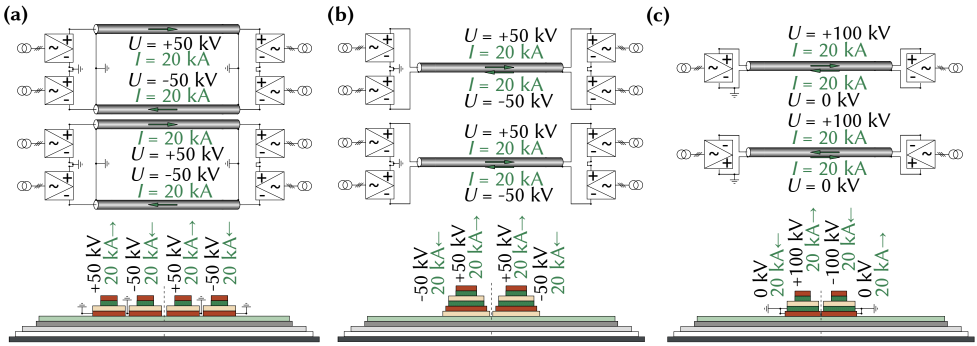

Figure 4.2: Topologies under examination: (a) Two rigid bipoles without metallic return; (b) Two coaxial rigid bipoles without metallic return; (c) Two coaxial monopoles with metallic return. Topology (c) has been proposed.

An alternative topology to suppress the external magnetic field of the cables is shown in figure 4.2 (b). The topology consists of a pair of coaxial rigid bipoles in the absence of a metallic return. This is equivalent to two coaxial cables, each of them transmitting 2 GW_e at $\pm$50 kV, 20 kA. Each outer phase is without a ground connection. The corresponding cable configuration enlarges the cable diameter because the outer phase must have an outer electric insulator to avoid a breakdown with the pipe. Therefore, the cable loses physical flexibility, which complicates its transportation. Without a grounded outer phase, voltage can be induced owing to current variations. Besides, based on the available information, this cable configuration has not been proven outside of research facilities.

The topology in figure 4.2 (c) is composed of two parallel coaxial monopoles with a metallic return. Each coaxial monopole transmits 2 GW_e. In the inner phase, one monopole operates at +100 kV and the other at −100 kV. The outer phase of both monopoles is grounded and thereby at 0 kV. Every phase conducts 20 kA. The grounded outer phase reduces the induced voltage during current variations and allows the omission of an outer electric insulator. Consequently, the shorter cable diameter leads to a more flexible cable that can be transported using drums. In the cable surroundings, the induced magnetic field is nearly zero, caused by opposite current flows in the inner and outer phases (see section 4.2.3). For these reasons, the topology and cable configuration shown in figure 4.2 (c) were selected.

Each of the mentioned topologies supports redundancy for 2 GW_e, since one cable can still be in service, although the other cable does not function. Considering a monopole outage, such topologies enhance the ease of maintenance and reliability of supply. A comparable topology has been proposed in [205]. Still, this work does not examine the redundancy for the case of a failure of the complete electrical system, like when there is no coolant flowing. For such a scenario, the scholars in [202] have suggested a parallel copper cable with equivalent transmission capacity. Other researchers have proposed the use of various small hybrid pipelines in parallel [201].

For the transmission of 4 GW_e, a rated voltage U_0 of $\pm$100 kV and a rated current I_0 of 20 kA were selected. Other rated parameters, for example, $\pm$50 kV and 40 kA, could also have been reasonable. A line operating at $\pm$100 kV is classified into the high-voltage power grid, while a line operating at $\pm$50 kV is categorized into the medium-voltage power network [247]. The medium voltage enables the use of smaller converter stations [248]. As a result, the likely cost of the complete electric system can be reduced. Nevertheless, doubling the rated voltage from $\pm$50 kV to $\pm$100 kV halves the rated current from 40 to 20 kA. Consequently, less superconductor length is needed. Thus, the potential expenditures for the cable decrease. The quantitative influence of high and medium voltage on the required length of superconductor will be discussed later in section 4.2.2.

To establish a safety factor of 1.25 to the rated current I_0 of 20 kA, it is assumed that the minimum expected self-field critical current $I_{c,\mathrm{min}}$ should be 25 kA. Section 4.2.3 will present the method to determine the self-field critical current in the inner phase $I_{c,1}$ and the outer phase $I_{c,2}$. While the liquid hydrogen cools the cable to approximately 20 K under nominal operation, the design temperature T_{des} is conservatively assumed to be 30 K to mitigate electrical design risks.

4.2.2 Determination of the Cable Layout

The radius of the inner copper stabilizer $r_{1,\mathrm{cu}}$ has a decisive influence on the cable layout. The inner copper stabilizer is the core of the cable and its radius determines the largest number of REBCO tapes that can be located in the inner phase. The radius, or rather the size, of the copper core also defines the electrical performance of the cable if a short circuit occurs. The proposed cable design is based on a copper stabilizer with inner radius $r_{1,\mathrm{cu}}$ of 13.9 mm. This is a common size for copper cores, since they typically have a radius between 5 mm and

20 mm [249]. The simulations that result in this value will be introduced later in sections 4.2.3 and 4.2.4. First, the geometrical effects of the radius of the inner copper core will be discussed.

Equation 4.1 shows how the number of tapes per layer in the inner phase has been calculated. This equation relates the formula of the surface of a circle to the trigonometric equation considering the lay angle of the tape:

$$N_{1,\text{tapes}} = \left\lfloor \frac{2 \cdot \pi \cdot r_{1,\text{cu}}}{a_{\text{tape}} / \cos(\theta_1)} \right\rfloor , \tag{4.1}$$

where the radius of the copper core $r_{1,\text{cu}}$ is assumed to be 13.9 mm, the inner tape angle θ_1 is a common lay angle of 15° [249], and the tape width a_{tape} is 4.0 mm, resulting in a number of tapes in the inner phase $N_{1,\text{tapes}}$ of 21 tapes. Considering the tape thickness s_{tape} of approximately 100 µm (see figure 3.1), and a single layer of REBCO tapes on top of the inner copper stabilizer, the outer radius of the superconducting tape in the inner phase $r_{1,\text{hts}}$ is 14.0 mm.

In coaxial cables, the electric field between two phases is given by the equation [250]:

$$E(r) = \frac{U}{r \cdot \ln\left(\frac{r_\text{o}}{r_\text{i}}\right)} , \tag{4.2}$$

where E is the electric field at radius r of a cylindrical capacitor with outer radius r_o and inner radius r_i at a voltage U. For safety reasons, it is assumed that the highest electric field E_{lim} during operation is 10 kV mm^{-1}. This assumption will be examined later in this section. The maximum electric field occurs where the radius r is equivalent to the inner radius r_i. Therefore, the outer radius of the electrical insulator $r_{1,\text{ins}}$ can be determined using the equation:

$$r_{1,\text{ins}} = r_{1,\text{hts}} \cdot \exp\left(\frac{U_0}{E_{\text{lim}} \cdot r_{1,\text{hts}}}\right) , \tag{4.3}$$

where equation 4.2 has been solved for the outer radius r_o, here equivalent to $r_{1,\text{ins}}$, and the inner radius r_i has been replaced by the outer tape radius $r_{1,\text{hts}}$. The voltage U in equation 4.2 is equivalent to the rated voltage U_0 in equation 4.3 and the electric field E is equal to the expected highest electric field E_{lim}. This results in an electrical insulator outer radius $r_{1,\text{ins}}$ of 28.6 mm.

The assumption of a maximum electric field E_{lim} equal to 10 kV mm^{-1} proceeds from past high-voltage superconducting (420 kV) and conventional (380 kV) cable projects that are designed on the basis of maximum electric fields in the same order of magnitude [251]. This assumption can be verified as follows. At present, formal standards do not define the testing voltage of paper-lapped high-voltage DC cables at cryogenic temperature levels. For that reason, the authors in [252] proposed to use the standard for extruded insulation materials, as defined in IEC 62895:2017 [253]. According to this standard, the testing voltage U_{T} must be 1.85 times the nominal voltage U_0. That means that the testing voltage U_{T} in this work would be equal to 185 kV. Moreover, the authors in [249] assumed that the breakdown voltage E_{b} of paper insulation in a DC cable operating in liquid hydrogen would be equal to 20 kV mm^{-1}. These considerations result in a moderately smaller insulator radius than $r_{1,\mathrm{ins}}$ in equation 4.3, namely,

$$r_{1,\mathrm{ins}} > r_{1,\mathrm{hts}} \cdot \exp\left(\frac{U_{\mathrm{T}}}{E_{\mathrm{b}} \cdot r_{1,\mathrm{hts}}}\right). \tag{4.4}$$

It is considered that the electric insulator is Kapton® or polypropylene laminated paper (PPLP), which are insulating materials that are traditionally used in superconducting cables immersed in liquid nitrogen. It is known that the dielectric strength of liquid hydrogen at 20 K slightly exceeds the dielectric strength of liquid nitrogen at 77 K [254]. However, the dielectric strengths of Kapton® and PPLP in liquid hydrogen have not been experimentally tested. Until now, only a kind of crepe insulation paper has been successfully tested in liquid hydrogen up to 50 kV, but the authors did not mention what kind of crepe insulation paper they examined [26].

The highest number of tapes that can be wound per layer in the outer phase can be determined in a similar way as in equation 4.1. In addition to the lay angle, the outer phase allows variations in the number of tapes used. Three different winding types for the outer phase are shown in figure 4.3. In type I, the number of tapes in the inner phase $N_{1,\mathrm{tapes}}$ and outer phase $N_{2,\mathrm{tapes}}$ are equal, but the lay angle of the outer tapes θ_2 is higher than that of the inner tapes θ_1 to achieve a fully wound outer phase. In type II, the lay angle of the tapes in the outer phase θ_2 is the same as in the inner phase θ_1, but the number of tapes in the outer phase $N_{2,\mathrm{tapes}}$ is higher than that in the inner phase $N_{1,\mathrm{tapes}}$, so that it can be fully wound. In type III, the number of tapes and the lay angles are equal in both phases, but this means that the outer phase is not completely filled.

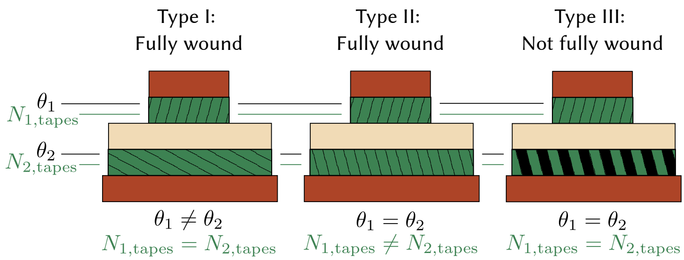

Figure 4.3: Three different winding types for the REBCO tapes in the outer phase. The lay angles in the inner phase θ_1 and in the outer phase θ_2 can be equal or not, depending on the winding type. Similarly, the number of tapes in the inner phase $N_{1,\text{tapes}}$ and in the outer phase $N_{2,\text{tapes}}$ can be the same in both phases or not. Type III has been selected.

The winding type II has been commonly used in multiple DC and AC superconducting cable designs, for example in [255–259]. Nevertheless, the principal benefit of type III is that notably lower superconductor length is required, in comparison with winding types I and II. A comparison of the superconductor length and a compilation of the different radii in the cable layout is presented in table 4.1.

Designs A, B, and C share the same rated voltage U_0 of ± 100 kV and the rated current I_0 of 20 kA, as well as an identical configuration in the inner phase. However, they present different winding types in the outer phase. Design A has a winding type I, whereas design B is based on type II, and design C on type III. It can be seen that design C demands approximately 35% lower superconductor length than designs A and B.

Design D presents the alternative rated voltage U_0 of ± 50 kV and rated current I_0 of 40 kA, as discussed previously in section 4.2.1. Although both designs C and D exhibit the same winding type III, design C needs approximately 52% less superconductor length. The larger rated current I_0 in design D causes a larger number of tapes to be required in the inner phase $N_{1,\text{tapes}}$ and outer phase $N_{2,\text{tapes}}$ to conduct higher minimum critical currents in the inner phase $I_{c,1}$ and outer phase $I_{c,2}$, respectively. More details regarding the minimum critical currents will be discussed in section 4.2.3.

It should be noted that the required surface per cable A_{cable} is smaller in design D than in the other designs, owing to the smaller electric-insulation thickness caused by a lower rated voltage U_0. However, only larger radii of the copper stabilizer in the inner phase $r_{1,\text{cu}}$ and outer phase $r_{2,\text{cu}}$ can support the cable in the case of a short circuit at a higher rated current I_0.

Table 4.1 shows the gap between tapes in the inner phase $g_{1,\text{tapes}}$ and the outer phase $g_{2,\text{tapes}}$. In the following section 4.2.3, it will be shown that the magnetic flux density outside the cable in design C is sufficiently low to be negligible, although the gap $g_{2,\text{tapes}}$ in this design is wider than in the others. A detailed quantitative analysis of this result has been partly presented in [260]. If AC losses can be negligible despite the larger gap $g_{2,\text{tapes}}$, design C is proposed for the conceptual design of the hybrid pipeline in this study, owing to the significantly lower amount of superconductor required. It is important to note that no cable project is known to have used winding type III.

Table 4.1: Comparison of different cable designs. Each design consists of two identical monopoles. The presented values refer to a single monopole that delivers 2 GW$_e$ of electrical energy. Design C has been selected.

Parameter	Symbol	Design A	Design B	Design C	Design D
Outer phase layout	–	Type I	Type II	Type III	Type III
Rated power	P_0		4.0 GW$_e$ ($2 \cdot 2$ GW$_e$)		
Rated voltage	U_0		± 100.0 kV		± 50.0 kV
Rated current	I_0		20.0 kA		40.0 kA
HTS tape width	a_{tape}		4.0 mm		4.0 mm
HTS Tape thickness	s_{tape}		0.1 mm		0.1 mm
Outer radius of inner copper stabilizer	$r_{1,\text{cu}}$		13.9 mm		19.5 mm
Outer radius of inner HTS tape	$r_{1,\text{hts}}$		14.0 mm		19.7 mm
Outer radius of electrical insulator	$r_{1,\text{ins}}$		28.6 mm		25.4 mm
Outer radius of outer HTS tape	$r_{2,\text{hts}}$		28.7 mm		25.6 mm
Outer radius of outer copper stabilizer	$r_{2,\text{cu}}$		30.7 mm		29.7 mm
Cable cross-section of one monopole	A_{cable}		2 951.6 mm^2		2 774.3 mm^2
Number of tapes in inner phase	$N_{1,\text{tapes}}$		21		44
Gap between tapes inner phase	$g_{1,\text{tapes}}$		0.018 mm		1.428 mm
Number of layers in inner phase	$N_{1,\text{layers}}$		1		2
Lay angle in inner phase	θ_1		15.0°		15.0°
Number of tapes in outer phase	$N_{2,\text{tapes}}$		21		44
Gap between tapes outer phase	$g_{2,\text{tapes}}$	0.00 mm	0.04 mm	4.42 mm	3.11 mm

Continued on next page

Table 4.1: Comparison of different cable designs. Each design consists of two identical monopoles. The presented values refer to a single monopole that delivers 2 GW_e of electrical energy. Design C has been selected. (Continued)

Parameter	Symbol	Design A	Design B	Design C	Design D
Number of layers in outer phase	$N_{2,\text{layers}}$	1	1	1	2
Lay angle in outer phase	θ_2	62.1°	15.0°	15.0°	15.0°
Superconductor length per monopole	–	5 000 km	4 969 km	3 261 km	6 833 km
Total superconductor length	–	9 999 km	9 939 km	6 522 km	13 666 km

4.2.3 Calculation of the Critical Current

In the previous section, the number of superconducting tapes in the inner phase $N_{1,\text{tapes}}$ has been given by the maximum number of tapes that can be wound on top of the copper core (see equation 4.1). However, it must be verified whether this amount of superconductor can carry the minimum critical current $I_{c,\text{min}}$ of 25.0 kA. The same procedure must be carried out for the outer phase. Therefore, the self-field critical currents in the inner phase $I_{c,1}$ and the outer phase $I_{c,2}$ have been calculated under rated operating conditions at a conservative design temperature T_{des} of 30 K. The fitting functions of the REBCO tape measurements—presented in sections 3.3 and 3.4—have been used to determine the critical current dependencies on field angle, magnetic flux density, and temperature.

Figure 4.4 (a) shows the 2D cross-section of the superconducting cable that has been considered for the calculation. Every REBCO tape has been partitioned into nodes perpendicular to the cross-section. Each current node is defined by a position $\vec{r}$ and a normal vector $\vec{n}_c$ that describes the tape direction in the layer. For every REBCO tape, 10 nodes per millimeter width have been assumed (see figure 4.4 (b)). Consequently, the total number of nodes N_{nodes} is given by:

$$N_{\text{nodes}} = 10 \cdot a_{\text{tape}} \cdot \left(N_{1,\text{layers}} \cdot N_{1,\text{tapes}} + N_{2,\text{layers}} \cdot N_{2,\text{tapes}} \right) , \tag{4.5}$$

where a_{tape} is the superconducting tape width, $N_{1,\text{tapes}}$ is the number of tapes in the inner phase, $N_{1,\text{layers}}$ is the number of layers in the inner phase, $N_{2,\text{tapes}}$ is the number of tapes in the outer phase, and $N_{2,\text{layers}}$ is the number of layers in the outer phase. Considering the values in table 4.1, design A has 1 680 nodes.

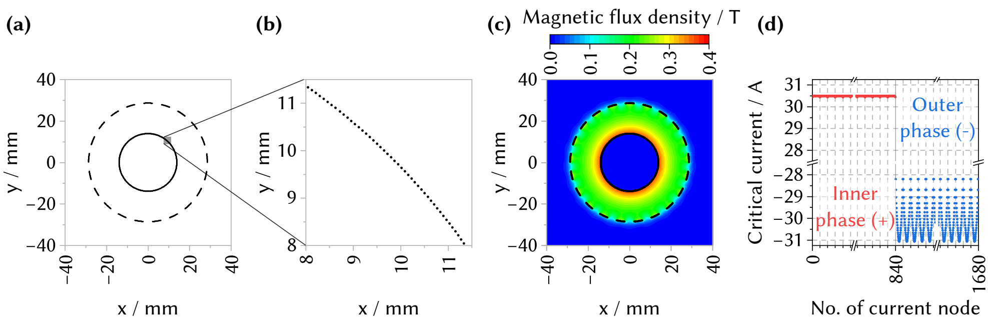

Figure 4.4: Calculation of the critical current of the high-temperature superconducting cable for the selected design A: (a) Partition of the cable cross-section into current nodes; (b) Magnification of the gray section in (a); (c) Flux density distribution in and around the cable; (d) Critical current of each of the 1 680 current nodes considered.

The magnetic field $\vec{B}_l$ at a location $\vec{r}_l$ of a sufficiently long, straight thread is given by the equation:

$$\vec{B}_l\left(I_i, \vec{r}_l, \vec{r}_i\right) = \frac{\mu_0 \cdot I_i}{2 \cdot \pi \cdot \left\|\vec{r}_l - \vec{r}_i\right\|^2} \cdot \begin{pmatrix} y_i - y_l \\ x_l - x_i \end{pmatrix}, \tag{4.6}$$

where μ_0 is the vacuum permeability, and I_i is the self-field critical current of a node i located at $\vec{r}_i$. Equation 4.6 can be employed to determine the magnetic field vector produced by each node on the other nodes. This results in a total magnetic field profile that is generated by all nodes. The total field profile is used in the elliptical model—described in equation 3.1—to obtain the self-field critical current of each node I_i. The direction of the electrical current is positive in the inner phase and negative in the outer phase.

Using $I_{c,\mathrm{ellip}}$ from table 3.1 as the initial input parameter for each node current I_i in equation 4.6, equations 4.6 and 3.1 are iterated until self-consistent magnetic flux densities and critical current distributions are reached. The iteration converges after approximately seven loops, when the convergence criterion of a relative current change of 10^{-7} is satisfied. Afterwards, the magnetic flux density distribution is calculated at arbitrary positions, according to equation 4.6. Figure 4.4 (c) illustrates the resultant magnetic field distribution. Outside the cable, the magnetic field cancels and can be neglected. The largest magnetic field magnitude occurs near the inner phase and amounts to approximately 0.34 T.

Figure 4.4 (d) shows the critical currents of multiple representative nodes inside the tapes. At the edges of each tape, the critical current is lower compared with the middle of the tape, owing to larger vertical magnetic field components. This effect is more pronounced in the negative outer phase because of the wider gap between tapes. The absolute magnitudes in figure 4.4 (d) correspond to the expected critical current values obtained from the measurements at 30 K and magnetic flux densities lower than 0.2 T in figure 3.2. Approximately 30 A per node is equivalent to about 3 000 A cm^{-1}, since there are 10 nodes per mm width.

The sum of the self-field critical currents of all nodes is equivalent to the self-field critical currents in the inner phase $I_{c,1}$ and outer phase $I_{c,2}$. The corresponding values are presented in table 4.2 for each of the designs discussed previously in section 4.2.2. These results confirm that the number of superconducting tapes is adequate, because the currents $I_{c,1}$ and $I_{c,2}$ are higher than the required minimum self-field critical current $I_{c,\min}$.

Table 4.2: Calculated critical currents in the inner phase $I_{c,1}$ and the outer phase $I_{c,2}$ for a signle monopole across different cable designs. Design C has been selected.

Parameter	Symbol	Design A	Design B	Design C	Design D
Outer phase layout	–	Type I	Type II	Type III	Type III
Rated power	P_0		4.0 GW$_e$		4.0 GW$_e$
Rated voltage	U_0		± 100.0 kV		± 50.0 kV
Rated current	I_0		20.0 kA		40.0 kA
Required minimum self-field critical current	$I_{c,\min}$		25.0 kA		50.0 kA
Calculated critical current inner phase	$I_{c,1}$		25.6 kA		50.8 kA
Calculated critical current outer phase	$I_{c,2}$	−26.1 kA	−26.1 kA	−25.1 kA	−50.3 kA

4.2.4 Simulation of the Cable in the Case of a Short Circuit

The cable must operate safely, even when a short circuit occurs. An adiabatic, lumped-parameter, Python-coded cable model has been developed to reproduce the current, voltage, resistance, and temperature of every material in the cable during a short circuit. This model provides the necessary information to determine whether safety is guaranteed.

The simulation is based on the electrical diagram shown in figure 4.5. The positive and negative phases represent one of the two monopoles in the hybrid pipeline (see figure 4.2 (c)). The other monopole is equivalent to the one in figure 4.5, but its current directions are opposite. Under rated operating conditions, a current I_r passes through a load R_r that is equal to $U_0 \cdot I_0^{-1}$. When a short circuit occurs, a current I_sc passes through the resistance R_sc, which is significantly smaller than the load R_r. The model considers a short circuit that takes place between the phases at the distant end of one monopole.

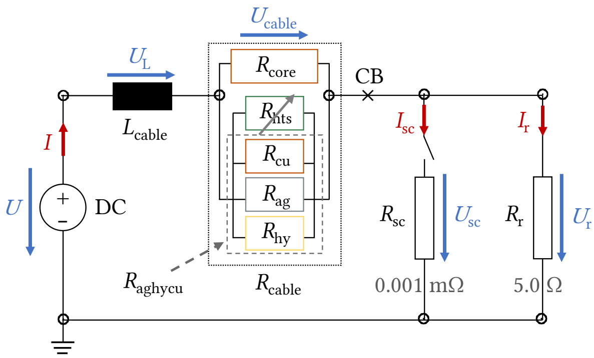

Figure 4.5: Electrical diagram of a monopole in the case of a short circuit, where U is the source voltage, I is the source current, U_L is the voltage across the cable inductance L_{cable}, U_{cable} is the voltage across the equivalent cable resistance R_{cable}, U_{sc} and I_{sc} are the voltage and current across the short-circuit resistance R_{sc}, respectively, and U_r and I_r are the voltage and current across the load R_r, respectively. The inner phase of the cable is made of a copper stabilizer with resistance R_{core}, which is connected in parallel to the resistances of the REBCO tape: the high-temperature superconductor resistance R_{hts}, and the resistance R_{aghycu}, which equals the parallel combination of copper R_{cu}, silver R_{ag}, and Hastelloy® R_{hy}. CB denotes the circuit breaker.

A circuit breaker requires a specific latency time to isolate the cable from the electric network after a short circuit. A converter manufacturer supplied a current profile I, where the circuit breaker responds within 50 ms. Before the monopole is disconnected, it is assumed that the cable must withstand a current seven times larger than the minimum critical current $I_{c,\text{min}}$, i.e., the maximum current I_{max} is 175 kA. This assumption is based on private communication with a manufacturer of superconducting cable terminations [261], after examining currents between five and ten times the minimum critical current, similar to the values analyzed in [262].

Copper Stabilizer

Since the selected number of REBCO tapes is intended to conduct only the current $I_{c,\text{min}}$, the copper stabilizers in the inner and outer phases provide electrical support at higher currents. The purpose of the simulation model is to calculate an appropriate cross-section of the copper stabilizer A_{cu} capable of carrying the fault current until the circuit breaker isolates the cable from the electrical grid. The cross-section A_{cu} will have the same value for the inner and outer copper stabilizers.

The electrical conductance of copper depends on its purity, which is usually defined by the residual resistivity ratio (RRR). By definition, this is the ratio of copper's resistivity at 293 K to that at 4.2 K. Commercially available pure copper has RRRs between 50 and 500 [263]. Following a conservative approach and to keep material costs low, the copper in the model is assumed to have an RRR of 50. It is important to note that copper typically resists hydrogen embrittlement, unless oxygen or copper oxide is present inside [264].

In the inner phase, a stranded copper wire is assumed to have a fill factor f_{fill}, so that the copper cross-section is given by:

$$A_{\text{cu}} = f_{\text{fill}} \cdot \pi \cdot r_{1,\text{cu}}^2, \tag{4.7}$$

where $r_{1,\text{cu}}$ is the radius of the copper stabilizer in the inner phase. Copper-stranded wires with high power density usually have a fill factor f_{fill} of 60% [265]. In the cable core, a stranded wire offers mechanical flexibility and an adequate volume to wind the necessary number of superconducting tapes. At the same time, only a fragment f_{fill} of copper is required.

In the outer phase, solid-drawn copper tapes are assumed to have the same thickness as the REBCO tapes (approximately 100 μm, see figure 3.1). Given that the cross-section A_{cu} is equal in both the inner and outer phases, the radius of the copper stabilizer $r_{2,\text{cu}}$ can be calculated using the equation:

$$\pi \cdot r_{2,\text{cu}}^2 = \pi \cdot r_{2,\text{hts}}^2 + A_{\text{cu}}, \tag{4.8}$$

where $r_{2,\text{hts}}$ is the outer radius of the superconducting tapes in the outer phase. Solid-drawn copper tapes provide mechanical flexibility, a more compact cable cross-section, and a smoother cable surface than stranded wires in contact with liquid hydrogen in the pipeline.

Current Density, Resistivity, and Temperature

The current through each material in the cable is subject to its electrical resistivity ϱ. Figure B.1, in appendix B, presents the resistivities of copper, silver, Hastelloy®, and YBCO as a function of temperature. Below the critical temperature T_c of 93 K, the differential resistivity of YBCO is given by re-expressing the E-J power law as [266]:

$$\varrho_{\text{hts}}\left(T_{\text{cable}}\right) = \frac{E}{J_{\text{hts}}\left(T_{\text{cable}}\right)} = \frac{E_c}{J_{\text{hts}}} \cdot \left[\frac{J_{\text{hts}}}{J_c\left(T_{\text{cable}}\right)}\right]^n \quad \text{with} \quad T_{\text{cable}} < 93\text{ K}, \tag{4.9}$$

where J_{hts} is the current density of the superconductor, J_c is the critical current density dependent on the cable temperature T_{cable}, n is the power-law exponent, and E_c is the electric-field criterion for J_c. It is assumed that the electric field criterion E_c is 1 μV cm^{-1}, and that the power-law exponent n is 30. In the flux-flow regime, the electric-field criterion E_c is assumed to be 1 mV cm^{-1}, and the power-law exponent n is assumed to be 4.

The differential resistivity of the HTS material ϱ_{hts} is subject to the electric current density, as seen in equation 4.9. For that reason, the current passing through the HTS material must be updated at each time step. Moreover, the critical current density J_c depends on the cable temperature T_{cable}. Therefore, the temperature of the HTS material must be calculated at each time step as well. Since an adiabatic model is assumed, where the heat exchange between the material layers is not considered, the rise in cable temperature can be determined as [266]:

$$C_{\mathrm{cable}} \frac{\mathrm{d}T_{\mathrm{cable}}}{\mathrm{d}t} = W_{\mathrm{J,cable}}, \tag{4.10}$$

where C_{cable} is the heat capacity of the cable and $W_{\mathrm{J,cable}}$ is the Joule-heating loss of the cable. The heat capacity C_{cable} is given by:

$$\begin{aligned} C_{\mathrm{cable}} &= C_{\mathrm{core}} + C_{\mathrm{hts}} + C_{\mathrm{aghycu}}, \\ C_{\mathrm{core}} &= c_{\mathrm{core}} \cdot V_{\mathrm{core}} \cdot \rho_{\mathrm{core}}, \\ C_{\mathrm{hts}} &= c_{\mathrm{hts}} \cdot V_{\mathrm{hts}} \cdot \rho_{\mathrm{hts}}, \\ C_{\mathrm{aghycu}} &= c_{\mathrm{ag}} \cdot V_{\mathrm{ag}} \cdot \rho_{\mathrm{ag}} + c_{\mathrm{hy}} \cdot V_{\mathrm{hy}} \cdot \rho_{\mathrm{hy}} + c_{\mathrm{cu}} \cdot V_{\mathrm{cu}} \cdot \rho_{\mathrm{cu}}, \end{aligned} \tag{4.11}$$

where C_{core}, C_{hts}, and C_{aghycu} are the heat capacities of the copper stabilizer, the HTS material, and the remaining materials in the tape (silver, Hastelloy®, and copper), respectively. The temperature dependent specific heat capacities c_{core}, c_{hts}, c_{ag}, c_{hy}, and c_{cu} (see figure B.2), the volumes along the 75 km long hybrid pipeline V_{core}, V_{hts}, V_{ag}, V_{hy}, and V_{cu}, and the mass densities ρ_{core}, ρ_{hts}, ρ_{ag}, ρ_{hy}, and ρ_{cu} (see table B.1) correspond to the copper stabilizer, the HTS material, and the remaining materials in the tape—silver, Hastelloy®, and copper—respectively. The mass density of the copper stabilizer ρ_{core} equals the mass density of copper ρ_{cu}.

The Joule heating loss $W_{\mathrm{J,cable}}$ in equation 4.10 is calculated as:

$$\begin{aligned} W_{\mathrm{J,cable}} &= W_{\mathrm{J,core}} + W_{\mathrm{J,hts}} + W_{\mathrm{J,aghycu}}, \\ W_{\mathrm{J,core}} &= R_{\mathrm{core}} \cdot I_{\mathrm{core}}^2, \\ W_{\mathrm{J,hts}} &= R_{\mathrm{hts}} \cdot I_{\mathrm{hts}}^2, \\ W_{\mathrm{J,aghycu}} &= R_{\mathrm{aghycu}} \cdot I_{\mathrm{aghycu}}^2. \end{aligned} \tag{4.12}$$

Similarly, the Joule-heating losses $W_{\mathrm{J,core}}$, $W_{\mathrm{J,hts}}$, and $W_{\mathrm{J,aghycu}}$, the currents I_{core}, I_{hts}, and I_{aghycu}, and the resistances R_{core}, R_{hts}, and R_{aghycu} correspond to the copper stabilizer, the HTS material, and the remaining materials in the tape, respectively.

To model the non-linear resistivity of the superconductor below its critical temperature, the two-branches model and the current-iterative process have been used. A detailed description of this approach can be found in [266]. By means of the Euler method, equation 4.10 has been solved numerically [267]. To determine the self-field critical current density J_c, the fitting functions of the REBCO tape measurements have been employed (see equations 3.1 and 3.2). Since it has been assumed that the short circuit takes place at the distant end of the hybrid pipeline, the simulation start temperature T_0 is equal to the outlet temperature of the liquid hydrogen, i.e., 26 K. Section 4.3.2 will present that one of the highest outlet temperatures, approximately 26 K, occurs for low mass flows.

Voltage

To analyze the voltage variations in the cable, Kirchhoff's voltage law has been applied to the electrical diagram shown in figure 4.5 [268]. The resultant source voltage U depends on time t and is given by:

$$\begin{aligned} U(t) &= L_{\mathrm{cable}} \cdot \frac{\mathrm{d}I(t)}{\mathrm{d}t} + I(t) \cdot R_{\mathrm{cable}} \cdot (T_{\mathrm{cable}}) + \frac{I(t)}{\frac{1}{R_{\mathrm{sc}}} + \frac{1}{R_{\mathrm{r}}}}, \\ &= U_{\mathrm{L}} + U_{\mathrm{cable}} + \frac{I(t)}{\frac{1}{R_{\mathrm{sc}}} + \frac{1}{R_{\mathrm{r}}}}, \end{aligned} \tag{4.13}$$

where R_{cable} is the cable resistance and T_{cable} is the cable temperature, both considered along the 75 km long cable. The load R_{r} is equal to $U_0 \cdot I_0^{-1}$ and is much larger than the short-circuit resistance R_{sc}, where the short circuit occurs, as discussed earlier this section. The current profile I includes a capacitance in the network. However, because this capacity has almost no effect on the heating of the REBCO tape (the focus of this section), it has been neglected.

In equation 4.13, the inductance of the coaxial cable L_{cable} is determined as:

$$L_{\text{cable}} = \frac{\mu_{\text{ins}} \cdot \ell}{2 \cdot \pi} \cdot \ln\left(\frac{r_{1,\text{ins}}}{r_{1,\text{hts}}}\right), \tag{4.14}$$

where ℓ is the cable length and μ_{ins} is the permeability of the electric insulator, which equals the vacuum permeability μ_0 multiplied by the relative permeability of a synthetic material μ_{rel}. It is assumed that the relative permeability of the synthetic material is 1.0.

Results

The simulation results for the behavior of the cable during a short circuit are presented in figure 4.6. Temporally, three stages can be defined as follows:

1. Rated operating conditions, until time t reaches 0.0 s;
2. Short circuit occurs at 0.0 s. Shortly after, the source current I rises and stays at a maximum I_{max} of 175 kA;
3. Current diminishes from 0.05 s onward, when the circuit breaker disconnects the cable from the grid. The source current I disappears entirely at approximately 0.6 s.

Under rated operating conditions, i.e., for $t < 0.0$ s, the source current I is carried entirely by the superconducting material, so that $I = I_{\text{hts}}$ (see figure 4.6 (a)). This occurs because the superconductor has zero resistance ($R_{\text{hts}} = 0$). The resistance of the inner copper stabilizer R_{core} is low but still higher than R_{hts} (about 0.07 Ohm). The resistance R_{aghycu} represents the equivalent parallel resistance of the other materials in the REBCO tape and is significantly higher than the resistances R_{hts} and R_{core}, as it can be seen in figure 4.6 (d).

Between 0.0 s and approximately 0.3 s, figure 4.6 (a) shows that the current is mainly carried by the inner copper core, because the current I_{core} is much larger than the current through the superconductor I_{hts}. The electrical energy flowing through copper raises the cable temperature T_{cable} (see figure 4.6 (b)). The higher temperature noticeably increases the resistance R_{aghycu} (figure 4.6 (d)), while the copper core resistance R_{core} grows only slightly. The HTS resistance R_{hts} increases because of the larger source current and the temperature rise. Although the temperature reaches a final level of about 52.8 K, the superconductor can still carry the residual current after $t \approx 0.3$ s.

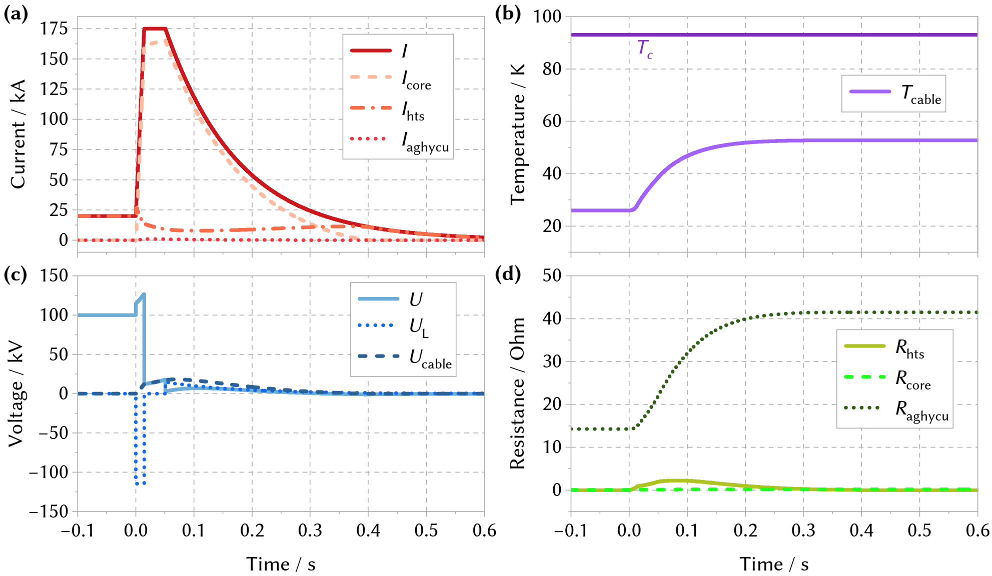

Figure 4.6: Simulation results of the cable during a short circuit: (a) Current variations in the source current I, in the copper core I_{core}, in the high-temperature superconductor I_{hts}, and in the remaining materials of the REBCO tape I_{aghycu} (silver, Hastelloy®, and copper); (b) Temperature development in the cable T_{cable} together with the critical temperature T_c of the superconductor; (c) Voltage changes in the source U, in the inductance U_{L}, and in the cable U_{cable}; (d) Resistance changes in the superconductor R_{hts}, in the copper core R_{core}, and in the remaining materials of the tape R_{aghycu}.

The voltage variations in the source U, in the cable U_{cable}, and in the inductance U_{L} are shown in figure 4.6 (c) and are defined by equation 4.13. When the short circuit suddenly raises the source current, the inductance opposes the change, inducing a negative voltage. Once the source current I settles at the constant maximum $I_{\text{max}} = 175\,\text{kA}$, the inductive voltage U_{L} becomes zero. When the source current I falls, the voltage U_{L} becomes positive because the inductance continues to oppose the decreasing current. Both U_{L} and the cable voltage U_{cable} decrease as the source current I approaches zero. A peak source voltage U_{max} of 126.9 kV occurs shortly before the source current begins to decline. This maximum voltage is lower than the test voltage U_{T} of 185 kV, which the cable must withstand (see section 4.2.2).

The results displayed in figure 4.6 prove that the cable operates safely, even during a short circuit, considering the following aspects:

- The cross-section of the copper core A_{core} has an appropriate size to transmit the current that can not be conducted by the superconductor during the fault.

- The radius of the copper core $r_{1,\text{cu}}$ is sufficiently large to wind the required number of REBCO tapes that should transmit the minimum critical current $I_{c,\text{min}}$ (see section 4.2.3).
- The radius of the copper core $r_{1,\text{cu}}$ leads to an adequate electric-insulation thickness, as defined by equation 4.3, because the maximum voltage U_{max} remains below the test voltage U_{T} of 185 kV, as discussed in section 4.2.2. This is partly owing to the selected insulator thickness, which directly affects the inductance magnitude L_{cable} and thereby the maximum voltage U_{max}, as shown in equations 4.13 and 4.14.

It is important to note that the assumed adiabatic model does not consider the heat exchange among the tape layers or between the warm cable and liquid hydrogen. Regarding the increase of cable temperature, the results presented in [269] demonstrate that the difference between an adiabatic and a non-adiabatic model is negligible for a short-circuit event. The reason is that the temperature rises in such a short period that heat transfer to the coolant is not fast enough to keep the cable cooled. Nevertheless, a non-adiabatic model can simulate how the liquid hydrogen dissipates the heat from the tapes after the fault. Hence, the adiabatic model represents a worst-case scenario for the thermal behavior of the superconducting cable; the final temperature in a non-adiabatic model would be even lower.

The assumed lumped-parameter model ignores spatial developments, but focuses on the time-dependent variations inside the cable. In this lumped-parameter model, the cable temperature rises uniformly along the entire cable length. A 1D or 2D model can simulate the risk of coolant boiling caused by a short circuit more accurately [269]. Nevertheless, the following simplified heat transfer calculation shows that the resulting final temperature of 52.8 K does not cause liquid hydrogen boiling.

A worst-case scenario is defined in which there is no liquid hydrogen flow (the coolant volume is constant), the heat generated by the short circuit is completely transferred to the coolant, and the total coolant volume is at the outlet temperature and pressure of approximately 25.9 K and 528 kPa, respectively (see sections 4.3.2 and 4.3.3). The magnitude of heat transfer equals the temperature difference between the heated cable and the coolant, i.e., 664.5 MJ, because the cable heat capacity C_{cable} is 24 760 kJ K^{-1} at 52.8 K, as described by equation 4.11. The density and specific heat capacity of liquid hydrogen at constant volume for the assumed outlet temperature and pressure are 63.3 kg_{H2} m^{-1} and 6 113 J kg^{-1}, respectively [50]. Considering a specific volume of 15.8 cm^3 g_{H2}^{-1}—which is defined by the inner pipeline dimensions that will be selected in section 4.3.5—the resulting liquid hydrogen temperature and pressure would be approximately 26.2 K and 691 kPa, respectively. At these conditions, hydrogen remains in the liquid phase and maintains a safe distance from the boiling curve (see section 4.3.3).

4.3 Thermal-hydraulic Design

The main requirement for the thermal-hydraulic design is to transmit liquid hydrogen through a 75 km long pipeline without coolant boiling and without intermediate cooling stations. It is assumed that large cryogenic storage tanks are situated at the starting and ending points of the hybrid pipeline. On the upstream (supply) side, the tank contains liquid hydrogen at thermodynamic equilibrium at 20.4 K and 150 kPa. A transfer pump delivers the liquid hydrogen at an inlet pressure p_{in} of 600 kPa to the hybrid pipeline. Based on an interview with an established manufacturer, such transfer pipes—capable of sustaining a differential pressure of 450 kPa—are commercially available and can produce mass flows as large as 50 $\mathrm{t_{H2}\,h^{-1}}$ (≈ 13.9 $\mathrm{kg_{H2}\,s^{-1}}$). The inlet temperature of the hybrid pipeline T_{in} (20.4 K) is assumed to be equal to the temperature in the cryogenic tank, because any heat generated by the transfer pipe is compensated by heat transfer to the stored coolant.

4.3.1 Design Equations

The principal goal of the thermal-hydraulic simulation is to determine the temperature increase and pressure drop of liquid hydrogen over the pipeline length. A Python-based model calculates the outlet temperature T_{out} and outlet pressure p_{out} of the transported liquid hydrogen at the end of the hybrid pipeline. The computational method is defined by a reduced version of the one-dimensional compressible flow equations for the balance of mass, momentum, and energy. Because the pipeline length is significantly longer than its diameter, the differences in temperature and pressure between the inlet and outlet are given by [18]:

$$\bar{c}_{p,\mathrm{LH2}} \cdot \frac{T_{\mathrm{out}} - T_{\mathrm{in}}}{\ell} = \left(1 - \bar{\alpha}_{\mathrm{LH2}} \cdot \bar{T}\right) \cdot F + \frac{q_{\mathrm{l}}}{\dot{m}_{\mathrm{LH2}}}, \tag{4.15}$$

$$\frac{1}{\bar{\rho}_{\mathrm{LH2}}} \cdot \frac{p_{\mathrm{in}} - p_{\mathrm{out}}}{\ell} = F + \frac{\bar{\alpha}_{\mathrm{LH2}} \cdot \nu_{\mathrm{LH2}}^2}{\bar{c}_{p,\mathrm{LH2}}} \cdot \frac{q_{\mathrm{l}}}{\dot{m}_{\mathrm{LH2}}}, \tag{4.16}$$

$$F = \frac{\zeta}{D_h} \cdot \frac{\nu_{\mathrm{LH2}}^2}{2}, \tag{4.17}$$

where T_{in}, T_{out}, p_{in}, and p_{out} are the inlet and outlet temperatures and pressures, respectively; ℓ is the pipeline length; $\bar{T}$ is the average of the inlet and outlet temperatures; q_{l} is the total heat load per unit length; F is correlated to the friction factor ζ; and D_h is the hydraulic diameter. The following symbols refer to the transported liquid hydrogen: $\bar{c}_{p,\mathrm{LH2}}$ is the average specific heat capacity at constant pressure, $\bar{\alpha}_{\mathrm{LH2}}$ is the average thermal expansivity factor, $\bar{\rho}_{\mathrm{LH2}}$ is the average mass density, $\dot{m}_{\mathrm{LH2}}$ is the mass flow rate, and ν_{LH2} is the flow speed.

Equations 4.15 and 4.16 are the reduced version of the equations presented in [18] because of the following assumptions:

- It has been assumed that the inclination between the beginning and end of the pipeline is negligible, because the elevation difference between Brunsbüttel and Hamburg is very small, especially near the Elbe river.
- Since the ratio of the liquid-hydrogen flow speed ν_{LH2} to the speed of sound in liquid hydrogen is considerably small [50], the Mach number is assumed to be zero [18]. The liquid-hydrogen flow speed ν_{LH2} is determined by the hydrogen demand in Hamburg (see table 2.5) and will be calculated later in this section.

The next paragraphs will define in more detail the variables appearing in equations 4.15, 4.16, and 4.17.

Hydraulic Diameter

The hydraulic diameter D_h is commonly used as a basic estimate to treat arbitrary cross-sections as equivalent circular pipes. Since the pipeline transmitting liquid hydrogen contains two superconducting cables, the hydraulic diameter D_h is calculated using [270]:

$$D_h = \frac{4 \cdot A_{\mathrm{pipe}}}{l_w} = \frac{2 \cdot \left(r_{\mathrm{LH2,i}}^2 - 2 \cdot r_{\mathrm{2,cu}}^2\right)}{r_{\mathrm{LH2,i}} + 2 \cdot r_{\mathrm{2,cu}}}, \tag{4.18}$$

$$A_{\mathrm{pipe}} = \pi \cdot r_{\mathrm{LH2,i}}^2 - 2 \cdot \pi \cdot r_{\mathrm{2,cu}}^2, \tag{4.19}$$

$$l_{\mathrm{w}} = 2 \cdot \pi \cdot r_{\mathrm{LH2,i}} + 2 \cdot \left(2 \cdot \pi \cdot r_{\mathrm{2,cu}}\right), \tag{4.20}$$

where $r_{\mathrm{LH2,i}}$ is the inner radius of the pipe that carries liquid hydrogen, $r_{\mathrm{2,cu}}$ is the outer radius of each superconducting cable located inside the pipe, A_{pipe} is the effective flow cross-section, and l_{w} is the wetted perimeter (the perimeter in contact with the fluid).

Heat Load

Although the hybrid pipeline is thermally insulated, an unavoidable total heat load per unit length q_l acts on the inner pipe, which is calculated as:

$$q_l = q_{l,0} + q_A \cdot \pi \cdot D_{LH2,i}, \tag{4.21}$$

where q_A is the heat flux and $q_{l,0}$ is a diameter-independent offset [249]. The related surface is the cylindrical jacket of the pipe transmitting liquid hydrogen, which has an inner diameter $D_{LH2,i}$. It is evident that the heat load q_l increases linearly with a larger pipe inner diameter. A heat flux q_A equal to 3.2 W m^{-2} and a diameter-independent offset $q_{l,0}$ equal to 0.25 W m^{-1} were taken as an average based on the following references. The validity of this theoretical assumption should be confirmed experimentally in future research, which lies beyond the scope of the present study:

1. The author in [271] examined vacuum jacketed pipes with different diameters transmitting liquid hydrogen. The data were linearly fitted, yielding a heat flux q_A of 3.3 W m^{-2} and a diameter-independent offset $q_{l,0}$ of 0.25 W m^{-1}.
2. The scholars in [249] assumed that combining vacuum insulation with 30 layers of MLI produces a heat flux q_A of 1.2 W m^{-2} for a temperature difference between 300 K and 21 K. The offset $q_{l,0}$ was omitted, as it is linked to electromagnetic losses that are less influential in a DC context.
3. Two further studies reported a heat load per unit length q_l of 2.0 W m^{-1}. In the first study, the authors examined inner diameters of 12.6 cm and 15.2 cm [202]. In the second work, diameters up to 19.8 cm were considered [201]. These assumptions lead to a heat flux q_A between 3.2 W m^{-2} and 5.0 W m^{-2}, if the offset $q_{l,0}$ is taken as zero and diameters equal to or larger than 12.6 cm are used.

At the starting and ending points of the transmission line, additional thermal losses occur due to the transition from ambient temperature to low temperatures of the current leads and cryostat terminations. Conventional, bath cooled current leads generate a minimum parasitic load per pole of about 42 W kA^{-1} when transitioning from 300 K to 77 K, because liquid nitrogen is used as an intermediate cooling level [272].

In contrast, superconducting current leads can produce a notably lower heat load on the cold side—approximately 3 W for a current of 20 kA with a temperature drop from 60 K to 4.5 K [273]. Assuming the use of superconducting current leads, and accounting for an unavoidable, load-independent loss of 20 W caused by the cryostat terminations (an empirical value according to [251]), the thermal losses at the extremities of the hybrid pipeline can be neglected. This is enabled by the relatively high mass flow requirement of at least 5.20 $\mathrm{kg_{H2}\ s^{-1}}$ (see table 2.5), which limits the temperature rise caused by the termination losses.

Friction Factor, Surface Roughness, and Reynolds Number

The friction factor ζ for the liquid-hydrogen flow is determined by means of the Newton-Raphson method applied to the Colebrook-White implicit equation, namely:

$$\frac{1}{\sqrt{\zeta}} = -\,2 \cdot \log\left(\frac{\epsilon}{3.7 \cdot D_h} + \frac{2.51}{\mathrm{Re} \cdot \sqrt{\zeta}}\right), \tag{4.22}$$

where ϵ is the surface roughness, D_h is the hydraulic diameter, and Re is the Reynolds number. It has been shown that the hydraulic diameter D_h can be used to determine the friction factor ζ for turbulent flow (Re larger than 4 000) in non-circular cross-sections, provided that there are no sharp edges inside the conduit [270]. A more precise calculation of the friction factor ζ for the considered cross-section is beyond the scope of this work.

Two components are mainly in contact with the transmitted liquid hydrogen: the outer drawn copper layer of the cable and the inner pipe made of Invar. Consequently, the surface roughness ϵ must be evaluated for these materials. References [274–276] indicated that commercial steel pipes exhibit a surface roughness ϵ of 0.046 mm, which is the nearest literature value to the roughness of Invar. The surface roughness of drawn copper is 0.0015 mm [274]. To adopt a conservative approach, the surface roughness ϵ is assumed to be 0.046 mm in equation 4.22.

The Reynolds number Re in equation 4.22 is calculated as:

$$\mathrm{Re} = \frac{\nu_{\mathrm{LH2}} \cdot D_h \cdot \bar{\rho}_{\mathrm{LH2}}}{\bar{\mu}_{\mathrm{LH2}}} \quad \text{with} \quad \nu_{\mathrm{LH2}} = \frac{\dot{m}_{\mathrm{LH2}}}{\bar{\rho}_{\mathrm{LH2}} \cdot A_{\mathrm{pipe}}}, \tag{4.23}$$

where $\bar{\mu}_{\mathrm{LH2}}$ denotes the average viscosity of the transmitted liquid hydrogen.

Initialization and Iteration Method

The mean values of the liquid hydrogen properties—mass density $\bar{\rho}_{\mathrm{LH2}}$, specific heat capacity $\bar{c}_{p,\mathrm{LH2}}$, thermal expansivity factor $\bar{\alpha}_{\mathrm{LH2}}$, and viscosity $\bar{\mu}_{\mathrm{LH2}}$—used in equations 4.16, 4.17, and 4.23 are obtained from the para-hydrogen data in REFPROP [50]. They are evaluated at the average inlet-outlet temperature and pressure, i.e., $\bar{\rho}_{\mathrm{LH2}}(\bar{T},\bar{p})$, $\bar{c}_{p,\mathrm{LH2}}(\bar{T},\bar{p})$, $\bar{\alpha}_{\mathrm{LH2}}(\bar{T},\bar{p})$, $\bar{\mu}_{\mathrm{LH2}}(\bar{T},\bar{p})$, where

$$\bar{T} = \frac{T_{\mathrm{in}} + T_{\mathrm{out}}}{2}, \ \bar{p} = \frac{p_{\mathrm{in}} + p_{\mathrm{out}}}{2}. \tag{4.24}$$

The initial values for the outlet temperature T_{out} and pressure p_{out} are obtained by specifying a maximum pressure drop, for example 300 kPa. At this assumed outlet pressure p_{out}, the saturation temperature T_{sat} of liquid hydrogen is determined. To provide a safety margin, the maximum outlet temperature T_{out} of the transmitted liquid hydrogen must be at least 1 K below the boiling curve, i.e.,

$$T_{\mathrm{out}} \leq T_{\mathrm{sat}}(p_{\mathrm{out}}) - 1\,\mathrm{K}. \tag{4.25}$$

Once the initial values for the outlet temperature T_{out} and outlet pressure p_{out} are set, the inlet temperature $T_{\mathrm{in}} = 20.4$ K and inlet pressure $p_{\mathrm{in}} = 600$ kPa (as described at the beginning of this section) are used to calculate the mean temperature $\bar{T}$ and mean pressure $\bar{p}$ via equation 4.24. These averaged parameters are then employed in equations 4.16, 4.17, and 4.23 for a given mass flow $\dot{m}_{\mathrm{LH2}}$ and pipe inner diameter $D_{\mathrm{LH2,i}}$, iterating until self-consistent values of T_{out} and p_{out} are obtained. The iteration typically converges after eight repetitions, when the relative change in the outlet temperature T_{out} and pressure p_{out} falls below 10^{-7}.

Table 4.3 shows an example of the model values when the pipe inner diameter $D_{\mathrm{LH2,i}}$ is set to 36 cm and the liquid hydrogen mass flow m_{LH2} is 6.0 $\mathrm{kg_{H2}\ s^{-1}}$.

Table 4.3: Example of thermal-hydraulic model values for a pipe inner diameter of 36 cm and a liquid hydrogen mass flow of 6.0 $\mathrm{kg_{H2}\ s^{-1}}$.

Parameters	Symbol	Value
Inlet temperature	T_{in}	20.4 K
Inlet pressure	p_{in}	600.0 kPa
Heat flux	q_{A}	3.2 W m^{-2}
Offset heat load per unit length	$q_{\mathrm{l,0}}$	0.25 W m^{-1}
Total heat load per unit length	q_{l}	3.857 W m^{-1}
Pipe inner diameter	$D_{\mathrm{LH2,i}}$	36.0 cm

Continued on next page

Table 4.3: Example of thermal-hydraulic model values for a pipe inner diameter of 36 cm and a liquid hydrogen mass flow of 6.0 kg_{H2} s^{-1}. (Continued)

Parameters	Symbol	Value
Hydraulic diameter	D_h	25.3 cm
Effective flow cross-section	A_{pipe}	958.8 cm^2
Wetted perimeter	l_{w}	151.6 cm
Liquid hydrogen mass flow	$\dot{m}_{\mathrm{LH2}}$	6.0 kg_{H2} s^{-1}
Liquid hydrogen flow speed	ν_{LH2}	0.913 m s^{-1}
Surface roughness	ϵ	0.046 mm
Reynolds number	Re	1 371 075
Friction factor	ζ	0.0142
Average temperature	$\bar{T}$	22.6 K
Average pressure	$\bar{p}$	539.7 kPa
Average mass density	$\bar{\rho}_{\mathrm{LH2}}$	68.5 kg_{H2} m^{-3}
Average specific heat capacity	$\bar{c}_{p,\mathrm{LH2}}$	11 044.0 J kg_{H2}^{-1} K^{-1}
Average thermal expansivity factor	$\bar{\alpha}_{\mathrm{LH2}}$	0.0196 K^{-1}
Average viscosity	$\bar{\mu}_{\mathrm{LH2}}$	11.55 µPa s
Outlet temperature	T_{out}	24.9 K
Outlet pressure	p_{out}	479.4 kPa

4.3.2 Temperature Increase

Figure 4.7 presents the results of the thermal-hydraulic model for the outlet temperature T_{out} as a function of the mass flow $\dot{m}_{\mathrm{LH2}}$. Five different pipe inner diameters $D_{\mathrm{LH2,i}}$ are compared: 33 cm, 34 cm, 36 cm, 38 cm, and 40 cm. The requirement established by equation 4.25 guarantees that the shown combinations of diameter $D_{\mathrm{LH2,i}}$ and mass flow $\dot{m}_{\mathrm{LH2}}$ keep hydrogen in the liquid phase even after 75 km of transmission and without intermediate cooling stations, wherever an outlet temperature T_{out} is displayed. The smallest integer pipe inner diameter that satisfies this condition is 33 cm. Larger diameters—greater than 40 cm—are also suitable; however, they would eliminate the lowest mass flow values $\dot{m}_{\mathrm{LH2}}$ because they are more appropriate for higher mass flow ranges. The reasons for this will be discussed as follows.

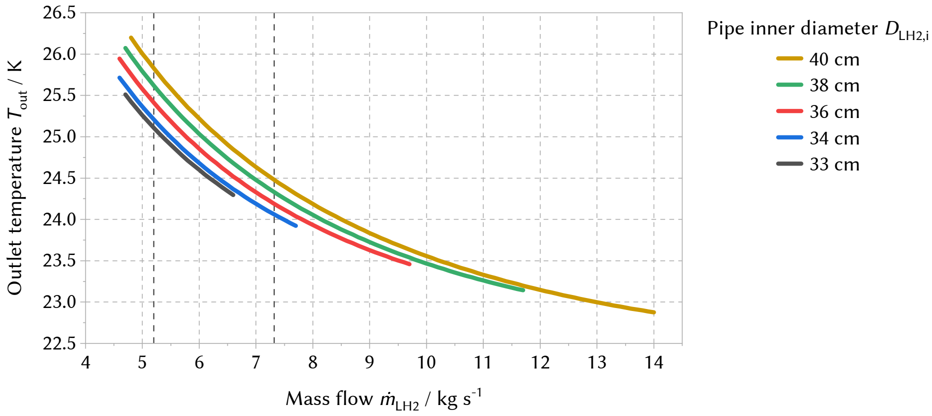

Figure 4.7: Outlet temperature T_{out} of the liquid hydrogen as a function of its mass flow $\dot{m}_{LH2}$ after transmission in the hybrid pipeline. Five different pipe inner diameters $D_{LH2,i}$ are compared: 33 cm, 34 cm, 36 cm, 38 cm, and 40 cm. The vertical dashed lines indicate the lower and upper limits of the hydrogen demand in the selected case study: 5.20 kg$_{H2}$ s^{-1} (0.62 GW$_t$) and 7.32 kg$_{H2}$ s^{-1} (0.87 GW$_t$). An inner diameter $D_{LH2,i}$ of 36 cm has been selected.

The variation of the pipe inner diameter $D_{LH2,i}$ shows that, for a given mass flow $\dot{m}_{LH2}$, the outlet temperature T_{out} is higher for larger diameters. This is a consequence of the higher heat load q_l (see equation 4.21). Consequently, smaller pipe diameters produce lower cryogenic losses, which in turn allow slower flow speeds ν_{LH2} and therefore lower mass flow rates $\dot{m}_{LH2}$ (cf. equation 4.23). However, thinner pipes increase frictional losses. Hence, larger diameters $D_{LH2,i}$ enable higher ranges of mass flow $\dot{m}_{LH2}$, in accordance with equations 4.15 and 4.16.

For all pipe inner diameters, increasing the mass flow $\dot{m}_{LH2}$ lead to a lower outlet temperature T_{out}. This follows from equation 4.15, because the liquid hydrogen is transported faster. Conversely, lower mass flows produce higher outlet temperatures due to reduced velocity values ν_{LH2}. The simulation shows that the outlet temperature ranges from 22.9 K to 26.2 K, depending on the selected mass flow $\dot{m}_{LH2}$ and pipe inner diameter $D_{LH2,i}$. The following section explains why a pipe inner diameter of 36 cm has been chosen for the design.

4.3.3 Pressure Drop

The results of the thermal-hydraulic model are presented in figure 4.8 in terms of the pressure difference $p_{in} - p_{out}$ (with p_{in} = 600 kPa), as a function of the mass flow $\dot{m}_{LH2}$. It can be seen that, at higher mass flow values $\dot{m}_{LH2}$, the pressure difference $p_{in} - p_{out}$ is larger, caused by higher frictional losses, as previously discussed. In contrast, low mass flow values and larger pipe inner diameters $D_{LH2,i}$ result in smaller pressure drop owing to reduced frictional losses, as described by equations 4.16 and 4.17. When the pipe inner diameter $D_{\mathrm{LH2,i}}$ is equal to 33 cm, the pressure difference varies from 125–241 kPa. If a pipe inner diameter $D_{\mathrm{LH2,i}}$ of 40 cm is considered, the pressure difference ranges from 43–341 kPa. Analogous to figure 4.7, all shown pressure-difference values ensure that hydrogen remains in the liquid state after the 75 km long transmission.

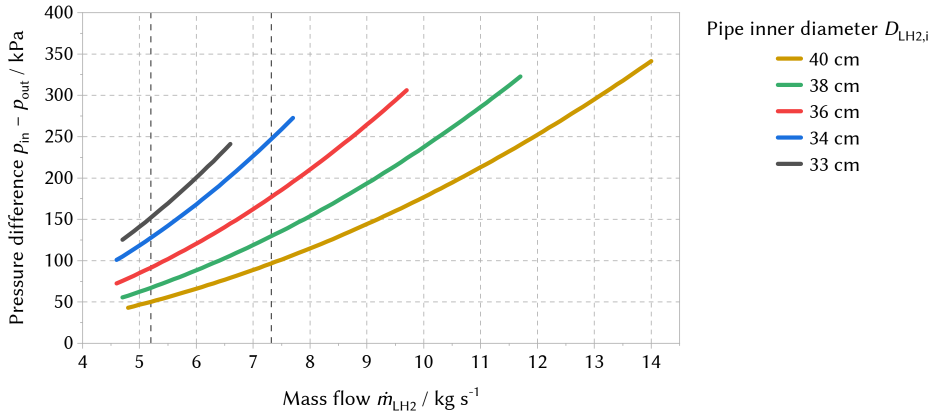

Figure 4.8: Outlet pressure p_{out} of the liquid hydrogen as a function of its mass flow $\dot{m}_{\mathrm{LH2}}$ after transmission in the hybrid pipeline. Five different pipe inner diameters $D_{\mathrm{LH2,i}}$ are compared: 33 cm, 34 cm, 36 cm, 38 cm, and 40 cm. The vertical dashed lines show the lower and upper limits of the hydrogen demand in the selected case study: 5.20 kg$_{\mathrm{H2}}$ s^{-1} (0.62 GW$_{\mathrm{t}}$) and 7.32 kg$_{\mathrm{H2}}$ s^{-1} (0.87 GW$_{\mathrm{t}}$). An inner diameter $D_{\mathrm{LH2,i}}$ of 36 cm has been selected.

The vertical dashed lines in figures 4.7 and 4.8 indicate the lower and upper limits of the hydrogen demand in the selected case study, e.g., 5.20 kg$_{\mathrm{H2}}$ s^{-1} (0.62 GW$_{\mathrm{t}}$) and 7.32 kg$_{\mathrm{H2}}$ s^{-1} (0.87 GW$_{\mathrm{t}}$), in accordance with table 2.5. These limits guide the selection of an appropriate pipe inner diameter $D_{\mathrm{LH2,i}}$.

On the one hand, the hybrid pipeline should operate even when the flow of liquid hydrogen is lower than the expected regular demand. Minimum mass flow values $\dot{m}_{\mathrm{LH2}}$ of 4.6 kg$_{\mathrm{H2}}$ s^{-1} (0.55 GW$_{\mathrm{t}}$) are feasible when the pipe inner diameter $D_{\mathrm{LH2,i}}$ equals 34 cm or 36 cm. On the other hand, the liquid hydrogen demand in Hamburg may later increase, as discussed in section 2.5. A pipe inner diameter $D_{\mathrm{LH2,i}}$ of 36 cm has been selected because this size enables a liquid hydrogen flow up to 9.7 kg$_{\mathrm{H2}}$ s^{-1} (1.15 GW$_{\mathrm{t}}$) with only a modest increase in diameter. In contrast, the smaller diameter $D_{\mathrm{LH2,i}}$ = 34 cm allows a maximum mass flow of 7.7 kg$_{\mathrm{H2}}$ s^{-1} (0.91 GW$_{\mathrm{t}}$).

The thermal-hydraulic simulation has demonstrated how to keep hydrogen in its liquid state and has led to the selection of the pipe inner diameter $D_{\mathrm{LH2,i}}$. However, this procedure has some limitations. The estimate of the inner diameter $D_{\mathrm{LH2,i}}$ tends to be conservative, because no curves, fittings, or support structures were considered inside the inner pipe. Moreover, this work does not examine preventive measures for incidents that could compromise the safe transmission of liquid hydrogen. At a minimum, it should be clear that emergency valves must be installed at regular intervals along the hybrid pipeline to provide controlled release of hydrogen vapor in the event of liquid hydrogen boiling and a corresponding excess pressure.

4.3.4 Density Variation

The average thermal expansivity factor $\bar{\alpha}_{\mathrm{LH2}}$ was introduced by Trevisani et al. in equations 4.15 and 4.16 to account for the compressibility of liquid hydrogen, in contrast to other coolants such as liquid nitrogen (which is essentially incompressible) [18]. Figure 4.9 illustrates the density variation of liquid hydrogen between the inlet and outlet conditions, using the results of the previous sections. The color map shows the liquid hydrogen density as a function of temperature (x-axis) and pressure (y-axis), based on data from REFPROP [50]. The white curve indicates the outlet temperature T_{out} and outlet pressure p_{out} for the selected pipe inner diameter $D_{\mathrm{LH2,i}}$ = 36 cm over its operational mass flow range $\dot{m}_{\mathrm{LH2}}$ of 4.6–9.7 $\mathrm{kg_{H2}\ s^{-1}}$. For reference, the inlet temperature T_{in} and inlet pressure p_{in} are marked. The black curve delineates the phase boundary between the gaseous and liquid states.

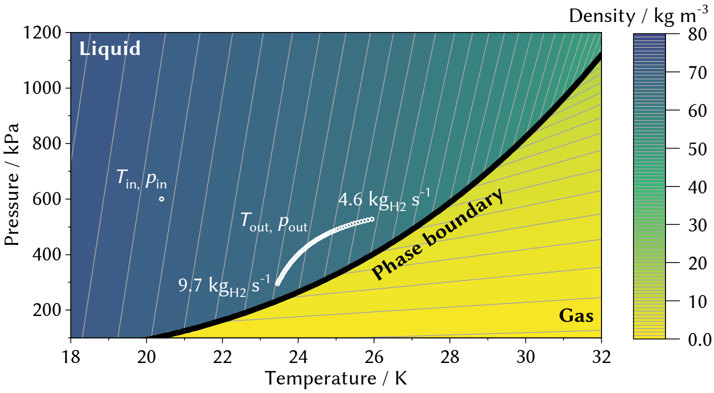

Figure 4.9: Density of liquid hydrogen (para-hydrogen) as a function of its temperature and pressure, based on data from [50]. The black curve represents the phase boundary between the gaseous and liquid states. The white curve shows the possible outlet temperature T_{out} and pressure p_{out} of the hybrid pipeline, given the inlet temperature T_{in} and pressure p_{out} for a pipe inner diameter of 36 cm at mass flow rates of 4.6–9.7 $\mathrm{kg_{H2}\ s^{-1}}$.

The results in figure 4.9 show that the density of liquid hydrogen at the inlet conditions is approximately 71.4 kg_{H2} m^{-3}. When liquid hydrogen is transmitted through the 75 km long hybrid pipeline at 9.7 kg_{H2} s^{-1}, the density drops to roughly 66.9 kg_{H2} m^{-3}, i.e., a reduction of about 6.2%. If the mass flow $\dot{m}_{\mathrm{LH2}}$ is reduced to 4.6 kg_{H2} s^{-1}, the density further declines to 63.3 kg_{H2} m^{-3}, corresponding to an approximate 11.2% decrease.

4.3.5 Pipe Layout

This section describes the aspects that were considered in the design of the pipe layout, namely the thicknesses of the inner and outer pipes (see the profile view of the hybrid pipeline in figure 4.1). The inner pipe must resist the inlet pressure p_{in} of 600 kPa on its inner side and a very low pressure close to vacuum on its outer side. For safety reasons, the inner pipe is assumed to be rated for PN 16 (nominal pressure 1600 kPa). Its wall thickness was determined in accordance with the AD 2000 set of rules for pressure equipment, resulting in a thickness of 5 mm (the difference between the outer radius $r_{\mathrm{LH2,o}}$ and the inner radius $r_{\mathrm{LH2,i}}$). However, an additional assessment is required because the inner-pipe material, Invar, is not covered by AD 2000 for hydrogen and low-temperature applications.

To reduce thermal losses by convection and conduction, the gap between the inner and outer pipes is filled with a layer of multi-layer insulation (MLI) and a vacuum region, respectively. The MLI thickness is suggested to be 20 mm to accommodate 40 insulation layers. Between the MLI's outer radius $r_{\mathrm{MLI,o}}$ and the inner radius of the outer pipe $r_{\mathrm{pipe,i}}$, a clearance of 10 mm is proposed. Cryostats must maintain a low-pressure vacuum for at least 25 years, which can be achieved through getter-filled terminations and accessible pumping ports [277]. During construction, cryogenic pipes are vacuum pumped segment by segment and assembled with suitable couplings [278]. It is assumed that vacuum pumps are employed during construction and reused through accessible pumping ports when necessary.

The outer pipe thickness was designed according to the conservative design guideline of a 1/50 wall-thickness-to-diameter ratio for long vacuum carbon steel pipes [279], which yields a wall thickness of 9 mm. The proposed pipe layout is presented in table 4.4, together with a summary of the hybrid pipeline design.

4.4 Design Summary

The previous sections have discussed the design of the electrical cable and the liquid hydrogen pipe for the proposed 75 km long hybrid pipeline. Table 4.4 summarizes the selected design. Outcomes from earlier studies that are not incorporated in this work are summarized in [241].

Table 4.4: Design summary of the hybrid pipeline including: cable rated parameters, cable layout, pipeline rated parameters, and pipeline layout.

Parameters	Symbol	Value
Cable rated parameters		
Rated power	P_0	4.0 $\mathrm{GW_e}$
Rated voltage	U_0	± 100.0 kV
Rated current	I_0	20.0 kA
Required minimum self-field critical current	$I_{c,\min}$	25.0 kA
Cable layout		
HTS tape width	a_{tape}	4.0 mm
HTS tape thickness	s_{tape}	0.1 mm
Outer radius of inner copper stabilizer	$r_{1,\text{cu}}$	13.9 mm
Outer radius of inner HTS tape	$r_{1,\text{hts}}$	14.0 mm
Outer radius of electrical insulator	$r_{1,\text{ins}}$	28.6 mm
Outer radius of outer HTS tape	$r_{2,\text{hts}}$	28.7 mm
Outer radius of outer copper stabilizer	$r_{2,\text{cu}}$	30.7 mm
Cable cross-section of one monopole	A_{cable}	2 951.6 $\mathrm{mm^2}$
Number of tapes in inner phase	$N_{1,\text{tapes}}$	21
Gap between tapes inner phase	$g_{1,\text{tapes}}$	0.018 mm
Number of layers in inner phase	$N_{1,\text{layers}}$	1
Lay angle in inner phase	θ_1	15.0°
Calculated critical current inner phase	$I_{c,1}$	25.6 kA
Outer phase layout	–	Type III
Number of tapes in outer phase	$N_{2,\text{tapes}}$	21
Gap between tapes outer phase	$g_{2,\text{tapes}}$	4.42 mm

Continued on next page

Table 4.4: Design summary of the hybrid pipeline including: cable rated parameters, cable layout, pipeline rated parameters, and pipeline layout. (Continued)

Parameters	**Symbol**	**Value**
Number of layers in outer phase	$N_{2,\text{layers}}$	1
Lay angle in outer phase	θ_2	15.0°
Calculated critical current outer phase	$I_{c,2}$	−25.2 kA
Superconductor length per monopole	–	3 261 km
Total superconductor length	–	6 522 km
	Pipeline rated parameters	
Inlet temperature	T_{in}	20.4 K
Inlet pressure	p_{in}	600 kPa
Total heat load per unit length	q_{l}	3.857 W m^{-1}
Surface roughness	ϵ	0.046 mm
Pipe inner diameter	$D_{\text{LH2,i}}$	36.0 cm
Liquid hydrogen mass flow	$\dot{m}_{\text{LH2}}$	4.6−9.7 kg_{H2} s^{-1}
Chemical power	P_{t}	0.55−1.15 GW_{t}
Outlet temperature	T_{out}	25.9−23.5 K
Outlet pressure	p_{out}	527.5−293.9 kPa
	Pipeline layout	
Inner radius of inner pipe	$r_{\text{LH2,i}}$	180.0 mm
Outer radius of inner pipe	$r_{\text{LH2,o}}$	185.0 mm
Outer radius of multi-layer insulation	$r_{\text{MLI,o}}$	205.0 mm
Inner radius of outer pipe	$r_{\text{pipe,i}}$	215.0 mm
Outer radius of outer pipe	$r_{\text{pipe,o}}$	224.0 mm

5 Techno-economic Assessment of the Transmission Alternatives

The hybrid pipeline will only move from concept to market if it can be more cost-effective than conventional alternatives. The techno-economic assessment will examine under which conditions this is feasible. A clear definition of the context, system limits, and all components needed for the transmission of both hydrogen and electrical energy is required. Based on the case study and conceptual design discussed in the previous chapters, this chapter presents the system limits and comparison method for the techno-economic assessment. This includes a systematic evaluation of the components required for energy transmission. The results will include the investment and operating costs of the hybrid pipeline, as well as a comparison with current standards. A sensitivity analysis will clarify the influence of length and other parameters on the results.

5.1 Definition of the System Limits

The requirements for the selected case study Brunsbüttel–Hamburg in northern Germany are: 75 km of transmission length, 4 GW_e of electric power, and 0.62–0.87 GW_t of liquid hydrogen transport (see table 2.5). Figure 5.1 shows the system limits for the techno-economic assessment of this case study, divided into the upstream (supply), midstream (transmission), and downstream (demand). The techno-economic assessment will focus on the comparison of two transmission alternatives inside the system limits: the hybrid pipeline alternative and the conventional alternative, which is mainly composed of an HVDC underground cable and a gaseous hydrogen pipeline (see section 2.6). Outside the system limits, the case study establishes the conditions that remain constant for both transmission alternatives.

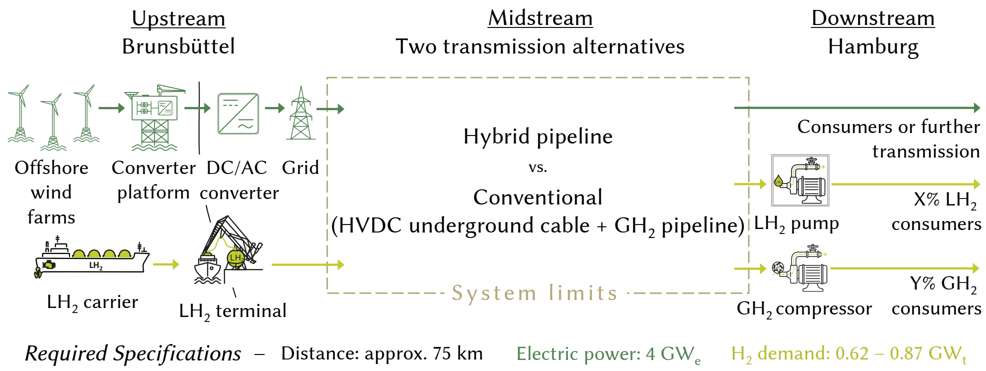

Figure 5.1: System limits of the techno-economic assessment between the hybrid pipeline alternative and the conventional alternative, which is mainly composed of a high-voltage direct-current (HVDC) underground cable and a gaseous hydrogen (GH_2) pipeline. Two final products will be considered: liquid hydrogen (LH_2) and GH_2.

On the electrical upstream, the offshore wind farms HelWin1 [280], HelWin2 [281], and SylWin1 [282] have delivered since 2015 approximately 2.1 GW_e of electrical energy to the Brunsbüttel area. Starting in 2027, BorWin6 will transmit 980 MW_e to the same interconnection point. All offshore wind farms are connected to corresponding converter platforms that convert AC to HVDC for more efficient transmission to the coast. Once ashore, the electrical energy is converted back into AC for the high-voltage grid [283]. Additional electrical energy will be transmitted through this region from Denmark [166] to the south of the country [167, 168].

On the chemical upstream, a stationary terminal in Brunsbüttel will receive hydrogen imports by liquid hydrogen carriers, as discussed in section 2.5. Some specifications about liquid hydrogen carriers and terminals, which are outside the system limits, are presented in appendix C.

On the downstream, the electrical energy will be delivered to the grid in the Hamburg area, where different kinds of consumers are located or where the electrical energy can be further transmitted. Regarding hydrogen transfer, the demand side can obtain two valuable but distinct products: liquid hydrogen or gaseous hydrogen. For this reason, the comparison will be presented for the two final products, as shown in table 5.1. The next sections will describe the components inside the system limits for each of the two final products. Outside the downstream limits, it is assumed that either a liquid hydrogen pump or a gaseous hydrogen compressor increases the pressure for the final hydrogen delivery to the corresponding consumers.

Table 5.1: Overview of final products and alternatives in the techno-economic assessment.

Final product	**Alternatives**
Liquid hydrogen	Hybrid pipeline
	Conventional
Gaseous hydrogen	Hybrid pipeline
	Conventional

5.1.1 Liquid Hydrogen as Final Product

In the first comparison, hydrogen will be delivered in its liquid state. Figure 5.2 shows the detailed configuration inside the system limits for this final product. It includes all components in each transmission alternative.

The electrical energy enters the system from the high-voltage grid at 380 kV. In the hybrid pipeline alternative, AC/DC converter stations reduce the voltage to ± 100 kV, which is the rated voltage proposed for the hybrid pipeline (see table 4.4). In the conventional alternative, AC/DC converter stations increase the voltage to ± 525 kV, which is the rated voltage of extra-high-voltage DC underground cables, as presented in section 2.6.1. On the downstream side, DC/AC converter stations will raise or lower the voltage to feed back into the 380 kV grid, depending on the transmission alternative.

The hydrogen transfer in the hybrid pipeline alternative proceeds as follows. Liquid hydrogen enters the system at 150 kPa (1.5 bar) and 20.4 K (see section 4.3). A transfer pump with a differential pressure of 450 kPa (4.5 bar) raises the pressure to 600 kPa (6 bar), as specified for the inlet pressure p_{in} in table 4.4. Any temperature rise caused by the transfer pipe is compensated by heat transfer to the stored coolant (see section 4.3).

With an outer diameter of approximately 45 cm, the hybrid pipeline transmits 0.55–1.15 GW_{t} (i.e., 397–838 $\text{t}_{\text{H2}}\ \text{d}^{-1}$) of liquid hydrogen, based on the lower heating value of para-hydrogen (see section 2.4). The liquid hydrogen is then delivered directly to the consumers or temporarily stored in a buffer of 1 000 t_{H2}. This size was chosen because the maximum transmission capacity of the hybrid pipeline is 838 $\text{t}_{\text{H2}}\ \text{d}^{-1}$, which is rounded to 1 000 t_{H2} to ensure security of supply. When the storage is used, approximately 0.5% of liquid hydrogen will boil [284,285] and the resulting boil-off gas can be supplied to consumers of gaseous hydrogen.

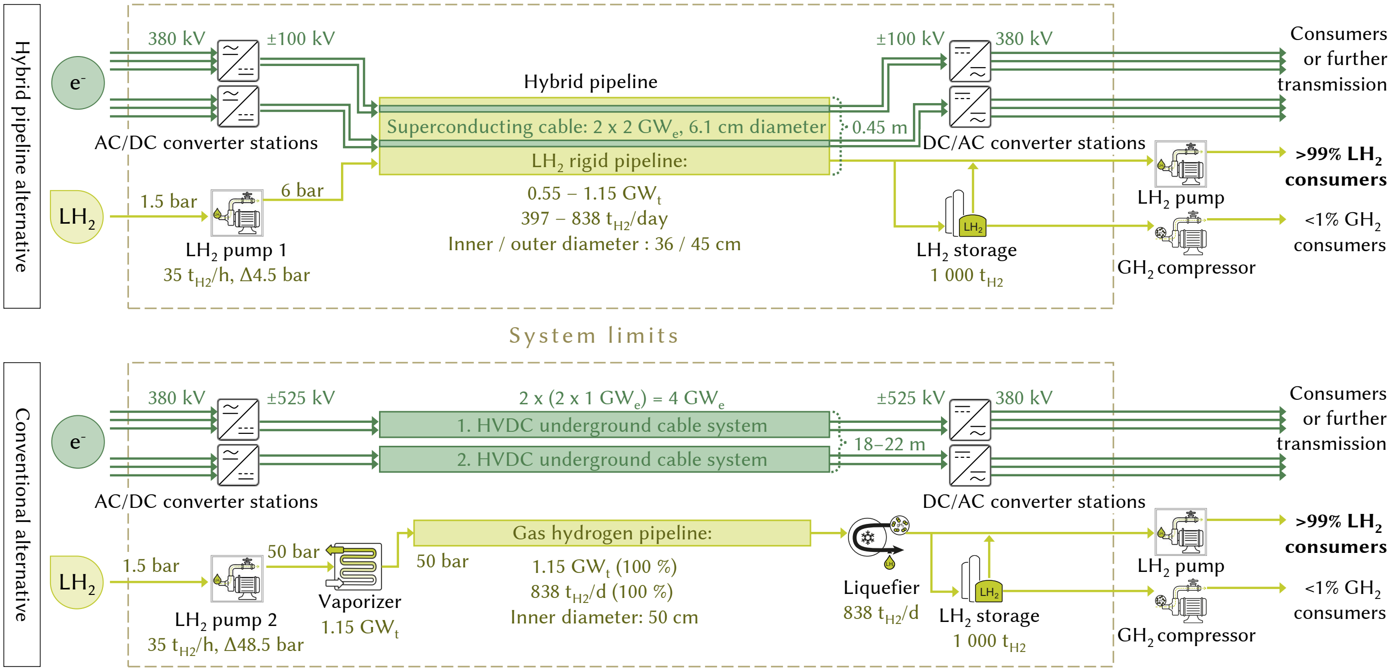

Figure 5.2: Detailed configuration of the two alternatives with liquid hydrogen (LH_2) as final product. A very small portion is delivered in the form of gaseous hydrogen (GH_2), when the LH_2 storage is used.

In the conventional alternative, it is assumed that a newly built, 50 cm wide pipeline transmits hydrogen in its gaseous state. This assumption is based on the absence of a natural gas pipeline between Brunsbüttel and Hamburg that could be repurposed[1] (see figures A.1 and A.2). The 50 cm diameter was chosen because such a gaseous pipeline exhibits a similar thickness and capacity as that of the hybrid pipeline, i.e., 1.2 GW_t at 100% load (see section 2.6.2).

The operating pressure of the gaseous pipeline is 5 000 kPa (50 bar) [53]. Consequently, pressure must be increased from 150 kPa (1.5 bar) to 5 000 kPa (50 bar). Traditionally, compressors raise the pressure at the inlet. However, it is far more energy efficient to pump liquid hydrogen to a higher pressure than to compress gaseous hydrogen to the same level. Hence, a pump with a differential pressure of 4 850 kPa (48.5 bar) is used to pressurize the liquid hydrogen. Alternatively, pressure could be increased by re-gasifying the liquid hydrogen at constant volume [66], but this route is not pursued because pressurizing before regasification is standard in the LNG industry [287] and in other liquid hydrogen regasification designs [288, 289].

A vaporizer must evaporate the liquid hydrogen for transmission through a conventional gaseous hydrogen pipeline. Since in this case consumers expect liquid hydrogen as the end-use product, a liquefier converts the gaseous hydrogen back into liquid after transmission. Analogously to the hybrid pipeline alternative, a buffer of 1 000 t_{H2} is located after transmission to ensure security of supply.

Importantly, the hybrid pipeline requires only about 0.45 m of width to transmit both liquid hydrogen and electrical energy. In comparison, 18–22 m are required for the operation of HVDC underground cables alone [187].

5.1.2 Gaseous Hydrogen as Final Product

Figure 5.3 presents the detailed transmission configuration when gaseous hydrogen is assumed to be the final product. The electrical pathways are the same as for the liquid hydrogen case. The left side of the hydrogen transmission (i.e., the components before the hybrid pipeline and the gaseous pipeline) also remains unchanged for both final products.

[1] As of June 2026, a natural gas pipeline now runs through this region [286]. Since this project was already at an advanced stage before the new natural gas pipeline was identified, the assumption of a newly built pipeline remained. Although repurposed gaseous hydrogen pipelines are less expensive than newly built ones, the results in section 5.4 will show that this assumption has a small effect on the total costs.

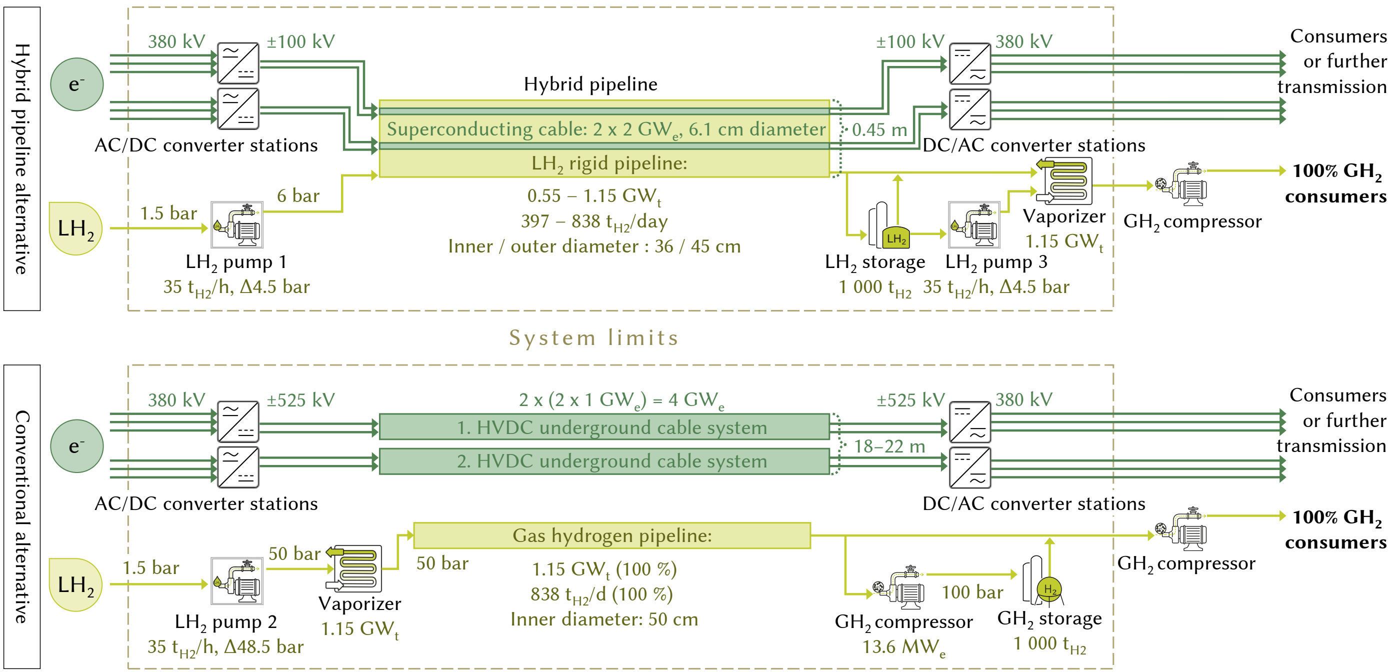

Figure 5.3: Detailed configuration of the two alternatives with gaseous hydrogen as final product. Hydrogen enters the system in its liquid state (LH_2).

The difference between figures 5.2 and 5.3 lies in the hydrogen treatment after transmission. In the hybrid pipeline alternative, liquid hydrogen can be temporarily stored in a 1 000 t_{H2} storage before further transmission to consumers. A liquid hydrogen pump is then required to extract the liquid from storage, and a vaporizer with the same maximum load as the hybrid pipeline evaporates the liquid hydrogen for delivery in its gaseous state.

In the conventional alternative, gaseous hydrogen can be transmitted directly to the consumers without further treatment. For security of supply and to keep the two alternatives consistent, a gaseous hydrogen storage of 1 000 t_{H2} is considered as buffer before direct delivery.

Because gaseous hydrogen has a low volumetric energy density, it must be compressed for storage. Consequently, a compressor is placed before feeding gas into the storage. Section 5.3.5 will explain why the electric power rating of the compressor is 13.6 MW_e. Section 5.3.6 will justify the selection of a storage pressure level of 1 000 kPa (100 bar).

5.2 Assessment Method

In this study, both the annuity method and the present-value method are applied to provide a comprehensive comparison of transmission alternatives. Each approach highlights a different economic perspective: annual cost expenditures versus lifetime costs. Using them in parallel offers a more solid basis for evaluating transmission options with varying lifetimes and operating profiles.

Annuity Method

The annuity method is used to convert upfront investment costs into equivalent annual costs by means of an annuity factor [290]. This allows the evaluation of capital and operating expenditures on a consistent annual basis. The annual total expenditures of the system $\mathrm{TOTEX}^{\mathrm{annual}}$ $\mathrm{TOTEX}^{\mathrm{annual}}$ $\mathrm{TOTEX}_{\mathrm{annual}}$ $\mathrm{TOTEX}_{\mathrm{annual}}$ $\mathrm{TOTEX}^{\mathrm{annual}}_{\mathrm{annual}}$ $\mathrm{TOTEX}^{\mathrm{annual}}_{\mathrm{annual}}$ are the sum of the annual total expenditures of each component i in the considered transmission alternative:

$$\mathrm{TOTEX}^{\mathrm{annual}} = \sum_{i=1}^{M} \mathrm{TOTEX}_i^{\mathrm{annual}}. \tag{5.1}$$

The total expenditures $\mathrm{TOTEX}_i^{\mathrm{annual}}$ of a component i are composed of the annualized investment costs $\mathrm{CAPEX}_i^{\mathrm{annual}}$ plus the annual fixed and variable operating costs $\mathrm{fixOPEX}_i^{\mathrm{annual}}$ and $\mathrm{varOPEX}_i^{\mathrm{annual}}$, respectively:

$$\mathrm{TOTEX}_i^{\mathrm{annual}} = \mathrm{CAPEX}_i^{\mathrm{annual}} + \mathrm{fixOPEX}_i^{\mathrm{annual}} + \mathrm{varOPEX}_i^{\mathrm{annual}}. \tag{5.2}$$

The variable operating expenditures $\mathrm{varOPEX}_i^{\mathrm{annual}}$ pertain to the specific electrical energy demand. They are the product of the component-specific electrical energy consumption $w_{\mathrm{e},i}$ and the electricity cost κ_{e}:

$$\mathrm{varOPEX}_i^{\mathrm{annual}} = w_{\mathrm{e},i} \cdot \kappa_{\mathrm{e}}. \tag{5.3}$$

The fixed operating expenditures $\mathrm{fixOPEX}_i^{\mathrm{annual}}$ are determined by the operation and maintenance costs $\mathrm{O\&M}_i$, which are represented as a percentage of the initial capital cost $\mathrm{CAPEX}_i^{\mathrm{initial}}$:

$$\mathrm{fixOPEX}_i^{\mathrm{annual}} = \mathrm{CAPEX}_i^{\mathrm{initial}} \cdot \mathrm{O\&M}_i \tag{5.4}$$

The calculation of the initial capital cost $\mathrm{CAPEX}_i^{\mathrm{initial}}$ will be discussed later in equation 5.13. The annualized capital expenditures of a component $\mathrm{CAPEX}_i^{\mathrm{annual}}$ in equation 5.2 are the product of the annuity factor $\mathrm{AF}^{\mathrm{annual}}$ and the present-value investment cost of that component $\mathrm{CAPEX}_i^{\mathrm{present}}$:

$$\mathrm{CAPEX}_i^{\mathrm{annual}} = \mathrm{CAPEX}_i^{\mathrm{present}} \cdot \mathrm{AF}^{\mathrm{annual}}. \tag{5.5}$$

The annuity factor $\mathrm{AF}^{\mathrm{annual}}$ is defined using the system lifetime τ_{sys} and the weighted average cost of capital WACC. The system lifetime τ_{sys} is set at 40 years because each of the main transmission components (the hybrid pipeline, HVDC underground cable, and gaseous hydrogen pipeline) has a 40 year service life (see section 5.3). The selection of the weighted average cost of capital WACC will be discussed later. The annuity factor is given by [290]:

$$\mathrm{AF}^{\mathrm{annual}} = \frac{(1+\mathrm{WACC})^{\tau_{\mathrm{sys}}} \cdot \mathrm{WACC}}{(1+\mathrm{WACC})^{\tau_{\mathrm{sys}}} - 1}. \tag{5.6}$$

In equation 5.5, the present-value investment cost of a component $\mathrm{CAPEX}_i^{\mathrm{present}}$ depends on the component lifetime. If the component lifetime τ_i is shorter than the system lifetime τ_{sys}, replacement costs occurring at intervals τ_i are included and discounted to the present. If the final replacement is not fully utilized by the end of the system lifetime, the unused fraction of the component value is discounted back to the present [291]. Using the notation presented so far, these considerations are written as:

$$\mathrm{CAPEX}_i^{\mathrm{present}} = \mathrm{CAPEX}_i^{\mathrm{initial}} \cdot \left[\sum_{j=0}^{\lfloor \tau_{\mathrm{sys}}/\tau_i \rfloor} d^{-j \cdot \tau_i} - \frac{\tau_i - \mathrm{mod}(\tau_{\mathrm{sys}}, \tau_i)}{\tau_i} \cdot d^{-\tau_{\mathrm{sys}}} \right], \tag{5.7}$$

where $\mathrm{CAPEX}_i^{\mathrm{present}} = \mathrm{CAPEX}_i^{\mathrm{initial}}$ when the component lifetime τ_i equals the system lifetime τ_{sys}, and d is the discount factor defined by the weighted average cost of capital WACC as:

$$d = 1 + \mathrm{WACC}. \tag{5.8}$$

Present-value Method

The present-value method discounts all future operating costs to their value at the start of the project and adds them to the initial investment, providing a cumulative lifetime cost expressed in today's monetary terms [251]. In this method, the total present-value expenditures of the system $\mathrm{TOTEX}^{\mathrm{present}}$ are the sum of the present-value expenditures of each component i in the corresponding transmission alternative:

$$\mathrm{TOTEX}^{\mathrm{present}} = \sum_{i=1}^{M} \mathrm{TOTEX}_i^{\mathrm{present}}. \tag{5.9}$$

Analogously to equation 5.2, the total present-value expenditures of a component i are composed of the present-value investment costs (see equation 5.7) plus the present-value fixed and variable operating costs of the component. The present-value annuity factor r^b therefore aggregates recurring annual operating costs into a single discounted value, enabling a direct comparison of long-term expenditures:

$$\mathrm{TOTEX}_i^{\mathrm{present}} = \mathrm{CAPEX}_i^{\mathrm{present}} + \left(\mathrm{fixOPEX}_i^{\mathrm{annual}} + \mathrm{varOPEX}_i^{\mathrm{annual}} \right) \cdot \mathrm{AF}_{\mathrm{present}}, \tag{5.10}$$

where the present-value annuity factor $\mathrm{AF}^{\mathrm{present}}$ is calculated as [251]:

$$\mathrm{AF}^{\mathrm{present}} = \frac{d^{\tau_{\mathrm{sys}}} - 1}{d^{\tau_{\mathrm{sys}}} \cdot (d-1)} = \frac{1}{\mathrm{AF}^{\mathrm{annual}}}. \tag{5.11}$$

Here, τ_{sys} is the system lifetime and d is the discount factor determined by the weighted average cost of capital WACC, as defined in equation 5.8.

Weighted Average Cost of Capital (WACC)

The private cost of capital represents the compensation that commercially oriented investors request in exchange for providing financial means, whether by borrowing or shareholding. This compensation varies with the specific characteristics of a project because the probability of recovering the invested money is influenced by various risk factors, such as the underlying technology and the regional regulatory or policy conditions. The weighted average cost of capital (WACC) is a special case of the cost of capital. The WACC denotes the situation in which capital is obtained from both debt and equity funding [292].

To strengthen the reliability of results based on techno-economic analyses, Lonergan et al. advocate explaining the associated assumptions regarding the cost of capital and considering the dimensions of geography, time, and technology when choosing the cost of capital rate [292]. The selection of WACC rates in this work follows three arguments:

- **Geography**: The case study is limited to Germany. Therefore, no geographical differentiation is assumed because the regulatory and policy environment can be regarded as uniform. Nevertheless, the assumptions are based on German data.
- **Time**: The cost of capital varies over the system lifetime of 40 years, but the temporal dimension is omitted owing to uncertainty and for simplicity.
- **Technology**: The varying maturity of components considered in the techno-economic assessment creates distinct risk factors for capital providers. Consequently, multiple WACC rates are considered by technology.

For new investments in the electricity and hydrogen transmission network, Germany currently has no officially adopted WACC value. A new regulatory system is under consultation. In contrast, for new investments of electricity distributors, natural gas distributors, and natural gas TSOs, the German Federal Network Agency reports an annual WACC based on equity (40%) and debt (60%), as shown in table 5.2. The annual WACC applies only to the current regulatory period (2024–2029 for electricity and 2023–2028 for gas). From 2030 for electricity and from 2029 for gas onward, a single WACC will be applied for the entire five-year regulatory period [293].

Table 5.2: Return on equity, cost of debt, and weighted average cost of capital as published in 2026 by the German Federal Network Agency for new investments on the electrical and natural gas distribution networks, and on the natural gas transmission network [293].

Year	Return on equity	Cost of debt	Weighted average cost of capital (WACC)
2023	5.07%	1.71%	3.05%
2024	6.93%	3.87%	5.09%
2025 (projected)	6.95%	3.87%	5.10%
2026 (projected)	7.00%	3.67%	5.00%

For investments in the existing network infrastructure, the energy consulting firm BET expects the Federal Network Agency to increase the return on equity before tax from the current 5.07% to 6.5–7.0% for the next regulatory period because of a shorter-term view of interest rate levels [294]. Based on BET's argument, the WACC for new investments in the electrical distribution network is assumed to be higher in the next regulatory period than the 5.00% projected for 2026 in the current period (see table 5.2). Assuming a similar trend for distribution and transmission networks, a WACC of 6.5% is estimated for new investments on the electrical transmission network in this work.

Estimating a WACC for new investments in the hydrogen transmission network should consider that the infrastructure is in an early deployment stage, which entails higher risks for investors than for the electrical grid (see sections 2.2.1 and 2.6.2). Therefore, a WACC of 8.0% is assumed for new hydrogen transmission investments. This value applies to the gaseous hydrogen pipeline and to auxiliary components in the hydrogen supply chain, such as compressors, pumps, liquefiers, storage, and vaporizers. Hatton et al. expected an identical WACC of 8.0% for hydrogen production by electrolysis in Germany in 2025 [295], whereas other scholars estimated substantially higher rates of 13.8–16.9% for the same technology [296]. This reflects the relatively high level of uncertainty in the assumptions.

Given that the hybrid pipeline is at TRL 4 (laboratory-validated, see section 2.7), its WACC is set higher at 12.0%. For comparison, Lux et al. assumed a WACC of 12.0% as an upper limit for e-fuel imports from the Middle East and North Africa to Europe [297]. The different WACC values will be summarized later in table 5.3.

Availability and Losses

For each component i, specific capital expenditures $\text{CAPEX}_i^{\text{specific}}$ are multiplied by the component's effective size $S_i^{\text{effective}}$ to obtain the initial investment cost $\text{CAPEX}_i^{\text{initial}}$:

$$\text{CAPEX}_i^{\text{initial}} = \text{CAPEX}_i^{\text{specific}} \cdot S_i^{\text{effective}}. \tag{5.12}$$

To enable a consistent cost comparison of transmission alternatives, the nominal size of each component S_i^{nominal} is converted to an equivalent effective size $S_i^{\text{effective}}$, corrected for technical availability and losses:

$$S_i^{\text{effective}} = S_i^{\text{nominal}} \cdot f_i^{\text{availability}} \cdot f_i^{\text{loss}}, \tag{5.13}$$

where the inverse factors $f_i^{\text{availability}}$ and f_i^{loss} are dimensionless values ≥ 1. The component-specific inverse availability factor $f_i^{\text{availability}}$ accounts for planned and forced outages. The inverse loss factor f_i^{loss} considers performance differences arising from component-specific transmission losses. For example, if a component exhibits 2% hydrogen losses and is technically unavailable during 5% of the time per year because of planned and forced downtime, then:

$$\begin{aligned} f_i^{\text{loss}} &= \frac{100\%}{100\% - 2\%} = 1.02, \\ f_i^{\text{availability}} &= \frac{100\%}{100\% - 5\%} = 1.05. \end{aligned} \tag{5.14}$$

The component downtime owing to unexpected outages is out of the scope of this work. Each component is assumed to operate continuously, unless it is intended for occasional use, such as the liquid and gaseous hydrogen storage tanks in figures 5.2 and 5.3. Consequently, for such components the operating hours per year $t_{\text{op},i}$ will be determined.

Inflation Year and Currency Exchange

For each component and material, multiple data sources were compared where more than one reference was available. This comparison provides a more realistic range of costs associated with each item. Costs were adjusted to EUR_{2023} using the consumer price index to enable comparison of all cost parameters, i.e.:

$$\mathrm{Cost}_{\mathrm{EUR},2023} = \mathrm{Cost}_{\mathrm{EUR,year}} \cdot f_{\mathrm{EUR,year}}, \tag{5.15}$$

where $\mathrm{Cost}_{\mathrm{EUR},2023}$ is the cost in EUR_{2023}, $\mathrm{Cost}_{\mathrm{EUR,year}}$ is the cost in euros at the price level of the given year, and $f_{\mathrm{EUR,year}}$ is the inflation-adjustment factor that converts euros from that year to euros in 2023. The inflation-adjustment factors can be found in table C.2.

If the costs are expressed in a currency other than euros, the inflation adjustment is applied in that currency to the 2023 price level, and conversion into euros is performed with the exchange rate at the end of 2023, for example:

$$\mathrm{Cost}_{\mathrm{EUR},2023} = \mathrm{Cost}_{\mathrm{USD,year}} \cdot f_{\mathrm{USD,year}} \cdot f_{\mathrm{USD/EUR}}, \tag{5.16}$$

where $\mathrm{Cost}_{\mathrm{USD},2023}$ is the cost in US dollars at the price level of the given year, $f_{\mathrm{USD,year}}$ is the inflation-adjustment factor that converts US dollars from that year to US dollars in 2023, and $f_{\mathrm{USD/EUR}}$ is the exchange rate (USD to EUR) on 31 December 2023. The exchange rates can be found in table C.3.

If a source does not specify the inflation year for the reported costs, it is assumed to coincide with the publication year.

Cost Accounting Parameters

Table 5.3 summarizes the general cost accounting parameters used for the techno-economic assessment, as discussed in this section. The electrical energy cost κ_{e} is defined as the average of the industrial electricity cost in the past three years (2023–2025) [298]. The industrial electrical energy costs are adjusted to EUR_{2023} using the consumer price index (see table C.2).

Table 5.3: Assumed parameters for cost accounting.

Description	Variable	Value
System lifetime	τ_{sys}	40 years
Industrial electrical energy cost	κ_{e}	$0.194\ \mathrm{EUR}_{2023}\ \mathrm{kWh}_{\mathrm{e}}^{-1}$

Continued on next page

Table 5.3: Assumed parameters for cost accounting. (Continued)

Description		Variable	Value
Weighted average cost of capital	Electrical components	$WACC_{low}$	6.5%
	Gaseous and liquid hydrogen components	$WACC_{mid}$	8.0%
	Hybrid pipeline	$WACC_{high}$	12.0%
Annuity factor	Electrical components	AF^{annual}_{low}	0.0707
	Gaseous and liquid hydrogen components	AF^{annual}_{mid}	0.0839
	Hybrid pipeline	AF^{annual}_{high}	0.1213
Present-value of annuity factor	Electrical components	$AF^{present}_{low}$	14.146
	Gaseous and liquid hydrogen components	$AF^{present}_{mid}$	11.925
	Hybrid pipeline	$AF^{present}_{high}$	8.244

5.3 Components Properties and Cost Assumptions

The following sections examine the technical properties, investment, and operational costs of each component inside the limits of the techno-economic assessment. The results are based on a systematic literature review and on a few expert interviews. In a first instance, the investment-cost estimates of each component are discussed. Further techno-economic parameters, such as the component lifetime and the operation and maintenance cost rates, will then be introduced. Unless otherwise indicated, all tabulated values in section 5.3 are derived from the cited references.

5.3.1 Hybrid Pipeline

The conceptual design of the hybrid pipeline—presented in chapter 4—provides all the technical information needed to estimate its investment costs. Given the geometry of the single material layers (see table 4.4), the quantity of required material is calculated.

Specific material-cost estimates for HTS REBCO tapes, copper, electrical insulator, Invar, carbon steel, and thermal multi-layer insulation (MLI) can be found in table C.4 of appendix C. For each entry, optimistic, mean, and pessimistic costs are calculated based on the available sources. The optimistic and pessimistic cost estimates are derived from the items with the lowest and highest investment costs, respectively. The mean costs are the arithmetic mean of the available data.

Table 5.4 presents the mean investment-cost estimates of the hybrid pipeline, divided into material costs, direct costs (material, fabrication, pipe laying, and terminations), and indirect costs, which will be discussed later.

The fabrication costs are an estimate based on 10% (optimistic) or 15% (pessimistic) of the total material costs. It is assumed that the use of vacuum pumps during construction is included in the fabrication costs (see section 4.3.5). Although the manufacture cost estimate originally stems from the fabrication of superconducting cables without synergetic chemical energy transmission [251], it represents the most suitable approximation identified in the literature.

Table 5.4: Mean specific and total investment-cost estimates of a hybrid pipeline for the case study Brunsbüttel–Hamburg based on data from table C.4.

Description	Quantity	Specific costs	Total costs
HTS REBCO tape (4.0 mm width)	6 522.24 km	9.55 $\mathrm{EUR_{2023}\ m^{-1}}$	62.29 $\mathrm{MEUR_{2023}}$
Electrical insulator (Kapton®)	293.05 $\mathrm{m^3}$	266.91 $\mathrm{kEUR_{2023}\ m^{-3}}$	78.22 $\mathrm{MEUR_{2023}}$
Copper	976.76 t	10.41 $\mathrm{kEUR_{2023}\ t^{-1}}$	10.17 $\mathrm{MEUR_{2023}}$
Invar	3 483.04 t	34.12 $\mathrm{kEUR_{2023}\ t^{-1}}$	118.85 $\mathrm{MEUR_{2023}}$
Carbon steel	7 307.82 t	915.00 $\mathrm{EUR_{2023}\ t^{-1}}$	6.69 $\mathrm{MEUR_{2023}}$
MLI (40 layers)	87 179.20 $\mathrm{m^2}$	151.70 $\mathrm{EUR_{2023}\ m^{-2}}$	13.22 $\mathrm{MEUR_{2023}}$
Total material costs			289.44 $\mathrm{MEUR_{2023}}$
Fabrication	-	12.5% of material costs	36.18 $\mathrm{MEUR_{2023}}$
Pipe laying	75 km	931.81 $\mathrm{kEUR_{2023}\ km^{-1}}$	69.89 $\mathrm{MEUR_{2023}}$
Terminations	Both ends	-	2.32 $\mathrm{MEUR_{2023}}$
Total direct costs: material, fabrication, pipe laying, and terminations			397.85 $\mathrm{MEUR_{2023}}$
Total indirect costs		40.0% of direct costs	159.13 $\mathrm{MEUR_{2023}}$
Mean total hybrid pipeline investment costs			556.96 $\mathrm{MEUR_{2023}}$

The total investment costs for terminations with a capacity of 4 $\mathrm{GW_e}$ is estimated at 2.00 $\mathrm{MEUR_{2021}}$, based on an interview with a termination manufacturer. This amount is equivalent to 2.32 $\mathrm{MEUR_{2023}}$ and includes the terminations on both sides of the pipeline.

The cost estimates for pipe laying in Germany are based on the data presented in table C.5. Indirect costs, such as the owner's costs, unforeseen events, and engineering and design, are specified in table C.6. The indirect costs are calculated as 40% of the total direct costs, in accordance with [299, 300].

Figure 5.4 presents the resulting investment-cost estimates for the hybrid pipeline. The results indicate that the investment would amount to 321.39 $MEUR_{2023}$ in an optimistic scenario, 556.96 $MEUR_{2023}$ under average assumptions, and 809.96 $MEUR_{2023}$ in a pessimistic scenario.

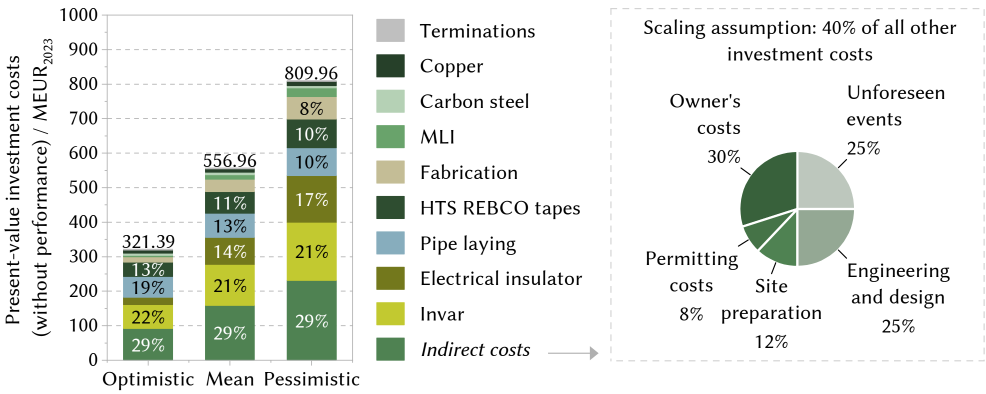

Figure 5.4: Present-value optimistic, mean, and pessimistic investment-cost estimates of the hybrid pipeline (without performance factors $f^{\text{availability}}_{\text{HyPipe}}$, $f^{\text{loss}}_{\text{HyPipe}}$) and breakdown of the indirect costs (based on [299, 300]).

It should be noted that the hybrid pipeline is currently at a comparatively low technology readiness level (TRL 4, see section 2.7). Consequently, additional system components or design adaptations not yet considered may be required during further development stages, potentially increasing the overall investment costs beyond the values reported here. Nevertheless, within the scope of the available data and assumptions, these estimates constitute the most detailed and robust approximation of the investment costs for the hybrid pipeline presented in this work and provide a baseline for future cost improvement.

In the optimistic, mean, and pessimistic scenarios, Invar accounts for the largest share of cost (22–21%.) The electrical insulator (Kapton®) represents the second-largest share in the mean and pessimistic estimates (14% and 17%, respectively). In contrast to PPLP, costs for Kapton® are publicly available (see table C.4). PPLP manufacturers were directly contacted, but no positive answer was received. However, it is commonly known that Kapton® is considerably more costly than PPLP [301]. Therefore, the costs for electrical insulation could be lower when using PPLP, provided the material is suitable for use in liquid hydrogen (see section 4.2.2).

To calculate the initial investment cost of the hybrid pipeline $\mathrm{CAPEX}_{\mathrm{HyPipe}}^{\mathrm{initial}}$ (equation 5.12), specific capital expenditures $\mathrm{CAPEX}_{\mathrm{HyPipe}}^{\mathrm{specific}}$ are obtained by dividing the mean investment costs presented in figure 5.4 by the pipeline length of 75 km. The resulting value of 7.43 $\mathrm{MEUR\ km^{-1}}$ is not transferable and applies only to the hybrid pipeline proposed in this work. This is because a hybrid pipeline is a custom-engineered product designed for a specific application context.

A consistent cost comparison with conventional transmission alternatives is possible if the specific investment-cost estimates of the hybrid pipeline $\mathrm{CAPEX}_{\mathrm{HyPipe}}^{\mathrm{specific}}$ are divided into electrical and chemical cost equivalents. For shared infrastructure delivering multiple energy vectors, investment costs cannot be uniquely attributed and therefore require allocation based on proportional rules [302]. For this purpose, the rated capacities of the superconducting cable and the liquid hydrogen pipeline are used as weighting metrics for cost allocation:

$$
\begin{aligned}
\mathrm{CAPEX}_{\mathrm{HyPipe,e}} &= \mathrm{CAPEX}_{\mathrm{HyPipe}}^{\mathrm{specific}} \cdot \frac{4.0\ \mathrm{GW_e}}{4.0\ \mathrm{GW_e} + 1.15\ \mathrm{GW_t}}, \\
\mathrm{CAPEX}_{\mathrm{HyPipe,t}} &= \mathrm{CAPEX}_{\mathrm{HyPipe}}^{\mathrm{specific}} \cdot \frac{1.15\ \mathrm{GW_t}}{4.0\ \mathrm{GW_e} + 1.15\ \mathrm{GW_t}},
\end{aligned} \tag{5.17}
$$

where 4.0 $\mathrm{GW_e}$ and 1.15 $\mathrm{GW_t}$ are the rated electrical and chemical transmission capacities of the hybrid pipeline, respectively. This allocation is more appropriate than a simple split into cable and pipe material costs because the electrical and thermal-hydraulic designs are closely interconnected. A neutral capacity-weighted allocation is applied, assuming equal weighting between electrical and chemical capacities. The resulting carrier-specific costs are then expressed per unit capacity:

$$
\begin{aligned}
\mathrm{CAPEX}_{\mathrm{HyPipe,e}}^{\mathrm{specific}} &= \frac{\mathrm{CAPEX}_{\mathrm{HyPipe,e}}}{4.0\ \mathrm{GW_e}} = 1.44\ \mathrm{MEUR_{2023}\ GW_e^{-1}\ km^{-1}}, \\
\mathrm{CAPEX}_{\mathrm{HyPipe,t}}^{\mathrm{specific}} &= \frac{\mathrm{CAPEX}_{\mathrm{HyPipe,t}}}{1.15\ \mathrm{GW_t}} = 1.44\ \mathrm{MEUR_{2023}\ GW_t^{-1}\ km^{-1}}.
\end{aligned} \tag{5.18}
$$

These results are also valid only for the specific hybrid pipeline design presented in this work. The values in equation 5.18 will be compared with the specific-cost estimates of conventional alternatives in section 5.4. Section 5.5 will determine the costs for transmission distances shorter and larger than 75 km.

The hybrid pipeline is assumed to have the same yearly technical availability as gaseous hydrogen pipelines. This assumption is based on the similar treatment of gaseous and liquid hydrogen piping by the Argonne National Laboratory (ANL) on behalf of the U.S. American Department of Energy (DOE) [300, 303]. The inverse availability factor $f_{\mathrm{HyPipe}}^{\mathrm{availability}}$ of 1.11 is adopted from a yearly availability of 90%, as presented in [299] (see section 5.3.4). Since the superconducting cable is assumed to have similar operation and maintenance costs as conventional underground cables (as considered by Kottonau et al. [251]), the maintenance downtime caused by the superconducting cable is lower than that caused by the liquid hydrogen pipeline (see section 5.3.3).

To determine the inverse loss factor $f_{\mathrm{HyPipe}}^{\mathrm{loss}}$, the losses caused by the superconducting cable and the liquid hydrogen pipeline are treated separately. A superconducting cable exhibits electromagnetic losses, such as hysteresis and Eddy-current losses [304]. Under DC operation, at a rated current I_A = 20 kA, and a minimum self-field critical current $I_{c,\mathrm{min}}$ = 25 kA, the electromagnetic losses are negligible compared with cryostat losses [211]. Therefore, it is assumed that the superconducting cable adds no losses to the hybrid pipeline ($f_{\mathrm{HyPipe,e}}^{\mathrm{loss}} = 1.0$).

Thermal losses through the cryostat are already accounted for in the thermal-hydraulic design, resulting in liquid hydrogen at a higher temperature than at the inlet of the hybrid pipeline. The temperature difference between liquid hydrogen products in each transmission alternative is neglected as a form of loss for simplicity; only hydrogen leakages are considered. An inverse loss factor for the liquid hydrogen pipeline $f_{\mathrm{HyPipe,t}}^{\mathrm{loss}}$ of 1.004 is derived from the expected mean hydrogen loss in gaseous transport pipelines: 0.7% in 2030 (Air Liquide) [305] and 0.04–0.48% in 2050 (Frazer-Nash Consultancy) [306] (see section 5.3.4). The combined value is:

$$f_{\mathrm{HyPipe}}^{\mathrm{loss}} = f_{\mathrm{HyPipe,e}}^{\mathrm{loss}} \cdot f_{\mathrm{HyPipe,t}}^{\mathrm{loss}} = 1.004 \tag{5.19}$$

A 40 year service life is assumed for the superconducting cable, following the assumptions in [251] for a superconducting transmission cable. Since ANL and DOE consider gaseous and liquid hydrogen pipelines equivalent in terms of reliability [300,303], the same 40 year lifetime is assigned to the liquid hydrogen pipeline, based on the studies of gaseous hydrogen pipelines from [52, 307, 308] (see section 5.3.4). Consequently, the lifetime of the hybrid pipeline τ_{HyPipe} is set to 40 years.

The yearly fixed operating expenditure of the hybrid pipeline $\mathrm{fixOPEX}_{\mathrm{HyPipe}}^{\mathrm{annual}}$ is given by equation 5.4. The operation and maintenance cost rate $\mathrm{O\&M}_{\mathrm{HyPipe}}$ is a percentage of the initial capital expenditures $\mathrm{CAPEX}_{\mathrm{HyPipe}}^{\mathrm{initial}}$ and is derived from:

$$\mathrm{O\&M}_{\mathrm{HyPipe}} = \frac{\mathrm{O\&M}_{\mathrm{HyPipe,e}} \cdot \mathrm{CAPEX}_{\mathrm{HyPipe,e}} + \mathrm{O\&M}_{\mathrm{HyPipe,t}} \cdot \mathrm{CAPEX}_{\mathrm{HyPipe,t}}}{\mathrm{CAPEX}_{\mathrm{HyPipe}}^{\mathrm{specific}}}, \tag{5.20}$$

where $O\&M_{HyPipe,e}$ and $O\&M_{HyPipe,t}$ are the operation and maintenance cost rates for the superconducting cable and the liquid hydrogen pipeline, respectively, and $CAPEX_{HyPipe,e}$ and $CAPEX_{HyPipe,t}$ are defined in equation 5.17. Following the argumentation in [251], the maintenance and repair costs are similar for superconducting cables and conventional underground cables. Because the losses are treated separately, the same operation and maintenance cost rate $O\&M_{HyPipe,e}$ of 3.34% is assumed for both conventional and superconducting cable technologies (see section 5.3.3). This value is the average of the rates presented in [309–311].

The ANL applies identical operation and maintenance cost rates to gaseous and liquid hydrogen pipelines. Their analysis focus on short-distance networks, such as refueling stations, liquid hydrogen terminals, and city-scale distribution [300]. In contrast, the case study Brunsbüttel–Hamburg proposes a 75 km long transmission pipeline, which entails stricter operation and maintenance requirements, e.g., the reuse of vacuum pumps (see section 4.3.5). This suggests higher operation and maintenance cost rates for longer lines. Therefore, the upper bound of the gaseous pipeline operation and maintenance cost rate is adopted for the cryogenic pipeline, giving $O\&M_{HyPipe,t} = 5.0\%$, as reported in [312] (see section 5.3.4).

Table 5.5 summarizes the techno-economic parameters for the hybrid pipeline.

Table 5.5: Techno-economic parameters for hybrid pipeline.

Parameter	Variable	Value	Source
Mean specific investment-cost estimate: hybrid pipeline alternative	$CAPEX^{specific}_{HyPipe}$	7.43 $MEUR_{2023}$ km^{-1}	Own calculation
Nominal size:	$S^{nominal}_{HyPipe}$	75 km	Own assumption
Mean specific investment-cost estimate: electrical equivalent	$CAPEX^{specific}_{HyPipe,e}$	1.44 $MEUR_{2023}$ GW_e^{-1} km^{-1}	Own calculation
Nominal size electrical equivalent	$S^{nominal}_{HyPipe,e}$	4.0 $GW_e \cdot 75$ km	Own assumption
Mean specific investment-cost estimate: chemical equivalent	$CAPEX^{specific}_{HyPipe,t}$	1.44 $MEUR_{2023}$ GW_t^{-1} km^{-1}	Own calculation

Continued on next page

Table 5.5: Techno-economic parameters for hybrid pipeline. (Continued)

Parameter	Variable	Value	Source
Nominal size: chemical equivalent	$S_{\mathrm{HyPipe,t}}^{\mathrm{nominal}}$	$1.15\ \mathrm{GW_t} \cdot 75\ \mathrm{km}$	Own assumption
Inverse availability factor	$f_{\mathrm{HyPipe}}^{\mathrm{availability}}$	1.11	[299]
Inverse loss factor	$f_{\mathrm{HyPipe}}^{\mathrm{loss}}$	1.004	[305, 306]
Lifetime	τ_{HyPipe}	40 a	[52, 251, 307, 308]
Operation and maintenance	$\mathrm{O\&M_{HyPipe}}$	3.71%	[309–312]

5.3.2 High-voltage Converter Stations

Several German and European public sources provide specific investment-cost estimates of high-voltage converter stations per $\mathrm{GW_e}$ (see figure 5.5). In Germany, the Network Development Plan (NEP) of 2023 [313] and 2021 [314] listed costs of voltage-source converters (VSC). The most recent report specified the use of onshore converter stations, the voltage level (320 kV or 525 kV), and whether the 525 kV converters include a DC circuit breaker and a dynamic braking system (DBS).

The European Ten-Year Network Development Plan 2024 (TYNDP) [315] and a 2023 report for the European Agency for the Cooperation of Energy Regulators (ACER) [316] presented specific investment-cost estimates of onshore converter stations announced by TSOs and project promoters, respectively. Both reports did not specify the voltage level or whether VSCs are considered. The ACER report presented the outcomes using the mean and quartiles as benchmark figures for the cost metrics.

A 2024 report of the *"Conseil International des Grands Réseaux Électriques"* (CIGRE) stated minimum and maximum specific investment-cost estimates for VSC and line-commutated converters (LCC), including installation, civil works, and project management, for the years 2014, 2020, 2030, 2040, and 2050 [317]. The data were adopted from the 2014 e-HIGHWAY study, which compiled costs from several older 2009–2013 studies [311]. For comparison with the VSC data from the NEP, figure 5.5 only presents the estimated costs for VSC from the e-HIGHWAY study.

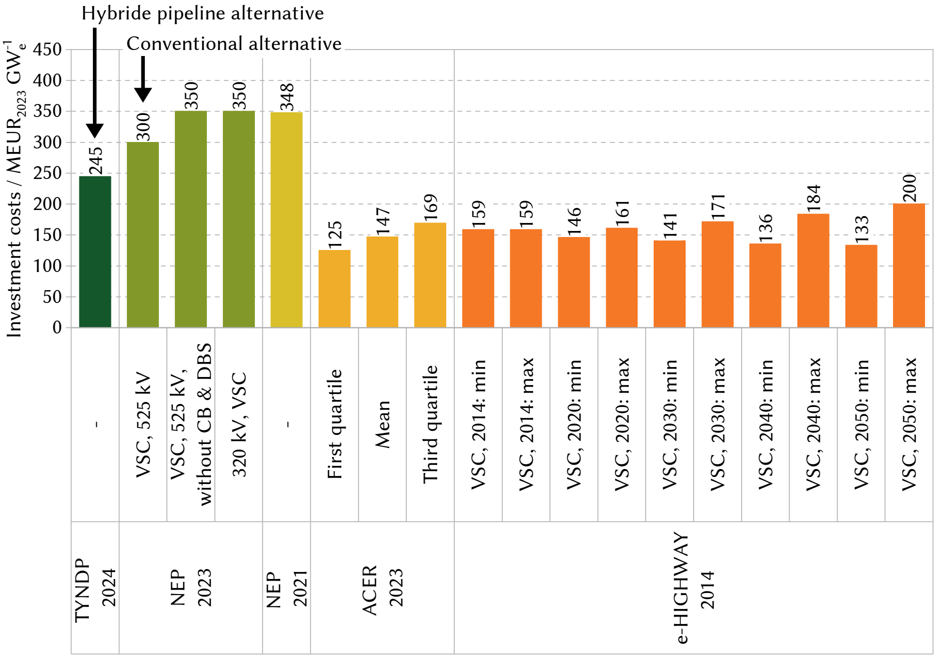

Figure 5.5: Specific investment costs of high-voltage, voltage-source converter (VSC) stations based on data from [311, 313–316]. The NEP 2023 source specifies when the converter does not include a breaker (CB) and a dynamic braking system (DBS) [313].

For the conventional alternative, the investment-cost estimates from the German NEP 2023 were used because the case study is located in Germany and assumes a voltage at ± 525 kV, as currently planned for extra-high-voltage DC underground cables (see section 2.6.1). Consequently, a specific investment cost of 300 $MEUR_{2023}$ GW_e^{-1}—including DC circuit breaker and DBS—is assumed.

For the hybrid pipeline alternative, the TYNDP source was adopted because the hybrid pipeline is designed for ±100 kV. The TYNDP did not specify the voltage level for which the converter units are designed, so the data is treated as a generic cost approximation applicable to different voltage categories. Moreover, converter stations at lower voltage levels are considerably smaller than those at higher voltages [318]. Hence, the converter stations in the hybrid pipeline alternative are estimated to cost 245 $MEUR_{2023}$ GW_e^{-1}. The investment costs are assumed to be equal in rectifier mode (AC/DC) and inverter mode (DC/AC).

CIGRE reported that the average unavailability of HVDC converter stations in more than 20 countries worldwide was 177 hours for the years 2017 and 2018 [319]. Related to 8 760 hours per year, this results in an inverse availability factor of approximately 1.02. CIGRE and Hofmann agree that HVDC converter stations have an efficiency of 99% [320,321], which is equivalent to an inverse loss factor of 1.01. CIGRE and Cabañas Ramos et al. estimated that the lifetime of HVDC converter stations is 25–30 years [322,323]. This work assumes a converter station lifetime of 30 years in accordance with the German TSO Amprion [324].

The operation and maintenance costs are estimated as 1.25% of the initial investment cost (see equation 5.4), after averaging the assumptions from the e-HIGHWAY study [311] and the German Energy Agency [325]. A summary of these parameters is presented in table 5.6.

Table 5.6: Techno-economic parameters for the HVDC converter stations.

Parameter	Variable	Value	Source
Specific investment-cost estimate: hybrid pipeline alternative	$\mathrm{CAPEX}_{\mathrm{converter}}^{\mathrm{specific}}$	245 $\mathrm{MEUR}_{2023}\ \mathrm{GW}_{\mathrm{e}}^{-1}$	[315]
Specific investment-cost estimate: conventional alternative	$\mathrm{CAPEX}_{\mathrm{converter}}^{\mathrm{specific}}$	300 $\mathrm{MEUR}_{2023}\ \mathrm{GW}_{\mathrm{e}}^{-1}$	[313]
Nominal size	$S_{\mathrm{converter}}^{\mathrm{nominal}}$	2 sides · 4.0 GW_{e}	Own assumption
Inverse availability factor	$f_{\mathrm{converter}}^{\mathrm{availability}}$	1.02	[319]
Inverse loss factor	$f_{\mathrm{converter}}^{\mathrm{loss}}$	1.01	[320, 321]
Lifetime	$\tau_{\mathrm{converter}}$	30 a	As reported in [322–324]
Operation and maintenance	$\mathrm{O\&M}_{\mathrm{converter}}$	1.25%	[311, 325]

5.3.3 HVDC Underground Cable Systems

The same reports that provided investment-cost estimates of high-voltage converter stations also give investment-cost estimates of HVDC underground cable systems per kilometer (see figure 5.6). However, only some sources specify the voltage level. The NEP 2023 considered both 320 kV and 525 kV cables. At the highest voltage level, cables with and without a metallic return are differentiated [313]. The 2023 report for ACER examined cables at 300–500 kV [316]. The e-HIGHWAY project listed only 320 kV cables [311].

Two further studies provided specific investment-cost estimates of HVDC underground cable systems. Vrana defined fixed, length-dependent, and power-dependent costs for 525 kV cables in Europe [326]. The 2023 European Pathway 2.0 project did not specify the voltage

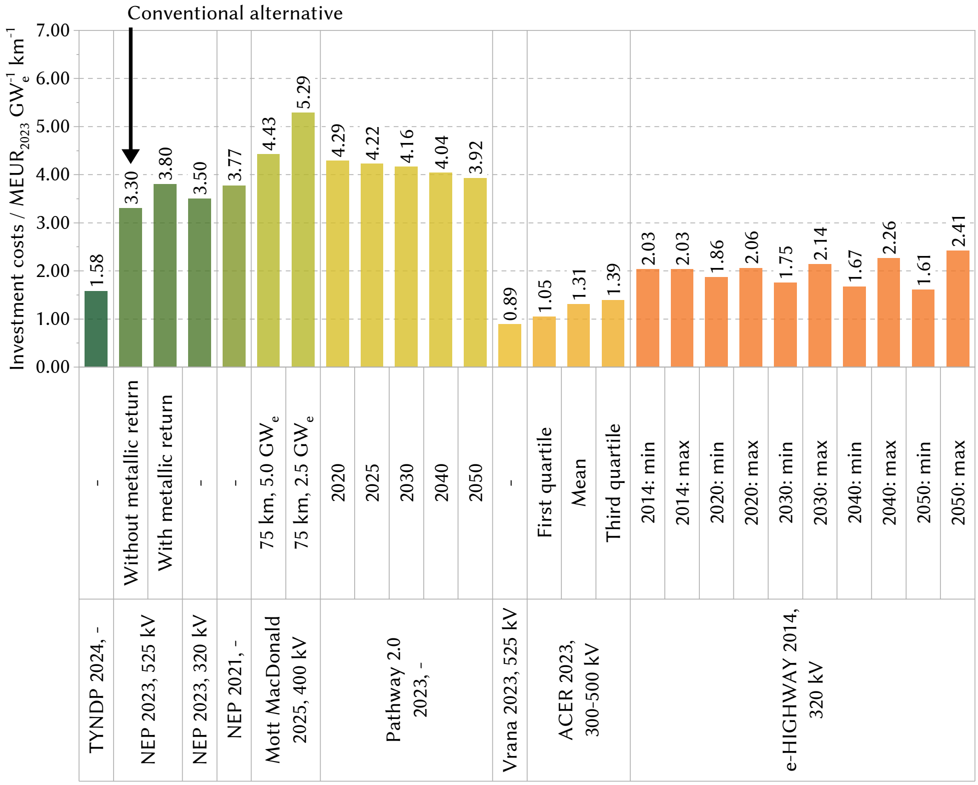

Figure 5.6: Investment-cost estimates of HVDC underground cable systems based on data from [309–311, 313–316, 326].

considered but listed specific investment costs of HVDC underground cables for the years 2020, 2025, 2030, 2040, and 2050 [310].

In 2025, Mott MacDonald and the Institution of Engineering and Technology (IET) published a comparison of electricity transmission technologies. Although the costs presented in this study are specially related to United Kingdom, figure 5.5 illustrates the investment-cost estimates for two different 75 km long, 400 kV, underground DC cable designs. The authors examined investment costs for transmission capacities of approximately 2.5 GW$_e$ and 5.0 GW$_e$, among others [309].

For the conventional alternative, the investment-cost estimates from the NEP 2023 are selected for two reasons. First, the NEP 2023 is a current German report. Second, the 525 kV cable without a metallic return corresponds to the HVDC underground cable design considered in this study (see section 2.6.1).

The technical unavailability of the HVDC underground cable is based on the data reported by CIGRE discussed in section 5.3.2 [319]. Under steady-state operation, the predominant losses in an HVDC cable are the Joule losses. The Prysmian Group, a manufacturer of HVDC cables, specifies an Ohmic resistance of 0.0060 Ohm km^{-1} for 525 kV DC cables [327]. However, this value applies at 20 °C. HVDC cables reach a temperature of 90 °C under operating conditions [328]. With a nominal copper cross-section of 3 000 mm^2 [329], the Ohmic resistance at 90 °C is 0.0073 Ohm km^{-1} per pole [50]. Therefore, four poles produce total power losses of approximately 106 kW$_e$ km^{-1} at the rated current of 1 GW per pole. Because HVDC cables rarely operate at a constant 100% load, assuming a 50% load results in total power losses of 26.5 kW$_e$ km^{-1}. In the 75 km long cable system of the conventional alternative, this leads to an efficiency of 99.95% and an inverse loss factor of 1.00.

The German Federal Network Agency [9] and Gatermann [330] estimate the lifetime of an HVDC underground at 40 years. The estimated operation and maintenance cost of 3.34% is an average of the percentages presented by the e-HIGHWAY (0.2%) and Pathway 2.0 projects (1.5%), and by the United Kingdom study by Mott MacDonald and IET (8.3%). A summary of the techno-economic parameters is presented in table 5.7.

Table 5.7: Techno-economic parameters for the HVDC underground cable systems.

Parameter	Variable	Value	Source
Specific investment-cost estimate: conventional alternative	$\mathrm{CAPEX}^{\mathrm{specific}}_{\mathrm{HVDCcable}}$	3.30 MEUR$_{2023}$ GW$_e^{-1}$ km^{-1}	[313]
Nominal size	$S^{\mathrm{nominal}}_{\mathrm{HVDCcable}}$	4.0 GW$_e$ · 75 km	Own assumption
Inverse availability factor	$f^{\mathrm{availability}}_{\mathrm{HVDCcable}}$	1.02	[319]
Inverse loss factor	$f^{\mathrm{loss}}_{\mathrm{HVDCcable}}$	1.00	Own calculation
Lifetime	$\tau_{\mathrm{HVDCcable}}$	40 a	As reported in [9, 330]
Operation and maintenance	$\mathrm{O\&M}_{\mathrm{HVDCcable}}$	3.34%	[309–311]

5.3.4 Gaseous Hydrogen Pipeline

Numerous reports have published specific investment-cost estimates of newly-built gaseous hydrogen pipelines per kilometer. Compressor costs are not included and will be treated in the next section. The pipe costs vary with the pipeline diameter, as can be seen in figure 5.7. The literature review includes investment-cost data from German projects that are part of the hydrogen core network (see figure A.1) [331], the EHB initiative section 2.6.2) [58], the European TYNDP 2024 [315], the U.S. American DOE [332], and multiple other scientific publications [213, 288, 290, 299, 312, 333–335].

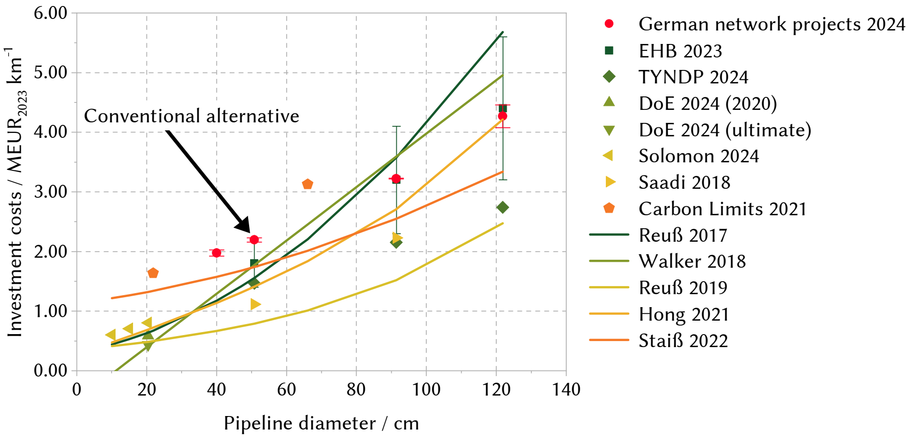

Figure 5.7: Investment-cost estimates of new gaseous hydrogen pipelines based on data from [58, 213, 288, 290, 299, 312, 315, 331–335].

Although all sources show a clear trend of higher cost estimates per kilometer for larger pipe diameters, the cost values for a given diameter vary widely. The larger the diameter, the greater the variation among sources. The EHB initiative reflected this uncertainty by specifying the standard deviation of its mean approximations. The standard deviation is presented as error bars in figure figure 5.7.

The German network projects include five lines in several federal states, with lengths between 6–120 km and a pipeline diameter of DN 500 [331], which is comparable to the diameter of the proposed hybrid pipeline. For the conventional alternative, the investment-cost estimates from the German network projects have been selected because they most closely resemble the proposed case study. This leads to optimistic (2.16 $MEUR_{2023}$ km^{-1}), mean (2.19 $MEUR_{2023}$ km^{-1}), and pessimistic (2.24 $MEUR_{2023}$ km^{-1}) investment costs. The average investment-cost estimates are presented as a red dot, and the standard deviation as red error bars. It is remarkable that the costs from this source are the highest for pipe diameters of approximately 50 cm. According to The Danish Energy Agency, the costs in Germany are slightly higher than in other European countries, probably owing to overhead costs additional to the installation [336].

In this work, the commonly reported unit EUR km^{-1} for the investment-cost estimates of gaseous hydrogen pipelines is replaced by EUR GW_t^{-1} km^{-1}. This allows a direct integration into the methodology presented in section 5.2 and a comparison with the other transmission alternatives. Considering a pipeline diameter of DN 500 (∼50 cm), an operating pressure of 50 bar, and a maximum capacity of 1.15 GW_t, the optimistic, mean, and pessimistic cost estimates become 1.88, 1.91, and 1.95 EUR_{2023} GW_t^{-1} km^{-1}, respectively.

Table 5.8 presents the techno-economic parameters used for the gaseous hydrogen pipelines. The inverse availability factor of 1.11 is based on a yearly availability of 90%, as proposed by Solomon et al. [299]. The average percentage of hydrogen leakage in transmission pipelines determines the inverse loss factor of 1.004, as estimated by Air Liquide (0.7% losses in 2030) [305] and the Frazer-Nash Consultancy (0.04–0.48% losses in 2050) [306]. The EHB initiative [307], Staiß et al. [52], and the IEA [308] expected a lifetime of 40 years for gaseous hydrogen pipelines.

The range of operation and maintenance costs estimated in the literature reflects the uncertainty in the associated costs. The five German network projects estimated operation and maintenance costs at 0.82% of initial investment costs, similar to the EHB initiative (0.9%), while Solomon et al., Reuß et al., and Walker et al. reported values of 2.6%, 4.0%, and 5.0%, respectively. Table 5.8 presents an average of these operation and maintenance cost estimates.

Table 5.8: Techno-economic parameters for gaseous hydrogen pipelines.

Parameter	Variable	Value	Source
Mean specific investment-cost estimate: conventional alternative	$CAPEX_{GH2pipe}^{specific}$	1.91 $MEUR_{2023}$ GW_t^{-1} km^{-1}	[331]
Nominal size	$S_{GH2pipe}^{nominal}$	1.15 $GW_t \cdot 75$ km	[307]
Inverse availability factor	$f_{GH2pipe}^{availability}$	1.11	[299]
Inverse loss factor	$f_{GH2pipe}^{loss}$	1.004	[305, 306]
Lifetime	$\tau_{GH2pipe}$	40 a	As reported in [52, 307, 308]
Operation and maintenance	$O\&M_{GH2pipe}$	2.66%	[290, 299, 307, 312, 331]

5.3.5 Gaseous Hydrogen Compressor

Multiple reports that published investment-cost estimates of gaseous hydrogen pipelines also provided investment-cost estimates of compressors. The costs are often dependent on the electrical power rating of the compressor P_{e}, which is directly related to the required shaft power P_{sh}, as will be discussed in this section.

The shaft power is the mechanical power rating of the compressor and is given in $\mathrm{MW_{sh}}$. This section explains how to calculate the electrical power rating P_{e} and the shaft power P_{sh} required for the pressure increase in the conventional alternative. Gaseous hydrogen coming from the conventional pipeline should be compressed to a storage pressure p_{GH2stor} of 100 bar (10 000 kPa) (see figure 5.3).

Compressor Inlet Pressure, Shaft Power, and Electrical Power Rating

The shaft power depends on the pressure difference between the inlet and outlet of the compressor. Therefore, the outlet pressure of gaseous hydrogen from the conventional pipeline must be known. The Darcy-Weisbach equation can be used to calculate the pressure drop over the transmission length ℓ of 75 km [337]:

$$\frac{p_{\mathrm{GH2pipe}} - p_{\mathrm{compres}}}{\ell} = \zeta_{\mathrm{GH2}} \cdot \frac{\bar{\rho}_{\mathrm{GH2}}}{2} \cdot \frac{\nu_{\mathrm{GH2}}^2}{D_{\mathrm{GH2}}}, \tag{5.21}$$

where p_{GH2pipe} is the inlet (operating) pressure of the gas pipeline (50 bar = 5 000 kPa), p_{compres} is the outlet pressure of the gas pipeline and simultaneously the inlet pressure of the compressor, ζ_{GH2} is the friction factor, $\bar{\rho}_{\mathrm{GH2}}$ is the average gas density, ν_{GH2} is the gas velocity, and D_{GH2} is the diameter of the conventional pipe (50 cm).

The friction factor ζ_{GH2} can be calculated with the Colebrook-White implicit equation (see equation 4.22), substituting the hydraulic diameter D_h with the conventional pipe diameter D_{GH2}:

$$\frac{1}{\sqrt{\zeta_{\mathrm{GH2}}}} = -2 \cdot \log\left(\frac{\epsilon}{3.7 \cdot D_{\mathrm{GH2}}} + \frac{2.51}{Re_{\mathrm{GH2}} \cdot \sqrt{\zeta_{\mathrm{GH2}}}}\right). \tag{5.22}$$

The surface roughness ϵ of the conventional pipe is assumed to be the typical roughness of commercial steel pipes, which is 0.046 mm (see section 4.3.1).

The Reynolds number Re_{GH2} for the friction factor ζ_{GH2} is determined as in equation 4.23, but replacing the liquid hydrogen parameters with gaseous hydrogen parameters, that is:

$$Re_{\mathrm{GH2}} = \frac{\nu_{\mathrm{GH2}} \cdot D_{\mathrm{GH2}} \cdot \bar{\rho}_{\mathrm{GH2}}}{\bar{\mu}_{\mathrm{GH2}}} \quad \text{with} \quad \nu_{\mathrm{GH2}} = \frac{\dot{m}_{\mathrm{GH2}}}{\bar{\rho}_{\mathrm{GH2}} \cdot A_{\mathrm{GH2pipe}}}, \tag{5.23}$$

where $\bar{\mu}_{\mathrm{GH2}}$ is the average gas viscosity and A_{GH2pipe} is the pipeline cross-section. It is assumed that the gas mass flow $\dot{m}_{\mathrm{GH2}}$ equals the liquid hydrogen mass flow $\dot{m}_{\mathrm{LH2}}$ in the hybrid pipeline alternative, i.e., 4.6–9.7 $\mathrm{kg_{H2}\ s^{-1}}$.

The average values of the gas density $\bar{\rho}_{\mathrm{GH2}}(\bar{T}_{\mathrm{GH2}}, \bar{p}_{\mathrm{GH2}})$ and the gas viscosity $\bar{\mu}_{\mathrm{GH2}}(\bar{T}_{\mathrm{GH2}}, \bar{p}_{\mathrm{GH2}})$ are obtained using by taking the arithmetic average of the inlet and outlet gas pressures $\bar{p}_{\mathrm{GH2}}$, which is determined using the same iteration method as in section 4.3.1. For simplicity, the gas temperature T_{GH2} is assumed to be constant at 283.15 K throughout the conventional pipeline. This assumption is reasonable because pipelines are typically buried 1–2 m below ground, where the soil temperature remains stable.

Equation 5.21 is solved using the values for ℓ, D_{GH2}, ϵ, and $\dot{m}_{\mathrm{GH2}}$. For $\bar{\rho}_{\mathrm{GH2}}$ and $\bar{\mu}_{\mathrm{GH2}}$, normal-hydrogen data values are used [50]. The resultant pressure drop between the inlet pressure p_{GH2pipe} and the outlet pressure p_{compres} of the gas pipeline is 1.2 bar (117.9 kPa) at a mass flow $\dot{m}_{\mathrm{GH2}}$ of 4.6 $\mathrm{kg_{H2}\ s^{-1}}$ and 5.8 bar (580.4 kPa) at 9.7 $\mathrm{kg_{H2}\ s^{-1}}$. Table 5.9 summarizes the assumptions and results for the pressure drop calculations.

Table 5.9: Assumptions and results for gaseous hydrogen pressure drop calculations.

Parameter	Symbol	Value
	Assumptions	
Gas temperature	T_{GH2}	283.15 K
Gas mass flow	$\dot{m}_{\mathrm{GH2}}$	4.6–9.7 $\mathrm{kg_{H2}\ s^{-1}}$
Gas pipeline inlet pressure	p_{GH2pipe}	50 bar (5 000 kPa)
Gas pipeline diameter	D_{GH2}	50 cm
Gas pipeline length	ℓ	75 km
Surface roughness	ϵ	0.046 mm
	Results	
Oulet pressure from gas pipeline and inlet pressure for compressor	p_{compres}	48.8–44.2 bar (4 882–4 420 kPa)

Once the inlet pressure of the compressor p_{compres} is obtained, the shaft power P_{sh} can be determined assuming a polytropic process (which is closer to real conditions than isothermal or adiabatic processes) [338]:

$$P_{\text{sh}} = \frac{1}{\eta_{\text{poly}}} \cdot \dot{m}_{\text{GH2}} \cdot \bar{Z} \cdot \frac{\text{R}}{M_{\text{H2}}} \cdot \frac{n_{\text{poly}}}{n_{\text{poly}} - 1} \cdot \left[\left(\frac{p_{\text{GH2stor}}}{p_{\text{compres}}} \right)^{\left(\frac{n_{\text{poly}} - 1}{n_{\text{poly}}} \right)} - 1 \right]. \tag{5.24}$$

Here, η_{poly} is the polytropic efficiency, $\bar{Z}$ is the average compressibility factor, R = 8.314 J mol^{-1} K^{-1} is the universal gas constant, M_{H2} = 2.016 kg$_{\text{H2}}$ kmol^{-1} is the molar mass of hydrogen [50], n_{poly} is the polytropic coefficient, and p_{GH2stor} is the storage pressure (100 bar = 10 000 kPa).

To simplify the analysis, the polytropic efficiency η_{poly} and coefficient n_{poly} are assumed to be 85% [339] and 1.33 [340], respectively. In a more detailed investigation, these parameters would be specific to the compressor type and manufacturer. The average compressibility factor $\bar{Z}$ is computed as the arithmetic mean of the inlet compressibility $Z_{\text{in}}(T_{\text{GH2}}, p_{\text{compres}})$ and the outlet compressiblity $Z_{\text{out}}(T_{\text{discharge}}, p_{\text{GH2stor}})$, using data from [50]. The discharge temperature $T_{\text{discharge}}$ follows from the polytropic compression relationship [341]:

$$\frac{T_{\text{discharge}}}{T_{\text{GH2}}} = \left(\frac{p_{\text{GH2stor}}}{p_{\text{compres}}} \right)^{\left(\frac{n_{\text{poly}} - 1}{n_{\text{poly}}} \right)}. \tag{5.25}$$

Equation 5.24 leads then to a shaft power P_{sh} of 12.6 MW$_{\text{sh}}$ at a mass flow $\dot{m}_{\text{GH2}}$ of 9.7 kg$_{\text{H2}}$ s^{-1} and 5.2 MW$_{\text{sh}}$ at 4.6 kg$_{\text{H2}}$ s^{-1}. The electrical power rating P_{e} can then be obtained as [213]:

$$P_{\text{e}} = \frac{P_{\text{sh}}}{\eta_{\text{mech}} \cdot \eta_{\text{e}}}, \tag{5.26}$$

where η_{mech} = 95% is the mechanical efficiency of the compressor and η_{e} is the electrical efficiency given by the empirically derived scaling function [213]:

$$\begin{aligned} \eta_{\text{e}} = 8 \cdot 10^{-5} \cdot x^4 - 0.0015 \cdot x^3 + 0.0061 \cdot x^2 + 0.0311 \cdot x + 0.7617, \\ \text{with } x = \log(P_{\text{sh}}). \end{aligned} \tag{5.27}$$

Solving equations 5.26 and 5.27 gives an electrical power rating P_{e} of 13.6 MW$_{\text{e}}$ when the maximum mass flow $\dot{m}$ of 9.7 kg$_{\text{H2}}$ s^{-1} is considered. Table 5.10 summarizes the assumptions and results for the electrical power rating calculations.

Table 5.10: Assumptions and results for compressor electrical power rating calculations.

Parameter	Symbol	Value
Assumptions		
Gas mass flow	$\dot{m}_{\mathrm{GH2}}$	9.7 $\mathrm{kg_{H2}\ s^{-1}}$
Inlet pressure for compressor	p_{compres}	44.2 bar (4 420 kPa)
Polytropic efficiency	η_{poly}	85.0%
Polytropic coefficient	n_{poly}	1.33
Storage inlet pressure	p_{GH2stor}	100 bar (10 000 kPa)
Mechanical efficiency	η_{mech}	95.0%
Electrical efficiency	η_{e}	97.2%
Results		
Discharge temperature	$T_{\mathrm{discharge}}$	346.8 K
Average compressibility factor	$\bar{Z}$	1.04
Shaft power	P_{sh}	12.6 $\mathrm{MW_{sh}}$
Electrical power rating	P_{e}	13.6 $\mathrm{MW_{e}}$

Compressor Investment and Operating Costs

Figure 5.8 presents the absolute and specific investment-cost estimates of compressors as a function of the electrical power rating P_{e}. The dependency on the electrical power rating is defined differently by each reference.

The EHB initiative [58] expected a linear dependency, as can be seen in figure 5.8 (b). The TYNDP used the same data as the EHB initiative. Solomon et al. [299], Hong et al. [288], and Reuß et al. [213, 290] expected a scale-economy cost, adopting a power function with a concave curve. Walker et al. also expected a scale-economy cost but because of fixed-cost amortization [312]. Staiß et al. [335] provided investment-cost estimates for a single compressor unit with a rated throughput of 240 $\mathrm{t_{H2}\ d^{-1}}$. Figure 5.8 illustrates the data for Staiß et al. if it is assumed that multiple compressor trains can be used in series.

The comparison of references in figure 5.8 shows that for larger values of the electrical power rating P_{e}, the costs estimated by the EHB initiative are considerably larger than those adopted by the other references. A notable point is that the data from Staiß et al., Solomon et al., and Reuß et al. are assumed for Germany, while the data from Walker et al. and Hong et al. are assumed for the United Kingdom and Southeast Asian Nations, respectively.

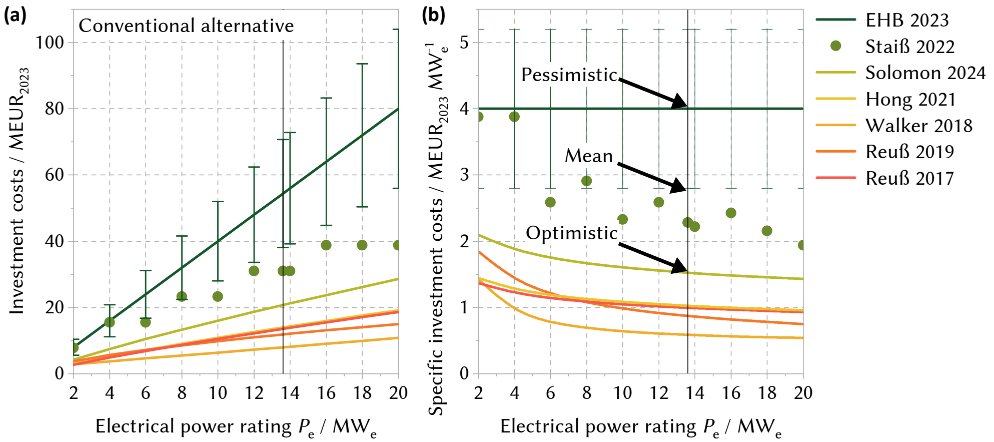

Figure 5.8: (a) Absolute and (b) specific investment-cost estimates of gaseous hydrogen compressors as a function of the electrical power rating. Based on data from [58, 213, 288, 290, 299, 312, 335].

Because of the large uncertainty in the range of investment-cost estimates, optimistic (1.52 $\mathrm{MEUR_{2023}\ MW_e^{-1}}$) and pessimistic cost values were assumed (4.00 $\mathrm{MEUR_{2023}\ MW_e^{-1}}$). The assumptions are based on the cost data from Solomon et al. and the EHB initiative, since the former focused on Germany and the latter aggregates information from multiple TSOs. Given a compressor capacity of 13.6 $\mathrm{MW_e}$, the mean investment-cost estimate for the conventional alternative is 37.57 $\mathrm{MEUR_{2023}}$.

The studies by Solomon et al. [299] and Hong et al. [288] reported availability factors of 90% for gaseous hydrogen compressors, resulting in an inverse availability factor of 1.11. An inverse loss factor of 1.005 is based on 5% hydrogen losses, as determined by Reuß et al. [213] and Hong et al. [288]. The EHB initiative estimated that a compressor with outlet pressures of 50–80 bar has a lifetime of 25 years [307], while Solomon et al. considered that compressors with outlet pressures of 70–540 bar have lifetimes of 15 years [299]. An average lifetime of 20 years is assumed in this work.

The estimated operation and maintenance costs differ among sources. Therefore, an average of 3.3% is adopted, given the values published by the EHB initiative (1.7%) [307], Staiß et al. (3.0%) [335], Reuß et al. (4.0%) [213], Hong et al. (4.0%) [288], and Solomon et al. (4.0%) [299].

To calculate the variable operating expenditures varOPEX, it should be noted that the compressor is used for the gaseous hydrogen storage, which is planned for security reasons only. It is assumed that the storage is used, for example, due to consumer-side outages or other constraints. Since the storage size is of 1 000 $\mathrm{t_{H2}}$, the tank is almost filled after 28 h when using the full pipeline mass flow of 35 $\mathrm{t_{H2}\ h^{-1}}$. Assuming that the storage tank is completely filled once per month (12 times per year), the annual operating hours of the compressor are 336 h.

Accordingly, the lower-bound variable annual operating expenditures can be calculated as [299]:

$$\mathrm{varOPEX}_{\mathrm{compres}}^{\mathrm{annual}} = S_{\mathrm{compres}}^{\mathrm{nominal}} \cdot t_{\mathrm{op,compres}} \cdot \kappa_{\mathrm{e}}, \tag{5.28}$$

where $S_{\mathrm{compres}}^{\mathrm{nominal}}$ is the nominal size of 13.6 $\mathrm{MW_e}$, $t_{\mathrm{op,compres}}$ are the annual operating hours, and κ_{e} is the electrical energy cost, as defined in section 5.2. Here, a lower-bound estimate of the electrical energy consumption at full-load operation is obtained by multiplying the electrical nominal size $S_{\mathrm{compres}}^{\mathrm{nominal}}$ by the annual operating time $t_{\mathrm{op,compres}}$.

Correspondingly, the lower-bound specific energy consumption $w_{\mathrm{e,compres}}$ is assumed to be 389.5 $\mathrm{kWh_e\ t_{H2}^{-1}}$ when dividing the nominal size $S_{\mathrm{compres}}^{\mathrm{nominal}}$ by the gas mass flow $\dot{m}_{\mathrm{GH2}}$ of approximately 35 $\mathrm{t_{H2}\ h^{-1}}$ (9.7 $\mathrm{kg_{H2}\ s^{-1}}$). The specific electrical energy consumption is of the same order of magnitude as the values reported by Staiß et al. (465.0 $\mathrm{kWh_e\ t_{H2}^{-1}}$) [335] and Hong et al. (570.0 $\mathrm{kWh_e\ t_{H2}^{-1}}$) [288].

A summary of the techno-economic parameters for the gaseous hydrogen compressor is presented in table 5.11.

Table 5.11: Techno-economic parameters for gaseous hydrogen compressors.

Parameter	Variable	Value	Source
Mean specific investment-cost estimate: conventional alternative	$\mathrm{CAPEX}_{\mathrm{compres}}^{\mathrm{specific}}$	2.76 $\mathrm{MEUR_{2023}\ MW^{-1}}$	[58, 299]
Nominal size	$S_{\mathrm{compres}}^{\mathrm{nominal}}$	13.6 $\mathrm{MW_e}$	Own calculation
Inverse availability factor	$f_{\mathrm{compres}}^{\mathrm{availability}}$	1.11	[288, 299]
Inverse loss factor	$f_{\mathrm{compres}}^{\mathrm{loss}}$	1.005	[213, 288]
Lifetime	τ_{compres}	20 a	[299, 307]
Operation and maintenance	$\mathrm{O\&M}_{\mathrm{compres}}$	3.3%	[213, 288, 299, 307, 335]
Annual operating hours	$t_{\mathrm{op,compres}}$	336 h	Own assumption
Electrical energy consumption	$w_{\mathrm{e,compres}}$	389.5 $\mathrm{kWh_e\ t_{H2}^{-1}}$	Own calculation

5.3.6 Gaseous Hydrogen Storage

Large-scale gaseous hydrogen storage systems are more cost-effective as caverns rather than as tanks [342]. However, cavern storage is geographically limited to locations with suitable conditions. In the conventional alternative, a gaseous hydrogen storage is proposed at the end of the gas pipeline, i.e., in Hamburg. Since no storage caverns exist in this area, the storage must consist of one or several tanks.

Several studies have estimated the investment costs of stationary gaseous hydrogen storage tanks [290, 342–344]. However, all of them derived their values from the U.S. American DOE [332] (see figure 5.9). The DOE estimated costs in USD_{2007} kg_{H2}^{-1} for two time horizons (2020 and "ultimate") and two pressure levels (160 bar or 430 bar). The "ultimate" target refers to long-term costs in a well-established hydrogen market.

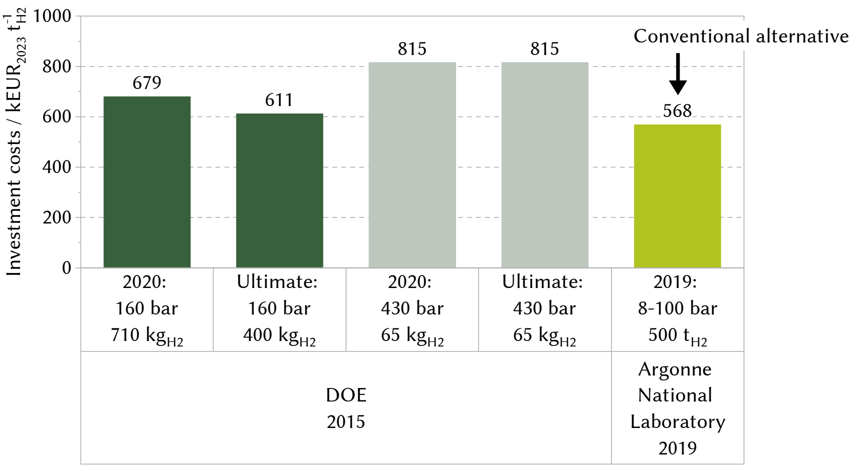

Figure 5.9: Investment-cost estimates of gaseous hydrogen storage tanks based on data from [332, 345].

At 160 bar, each tank has a storage size of 710 kg_{H2} for the 2020 horizon and 400 kg_{H2} for the ultimate target. The smaller ultimate tank size was chosen deliberately to reduce the cost per kilogram of stored gas. Tanks operating at 430 bar have a size of 65 kg_{H2} for both horizons [332]. Figure 5.9 clearly indicates that storage tanks are more cost-effective at 160 bar than at 430 bar because of the lower pressure requirements.

In 2019, the ANL presented 300 underground parallel-pipe tanks that can store 500 t_{H2} at operating pressures between 8–100 bar for a cost of 568 $kEUR_{2023}$ t_{H2}^{-1}. It is worth noting that, for this storage size, 450 000 m^2 ($\sim$110 acres) of land would be required [345]. The specific investment-cost estimate from ANL has been selected for the conventional alternative because it is the newest source and the storage size of 500 t_{H2} is closer to that proposed in this work (1 000 t_{H2}).

Table 5.12 outlines the techno-economic parameters for the gaseous hydrogen storage. As reported in [343], a stationary storage system is considered technically available on 350 days per year, resulting in an inverse availability factor of 1.043. The authors in [290, 342, 344] assumed 0.0% of hydrogen losses during storage, so the inverse loss factor is 1.00. In this work, a component lifetime of 30 years is assumed, as reported in [332,343,344]. The operation and maintenance cost rate of stationary gaseous hydrogen storage was identically defined as 2.0% by all authors in [290, 342, 344].

Table 5.12: Techno-economic parameters for gaseous hydrogen storage.

Parameter	Variable	Value	Source
Mean specific investment-cost estimate: conventional alternative	$\mathrm{CAPEX}_{\mathrm{GH2stor}}^{\mathrm{specific}}$	568 $\mathrm{kEUR}_{2023}\ t_{H2}^{-1}$	[345]
Nominal size	$S_{\mathrm{GH2stor}}^{\mathrm{nominal}}$	1 000 t_{H2}	Own assumption
Inverse availability factor	$f_{\mathrm{GH2stor}}^{\mathrm{availability}}$	1.043	[343]
Inverse loss factor	$f_{\mathrm{GH2stor}}^{\mathrm{loss}}$	1.00	[290, 342, 344]
Lifetime	τ_{GH2stor}	30 a	As reported in [332, 343, 344]
Operation and maintenance	$\mathrm{O\&M}_{\mathrm{GH2stor}}$	2.0%	As reported in [290, 342, 344]

5.3.7 Hydrogen Liquefier

Hydrogen liquefaction plants have been built since the late 1950s on an industrial scale (5–36 $t_{H2}\ d^{-1}$) [67]. As of May 2024, the USA possessed a total hydrogen liquefaction capacity of 794 $t_{H2}\ d^{-1}$ [346]. Other countries, such as Canada, France, Germany, the Netherlands, Russia, Japan, India, South Korea, China, and Australia, also have industrial or small liquefaction plants (0.3–3.4 $t_{H2}\ d^{-1}$) [67].

In 2024, South Korean SK E&S announced the completion of the world's largest hydrogen liquefaction plant, according to its own statements. The liquefier has a yearly capacity of 30 000 t_{H2} (approximately 82 $t_{H2}\ d^{-1}$) and occupies about 50 000 m^2 (12 acres) of land [347, 348]. In the USA, 145 t_{H2} d^{-1} of additional liquefaction capacity was under construction in 2024, and a further 345 t_{H2} d^{-1} was in the planning stage [346]. The largest known conceptual design of a hydrogen liquefaction plant has a capacity of 864 t_{H2} d^{-1} [66]. In this work, a liquefier capacity of 838 t_{H2} d^{-1} is required in the conventional alternative to supply the same amount of liquid hydrogen as in the hybrid pipeline alternative (see figure 5.2).

A relatively large number of studies have estimated the investment costs of hydrogen liquefiers, as can be seen in figure 5.10. Many of those studies [69, 290, 342, 349–351] derived their estimates from one or two primary sources: the 2006-present U.S. American *Hydrogen Delivery Scenario Analysis Model (HDSAM)* from the ANL [300], and the 2013 European project *Integrated Design for Demonstration of Efficient Liquefaction of Hydrogen (IdealHy)* [68]. Other reports—IEA [308, 352], DNV [353], DOE [332], Air Liquide [354], and Sadler et al. [355]—published their own investment-cost estimates. IRENA reviewed several of the references in 2022 [356].

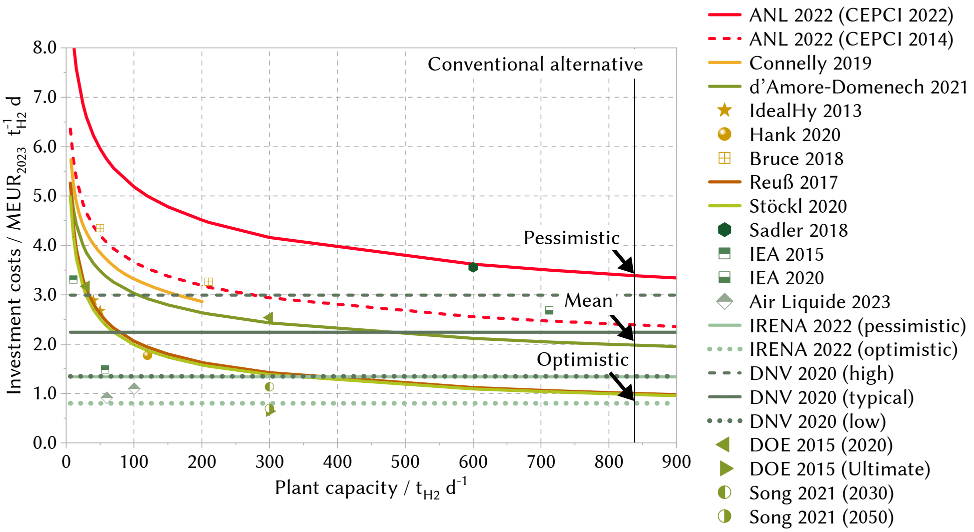

Figure 5.10: Investment-cost estimates of liquefaction plants based on data from [68, 69, 290, 300, 308, 332, 342, 344, 349–356]. The vertical line presents the required plant capacity in the conventional alternative of 838 t_{H2} d^{-1} and the selected optimistic, mean, and pessimistic specific investment costs.

Figure 5.10 presents the specific investment-cost estimates in $MEUR_{2023}$ t_{H2}^{-1} d as a function of the plant capacity in t_{H2} d^{-1}. Larger hydrogen liquefaction plants benefit from economies of scale, as shown by the ANL data [300] and other studies that used this dataset. IRENA noted that plants with a single liquefaction unit (train) are unlikely to exceed capacities of 200 t_{H2} d^{-1}

because the coldbox would reach its maximum practical dimensions for transport [356]. Most references, however, provide investment-cost estimates above this capacity limit.

The ANL defined a cost function dependent on the Chemical Engineering Plant Cost Index (CEPCI), a tool used to adjust process-construction costs from one year to another [300]. Figure 5.10 shows ANL results for CEPCI values in 2014 and 2022. Connelly et al. [349] and d'Amore-Domenech et al. [350] estimated liquefier investment costs based on the ANL data. Hank et al. [69] and Bruce et al. [351] based their estimations on the results from *IdealHy* [68], although Bruce et al. reported costs close to those from ANL. Reuß et al. [290] and Stöckl et al. [342] combined the datasets of both ANL and *IdealHy*, producing a curve similar to ANL's but with lower specific investment costs.

In the conventional alternative with liquid hydrogen as the final product, 838 t_{H2} d^{-1} (1.15 GW_t) must be liquefied after gaseous transmission. The vertical line in figure 5.10 illustrates that, at this plant capacity, the expected specific investment costs range from 0.8 to 3.4 $MEUR_{2023}$ t_{H2}^{-1} d. Because of this large uncertainty, optimistic, average, and pessimistic investment-cost values were selected. The optimistic value is 0.8 $MEUR_{2023}$ t_{H2}^{-1} d from IRENA [356]. The pessimistic value is 3.4 $MEUR_{2023}$ t_{H2}^{-1} d from ANL with CEPCI 2022 [300]. The arithmetic mean value is 2.1 $MEUR_{2023}$ t_{H2}^{-1} d.

Table 5.13 presents the techno-economic parameters for the hydrogen liquefier. The *IdealHy* study reported that a large-scale liquefaction plant is technically available for 8 000 h a^{-1} (91% of a year) [68], which is similar to the availability of 92% per year published in [351]. An average of both values leads to an inverse availability factor of 1.091.

Table 5.13: Techno-economic parameters for hydrogen liquefier.

Parameter	Variable	Value	Source
Mean specific investment-cost estimate: conventional alternative	$\mathrm{CAPEX}_{\mathrm{liquefi}}^{\mathrm{specific}}$	2.1 $MEUR_{2023}$ t_{H2}^{-1} d	[300, 356]
Nominal size	$S_{\mathrm{liquefi}}^{\mathrm{nominal}}$	838 t_{H2} d^{-1}	Own assumption
Inverse availability factor	$f_{\mathrm{liquefi}}^{\mathrm{availability}}$	1.091	[68, 351]
Inverse loss factor	$f_{\mathrm{liquefi}}^{\mathrm{loss}}$	1.012	[68, 290, 344, 356]
Lifetime	τ_{liquefi}	36 a	[68, 300, 349, 351, 352]
Operation and maintenance	$\mathrm{O\&M}_{\mathrm{liquefi}}$	4.0%	As reported in [68, 308, 342, 356]
Electrical energy consumption	$w_{\mathrm{e,liquefi}}$	6.76 MWh_e t_{H2}^{-1}	As reported in [68]

The authors of *IdealHy* estimated that hydrogen losses during the liquefaction process account for 1.63% of the produced hydrogen [68]. In comparison, IRENA considered that 0.0% hydrogen losses are possible in the long term [356]. The authors in [290, 344] derived hydrogen-loss data from other reports and assumed a value of 1.65 %. In this work, an average of all previous values is used for an inverse loss factor of 1.012.

Connelly et al., Bruce et al., and the ANL determined the liquefier lifetime as 40 years [300, 349, 351], while the IEA and *IdealHy* expected a component lifetime of 30 years [68, 352]. An average of the discussed values gives a liquefier lifetime of 36 years. The operation and maintenance costs are uniformly reported as 4.0% of the initial investment costs in [68, 308, 342, 356].

Multiple studies have reported specific energy consumption values between 6.4 $MWh_e\ t^{-1}_{H2}$ and 15.0 $MWh_e\ t^{-1}_{H2}$ for hydrogen liquefaction [64]. Assuming optimistic efficiency progress in the long term, the value of 6.76 $MWh_e\ t^{-1}_{H2}$ (including ancillary units) from the *IdealHy* project is adopted for this work. *IdealHy* also quantified the water consumption for cooling during the liquefaction process as 15.0 $m^3_{H2O}\ t^{-1}_{H2}$. However, the variable operation costs caused by water consumption are neglected in this work because of their much lower magnitude compared to electrical energy consumption costs [68].

5.3.8 Liquid Hydrogen Storage

Thermally insulated storage tanks constitute a mature technology for transporting liquid hydrogen by trailer, with typical capacities of 125 m^3. These tanks are also employed in stationary industrial applications, with commercially available capacities up to 400 m^3 [357]. Using the density of para-hydrogen at 20.0 K and 100 kPa (1.0 bar) as $\rho_{paraH2} = 71.144\ kg_{H2}\ m^{-3}$ [50], the corresponding payloads are approximately 8.9 t_{H2} and 28.5 t_{H2}, respectively. This density is used converting between metric tons of liquid hydrogen and cubic meters in this section.

Larger cryogenic storage tanks are required for bulk transport of liquid hydrogen. As a part of the Japanese *HySTRA* project, Kawasaki Heavy Industries obtained the approval in principle for a carrier with four single spherical tanks, each with a storage capacity of 40 000 m^3 ($\sim$2 800 t_{H2}), and a total capacity of 160 000 m^3 ($\sim$11 400 t_{H2}) [358]. In 2025, CB&I, Shell, and NASA built the first 100 000 m^3 ($\sim$7 100 t_{H2}) stationary liquid-hydrogen storage tank for international-trade applications [359]. In 2023, the consortium expected that the cost for a storage tank of this size would be less than 22.7 $kEUR_{2023}\ t^{-1}_{H2}$ (24.6 $kUSD_{2023}\ t^{-1}_{H2}$ or 175 $MUSD_{2023}$) [360].

Figure 5.11 presents specific investment-cost estimates of liquid hydrogen storage tanks with capacities up to 7 200 t_{H2}. Some authors—DNV [353], Song et al. [344], and Stöckl et al. [342]—assumed linear investment costs. Reuß et al. [290], Stöckl et al. [342], and Hank et al. [69] derived their calculations from U.S. American DOE data [332]. In contrast, ANL [300] and IRENA [356] expected a scale-economy cost (ANL due to fixed-cost amortization; IRENA because of a scaling exponent equal to 0.67). d'Amore-Domenech et al. [350] anticipated diseconomies of scale, that is, per-unit costs increase with storage capacity owing to a scaling exponent equal to 1.344.

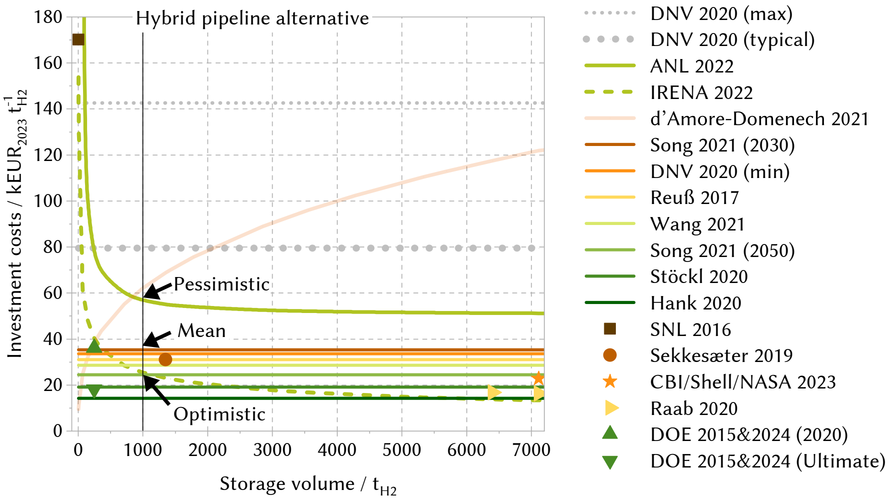

Figure 5.11: Investment costs of liquid hydrogen storage tanks based on data from [53, 69, 285, 289, 290, 300, 332, 342, 344, 350, 353, 356, 360–362]. The vertical line presents the storage capacity in the hybrid pipeline alternative of 1 000 t_{H2} and the selected optimistic, mean, and pessimistic specific investment costs.

The U.S. American Sandia National Laboratory (SNL) estimated high investment costs of 170 kEUR$_{2023}$ t_{H2}^{-1} for a relatively small tank of 61 m^3 (4.3 t_{H2}). A comparison with the estimated costs of the 100 000 m^3 (~7 080 t_{H2}) stationary liquid-hydrogen storage tank of 22.7 kEUR$_{2023}$ t_{H2}^{-1} from CBI, Shell, and NASA suggests that investment costs per unit decrease at larger capacities. Therefore, economies of scale appear to be more probable than diseconomies of scale.

For a storage capacity of 1 000 t_{H2} in the hybrid pipeline alternative, optimistic, mean, and pessimistic investment costs of 25.5 kEUR$_{2023}$ t_{H2}^{-1}, 39.2 kEUR$_{2023}$ t_{H2}^{-1}, and 56.8 kEUR$_{2023}$ t_{H2}^{-1} were selected, respectively. This selection reflects the large uncertainty in the investment-cost estimations. The selected values can be seen in figure 5.11.

Table 5.14 introduces the techno-economic parameters for the liquid hydrogen storage. Since the technical operational availability of stationary storage tanks is rarely reported, an approximate annual availability can be adopted from gaseous hydrogen storage tanks—namely 96% of the year (see section 5.3.6). This yields an inverse availability factor of 1.043.

The inverse loss factor is derived from the liquid hydrogen boil-off rate, which results from heat transfer through the thermal insulation. For cryogenic liquid hydrogen storage tanks, increasing the storage volume reduces the surface-to-volume ratio, thereby lowering relative heat ingress and boil-off losses [67]. The boil-off rate of large tanks ($>$ 40 t_{H2} [284]) with standard thermal insulation is less than 0.05% per day [285].

Since the liquid hydrogen storage is planned for security reasons only (see figure 5.2), it is assumed that the tank operates 336 hours (14 days) per year (see section 5.3.5). Assuming a conservative boil-off rate of 0.05% per day, a total of 0.7% of the liquid hydrogen would be boiled off annually. Additionally, to keep large cryogenic spherical tanks (40 000 $m^3 \approx$ 2 800 t_{H2}) sufficiently cold and avoid active re-cooling, a minimum fill level (heel) of approximately 5% of the liquid hydrogen is required [363]. Considering both the boil-off rate and the heel results in an inverse loss factor of 1.060.

The ANL expected that a liquid-hydrogen storage tank has a lifetime of 30 years, while Song et al. assumed a lifetime of 20 years. In this work, an average lifetime of 25 years is assumed. All authors in [53, 290, 342, 344, 353] considered the operation and maintenance costs of liquid hydrogen storage to be 2% of the initial investment cost.

Table 5.14: Techno-economic parameters for liquid hydrogen storage.

Parameter	Variable	Value	Source
Mean specific investment-cost estimate: hybrid pipeline alternative	$\mathrm{CAPEX}^{\mathrm{specific}}_{\mathrm{LH2stor}}$	39.2 kEUR_{2023} t_{H2}^{-1}	[300, 356]
Nominal size	$S^{\mathrm{nominal}}_{\mathrm{LH2stor}}$	1 000 t_{H2}	Own assumption
Inverse availability factor	$f^{\mathrm{availability}}_{\mathrm{LH2stor}}$	1.043	[343]
Inverse loss factor	$f^{\mathrm{loss}}_{\mathrm{LH2stor}}$	1.060	[67, 284, 285, 363]
Lifetime	τ_{LH2stor}	25 a	[300, 344]
Operation and maintenance	$\mathrm{O\&M}_{\mathrm{LH2stor}}$	2.0%	As reported in [53, 290, 342, 344, 353]
Annual operating hours	$t_{\mathrm{op,LH2stor}}$	336 h	Own assumption

5.3.9 Liquid Hydrogen Pump

A cryogenic pump transfers liquid hydrogen by creating a pressure difference that yields the required mass flow rate. The differential pressure is commonly expressed in bar, or as total head in meters of fluid column. Head and pressure are related by:

$$\Delta p = \rho_{\text{paraH2}} \cdot \text{g} \cdot H, \tag{5.29}$$

where Δp is the differential pressure in pascal, g is the gravitational acceleration (9.80665 m s^{-2}), and H is the total head in meters. The density ρ_{paraH2} is considered to be that of para-hydrogen at 20.0 K and 100 kPa (1 bar), that is, 71.144 kg$_{\text{H2}}$ m^{-3} [50].

Usually, centrifugal pumps or pistons move the liquid inside a thermally insulated vessel. Pumps for liquid hydrogen fueling stations handle relatively low volumes, for example 0.2 t$_{\text{H2}}$ h^{-1} with a differential pressure of 900 bar [364] or 0.5 t$_{\text{H2}}$ h^{-1} with a differential pressure of 16 bar [365]. Transfer pumps for international-trade terminals transport significantly larger volumes. Commercially available transfer pumps move 27–50 t$_{\text{H2}}$ h^{-1} with a differential pressure of 1.8–1.3 bar [366]. In the future, transfer pumps with flow rates of 231 t$_{\text{H2}}$ h^{-1} and a 2 bar pressure increase are expected [367].

Transfer pumps necessitate motors with higher power capacities, thereby producing significant amounts of heat, which causes boil-off losses. A recent preprint from SINTEF Energy Research reported boil-off losses ranging from 0.76% to 1.06% of the stored liquid hydrogen mass (up to 119 t$_{\text{H2}}$ of a 160 000 m^3 liquid hydrogen carrier) when using a fixed-speed pump. A pump with a variable speed drive and a hydraulic efficiency of 70% achieved losses of 0.0–0.24% [367]. A newer development are superconducting hydrogen pumps, which operate with negligible thermal losses at mass flow rates of, for example, 50 t$_{\text{H2}}$ h^{-1} with a differential pressure of 3.6 bar [368].

A review of the literature indicated that only two original studies have reported first-hand investment cost data for liquid hydrogen pumps used in transfer applications: the studies by Nexant et al. [369] and the U.S. American DOE [332]. Figure 5.12 presents the specific investment-cost estimates (kEUR$_{2023}$ t$_{\text{H2}}^{-1}$ h) of terminal pumps from these two primary sources and from secondary publications that derived their values from one of these sources [290, 342, 344]. Additionally, an interview with a manufacturer of liquid hydrogen pumps provided investment-cost estimates of 2.0 MEUR$_{2023}$ kg$_{\text{H2}}^{-1}$ h for a pump with a mass flow rate up to 50 t$_{\text{H2}}$ h^{-1} and a differential pressure of 4.5 bar [370]. All investment-cost data in figure 5.12 refer to conventional (non-superconducting) pumps.

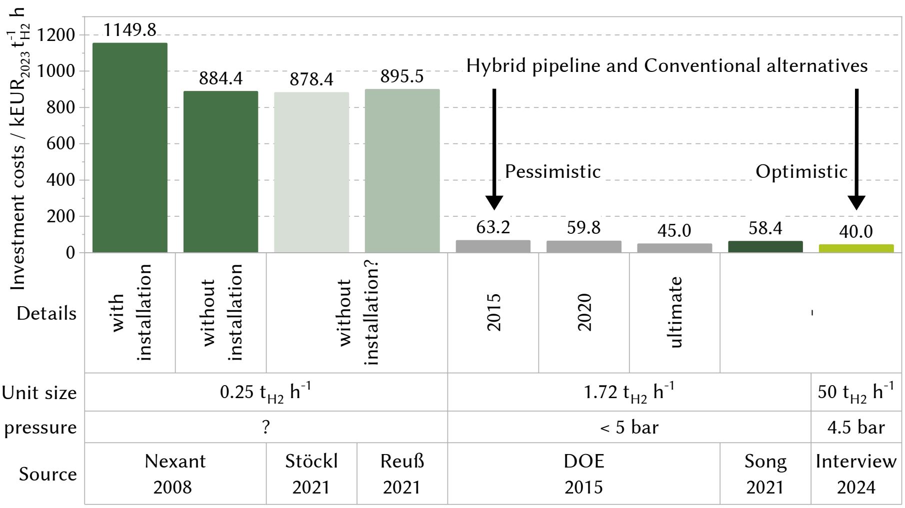

Figure 5.12: Specific investment cost of a liquid hydrogen transfer pump based on data from [290, 332, 342, 344, 369] and an interview with a pump manufacturer [370]. Stöckl et al. [342] and Reuß et al. [290] derived their values from Nexant [369]. Song et al. [344] based their estimate on DOE [332]. For larger capacities than the unit size, multiple pumps are used in parallel.

Nexant et al. estimated costs for single pumps with mass flow rates up to 0.25 $t_{H2}\ h^{-1}$ based on communication with vendors [369]. Larger transport capacities can be achieved by using multiple pumps in parallel. The differential pressure is not reported in this study. Cost estimates are shown both with and without installation. The authors assumed installation costs of 30% of the investment costs [369]. Stöckl et al. and Reuß et al. derived their cost estimations from Nexant et al. [290, 342].

The U.S. American DOE published cost data from developers of terminal pumps with mass flow rates up to 1.7 $t_{H2}\ h^{-1}$ and differential pressures < 5 bar. The investment costs were given for the status year 2015, target year 2020, and an ultimate target that predicts long-term costs in a well-established hydrogen market [332]. Song et al. derived their cost calculations from DOE [344].

Figure 5.12 shows that the cost estimate of Nexant et al. [369] is considerably higher than those of DOE [332] and the interviewed manufacturer [370]. This may be justified by the smaller unit size and by older data reported by Nexant et al. Moreover, the pressure difference of the study is unknown and the pumps might be designed for refueling stations.

Figure 5.12 shows that the cost estimate from the interviewed pump manufacturer (40.0 $kEUR_{2023}\ t_{H2}^{-1}\ h$) [370] is comparable to the costs estimated by DOE (45.0–63.2 $kEUR_{2023}\ t_{H2}^{-1}\ h$) [332]. Owing to the cost uncertainty at this scale, the DOE estimate for the status year 2015 is taken as pessimistic investment cost and the interview data as the optimistic investment cost for both the hybrid pipeline and conventional alternatives. The mean specific investment cost estimate is therefore 51.6 $kEUR_{2023}$ t^{-1}_{H2} h.

Table 5.15 outlines the techno-economic parameters for the liquid hydrogen pump. While liquid hydrogen transfer pumps are designed for highly reliable operation and extended service intervals [371], publicly available literature does not report quantified yearly operational availability values. The U.S. American DOE set a technical reliability target of more than 90% for liquid hydrogen fueling station pumps [372]. As a conservative assumption, a yearly reliability of 90% is adopted, leading to an inverse availability factor of 1.111.

The Norwegian SINTEF Energy Research study announced boil-off losses of 0.0–0.24% of the liquid hydrogen mass [367]. The higher loss value is adopted in this work, resulting in an inverse loss factor of 1.002. Only two original studies reported first-hand data on the expected lifetime of liquid hydrogen pumps: DOE (10 years) [332] and ANL (15 years) [300]. An average component lifetime of 12.5 years is assumed.

Reuß et al. estimated operation and maintenance costs of 3.0% of the initial investment cost [290], while Stöckl et al. considered 4.0% [342]. An average of 3.5% is adopted for the operation and maintenance costs of the liquid hydrogen pump.

On the upstream side of the techno-economic assessment (see figures 5.2 and 5.3), the liquid hydrogen pumps 1 and 3 are considered to be continuously operating. With a technical availability of 90% per year, the annual operating time is 7 884 h. In the hybrid pipeline alternative with gaseous hydrogen as the final product (see figure 5.3), pump 2 moves the stored liquid hydrogen from the tank used for security purposes. Pump 2 operates for 336 h of the year, consistent with the annual operating hours of the compressor (see section 5.3.5).

Pump Electrical Energy Consumption

Reuß et al. [290], Stöckl et al. [342], and Song et al. [344] approximated the electrical energy consumption of liquid hydrogen transfer pumps as 100 kWh_e t^{-1}_{H2}, 100 kWh_e t^{-1}_{H2}, and 1 kWh_e t^{-1}_{H2}, respectively. None of the authors specified the differential pressure of the pumps. Their values are based on DOE data for fueling-station pumps operating at 900 bar [332] and on Nexant et al. [369], which did not report inlet and outlet pressures.

In this work, the following methodology was used to calculate the electrical energy consumption of the pumps with a differential pressure of 4.5 bar (pumps 1 and 2) and 48.5 bar (pump 3). In fluid dynamics, the energy equation for a one-dimensional steady flow between an upstream side (in) and downstream side (out) results in a pump head H_{pump} determined as [373]:

$$H_{\text{pump}} = \left(\frac{p_{\text{out}}}{\rho \cdot \text{g}} - \frac{p_{\text{in}}}{\rho \cdot \text{g}}\right) + \left(\Phi_{\text{out}} \cdot \frac{\nu_{\text{out}}^2}{2 \cdot \text{g}} - \Phi_1 \cdot \frac{\nu_{\text{in}}^2}{2 \cdot \text{g}}\right) + (z_{\text{out}} - z_{\text{in}}) + H_{\text{friction}}, \tag{5.30}$$

where p_{in} and p_{out} are the inlet and outlet pressures, ρ is the fluid density (assumed constant in the formulation of equation 5.30), g is the gravitational acceleration, Φ_{in} and Φ_{out} are the kinetic-energy correction factors, ν_{in} and ν_{out} are flow velocities, z_{in} and z_{out} are relative elevations, and H_{friction} is the friction head loss. All terms are expressed in meters of fluid head. The parenthesized groups represent the pressure, kinetic, and potential energy contributions per unit weight, respectively.

Equation 5.30 is adapted to estimate the ideal hydraulic (shaft) work $w_{\text{sh,ideal}}$ of liquid hydrogen pumps by means of an infinitesimal pressure change analysis with the following assumptions. The kinetic and potential energy terms are neglected compared with the pressure head for sufficiently low flow velocities and when the pump inlet and outlet are at the same elevation. The friction head loss H_{friction} is initially omitted to obtain the minimum hydraulic work $w_{\text{sh,ideal}}$. Considering that liquid hydrogen exhibits a slight, liquid-phase compressibility:

$$w_{\text{sh,ideal}} = H_{\text{pump}} \cdot g \approx \int_{p_{\text{in}}}^{p_{\text{out}}} \frac{\mathrm{d}p}{\rho_{\text{LH2}}(p, T_{\text{ref}})}, \tag{5.31}$$

where p_{in} and p_{out} are the inlet and outlet pressures and the density ρ_{LH2} depends on the instantaneous pressure p and a reference temperature T_{ref}. Although equation 5.31 can be derived from the steady-flow energy equation 5.30, it is used here strictly as a mechanical energy balance for liquid pumping. As emphasized by White [373], the pump head represents mechanical energy added to the flow, and for lightly compressible liquids the energy equation is decoupled from thermodynamic state relations. Consequently, equation 5.31 is not interpreted as a thermodynamic process description and no isentropic constraint is imposed.

Equation 5.31 is solved numerically across 1 000 differential pressure steps using the para-hydrogen data from [50]. For simplicity, a constant reference temperature $T_{\text{ref}} = 20.4$ K is defined as the inlet temperature. Although the fluid temperature rises during pumping, the hydraulic work calculation assumes negligible temperature changes for moderate pressure levels. This assumption is justified by the weak liquid-phase compressibility of liquid hydrogen, its relatively large specific heat, and the contrast to the strongly compressible behavior of gases.

The irreversible mechanical losses associated with the friction head loss H_{friction} are embedded in the pump efficiency $\eta_{\text{pump,LH2}}$, which is combined with a motor efficiency $\eta_{\text{motor,LH2}}$ to determine the actual hydraulic work, i.e., the electrical energy consumption w_{e}:

$$w_{\text{e}} = \frac{w_{sh,\text{ideal}}}{\eta_{\text{pump,LH2}} \cdot \eta_{\text{motor,LH2}}}. \tag{5.32}$$

A pump efficiency $\eta_{\text{pump,LH2}}$ of 70% [367] and a motor efficiency $\eta_{\text{motor,LH2}}$ of 95% [288] were assumed. The resulting electrical energy consumption for pumps 1 and 3 (differential pressure of 4.5 bar) is 1.430 $\text{kWh}_\text{e}\ \text{t}_{\text{H2}}^{-1}$. For pump 2 (differential pressure of 48.5 bar), the consumption is 11.074 $\text{kWh}_\text{e}\ \text{t}_{\text{H2}}^{-1}$. These values are presented in table 5.15.

Table 5.15: Techno-economic parameters for liquid hydrogen pump.

Parameter	Variable	Value	Source
Mean specific investment-cost estimate: hybrid pipeline & conventional alternative	$\text{CAPEX}_{\text{LH2pump}}^{\text{specific}}$	51.6 $\text{kEUR}_{2023}\ \text{t}_{\text{H2}}^{-1}\ \text{h}$	[369, 370]
Nominal size	$S_{\text{LH2pump}}^{\text{nominal}}$	35 $\text{t}_{\text{H2}}\ \text{h}^{-1}$	Own assumption
Inverse availability factor	$f_{\text{LH2pump}}^{\text{availability}}$	1.111	[372]
Inverse loss factor	$f_{\text{LH2pump}}^{\text{loss}}$	1.002	[367]
Lifetime	τ_{LH2pump}	12.5 a	[300, 332]
Operation and maintenance	$\text{O\&M}_{\text{LH2pump}}$	3.5%	[290, 342]
Annual operating hours pumps 1 & 2	$t_{\text{op,LH2pump1}}$ $t_{\text{op,LH2pump2}}$	7 884 h	[372]
Annual operating hours pump 3	$t_{\text{op,LH2pump3}}$	336 h	Own assumption
Electrical energy consumption pumps 1 & 3	$w_{\text{e,pump1}}$ $w_{\text{e,pump3}}$	1.430 $\text{kWh}_\text{e}\ \text{t}_{\text{H2}}^{-1}$	Own calculation
Electrical energy consumption pump 2	$w_{\text{e,pump2}}$	11.074 $\text{kWh}_\text{e}\ \text{t}_{\text{H2}}^{-1}$	Own calculation

5.3.10 Liquid Hydrogen Vaporizer

A liquid hydrogen vaporizer—also called regasification plant—is essentially a heat exchanger that converts the cryogenic liquid back into its gaseous form. Today, no liquid hydrogen vaporizers are known at a GW_t-scale. However, LNG regasification plants are a mature technology, and the thermodynamics of LNG and liquid hydrogen regasification are considered comparable [374].

The three most common LNG vaporizing technologies are open rack vaporizers heated by seawater, ambient air vaporizers, and combustion heat vaporizers [289]. In this work, the combustion-heat option is neglected because it involves burning liquid hydrogen and thus represents a loss of high-value product. For simplicity, cold-energy utilization is omitted, although it could increase overall efficiency through electrical energy production (see section 2.4.5) and lessen the environmental impact of colder seawater outflow.

Open rack vaporizers require seawater temperatures above 5 °C (278.15 K) to operate reliably [375]. Ambient air vaporizers necessitate more space and a larger number of units because air has a much lower heat capacity than water [289]. Consequently, hybrid technologies—such as open rack vaporizers with ambient air vaporizers or combustion heat vaporizers—are increasingly employed for peak shaving [376]. Since the average seawater temperature off the coast near Brunsbüttel falls below 5 °C from January to March [377], a hybrid vaporizer concept is considered here.

Figure 5.13 presents specific investment-cost estimates for liquid hydrogen vaporizers reported in several studies. Sekkesæter published costs for ambient air vaporizers (448 $kEUR_{2023}$ MW_t^{-1}) and seawater vaporizers (118 $kEUR_{2023}$ MW_t^{-1}) at capacities of 14 MW_t (10 t_{H2} d^{-1}) and 1 167 MW_t (850 t_{H2} d^{-1}), respectively [289]. Sadler et al. provided a cost of 152 $kEUR_{2023}$ MW_t^{-1} for a capacity of 1 674 MW_t (1 220 t_{H2} d^{-1}) but did not specify whether the heat source was water or air [355].

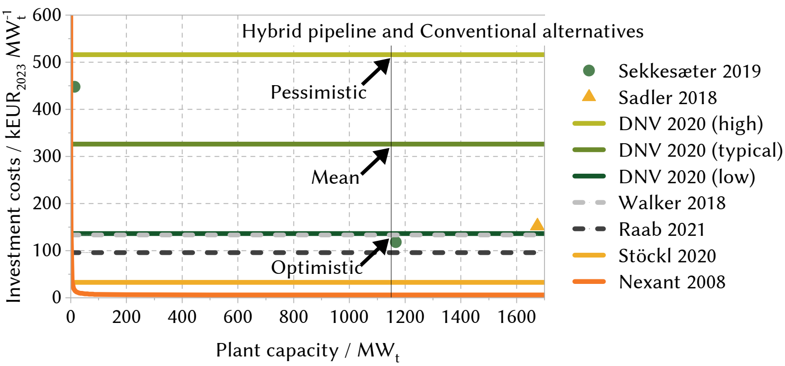

Figure 5.13: Specific investment costs of a liquid hydrogen vaporizer based on data from [289, 312, 342, 353, 355, 362, 369] and an interview with a pump manufacturer.

Nexant et al. considered a design of a terminal vaporizer that includes a liquid-circulating system with natural-gas combustion to prevent the heat-exchanger tubes from frosting [369]. This design is shown in figure 5.13 for reference, although using natural gas conflicts with climate-neutrality goals. Nexant et al. expected a scale-economy cost due to fixed-cost amortization [369]. Stöckl et al. used the data of Nexant et al. for their cost estimations [342].

Raab et al. reported linear investment-cost estimates of 96 $kEUR_{2023}$ MW_t^{-1} for an open rack vaporizer with a second closed-loop heat exchanger for improved temperature management [362]. DNV's cost data provide a wide range of low (136 $kEUR_{2023}$ MW_t^{-1}), typical (326 $kEUR_{2023}$ MW_t^{-1}), and high (516 $kEUR_{2023}$ MW_t^{-1}) investment-cost estimates for liquid hydrogen vaporizers [353], reflecting the estimates reported by Sekkesæter, Sadler et al., and Walker et al. This optimistic-mean-pessimistic range has been selected for the hybrid pipeline and conventional alternatives because of the uncertainty in the cost of a 1 150 MW_t hybrid vaporizing technology that could be employed in the case study.

Table 5.16 presents the techno-economic parameters for the liquid hydrogen vaporizer. The inverse availability factor of 1.111 is based on a yearly technical availability of 90%, as assumed in [288]. The inverse loss factor is set to 1.0, since the regasification process is assumed to exhibit no hydrogen losses [290, 353]. The vaporizer lifetime is estimated at 30 years [288], which is closer to the optimistic estimate of 35 years for an LNG vaporizer than to the pessimistic estimate of 15 years [378].

The operation and maintenance cost estimate was derived as the average of the values presented by Stöckl et al. (1.0%) [342], DNV (2.5 and 3.0%) [353], Reuß et al. (3.0%) [290], and Hong et al. (4.0%) [288]. This results in yearly expenditures of 2.7% of the initial investment-cost estimate.

There is large uncertainty in the electrical energy consumption of liquid hydrogen vaporizers because reported values range from 30 kWh_e t_{H2}^{-1} [289] to 600 kWh_e t_{H2}^{-1} [290]. IRENA noted that in [379], the authors estimated an electrical energy consumption of 1 665 kWh_e t_{H2}^{-1} [356]; however, this value was derived by IRENA from the 5% loss of the normal-hydrogen lower heating value reported in [379] due to regasification, which corresponds to lost chemical energy rather than an electrical energy input.

Most studies do not specify which components are included in their definition of the vaporization process. In contrast, two studies explicitly stated that their electrical energy-consumption estimate comprises the liquid hydrogen and water pressurization for an open rack vaporizer heated by seawater. Hong et al. calculated a total power demand of 47 kWh_e t_{H2}^{-1}, with 60% attributable to liquid hydrogen pressurization (Δ 40 bar) and 40% to water pressurization (Δ 2 bar) [288]. Sekkesæter reported a total consumption of 30 kWh_e t_{H2}^{-1}, composed of 67% for liquid hydrogen pressurization (Δ 43 bar) and 33% for water pressurization (Δ 2 bar). For an ambient air vaporizer, Sekkesæter estimated 20 $kWh_e\ t^{-1}_{H2}$ caused by a liquid hydrogen pump (Δ 49 bar), plus an additional heat demand of 80 kWh_t to raise the hydrogen temperature due to low ambient temperatures in Norway [289].

A hybrid seawater-ambient air technology in Brunsbüttel requires less heat than an ambient air vaporizer in Norway. Moreover, in this work, the electrical energy consumption of the liquid hydrogen pump is calculated independently of the vaporizer. Therefore, an electrical energy demand of 70 $kWh_e\ t^{-1}_{H2}$ is adopted, which corresponds to the lower bound reported by DNV in [353]. It is assumed that this power consumption comprises the water pump, the ambient air vaporizer, and ancillary electronic instruments.

Table 5.16: Techno-economic parameters for liquid hydrogen vaporizer.

Parameter	Variable	Value	Source
Mean specific investment-cost estimate: hybrid pipeline & conventional alternative	$CAPEX^{specific}_{LH2vap}$	326 $kEUR_{2023}\ MW^{-1}_t$	[353]
Nominal size	$S^{nominal}_{LH2vap}$	1 150 MW_t	Own assumption
Inverse availability factor	$f^{availability}_{LH2vap}$	1.111	[288]
Inverse loss factor	f^{loss}_{LH2vap}	1.0	[290, 353]
Lifetime	τ_{LH2vap}	30 a	[288, 378]
Operation and maintenance	$O\&M_{LH2vap}$	2.7%	[288, 290, 342, 353]
Electrical energy consumption	$w_{e,LH2vap}$	70 $kWh_e\ t^{-1}_{H2}$	[353]

5.4 Assessment Results and Analysis

The following sections will present and discuss the results of the techno-economic assessment. The analysis comprises the present-value and annualized investment and operating costs for the hybrid pipeline alternative and the conventional alternative, for both considered final products—liquid hydrogen and gaseous hydrogen.

5.4.1 Investment Costs of Transmission Alternatives

Table 5.17 summarizes the nominal size S_i^{nominal} and mean specific investment-cost estimates $\text{CAPEX}_i^{\text{specific}}$ of every component i in both transmission alternatives. One should be aware that, for several components, the mean specific investment-cost estimates $\text{CAPEX}_i^{\text{specific}}$ are subject to the application context (see section 5.3). The mean present-value and annualized investment cost $\text{CAPEX}_i^{\text{present}}$ and $\text{CAPEX}_i^{\text{annual}}$, respectively, are given for each of the considered final products considering the system lifetime τ_{sys} of 40 years.

Figure 5.14 (a) visualizes the mean present-value investment-cost estimates that are listed in table 5.17. The error bars exhibit the variations in the case of optimistic or pessimistic cost assumptions. The cost share of the components with the highest contribution is shown. The results demonstrate that the present-value investment-cost estimates of the hybrid pipeline alternative are considerably more cost-efficient than those of the conventional alternative, even for both final products.

If liquid hydrogen is the final product and the present-value method is considered, the hybrid pipeline alternative costs 45% of the conventional alternative (2 888 MEUR_{2023} versus 6 401 MEUR_{2023}, respectively). In other words, the hybrid pipeline alternative is 55% cheaper.

This result is driven by several factors. The 525 kV HVDC converter stations plus the underground cable system (3 726 MEUR_{2023}) are 24% more expensive than the hybrid pipeline and the 100 kV HVDC converter stations (2 836 MEUR_{2023}). Besides, the liquefaction and regasification of hydrogen add mean investment costs of 1 981 MEUR_{2023} and 457 MEUR_{2023}, respectively, which represent 38% of the present-value costs in the conventional alternative. Here, the large difference between the optimistic and pessimistic cost range stems mainly from the uncertainty on the investment costs of the liquefier (760–3 203 MEUR_{2023}) and the vaporizer (191–724 MEUR_{2023}).

Considering gaseous hydrogen as the final product, the present-value investment-cost estimate of the hybrid pipeline alternative is 66% of that of the conventional alternative (3 349 versus 5 055 MEUR_{2023}, respectively). This means that for gaseous hydrogen delivery, the cost advantage of the hybrid pipeline alternative reduces from 55% to 34%, compared to the case where liquid hydrogen is delivered. The hybrid pipeline alternative becomes more expensive mainly because an evaporator is required. On the other hand, the conventional alternative becomes less expensive since the liquefier is not necessary. However, the costs for the gaseous hydrogen storage reduce the cost-effectiveness of the conventional alternative (633 MEUR_{2023}). The costs for the gaseous hydrogen pipeline, compressor, liquid hydrogen storage, and pump contribute to less than 5% of the total present-value investment costs for both products in the conventional alternative.

Figure 5.14 (b) presents the comparison of annualized investment-cost estimates for the two transmission alternatives and each of the final products. For liquid hydrogen as the final product, the hybrid pipeline alternative costs 236.3 $MEUR_{2023}$ a^{-1} and the conventional alternative 481.7 $MEUR_{2023}$ a^{-1}. When gaseous hydrogen is desired, the total costs of the hybrid pipeline alternative are 268.9 $MEUR_{2023}$ a^{-1}, while the conventional alternative costs 368.8 $MEUR_{2023}$ a^{-1}. The result proportions between transmission alternatives are similar in the annualized and present-value investment-cost estimates, as expected. However, annualized costs provide a more intuitive representation of economic performance, as they express expenditures on a yearly basis rather than as a large aggregated present-value amount over the full project lifetime of 40 years.

The comparison of assessment methods also accentuates the influence of technology-specific assumptions regarding the WACC. Since the WACC of the hybrid pipeline is assumed to be higher than that of the other transmission technologies, the hybrid pipeline alternative benefits when costs are evaluated using a present-value aggregation. In this case, future expenditures are discounted more strongly, making them less significant from a present-value perspective. However, the hybrid pipeline alternative is penalized when costs are expressed as annualized payments, because a higher WACC implies more expensive capital and therefore larger annual capital recovery requirements. As a result, the total investment cost difference between transmission alternatives decreases from 55% to 51% (liquid hydrogen) and from 34% to 27% (gaseous hydrogen) when applying the annuity method instead of the present-value method.

Although it is not evident in figure 5.14, table 5.17 indicates that the mean investment-cost estimates of the hybrid pipeline are lower than the combined costs of the HVDC underground cable system and gaseous hydrogen pipeline, with a larger difference observed under the present-value method (621 $MEUR_{2023}$ versus 1 195 $MEUR_{2023}$) and a smaller difference under the annuity method (75.4 $MEUR_{2023}$ a^{-1} versus 87.0 $MEUR_{2023}$ a^{-1}). However, this cost advantage is still uncertain, as discussed in section 5.3.1.

Table 5.17: Mean investment-cost estimates of the components in the hybrid pipeline alternative and conventional alternative for each of the considered final products: liquid hydrogen (LH_2) and gaseous hydrogen (GH_2). The specific investment costs are not transferable to other applications unless specified in section 5.3.

Component	**Nominal size**	**Mean specific investment cost**	**Mean present-value investment cost ($MEUR_{2023}$)**		**Mean annualized investment cost ($MEUR_{2023}$ a^{-1})**	
i	$S_i^{nominal}$	$CAPEX_i^{specific}$	$CAPEX_i^{present}$		$CAPEX_i^{annual}$	
			LH_2	GH_2	LH_2	GH_2
			Hybrid pipeline alternative			
HVDC converter stations 100 kV	2 ends · 4 GW_e	244.7 $MEUR_{2023}$ GW_e^{-1}	2 214.9	2 214.9	156.6	156.6
Hybrid pipeline	75 km	7.4 $MEUR_{2023}$ km^{-1}	621.4	621.4	75.4	75.4
Vaporizer	1.15 GW_t	326.0 $MEUR_{2023}$ GW_t^{-1}	-	457.2	-	32.3
LH_2 storage	1 000 t_{H2}	39.3 $kEUR_{2023}$ t_{H2}^{-1}	48.9	48.9	4.1	4.1
LH_2 pump 1	35 t_{H2} h^{-1}	51.6 $kEUR_{2023}$ t_{H2}^{-1} h	3.1	3.1	0.3	0.3
LH_2 pump 3	35 t_{H2} h^{-1}	51.6 $kEUR_{2023}$ t_{H2}^{-1} h	-	3.1	-	0.3
Total	-	-	**2 888.3**	**3 348.6**	**236.3**	**268.9**
			Conventional alternative			
HVDC converters stations 525 kV	2 ends · 4 GW_e	300.0 $MEUR_{2023}$ GW_e^{-1}	2 715.5	2 715.5	192.0	192.0
Liquefier	838.1 t_{H2} d^{-1}	2.1 $MEUR_{2023}$ t_{H2}^{-1} d	1 981.4	-	166.2	-
HVDC underground cable system	4 GW_e · 75 km	3.3 $MEUR_{2023}$ GW_e^{-1} km^{-1}	1 010.9	1 010.9	71.5	71.5
GH_2 storage	1 000 t_{H2}	568.4 $kEUR_{2023}$ t_{H2}^{-1}	-	633.4	-	53.1
Vaporizer	1.15 GW_t	326.0 $MEUR_{2023}$ GW_t^{-1}	457.2	457.2	32.3	32.3
GH_2 pipeline 50 cm	1.15 GW_t · 75 km	1.91 $MEUR_{2023}$ GW_t^{-1} km^{-1}	183.7	183.7	15.4	15.4
LH_2 storage	1 000 t_{H2}	39.3 $kEUR_{2023}$ t_{H2}^{-1}	48.9	-	4.1	-
Compressor	13.6 MW_e	2.8 $MEUR_{2023}$ MW_e^{-1}	-	51.0	-	4.3
LH_2 pump 2	35 t_{H2} h^{-1}	51.6 $kEUR_{2023}$ t_{H2}^{-1} h	3.1	3.1	0.3	0.3
Total	-	-	**6 400.7**	**5 054.8**	**481.7**	**368.8**

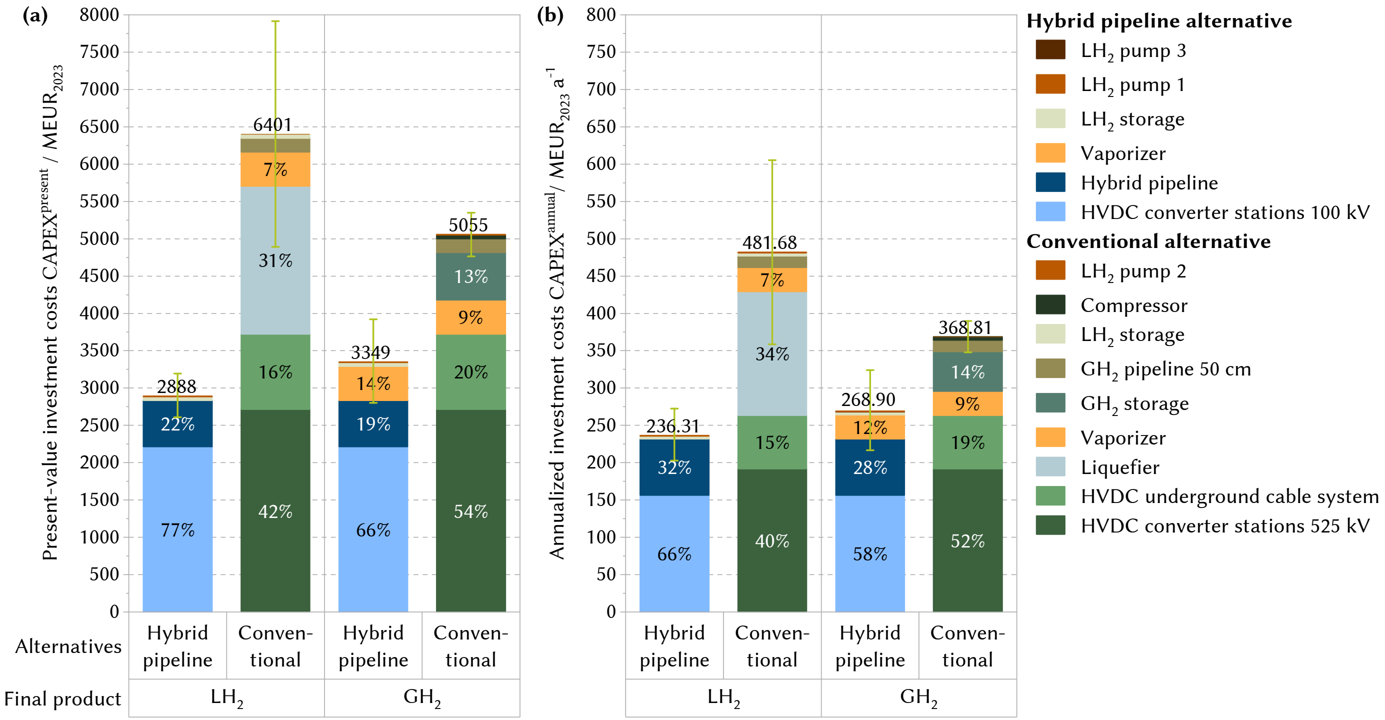

Figure 5.14: Comparison of (a) present-value and (b) annualized investment-cost estimates CAPEX of the two transmission alternatives, hybrid pipeline alternative versus conventional alternative, for each of the considered final products—liquid hydrogen (LH_2) and gaseous hydrogen (GH_2).

5.4.2 Operating Costs of Transmission Alternatives

Table 5.18 presents the mean present-value and annual fixed and variable operating cost estimates of each component i in both transmission alternatives. The observation period is 40 years (see table 5.3). The operation and maintenance cost rates $\mathrm{O\&M}_i$ are defined as a percentage of the initial capital cost $\mathrm{CAPEX}_i^{\mathrm{initial}}$, as given in equations 5.4 and 5.12, respectively. The derivation of these values and of the electrical energy consumption $w_{\mathrm{e},i}$, where applicable, can be found in section 5.3.

Figure 5.15 illustrates the results of table 5.18. Figure 5.15 (a) presents the amounts given by the present-value method, while figure 5.15 (b) represents the results using the annuity method. Both figures clearly demonstrate that the hybrid pipeline alternative is more cost-effective than the conventional alternative. Particularly for liquid hydrogen as the final product, the average operating costs of the hybrid pipeline alternative are 92% (present-value) and 91% (annually) lower than those of the conventional alternative.

The relatively high electrical energy consumption of the liquefier (6.76 $\mathrm{MW_e\ t_{H2}^{-1}}$ [68]) and electricity costs in Germany (0.194 $\mathrm{EUR_{2023}\ kWh_e^{-1}}$ derived from [298]) lead to variable operating expenses of 4 388 $\mathrm{MEUR_{2023}}$ and 368 $\mathrm{MEUR_{2023}\ a^{-1}}$ in the present-value and annuity methods, respectively. These amounts represent more than 7 times the total operating costs of the hybrid pipeline alternative in both methods (559 $\mathrm{MEUR_{2023}}$ and 49.3 $\mathrm{MEUR_{2023}\ a^{-1}}$, respectively). This result shows that liquid hydrogen is a high-value good. Producing it in Germany implies substantial costs, compared with transmitting liquid hydrogen via a hybrid pipeline from the import terminal to the consumers.

The fixed operating costs of the liquefier account for the largest share of the total fixed operating costs in the conventional alternative when liquid hydrogen is the final product (45% in the present-value method and 49% in the annuity method). Compared with the hybrid pipeline alternative, this item increases the total operating costs of the conventional alternative by 925 $\mathrm{MEUR_{2023}}$ and 77.6 $\mathrm{MEUR_{2023}\ a^{-1}}$ in the present-value and annuity methods, respectively. This is justified by the relatively high investment cost of the liquefier (see table 5.17) and the operation and maintenance cost rate of 4.0% (see table 5.18) relative to the other components.

Table 5.18: Mean operating cost estimates of the components in the hybrid pipeline alternative and conventional alternative for each of the considered final products: liquid hydrogen (LH_2) and gaseous hydrogen (GH_2). The operation and maintenance cost rates $O\&M_i$ are defined as a percentage of the initial capital cost.

Component	**Operation and maintenance cost rate**	**Electrical energy consumption**	**Mean present-value operating cost ($MEUR_{2023}$)**				**Mean annual operating cost ($MEUR_{2023}\ a^{-1}$)**			
i	$O\&M_i$	$w_{e,i}$	$fixOPEX_i^{present}$		$varOPEX_i^{present}$		$fixOPEX_i^{annual}$		$varOPEX_i^{annual}$	
			LH_2	GH_2	LH_2	GH_2	LH_2	GH_2	LH_2	GH_2
Hybrid pipeline alternative										
HVDC converter stations 100 kV	1.25%	-	356.8	356.8	-	-	25.2	25.2	-	-
Hybrid pipeline	3.71%	-	190.0	190.0	-	-	23.1	23.1	-	-
Vaporizer	2.70%	70.00 $kWh_e\ t_{H2}^{-1}$	-	159.1	-	169.4	-	11.2	-	14.2
LH_2 storage	2.00%	-	10.3	10.3	-	-	0.9	0.9	-	-
LH_2 pump 1	3.50%	1.43 $kWh_e\ t_{H2}^{-1}$	0.8	0.8	0.7	0.7	0.1	0.1	0.1	0.1
LH_2 pump 3	3.50%	1.43 $kWh_e\ t_{H2}^{-1}$	-	0.8	-	0.0	-	0.1	-	0.0
Total	-	-	**558.1**	**718.0**	**0.7**	**170.1**	**49.2**	**60.5**	**0.1**	**14.3**
Conventional alternative										
HVDC converters stations 525 kV	1.25%	-	437.5	437.5	-	-	30.9	30.9	-	-
Liquefier	4.00%	6.76 $MWh_e\ t_{H2}^{-1}$	925.0	-	4 388.2	-	77.6	-	368.0	-
HVDC underground cable system	3.34%	-	477.5	477.5	-	-	33.8	33.8	-	-
GH_2 storage	2.00%	-	-	141.4	-	-	-	11.9	-	-
Vaporizer	2.70%	70.00 $kWh_e\ t_{H2}^{-1}$	159.1	159.1	169.4	169.4	11.2	11.2	14.2	14.2
GH_2 pipeline 50 cm	2.66%	-	58.3	58.3	-	-	4.9	4.9	-	-
LH_2 storage	2.00%	-	10.3	-	-	-	0.9	-	-	-
Compressor	3.30%	389.50 $kWh_e\ t_{H2}^{-1}$	-	16.7	-	10.6	-	1.4	-	0.9
LH_2 pump 2	3.50%	11.07 $kWh_e\ t_{H2}^{-1}$	0.8	0.8	5.2	5.2	0.1	0.1	0.4	0.4
Total	-	-	**2 068.6**	**1 291.3**	**4 562.7**	**185.2**	**159.3**	**94.2**	**382.6**	**15.5**

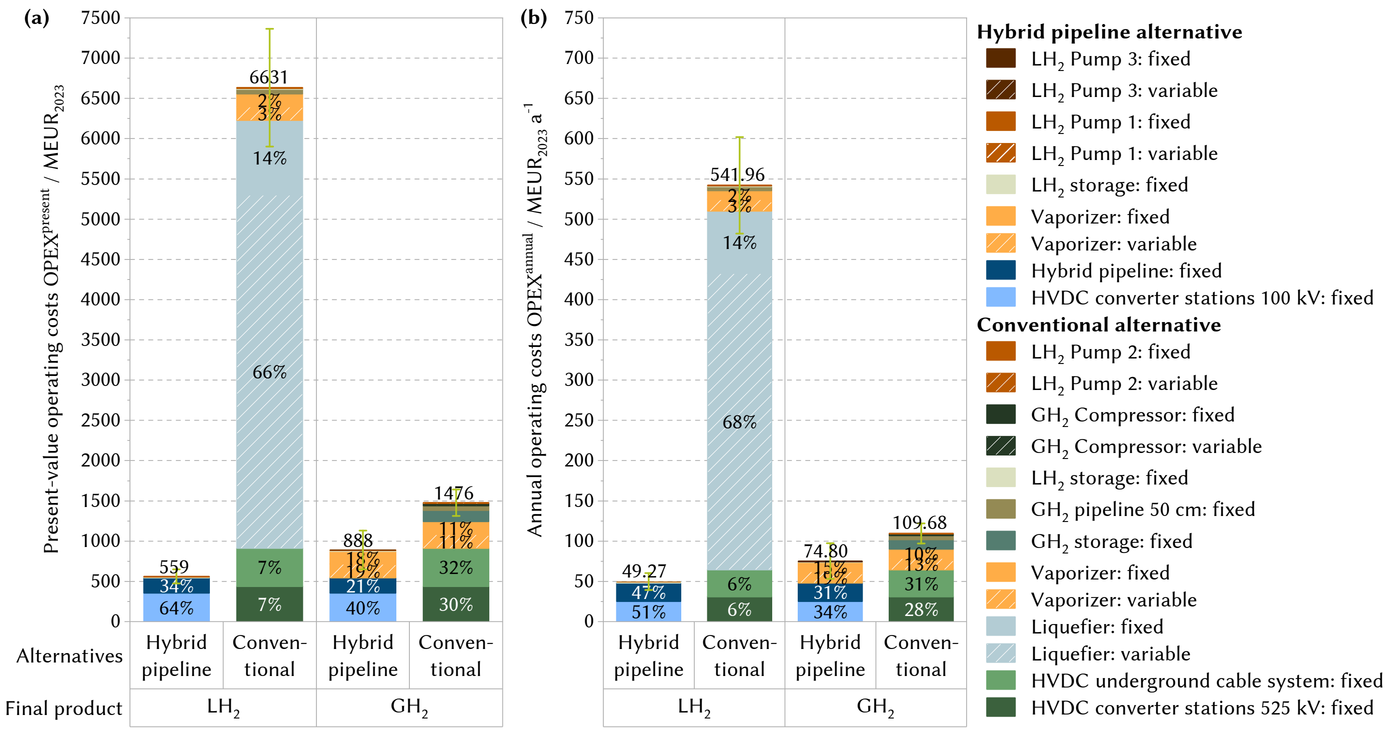

Figure 5.15: Comparison of (a) present-value and (b) annual operating cost estimates OPEX of the two transmission alternatives, hybrid pipeline alternative versus conventional alternative, for each of the considered final products—liquid hydrogen (LH_2) and gaseous hydrogen (GH_2).

Apart from the liquefier, the 525 kV converter stations and HVDC underground cable system in the conventional alternative contribute to 368 $MEUR_{2023}$ and 16.4 $MEUR_{2023}$ a^{-1} higher present-value and annual fixed operating costs, respectively, than those of the 100 kV converter stations and hybrid pipeline. This applies for both final products.

Owing to the fixed operation costs of the evaporator, the conventional alternative becomes 159 $MEUR_{2023}$ (present-value) or 11.2 $MEUR_{2023}$ a^{-1} (annualized) more expensive than the hybrid pipeline system when liquid hydrogen is considered as the final product. In comparison, the mean fixed present-value and annual operating costs of the gaseous hydrogen pipeline are 58 $MEUR_{2023}$ and 4.9 $MEUR_{2023}$ a^{-1}, respectively, relatively low. However, the combined fixed operating costs of the gaseous hydrogen pipeline and the HVDC underground cable system are higher than those of the hybrid pipeline alone: 536 $MEUR_{2023}$ versu 190 $MEUR_{2023}$ under the present-value method and 38.6 $MEUR_{2023}$ a^{-1} versus 23.0 $MEUR_{2023}$ a^{-1} under the annuity method.

If gaseous and not liquid hydrogen is desired as the final product, the operating cost advantage of the hybrid pipeline alternative decreases but remains significant compared with the conventional alternative. The mean operating costs of the hybrid pipeline alternative are in this case 40% (present-value) and 32% (annualized) lower than those of the conventional alternative. The main reasons for the cost difference are, in addition to the higher fixed operating costs of the converter stations and HVDC underground cable, the fixed operating costs of the gaseous hydrogen storage and pipeline. The vaporizer increases the operating costs equally in both transmission alternatives. Compared with the other components, the operating expenses for the hydrogen compressor, liquid hydrogen pumps, and storage are less significant under the assumptions made in this case study.

5.4.3 Total Cost Comparison of Transmission Alternatives

Figure 5.16 illustrates the total expenditure estimate comparison of transmission alternatives for both final products. The results in figure 5.16 (a) are based on the present-value method, while the values for figure 5.16 (b) were calculated using the annuity method (see section 5.2). The total expenditures are composed of the variable operating costs varOPEX, fixed operating costs fixOPEX, and investment costs CAPEX, as defined for each method in equations 5.2 and 5.10.

The findings provide clear evidence that, for the selected case study (Brunsbüttel–Hamburg), the hybrid pipeline alternative is more cost-efficient than the conventional alternative, especially when liquid hydrogen is the final product (see figure 5.2), but also when hydrogen is required in its gaseous state (see figure 5.3). Considering liquid hydrogen as the final product, the average total-cost difference between transmission alternatives is 74% under the present-value method and 72% under the annuity method. The cost difference between the cost accounting methods is given by the technology-specific selection of the WACC (see table 5.3). When gaseous hydrogen is defined as the final product, the average cost difference between transmission alternatives is 35% under the present-value method and 28% under the annuity method.

In absolute terms, the hybrid pipeline alternative costs 285.6 $MEUR_{2023}$ a^{-1} and 343.7 $MEUR_{2023}$ a^{-1} for liquid and gaseous hydrogen final products, respectively, while the conventional alternative costs 1 023.64 $MEUR_{2023}$ a^{-1} and 478.49 $MEUR_{2023}$ a^{-1} for the same products (see figure 5.16 (b)). For contextualization, the average total cost of the hybrid pipeline is 98.4 $MEUR_{2023}$ a^{-1} and represents 6% of the 2025 costs associated with network congestion management measures in Germany of 1 537 $MEUR_{2023}$ a^{-1} (1 609 $MEUR_{2025}$ a^{-1} [380]).

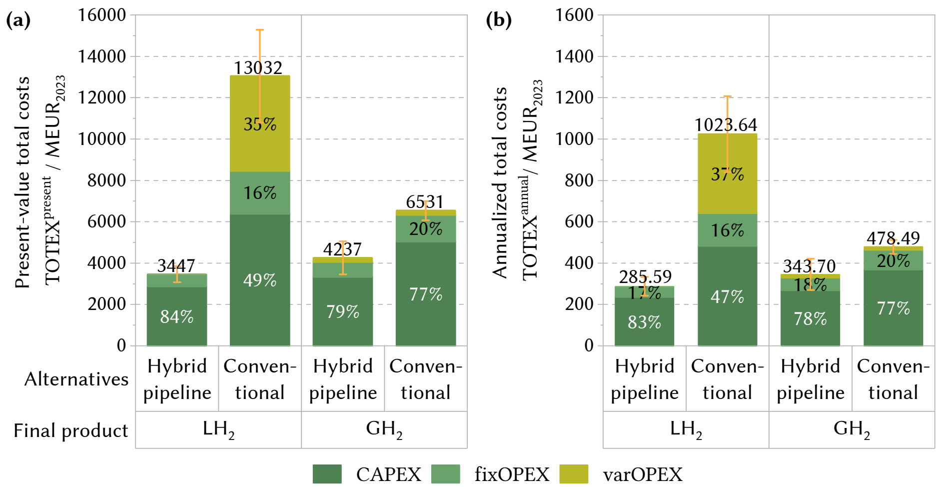

Figure 5.16: Total cost estimates TOTEX of the transmission alternatives divided into investment costs CAPEX, fixed operational costs fixOPEX, and variable costs varOPEX under the (a) present-value method and (b) annuity method for each final product—liquid hydrogen (LH_2) and gaseous hydrogen (GH_2).

As described in sections 5.4.1 and 5.4.2, the main reasons for the cost advantage of the hybrid pipeline alternative compared with the conventional alternative can be summarized as:

- When liquid hydrogen is the final product, regasification and liquefaction steps add substantial investment and operating costs to the conventional alternative. These steps are necessary when transporting hydrogen by pipeline in its gaseous state, although liquid hydrogen is desired.

- When gaseous hydrogen is the final product, the cost difference between transmission alternatives is lower because no liquefaction is needed and both transmission alternatives require vaporizers. The storage for gaseous hydrogen is more expensive than the liquid hydrogen storage, decreasing the cost advantage of the conventional alternative.
- Regardless of the product, the investment and operating costs of the 525 kV converter stations and HVDC underground cable systems in the conventional alternative are higher than those of the 100 kV converter stations and hybrid pipeline in the corresponding alternative.
- The investment and operating costs of the hybrid pipeline are lower than the combined costs of the HVDC underground cable system and gaseous hydrogen pipeline. However, this cost advantage is still uncertain due to the relatively low TRL 4 of the hybrid pipeline and should be refined in future development stages.

Section 5.3 indicated that the liquefier and vaporizer contribute most to the overall uncertainty in the range of optimistic and pessimistic investment costs, owing to their low maturity level at the scale considered in this work. The deviations from the mean cost estimates for the liquefier and vaporizer reveal a substantial uncertainty range, with the optimistic values falling up to 62% and 58% below the mean, and pessimistic values rising up to 62% and 58% above the mean, respectively.

The investment cost uncertainties of the gaseous compressor, liquid hydrogen storage, and pump are also considerable. However, their impact on the total optimistic and pessimistic cost range is smaller in absolute terms due to their lower overall investment costs. For the gaseous hydrogen storage tanks, the capital cost estimate is derived from a single reference. Therefore, a quantitative assessment of cost uncertainty is not available, despite a relatively low maturity level at this scale.

Table 5.19 presents the mean specific total cost estimates per kilometer of each transmission alternative under the present-value method. These values apply only for the 75 km long transmission systems and are not transferable to other distances. However, they enable the comparison per unit GW with other transmission systems of the same length using the following analysis.

The allocation method for shared infrastructure that transports multiple energy vectors—presented in equations 5.17 and 5.18—expresses the total costs of the hybrid pipeline per electrical unit (GW_e) and per thermal unit (GW_t). Auxiliary components are allocated to the proper energy vector based on their function. For example, converter stations belong to the electrical energy vector, whereas hydrogen storage tanks are accounted for under the chemical energy vector.

Table 5.19: Mean specific total cost (present-value) of each 75 km transmission alternative. Values are intendend solely for comparative assessment of alternatives spanning the same distance

Final product	Transmission alternative	Value
Liquid hydrogen	Hybrid pipeline	46.0 $MEUR_{2023}$ km^{-1}
	Conventional	173.8 $MEUR_{2023}$ km^{-1}
Gaseous hydrogen	Hybrid pipeline	56.5 $MEUR_{2023}$ km^{-1}
	Conventional pipeline	87.1 $MEUR_{2023}$ km^{-1}

Table 5.20 shows the resulting mean total cost estimates for each transmission alternative, split into electrical and chemical components, assuming liquid hydrogen as the final product and using the present-value method. Table 5.21 presents the analogous for gaseous hydrogen as the final product. Based on the presented allocation method, the results indicate that the hybrid pipeline incurs a lower mean cost per kilometer and unit power than the conventional alternatives for both electrical chemical transmission pathways.

Table 5.20: Mean specific total cost (present-value) of each 75 km transmission alternative, split into electrical and chemical components, for liquid hydrogen delivery. Values are intendend solely for comparative assessment of alternatives spanning the same distance.

Transmission alternative	Energy vector	Component	Value
Hybrid pipeline	Electrical	Hybrid pipeline	2.1 $MEUR_{2023}$ km^{-1} GW_e^{-1}
		Auxiliary	8.6 $MEUR_{2023}$ km^{-1} GW_e^{-1}
		Total system	10.7 $MEUR_{2023}$ km^{-1} GW_e^{-1}
	Chemical	Hybrid pipeline	2.1 $MEUR_{2023}$ km^{-1} GW_t^{-1}
		Auxiliary	0.7 $MEUR_{2023}$ km^{-1} GW_t^{-1}
		Total system	2.8 $MEUR_{2023}$ km^{-1} GW_t^{-1}

Continued on next page

Table 5.20: Mean specific total cost (present-value) of each 75 km transmission alternative, split into electrical and chemical components, for liquid hydrogen delivery. Values are intendend solely for comparative assessment of alternatives spanning the same distance. (Continued)

Transmission alternative	Energy vector	Component	Value
Conventional	Electrical	HVDC underground cable system	5.0 $MEUR_{2023}$ km^{-1} GW_e^{-1}
		Auxiliary	10.5 $MEUR_{2023}$ km^{-1} GW_e^{-1}
		Total system	15.5 $MEUR_{2023}$ km^{-1} GW_e^{-1}
	Chemical	Gaseous hydrogen pipeline	2.8 $MEUR_{2023}$ km^{-1} GW_t^{-1}
		Auxiliary	94.5 $MEUR_{2023}$ km^{-1} GW_t^{-1}
		Total system	97.3 $MEUR_{2023}$ km^{-1} GW_t^{-1}

Table 5.21: Mean specific total cost (present-value) of each 75 km transmission alternative, split into electrical and chemical components, for gaseous hydrogen delivery. Values are intendend solely for comparative assessment of alternatives spanning the same distance.

Transmission alternative	Energy vector	Component	Value
Hybrid pipeline	Electrical	Hybrid pipeline	2.1 $MEUR_{2023}$ km^{-1} GW_e^{-1}
		Auxiliary	8.6 $MEUR_{2023}$ km^{-1} GW_e^{-1}
		Total system	10.7 $MEUR_{2023}$ km^{-1} GW_e^{-1}
	Chemical	Hybrid pipeline	2.1 $MEUR_{2023}$ km^{-1} GW_t^{-1}
		Auxiliary	9.9 $MEUR_{2023}$ km^{-1} GW_t^{-1}
		Total system	12.0 $MEUR_{2023}$ km^{-1} GW_t^{-1}
Conventional	Electrical	HVDC underground cable system	5.0 $MEUR_{2023}$ km^{-1} GW_e^{-1}
		Auxiliary	10.5 $MEUR_{2023}$ km^{-1} GW_e^{-1}
		Total system	15.5 $MEUR_{2023}$ km^{-1} GW_e^{-1}
	Chemical	Gaseous hydrogen pipeline	2.8 $MEUR_{2023}$ km^{-1} GW_t^{-1}
		Auxiliary	19.1 $MEUR_{2023}$ km^{-1} GW_t^{-1}
		Total system	21.9 $MEUR_{2023}$ km^{-1} GW_t^{-1}

5.5 Sensitivity Analysis

Although the results in section 5.4.3 demonstrate that the hybrid pipeline alternative is more cost-efficient than the conventional alternative within the scope of the selected case study, the results are sensitive to the underlying assumptions.

For liquid hydrogen delivery, figure 5.17 presents the change in present-value average total cost of both transmission alternatives when the cost parameters of several components are varied. For gaseous hydrogen delivery, the absolute change is identical (values in $MEUR_{2023}$ next to each bar), but the relative change compared to the baseline differs.

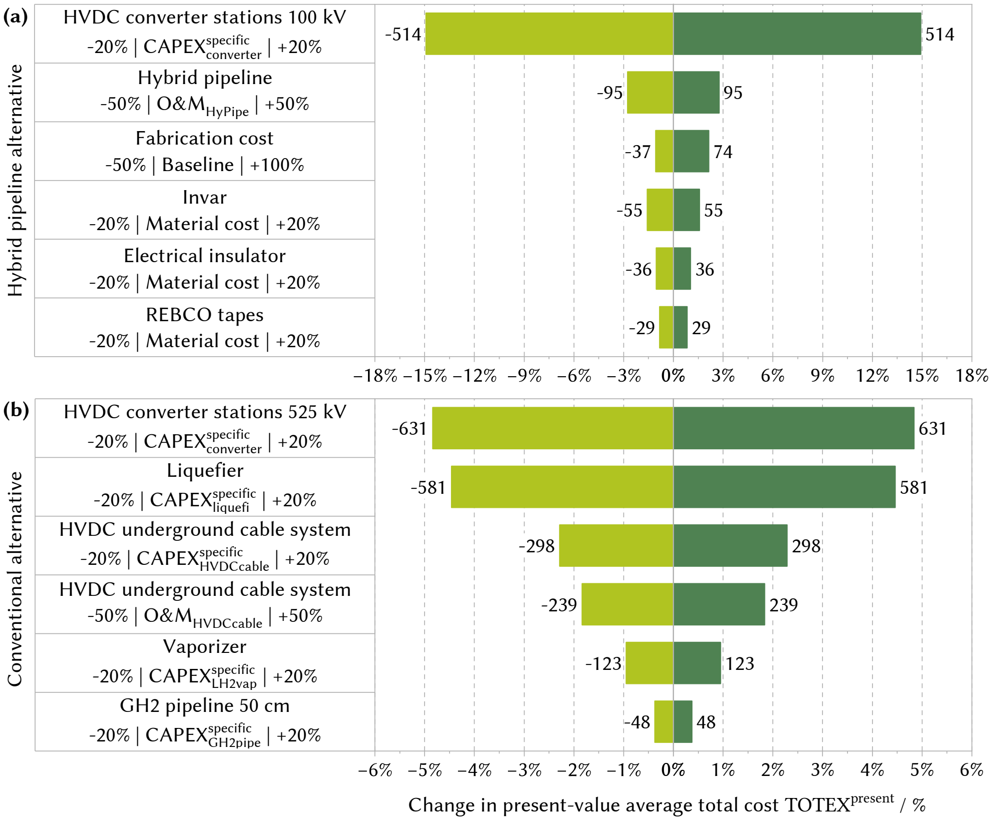

Figure 5.17: Change in present-value average total cost of the (a) hybrid pipeline alternative and (b) conventional alternative when varying specific cost parameters. The values next to the bars are the absolute change in $MEUR_{2023}$.

Figure 5.17 (a) shows that the specific investment cost of the HVDC converter stations at 100 kV has the largest influence on the average total cost of the hybrid pipeline alternative ($\approx$ 15%). The second largest effect is cause by the variation of the O&M cost of the hybrid pipeline ($\pm$50% compared to the baseline $O\&M_{HyPipe}$ = 3.71% of the corresponding investment cost). If the fabrication cost of the hybrid pipeline doubles, the increase in total system cost is less than 3% compared to the baseline.

Figure 5.17 (b) illustrates that the variation of the specific investment cost of the HVDC converter stations also has the most significant impact on the average total cost of the conventional alternative, followed by changes in the specific investment costs of the liquefier and the underground HVDC cable. However, the relative total cost change is $<$ 5% in all variations.

To evaluate the effect of length and variations of three relevant components on the total costs, the following sections will present further sensitivity analyses.

5.5.1 Length

The hybrid pipeline is a custom-engineered technology designed for a specific application context. Therefore, the resulting investment costs of the proposed 75 km long hybrid pipeline are not transferable to other lengths. To evaluate the effect of shorter and longer transmission distances on the total costs of the hybrid pipeline alternative, new hybrid pipeline designs for 50 km and 150 km lengths are developed. The design procedure is identical to that presented in chapter 4 and includes modifying the length in the following steps:

1. Determination of the cable layout and critical current
2. Simulation of the cable in case of a short circuit
3. Modeling of the temperature increase and pressure drop of the transmitted liquid hydrogen
4. Determination of the pipe layout

The resulting cable and pipeline layouts are presented for the 50 km and 150 km lengths in appendix C, table C.7. Here, the consequences of reducing and enlarging the hybrid pipeline length are discussed. At the end of this section, a comparison of total costs is presented for both transmission alternatives at each length.

Length Decrease: 50 km

Reducing the pipeline length from 75 km to 50 km does not influence the self-field critical current of each monopole, as determined in section 4.2.3. This is because only the cross-section has an effect on the calculated critical current. The only difference in the cable layout of the new 50 km design is a lower total superconductor length of 4 348 km compared to 6 522 km of the 75 km design C in table 4.1.

The simulation of the 50 km long cable in case of a short circuit demonstrates that decreasing the cable length does not compromise the hybrid pipeline safety during an electric fault. On one side, the maximum source voltage U_{max} equals the rated voltage U_0 of 100 kV, providing a significant safety margin to the test voltage U_{T} of 185 kV (see section 4.2.2). This means that the electrical insulation has an adequate thickness. On the other side, at the final temperature of 52.8 K, hydrogen remains in its liquid state and stays well below the boiling curve (see section 4.2.4).

For a 50 km pipe length, the thermal-hydraulic model shows that the inner diameter $D_{\mathrm{LH2,i}}$ can be reduced from 36 cm to 33 cm−compared to the 75 km pipe—while hydrogen still arrives in its liquid state. A smaller pipe inner diameter $D_{\mathrm{LH2,i}}$ reduces the heat load per unit length q_{l}, although thinner pipes increase the frictional losses (see section 4.3.2). Additionally, a shorter transmission length ℓ reduces the temperature and pressure differences between inlet and outlet (see equations 4.15 and 4.16), allowing a wider range of mass flow $\dot{m}_{\mathrm{LH2}}$. The resulting mass flow range of the 50 km long pipe is 4.0−10.1 $\mathrm{kg_{H2}\ s^{-1}}$ (0.50−1.20 $\mathrm{GW_t}$), compared to 4.6−9.7 $\mathrm{kg_{H2}\ s^{-1}}$ (0.55−1.15 $\mathrm{GW_t}$) for the 75 km pipe.

Length Increase: 150 km

When the cable length is increased to 150 km, the cable layout must be modified. This is mainly because the new length ℓ raises the cable inductance L_{cable} (see equation 4.14), which during a short circuit produces a maximum source voltage U_{max} (see equation 4.13) that exceeds the test voltage U_{T} of 185 kV. Therefore, keeping the same cable layout as in the 75 km design would compromise the cable's electrical breakdown strength and, consequently, the hybrid pipeline safety.

Setting the radius of the inner copper stabilizer $r_{\mathrm{1,cu}}$ to 18.6 mm assures safe operation of the 150 km long superconducting cable, even in the event of a fault (for comparison, $r_{\mathrm{1,cu}}$ = 13.9 mm in the 75 km design). The new radius of inner copper stabilizer $r_{\mathrm{1,cu}}$ enlarges the outer radius of the electrical insulator $r_{\mathrm{1,ins}}$ from 28.6 mm in the 75 km design to 31.9 mm in the 150 km design (see equation 4.3). This reduces the magnitude of the cable inductance

L_{cable} (see equation 4.14). Because the inner copper stabilizer now has a larger diameter, the number of superconducting tapes per layer increases from 21 to 28 to satisfy the winding conditions of type III (see figure 4.3). The new total amount of superconductor is 17 393 km.

During a short circuit (see section 4.2.4), the higher amounts of copper and superconductor lower the maximum temperature to just 35.5 K. Consequently, there is no risk of liquid hydrogen boiling caused by the fault. With the new layout, the maximum voltage U_{max} is 184 kV, i.e., lower than the test voltage U_T of 185 kV. This confirms the safe design of the cable layout.

The outer radius of the outer copper stabilizer $r_{2,cu}$, which defines the outer diameter of each monopole, increases from 30.7 mm (75 km design) to 35.1 mm (150 km design) because of the larger outer radius of the inner copper stabilizer $r_{1,cu}$ and the larger outer radius of the electrical insulator $r_{1,ins}$ (see equation 4.8). Considering the new cable outer diameter, a 150 km long pipeline that operates within the inlet and design parameters presented in section 4.3 can transmit liquid hydrogen without intermediate cooling stations. This is only possible if the pipe inner diameter $D_{LH2,i}$ and mass flow $\dot{m}_{LH2}$ increase considerably, as shown in figure 5.18.

The 150 km long hybrid pipeline requires a mass flow range of 15.5–16.5 $kg_{H2}\ s^{-1}$ (1.84–1.96 GW_e) when the pipe inner diameter $D_{LH2,i}$ is 61.0 cm to transmit liquid hydrogen without intermediate cooling stations. Since the hydrogen demand in the selected case study is considerably lower at 5.2–7.3 $kg_{H2}\ s^{-1}$ (0.62–0.87 GW_t, see vertical dashed lines in figure 5.18 and table 2.5), one pumping and re-cooling station becomes necessary to achieve the same hydrogen transmission rated power as in the 75 km design.

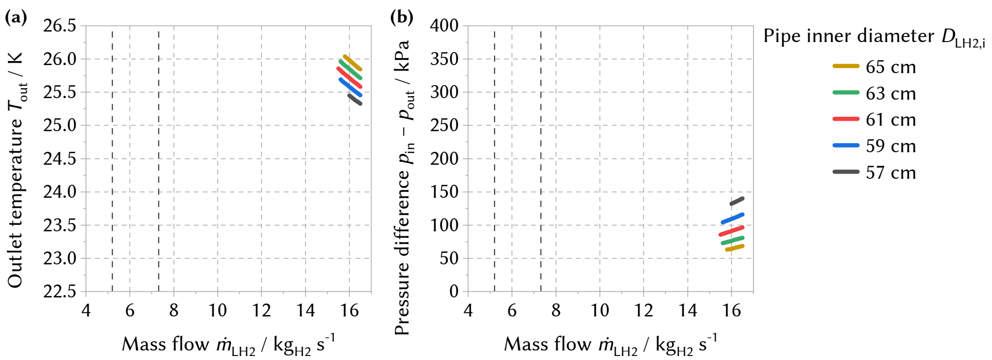

Figure 5.18: (a) Outlet temperature T_{out} and (b) pressure difference $p_{in} - p_{out}$ of liquid hydrogen, as a function of its mass flow $\dot{m}_{LH2}$, after transmission in a 150 km long hybrid pipeline without cooling stations, as discussed in section 5.5.1. Five different pipe inner diameters $D_{LH2,i}$ are compared. The vertical dashed lines present the lower and upper limits of the hydrogen demand in the selected case study.

To simplify the analysis, it is assumed that the cryocooler and pump are located in the middle of the 150 km transmission (at 75 km). They return the pressure and temperature of the transmitted liquid hydrogen to its inlet conditions of 20.4 K and 600 kPa. This assumption allows using the results for the 75 km design in section 4.3 for the inlet parameters of the cryocooler and the pump, and guarantees safe transmission of liquid hydrogen for the second 75 km section. In a more detailed analysis, the authors in [252] showed that the position of the re-cooling and pumping stations can be optimized to improve investment and operating costs and that the superconducting cable remains electrically continuous across intermediate stations.

To estimate the investment and operating costs of the cryocooler, the cooling power and electrical energy consumption must be determined. This is done using the mass flow rate $\dot{m}_{\mathrm{LH2}}$ and the liquid hydrogen enthalpy at its corresponding inlet and outlet temperature and pressure. The detailed methodology for this procedure and further techno-economic assumptions for the cryocooler are described in appendix C. The upper mass flow rate $\dot{m}_{\mathrm{LH2}}$ of 9.7 $\mathrm{kg_{H2}\ s^{-1}}$ (34.9 $\mathrm{t_{H2}\ h^{-1}}$) defines the cooling power at 421.05 $\mathrm{kW_t}$. Using the cost model for large-scale refrigerators presented in [252] and an equivalent cooling power of 81.37 $\mathrm{kW_t}$ at 4.5 K, the optimistic, mean, and pessimistic specific investment-cost estimates of the cryocooler $\mathrm{CAPEX}_{\mathrm{cryocool}}^{\mathrm{specific}}$ are 65.78 $\mathrm{kEUR_{2023}\ kW_t^{-1}}$, 87.71 $\mathrm{kEUR_{2023}\ kW_t^{-1}}$, and 109.64 $\mathrm{kEUR_{2023}\ kW_t^{-1}}$, respectively (see table 5.22).

The electrical energy consumption $w_{\mathrm{e,cryocool}}$ depends on the mass flow rate $\dot{m}_{\mathrm{LH2}}$. To calculate the average variable operating costs of the cryocooler $\mathrm{varOPEX_{cryocool}}$, it is assumed that the cryocooler operates half of the time at the lower mass flow rate of 4.6 $\mathrm{kg_{H2}\ s^{-1}}$ (16.6 $\mathrm{t_{H2}\ h^{-1}}$) and the remaining time at the upper mass flow rate of 9.7 $\mathrm{kg_{H2}\ s^{-1}}$ (34.9 $\mathrm{t_{H2}\ h^{-1}}$). The upper and lower bounds of the variable operating costs of the cryocooler $\mathrm{varOPEX_{cryocool}}$ are given by assuming that the cryocooler operates constantly at the highest or lowest mass flow rate $\dot{m}_{\mathrm{LH2}}$, respectively.

Results for Length Variations

Figure 5.19 presents the comparison of total costs for each product between transmission alternatives at lengths of 50 km, 75 km, and 150 km. Figures 5.19 (a) and (b) illustrate the results under the present-value and annuity methods, respectively. The total costs TOTEX are divided into investment costs CAPEX, fixed operational costs fixOPEX, and variable operational costs varOPEX.

When liquid hydrogen is the final product, the results demonstrate that the hybrid pipeline alternative remains considerably more cost-efficient than the conventional alternative, even

Table 5.22: Techno-economic parameters for cryocooler based on the methodology described in appendix C.

Parameter	Variable	Value	Source
Mean specific investment-cost estimate	$\mathrm{CAPEX}_{\mathrm{cryocool}}^{\mathrm{specific}}$	87.71 $\mathrm{kEUR_{2023}\ kW_t^{-1}}$	[252]
Nominal size	$S_{\mathrm{cryocool}}^{\mathrm{nominal}}$	421.05 $\mathrm{kW_t}$	Own calculation
Inverse availability and loss factors	$f_{\mathrm{cryocool}}^{\mathrm{availability}} \cdot f_{\mathrm{cryocool}}^{\mathrm{loss}}$	1.5	[252]
Lifetime	τ_{cryocool}	20 a	[252]
Operation and maintenance	$\mathrm{O\&M}_{\mathrm{cryocool}}$	4.0%	Own assumption
Electrical energy consumption	$w_{\mathrm{e,cryocool}}$	1 009.2–556.4 $\mathrm{kWh_e\ t_{H2}^{-1}}$ (16.6–34.9 $\mathrm{t_{H2}\ h^{-1}}$)	Own calculation
Annual operating hours	$t_{\mathrm{op,cryocool}}$	7 884 h	Own assumption

when an intermediate cooling station is required for a transmission distance of 150 km. If gaseous hydrogen is the desired product, the average total costs of the hybrid pipeline alternative are also lower than those of the conventional alternative for all considered lengths. However, adding an intermediate cooling station reduces the cost difference between transmission alternatives, principally because of the relatively high variable operating costs $\mathrm{varOPEX}_{\mathrm{cryocool}}$. In the case of pessimistic cost estimates, the hybrid pipeline has comparable total expenses to those of the conventional alternative at 150 km, when hydrogen is required in its gaseous state.

Additionally, this sensitivity analysis shows that the specific total costs of a hybrid pipeline cannot be extrapolated to an arbitrary length. For comparison, the mean specific present-value total cost of the hybrid pipelines are: 10.8 $\mathrm{MEUR_{2023}\ km^{-1}}$ for the 75 km case (tables 5.17 and 5.18), 10.9 $\mathrm{MEUR_{2023}\ km^{-1}}$ for 50 km, and 12.0 $\mathrm{MEUR_{2023}\ km^{-1}}$ for 150 km. For the longest case, the cooling station total cost of 3.0 $\mathrm{MEUR_{2023}\ km^{-1}}$ must be added.

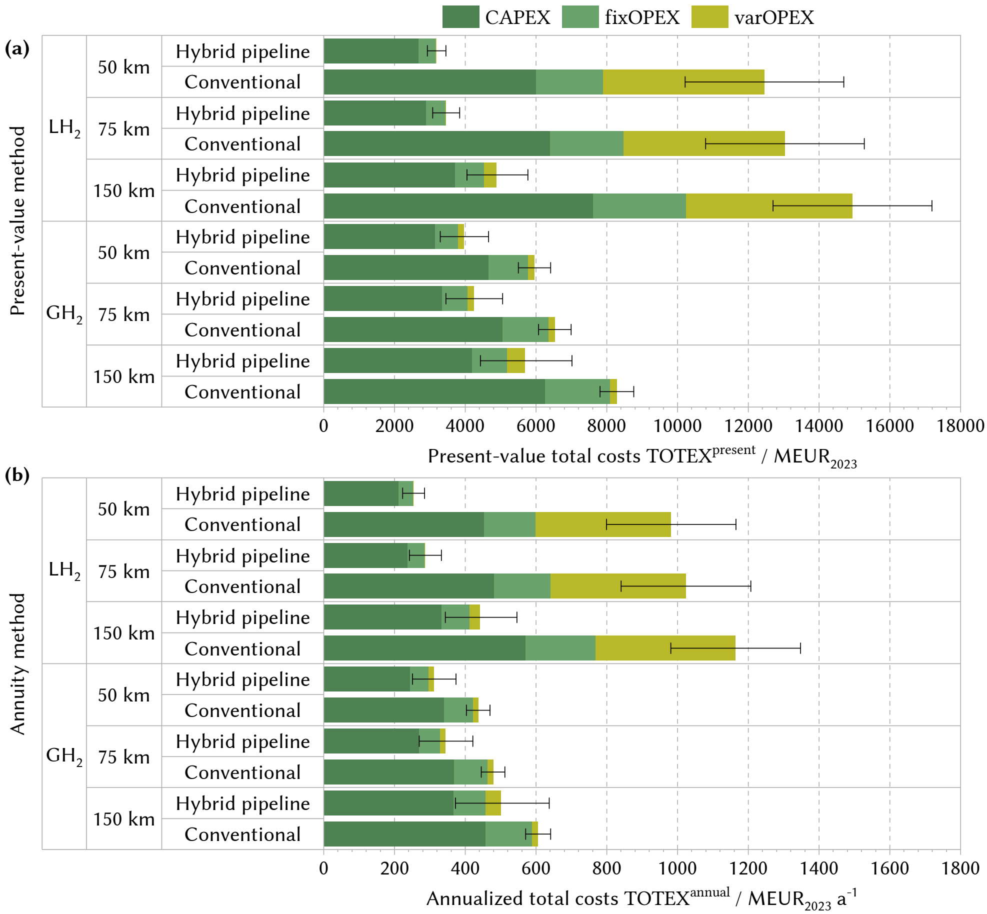

Figure 5.19: Comparison of (a) present-value and (b) annualized total costs between transmission alternatives at lengths of 50, 75, and 150 km. The total costs TOTEX are divided into investment costs CAPEX, fixed operational costs fixOPEX, and variable operational costs varOPEX for each product—liquid hydrogen (LH_2) and gaseous hydrogen (GH_2).

5.5.2 Variation of Assumptions for Three Components

Three component assumptions are varied to identify their influence on the comparison of total costs of transmission alternatives:

1. Converter stations – same specific investment-cost estimate for both 100 and 525 kV
2. HVDC overhead lines – use of overhead lines instead of underground cables in the conventional alternative

3. No hydrogen storage tanks – removal of liquid and gaseous hydrogen storage tanks and associated components in both alternatives

First, the justification for these variations is presented. Afterwards, the consequence of applying each and all component variations is assessed on the total cost difference between the two alternatives.

Converter Stations

In section 5.3.2, different specific investment-cost estimates were defined for the 525 kV converter stations in the conventional alternative (300 $\mathrm{MEUR_{2023}\ GW_e^{-1}}$) and the 100 kV converter stations in the hybrid pipeline alternative (245 $\mathrm{MEUR_{2023}\ GW_e^{-1}}$). This was justified by the lower voltage level of the hybrid pipeline alternative and consequently the smaller size of the converter stations [318]. The TYNDP cost estimates were used because they did not specify the voltage level of the converter stations and it was assumed that they were therefore general and valid for different voltage levels.

Since the investment costs of the converter stations account for the largest share of total investment costs in both transmission alternatives (see figure 5.14), this analysis evaluates the impact on total costs of assigning equal specific investment-cost estimates for both converter types. Accordingly, the specific investment costs of the 100 kV and 525 kV converter stations in the hybrid pipeline and conventional alternative are set at 300 $\mathrm{MEUR_{2023}\ GW_e^{-1}}$, respectively, since this amount is taken from the most recently approved German Network Development Plan 2023 [313].

HVDC Overhead Lines

Section 2.6.1 described that, currently, German law gives priority to new onshore HVDC connections [184] and HVDC overhead lines are only planned in exceptional cases, such as for environmental reasons [185]. This rule is often questioned because underground cables are more expensive than overhead lines [381]. Consequently, the German government is planning to establish HVDC overhead lines for new HVDC connections as mandatory [382] but with some exceptions [186] (see section 2.6.1).

The analysis replaces only the specific investment-cost estimate of the HVDC underground cable system (3.3 $\mathrm{MEUR_{2023}\ GW_e^{-1}\ km^{-1}}$) with that of HVDC overhead lines. The inverse availability factor $f_{\mathrm{HVDCcable}}^{\mathrm{availability}}$, inverse loss factor $f_{\mathrm{HVDCcable}}^{\mathrm{loss}}$, lifetime $\tau_{\mathrm{HVDCcable}}$, and operation and maintenance cost rate $O\&M_{HVDCcable}$ are held constant to facilitate comparison, although some or all of these values are likely to differ for HVDC overhead lines.

Cost estimates from the most recently approved German Network Development Plan 2023 are used to derive the specific investment-cost estimates for the HVDC overhead line [313]. Since this value is not explicitly available there, the cost for new construction of a 380 kV AC overhead line along a new route (double-circuit line, two circuits) is assumed to be identical to that of a 525 kV, 4.0 GW_e HVDC overhead line. This assumption has been previously made by the German TSOs [383] and leads to specific investment-costs of 1.125 $MEUR_{2023}$ GW_e^{-1}.

Hydrogen Storage

In sections 5.1.1 and 5.1.2, hydrogen storage tanks were placed downstream to improve supply security. so liquid hydrogen storage tanks appear in both transmission alternatives when liquid hydrogen is the final product (see figure 5.2). For gaseous hydrogen delivery, the hybrid pipeline alternative needs a liquid hydrogen pump and storage tank, whereas the conventional alternative requires a compressor and gaseous hydrogen storage tank (see figure 5.3). This sensitivity case assigns supply-security responsibilities to the hydrogen consumers, thereby removing the storage tanks and their related components (pump 3 and compressor) from the techno-economic assessment. The investment and operating costs of these components are neglected.

Results for Three Component Assumptions

Figure 5.20 shows the total cost difference between transmission alternatives when the single and combined assumption variations describes in this section are applied. Positive values indicate a cost advantage for the hybrid pipeline alternative, negative values indicate a cost advantage of the conventional alternative. The reference case (no variations) is included for comparison.

The results demonstrate that the replacement of HVDC underground cables by HVDC overhead lines produces the largest absolute decrease of total cost difference between the transmission alternatives. This variation affects equally both liquid and gaseous hydrogen products equally.

When liquid hydrogen is desired as the final product, the second largest total cost difference reduction occurs when the specific investment costs of the HVDC converter stations are set to equal values. When gaseous hydrogen is the final product, removing the hydrogen storage tanks and their related components becomes the second largest effect on the total cost difference. The variation of hydrogen storage has no impact on the comparison when liquid hydrogen is the product, because the same liquid hydrogen storage is removed from both alternatives.

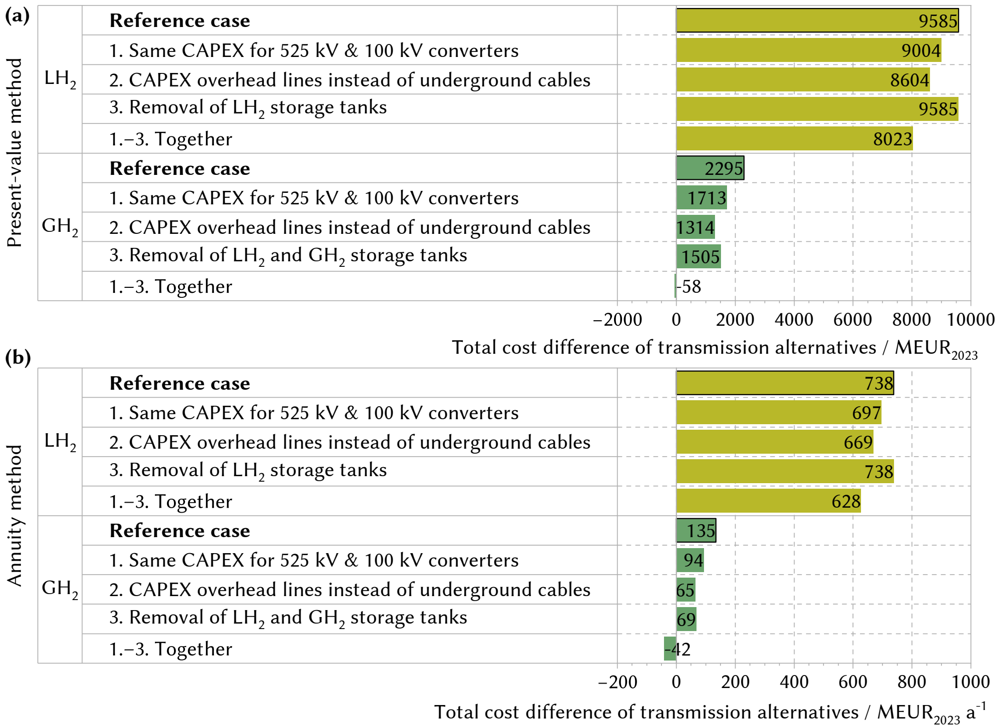

Figure 5.20: Total cost difference between transmission alternatives when varying single assumptions for converter stations, HVDC overhead lines, and hydrogen storage tanks with their related compressor or pump. For each final product—liquid hydrogen (LH_2) and gaseous hydrogen (GH_2)—figure (a) illustrates the results under the present-value method and (b) under the annuity method. Positive values indicate that the hybrid pipeline alternative is less expensive than the conventional alternative, whereas negative values indicate the opposite.

When all three variations are applied, the conventional alternative becomes less expensive than the hybrid pipeline alternative, but only when gaseous hydrogen is the final product. In that case, under the present-value and annuity methods, the conventional alternative costs 57 $MEUR_{2023}$ and 42 $MEUR_{2023}$ a^{-1} less than the hybrid pipeline alternative, respectively.

When liquid hydrogen is the final product, the hybrid pipeline alternative remains more cost-effective and costs 8 023 $MEUR_{2023}$ and 628 $MEUR_{2023}$ a^{-1} less than the conventional alternative under the present-value and annuity methods, respectively.

5.5.3 Liquid Hydrogen Pipe and HVDC Underground Cable as Additional Alternative

The results of the techno-economic assessment demonstrated that the liquefaction and re-gasification steps in the conventional alternative add substantial investment and operational costs when liquid hydrogen is the desired final product and a gaseous hydrogen pipeline is used for hydrogen transmission (see sections 5.4.2 and 5.4.3). To avoid the use of liquefaction plants and vaporizers, an additional alternative is introduced, in which a liquid hydrogen pipe performs the hydrogen transmission and a separate HVDC underground cable system transmits the electrical energy. This "LH_2 pipe & HVDC" alternative is presented in figure 5.21. The sensitivity analysis evaluates the additional alternative only for the case where liquid hydrogen is the final product and compares it with the other transmission alternatives.

The design of the liquid hydrogen pipe is based on the methodology and assumptions used for the hybrid pipeline but excludes the superconducting cable (see section 4.3). Accordingly, the inlet temperature T_{in}, inlet pressure p_{in}, total heat load per unit length q_{l}, and surface roughness ϵ are equal for both the hybrid pipeline alternative and the additional alternative (see table 4.3). The hydraulic diameter D_h is identical to the pipe inner diameter $D_{\mathrm{LH2,i}}$ in the absence of the superconducting cable.

The thermal-hydraulic model shows that the 75 km long liquid hydrogen pipe can transmit 4.1–9.7 kg_{H2} s^{-1} (0.49–1.15 GW_t) with a pipe inner diameter $D_{\mathrm{LH2,i}}$ of 32.1 cm without intermediate cooling stations. In comparison, the 75 km hybrid pipeline transfers 4.6–9.7 kg_{H2} s^{-1} (0.55–1.15 GW_t) using a pipe inner diameter $D_{\mathrm{LH2,i}}$ of 36.0 cm. Table 5.23 presents the liquid hydrogen pipe layout, which is composed of an inner Invar pipe, MLI, and outer carbon steel pipe.

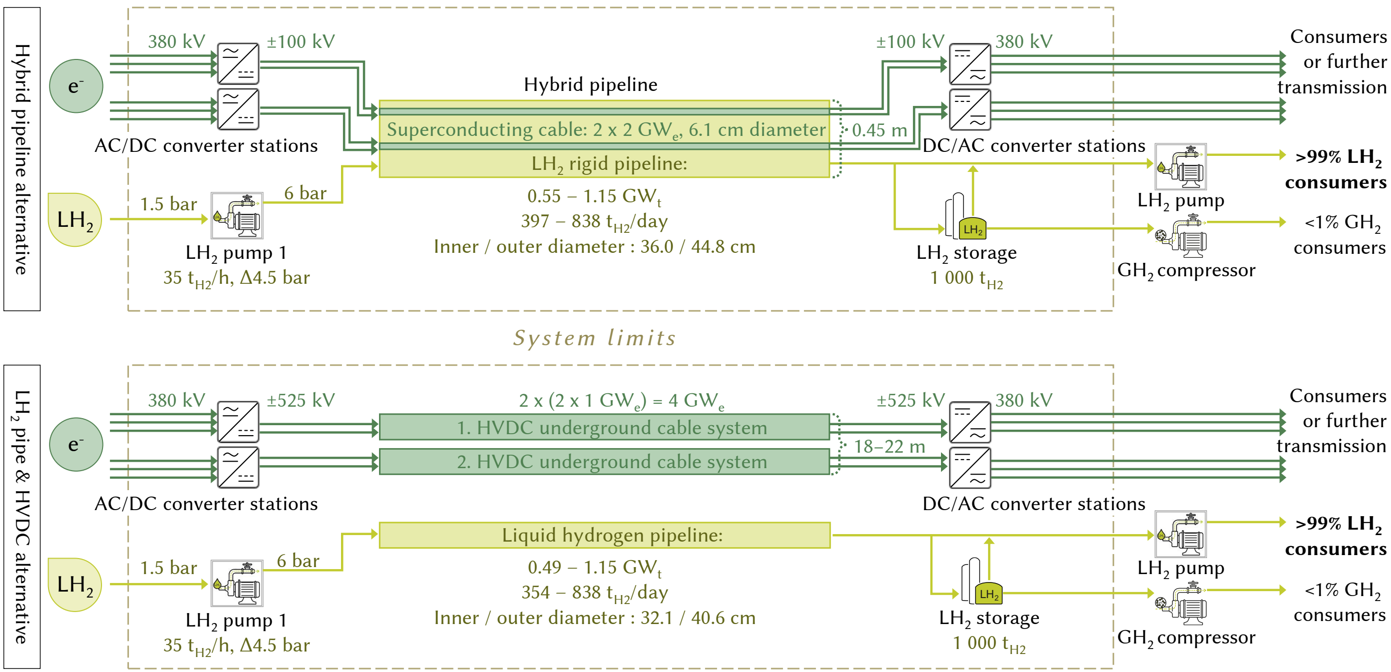

Figure 5.21: Detailed configuration of the hybrid pipeline alternative and the additional alternative based on a liquid hydrogen pipe and an HVDC underground cable system with liquid hydrogen (LH_2) as final product.

Table 5.23: Liquid hydrogen pipe layout for the additional alternative.

Parameters	Symbol	Value
Inner radius of inner pipe	$r_{\mathrm{LH2,i}}$	160.5 mm
Outer radius of inner pipe	$r_{\mathrm{LH2,o}}$	165.5 mm
Outer radius of multi-layer insulation	$r_{\mathrm{MLI,o}}$	185.5 mm
Inner radius of outer pipe	$r_{\mathrm{pipe,i}}$	195.5 mm
Outer radius of outer pipe	$r_{\mathrm{pipe,o}}$	203.0 mm

The mean specific investment costs for Invar, carbon steel, MLI, fabrication, pipe laying, and indirect costs are equal for the additional and hybrid pipeline alternatives (see table 5.4). It is assumed that the lifetime, operation and maintenance rate, inverse availability factor, and inverse loss factor are identical for both transmission alternatives as well (see table 5.5).

Figures 5.22 (a) and 5.22 (b) illustrate the total cost comparison between transmission alternatives under the present-value and annuity methods, respectively. When liquid hydrogen is considered as the final product, the hybrid pipeline alternative is 1 683 $\mathrm{MEUR_{2023}}$ (33%) less expensive under the present-value method and 99.42 $\mathrm{MEUR_{2023}\ a^{-1}}$ (26%) more cost-effective under the annuity method than the "LH_2 & HVDC" alternative, which uses a separate liquid hydrogen pipeline and an HVDC underground cable system. For comparison, figure 5.22 also includes the total costs of the hybrid pipeline alternative and conventional alternatives when gaseous hydrogen is defined as the final product.

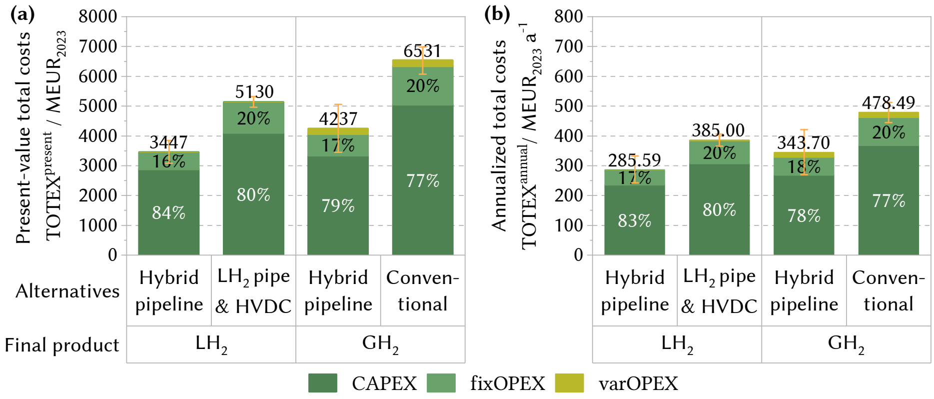

Figure 5.22: Comparison of total cost estimates TOTEX between the additional alternative "LH_2 pipe & HVDC"—based on a separate liquid hydrogen pipeline and an HVDC underground cable system—the hybrid pipeline alternative, and the conventional alternative under the (a) present-value method and (b) annuity method for each final product: liquid hydrogen (LH_2) and gaseous hydrogen (GH_2).

5.6 Discussion and Comparison of Results

While this assessment adopts a comprehensive system perspective that includes all components within the defined boundaries, it is useful to relate the results to existing literature, which often focuses primarily on the main transmission components. For this purpose, conditional specific cost values of the main electrical energy and hydrogen transmission infrastructure are discussed. As previous studies differ in their assumptions, system configurations, and boundary definitions, a direct comparison is not feasible. However, such a harmonized comparison still allows general trends and relative differences to be identified. The results should therefore be interpreted as indicative, particularly given the potentially significant cost contribution of auxiliary components.

This work extends existing research by reporting specific present-value total costs of the proposed hybrid pipelines for selected transmission lengths—50 km, 75 km, and 150 km—each corresponding to a distinct design configuration (see section 5.5.1). Table 5.24 presents the optimistic, mean, and pessimistic specific present-value total cost of the hybrid pipeline designs. For the 150 km design, the cooling station costs are included. The sensitivity analysis showed that specific costs cannot be extrapolated to arbitrary pipe lengths.

The fixed operating costs of the hybrid pipeline account for 3.71% of the investment costs (see table 5.5). In the 150 km design, the mean variable and fixed operating cost of the cooling station are 15% and 1% of the total hybrid pipeline costs, respectively. The 50 km and 75 km configurations do not require cooling stations.

Table 5.24: Optimistic, mean, and pessimistic specific present-value total costs of the hybrid pipeline designs.

Design length	Optimistic	Mean	Pessimistic
50 km	6.27 $MEUR_{2023}$ km^{-1}	10.85 $MEUR_{2023}$ km^{-1}	15.76 $MEUR_{2023}$ km^{-1}
75 km	6.24 $MEUR_{2023}$ km^{-1}	10.82 $MEUR_{2023}$ km^{-1}	15.73 $MEUR_{2023}$ km^{-1}
150 km	9.58 $MEUR_{2023}$ km^{-1}	14.96 $MEUR_{2023}$ km^{-1}	20.70 $MEUR_{2023}$ km^{-1}

Direct cost comparison with previous work is only conditionally possible because only a few studies have evaluated the cost-effectiveness of other superconducting hybrid energy pipeline designs and because their resulting EUR km^{-1} values are derived for different configurations. Moreover, proper comparison must incorporate transmission capacity, expressed in EUR km^{-1} GW_e^{-1} or EUR km^{-1} GW_t^{-1}. Consequently, the rated transmission capacity is used as the weighting metric for allocating costs between the electrical and chemical sides (see equations 5.17 and 5.18). For the hybrid pipeline proposed in this work, these assumptions lead to the specific costs presented in table 5.25.

Table 5.25: Optimistic, mean, and pessimistic specific present-value total costs of the hybrid pipeline designs using the rated transmission capacity as weighting metric for allocating costs between the electrical and chemical sides.

Design length	Electrical ($MEUR_{2023}$ km^{-1} GW_e^{-1})			Chemical ($MEUR_{2023}$ km^{-1} GW_t^{-1})		
	Optimistic	**Mean**	**Pessimistic**	**Optimistic**	**Mean**	**Pessimistic**
50 km	1.22	2.11	3.06	1.22	2.11	3.06
75 km	1.22	2.10	3.05	1.22	2.10	3.05
150 km	1.85	2.88	3.99	1.85	2.88	3.99

For simplicity, the following comparisons omit currency conversion and inflation. Qin et al. estimated total investment costs of 2 785 700 MUSD for a 20 000 km super energy pipeline with capacities of 100 GW_e for electrical energy transmission and 50 GW_t [29] for liquid hydrogen transmission. Their figures were obtained by extrapolating from specific cost values rather than from a bottom-up design. Applying the allocation method for shared infrastructure converts the total-cost estimates to 0.93 MUSD km^{-1} GW_e^{-1} for the electrical side and 0.93 MUSD km^{-1} GW_t^{-1} for the chemical side. However, these results should be interpreted with caution because variable operating costs are not explicitly included, the superconducting cable cost is derived from a 5 GW_e, 2 400 km HTS cable without losses [384], and the cryogenic pipeline and cooling system cost is taken from a 100 MW_e data center power supply system cooled with liquid nitrogen [385].

Since Mangiulli et al. [32] reported only investment costs and Cais et al. [33] employed only a fraction of the total costs for system-level modeling (see section 1.2), a direct comparison with those studies is not possible. A comparable work is that of Cavallucci et al., which analyzes DC transmission lines with MgB_2 wires immersed in liquid hydrogen [31].

At a transmission length of 10 km, Cavallucci et al. reported total costs of 7.2–10.6 MEUR km^{-1} for electrical energy capacities of 0.5–3.0 GW_e. For power levels of 0.5–1.5 GW_e, the cryostat transports roughly 170 g_{H2} s^{-1} (0.02 GW_t), while capacities above 2.5 GW_e, require 190–260 g_{H2} s^{-1} (0.02–0.03 GW_t) [31]. Using the allocation method, the highest capacities of 3.0 GW_e and 0.03 GW_t lead to specific costs of 3.51 MEUR km^{-1} GW_e^{-1} on the electrical side and 3.51 MUSD km^{-1} GW_t^{-1} on the chemical side. For lower transmission capacities, the allocated specific costs increase up to 13.93 MEUR km^{-1} GW_e^{-1} for electrical transmission and 13.93 MUSD km^{-1} GW_t^{-1} for chemical transmission when the line is designed for 0.5 GW_e and 0.02 GW_t.

When the electrical energy transmission is fixed at 2 GW_e, Cavallucci et al. examined four line lengths—5 km, 10 km, 50 km, and 100 km. Although they did not state the liquid hydrogen mass flow rate, it can be inferred to be about 190 g_{H2} s^{-1} (0.2 GW_t). The reported total cost figures range from approximately 9.46 MEUR km^{-1} for the 5 km line to about 7.53 MEUR km^{-1} for the 100 km line. Applying the allocation method to the longest design results in specific costs of 3.73 MEUR km^{-1} GW_e^{-1} on the electrical side and 3.73 MEUR km^{-1} GW_t^{-1} on the chemical side. Shorter configurations exhibit higher allocated costs. For instance, the 50 km line shows specific costs of 3.87 MEUR km^{-1} GW_e^{-1} for the electrical transmission and 3.87 MEUR km^{-1} GW_t^{-1} for the chemical transmission.

This analysis appears to suggest that, for the design lengths of 75 km and 150 km, the REBCO-based hybrid pipeline in this work may indicate lower allocated specific costs than the 100 km MgB_2 DC transmission lines that use MgB_2 wires immersed in liquid hydrogen. This may be justified by the relatively low transmission capacity of the MgB_2 line.

Previous studies have assumed that MgB_2 is more cost-effective than REBCO (e.g., [19, 33]), an idea supported by the specific costs per km. However, under the assumptions investigated in the present study, a different trend emerges when comparing the specific total costs per km and per GW. For a consistent assessment of both superconducting technologies, comparable transmission capacities, system configurations, and lengths will be required.

6 Summary, Conclusions, and Outlook

This chapter summarizes the main results of the dissertation and discusses their significance. It first introduces the principal findings, then derives the key conclusions, and lastly delineates the outlook for future research and practical implementation.

6.1 Summary

For the techno-economic assessment of a hybrid pipeline, this dissertation first examined the required background for the synergetic transmission of liquid hydrogen and electrical energy by high-temperature superconductivity. An extensive literature review was conducted to quantify and locate the expected supply and demand for both energy vectors in Germany. This analysis aimed to identify an appropriate case study.

Separate conventional transmission alternatives were determined for each energy carrier to benchmark the hybrid pipeline. The state of the art of superconducting energy pipelines was briefly summarized, providing examples of some built prototypes.

In a second step, the selected case study was used to develop the conceptual design of a hybrid pipeline. For this purpose, the technical properties and commercial availability of the superconducting material were discussed. For the electrical energy transmission, distinct topologies were compared. The amount of superconductor, electrical insulation, and stabilizing copper was calculated using Python-coded, lumped-parameter, adiabatic simulations of the cable operation, even in the event of a fault.

The chemical energy transmission was simulated by a Python-based thermal-hydraulic model, which estimated the temperature increase and pressure drop of the delivered liquid hydrogen at the pipeline outlet. The compressibility of liquid hydrogen was considered. This analysis led to the pipe layout.

In the last step, a comprehensive techno-economic assessment was carried out to assess the cost-effectiveness of a hybrid pipeline system compared to a conventional alternative. The system boundaries and auxiliary components were defined based on the selected case study.

Using the proposed conceptual design, the investment cost of the hybrid pipeline was estimated. A detailed literature review and some expert interviews were conducted to estimate the investment, fixed, and variable operating costs of the other components. Optimistic, mean, and pessimistic cost parameters were included to reflect the uncertainty of component and material costs.

The performance of each component was considered according to its availability and losses. Three distinct levels of financing parameters were defined based on the deployment stage of the technologies. Component replacement and discounting were considered for a system lifetime of 40 years. The results were evaluated under the present-value and annuity methods to highlight different economic perspectives. A sensitivity analysis quantified how varying underlying assumptions affect the cost-effectiveness of the transmission alternatives.

Lastly, the specific total cost of the hybrid pipeline was compared with that from previous studies. This was conditionally possible by using the rated transmission capacity as the weighting metric to allocate costs between the electrical and chemical sides. Such a methodology was selected because of the high interconnection of the electrical and chemical designs of the hybrid pipeline.

Main Results

By 2045, 60–70 GW_e of offshore wind capacity are projected in northern Germany. New transmission infrastructure is required to deliver the electrical energy to locations where demand is expected, e.g., in densely populated regions with demand estimates higher than 7 $GW_e\ km^{-2}$.

Germany's hydrogen supply is projected to be 13% to 51% through imports. Because of the expected involved costs, multiple studies indicated that most hydrogen imports are more likely to occur via pipelines than through terminals. However, the latest Approval of the Scenario Framework for the Natural Gas and Hydrogen Network Development Plan calls for a minimum of 4 $GWh_t\ h^{-1}$ of hydrogen imports by ship to ensure the security of supply.

A comparison of energy efficiencies in the import supply chain of various chemical energy carriers showed that liquid hydrogen imports achieve the highest efficiency when gaseous hydrogen is needed for end-use. Project partners determined that the levelized cost of hydrogen is the lowest for liquid hydrogen and ammonia imports when reconversion back to gaseous hydrogen and terminal costs are included. The analysis also indicated that the TRL of liquid hydrogen terminal components is lower than those for other chemical energy carriers.

The demand for liquid hydrogen is expected in sectors where its high energy density, high purity, and cryogenic temperature are particularly valuable. For aviation, the expected liquid hydrogen demand by 2050 in Germany ranges from 0.9 GW_t to 3.0 GW_t. For heavy-duty trucks, the projected hydrogen demand varies between 0.28 GW_t and 8.33 GW_t. An estimate of the hydrogen demand for the maritime sector on the European Atlantic coast was 28.2 GW_t, but the state of matter was not specified. Single semiconductor facilities require between 0.4 MW_t and 7.1 MW_t of high-purity hydrogen. Moreover, liquid hydrogen can be regasified and employed by industries with expected large hydrogen demand, such as steel and chemical manufacturers.

In northern Germany, Brunsbüttel is expected to become a node for electrical energy coming from offshore wind farms and northern countries. The industrial location has today an LNG import terminal that is projected to become a hydrogen import terminal. Approximately 75 km to the south, Hamburg is a big city, home to the largest airport in northern Germany and the largest German maritime port. The city is an extensive road-based transport hub and it has manufacturing industries for chips and steel. Thus, Brunsbüttel–Hamburg was selected as the case study. Based on current electrical transmission projects, a rated capacity of 4.0 GW_e of electrical energy was defined. Interviews with relevant local stakeholders indicated that at least 0.62–0.87 GW_t of hydrogen will be required in Hamburg.

For the electrical cable, REBCO was selected as the superconducting material owing to its high performance and widespread commercial availability. A topology consisting of two parallel DC coaxial monopoles with a metallic return path was selected because it leads to thinner cables, less induced voltage during current variations, and a lower magnetic field in the surroundings than other topologies. A rated current of 20 kA at $\pm$100 kV was selected to transmit 4.0 GW_e and to reduce the required amount of superconductor compared to higher currents at lower voltage levels.

The cable model determined a total superconductor amount of 6 522 km for 4 mm wide REBCO tapes. The simulations revealed that the proposed cable layout safely withstands a short circuit that leads to a maximum current of 175 kA during about 0.05 s. Moreover, the Joule losses that increase the cable temperature do not cause liquid hydrogen boiling. The thermal-hydraulic simulation demonstrated that liquid hydrogen has a safe margin to the boiling curve after 75 km of transmission in a rigid pipe without intermediate cooling stations. With an outer diameter of less than 45 cm, the hybrid pipeline can transmit 0.55–1.15 GW_t of liquid hydrogen and 4.0 GW_e of electricity.

The average investment cost of the hybrid pipeline was estimated to be 557 $MEUR_{2023}$. The values range from 321 $MEUR_{2023}$ to 810 $MEUR_{2023}$, depending on optimistic and pessimistic estimates. On average, the indirect costs—such as engineering, owner's costs, and unforeseen events—exhibited the largest cost share (159 $MEUR_{2023}$), followed by Invar (119 $MEUR_{2023}$) for the inner pipe, the electrical insulator (78 $MEUR_{2023}$), pipe laying (70 $MEUR_{2023}$), and the REBCO tapes (62 $MEUR_{2023}$).

Two possible valuable products were identified for end-use delivery: liquid and gaseous hydrogen. The conventional system comprised an underground HVDC cable system and a gaseous hydrogen pipeline. Within the system limits, the transmission alternatives included auxiliary components such as converter stations, liquefaction plants, vaporizers, pumps, compressors, and storage tanks for the liquid or gaseous state of hydrogen.

Based on the presented assumptions, the results revealed that, for liquid hydrogen delivery, the mean total cost of the hybrid pipeline alternative would be 286 $MEUR_{2023}$ a^{-1} (present-value 3 447 $MEUR_{2023}$) versus 1 024 $MEUR_{2023}$ a^{-1} (present-value 13 034 $MEUR_{2023}$) for the conventional alternative. In relative terms, the hybrid pipeline alternative is 72% less expensive than the conventional option (present-value 74%). For gaseous hydrogen delivery, the figures are 344 $MEUR_{2023}$ a^{-1} (present-value 4 237 $MEUR_{2023}$) versus 479 $MEUR_{2023}$ a^{-1} (present-value 6 533 $MEUR_{2023}$), respectively. Analogously, the hybrid pipeline system is 28% more cost-effective than the conventional alternative (present-value 35%). Parenthetical values correspond to the present-value calculations, which exhibit a larger cost difference than the annualized values owing to the three distinct levels of financing parameters.

The total cost difference between transmission alternatives was larger for liquid hydrogen delivery, mainly because of the required regasification (786 $MEUR_{2023}$) and liquefaction (7 295 $MEUR_{2023}$) in the conventional alternative. The variable operating cost for hydrogen liquefaction was the highest (4 0388 $MEUR_{2023}$) among the investment and operating expenses. The total costs of the converter stations represent the largest share in both alternatives (525 kV: 3 153 $MEUR_{2023}$; 100 kV: 2 572 $MEUR_{2023}$) when omitting the total cost of the liquefier. The largest total cost uncertainty exhibit both the liquefier (7 295 $MEUR_{2023}$ $\pm$ 1 792 $MEUR_{2023}$) and vaporizer (786 $MEUR_{2023}$ $\pm$ 419 $MEUR_{2023}$). The values in parentheses represent the average total costs under the present-value method.

The sensitivity analysis showed that the investment cost of the converter stations has the largest influence on the total cost of each system. Changing the transmission length demonstrated that the specific cost of the hybrid pipeline cannot be extrapolated. On average, the present-value specific total cost of the hybrid pipelines is 10.9 $MEUR_{2023}$ km^{-1} for the 50 km design, 10.8 $MEUR_{2023}$ km^{-1} for 75 km, and 15.0 $MEUR_{2023}$ km^{-1} for 150 km, which includes the total cost for one cooling station. The length sensitivity indicated that the hybrid pipeline alternative is more cost-effective than conventional infrastructure up to at least 150 km. Only under pessimistic cost parameters, the 150 km hybrid pipeline system's mean total cost per year becomes comparable to that of the conventional option for gaseous hydrogen delivery

Replacing the investment cost estimate of the underground HVDC cable system with that of HVDC overhead lines reduced the present-value cost advantage of the hybrid pipeline alternative by 10% for liquid hydrogen as the end-use product. When a separate liquid hydrogen pipe together with an underground HVDC cable was considered as a transmission alternative, the hybrid pipeline option remained more cost-effective, yielding 33% lower mean present-value expenses for liquid hydrogen transport.

These results provide the foundations for the conclusions derived as follows.

6.2 Conclusions

The main contribution of this work is providing evidence that hybrid pipelines can achieve considerably lower total costs than conventional infrastructure under a variety of conditions. The results demonstrate that a hybrid pipeline not only provides technical advantages, such as electrical and chemical energy transmission on a GW-scale with low material and space requirements. A hybrid pipeline also offers significant economic benefits in certain contexts.

The sensitivity analysis indicated that varying underlying parameters do not significantly affect the cost-effectiveness of the hybrid pipeline alternative compared to the conventional system. The results suggest that the cost advantage of the hybrid pipeline system is robust to length variations and component uncertainties. Although transmission distances beyond 150 km were not examined, the results do not exclude the possibility that the hybrid pipeline system could become more cost-effective than conventional infrastructure, especially when liquid hydrogen is the end-use product.

The length analysis demonstrated that the specific costs cannot be reliably extrapolated. Consequently, direct comparison with previous works is limited and requires matching transmission capacities and lengths.

While the bottom-up design of the hybrid pipeline showed how hydrogen and electrical energy can be transmitted synergetically using high-temperature superconductivity, the conceptual design also served to estimate the investment costs of the hybrid pipeline. The results indicated that the total cost of the hybrid pipeline represents only 6% of the 2025 cost associated with network congestion management measures in Germany. This suggests that a hybrid pipeline may be able to relieve network congestion at a relatively low cost.

The literature review indicated that liquid hydrogen imports are cost-competitive with ammonia imports and that several sectors will employ liquid hydrogen to enable decarbonization. While the TRL of several liquid hydrogen technologies is currently noticeably lower than those for other chemical energy carriers, international research is progressively maturing liquid hydrogen components to higher TRL stages for the coming decades. This findings suggest that imported liquid hydrogen will be available in significant amounts in the future.

From a practical perspective, the findings provide a solid quantitative basis for evaluating the economic viability of hybrid pipelines. In particular, the results support stakeholders, including electricity and hydrogen TSOs, policymakers, and regulatory authorities such as the German Federal Network Agency, in deciding how to expand the electricity and hydrogen transmission infrastructure.

At the same time, it is important to consider the limitations of the present study. The economic results apply only to the systems characterized by the assumptions presented in this work. If a hybrid pipeline system must include domestic hydrogen liquefaction, the results suggest that the conventional infrastructure would be more cost-effective for gaseous hydrogen delivery, even though that case was not explicitly quantified. This can be attributed to relatively high industrial electricity costs in Germany, in contrast to regions with lower electricity production costs. For liquid hydrogen delivery, the available evidence does not allow a direct determination of whether a local hybrid pipeline system with on-site liquefaction would become more cost-effective than conventional infrastructure.

Despite the contributions of this work, it does not evaluate the levelized costs of electrical energy and liquid hydrogen. These analyses would strengthen the cost-effectiveness of the hybrid pipeline and support a business case for stakeholder investment. A system-level analysis would further clarify the role of hybrid pipelines within integrated energy systems. While these limitations should be considered, the conclusions remain robust within the defined scope.

6.3 Outlook

Given the identified limitations, several directions for future research can be pursued. To advance the hybrid pipeline beyond TRL 4, targeted experimental liquid hydrogen projects—such as electrical insulation tests, determination of the heat load on a long-distance cryogenic pipe, and enhancement of thermal-hydraulic safety measures for high-range transmission—are required. The hydrogen integration platform at KIT could be used to test some of these aspects and implement them in future hybrid pipeline prototypes.

The accuracy of the hybrid pipeline investment cost estimate can be enhanced by benchmarking the presently derived fabrication costs against those from future prototype projects.

Although such a comparison still lacks data on long-distance applications, it refines the underlying cost assumptions and strengthens the overall techno-economic analysis.

A comprehensive comparison with further transmission systems would provide quantified results for evaluating cost-effectiveness. For example, one could compare a hybrid pipeline that transports liquid hydrogen after an upstream liquefaction plant versus a conventional pipeline that transmits gaseous hydrogen with liquefaction performed downstream at the delivery point. Further assessments might contrast the economics of delivering liquid hydrogen by road-based trailers with those of the hybrid pipeline concept.

An important extension would be to consider the levelized cost of electrical and chemical energy when delivering liquid hydrogen. In such studies, the coupling effects arising from the interdependent operation of the superconducting cable and the liquid hydrogen flow should be examined. A revenue model including avoided grid reinforcement costs could strengthen the profitability prospect of the hybrid pipeline. Its effective integration into the national energy system needs a system-level model.

For a consistent techno-economic assessment between different superconducting energy pipeline technologies, such as those based on MgB_2 and REBCO, future works should develop bottom-up designs with comparable configurations. Relevant configuration aspects include the electrical and chemical transmission capacities as well as the length.

The implementation of a hybrid pipeline in the energy system requires higher hydrogen liquefaction energy efficiency—shifting from present-day performance toward long-term theoretical targets. This holds for both liquid hydrogen imports from regions with abundant wind and solar resources as well as for domestic production. Moreover, the requirement is not exclusive for commercializing the hybrid pipeline, but several other energy sectors rely on the availability of liquid hydrogen to achieve decarbonization.

Beyond techno-economic aspects, the large-scale deployment of a hybrid pipeline also depends on a supportive regulatory regime. While this work demonstrates the technical and economical feasibility of a hybrid pipeline transmission system under the presented assumptions, its implementation will depend on consequent policies that facilitate further coupling of the hydrogen and electrical energy sectors.

Overall, the continued development of a consistent policy framework will be essential to support the further expansion of renewable energy systems and to reduce the use of fossil fuels. In addition, the active engagement of relevant societal actors is indispensable. Only through the combination of these elements can long-term economic development, stable socio-economic systems, and healthy ecosystems be enabled.

A Appendix: Background for Combined Energy Transition

Table A.1: Energy delivered in form of gaseous hydrogen (H_2, lower heating value) after losses in the production and import chain of liquid hydrogen (LH_2), liquid organic carriers (LOHC), and ammonia (NH_3) when using 100 kWh of electrical energy from renewable sources. IEA and Staiß et al. assumed a distance of 10 000 km for shipping, while Hank et al. considered 4 000 km. Hank et al. assumed a base case for 2020 and an optimistic case for $\sim$ 2030. Data based on [48, 52, 69].

Source	H_2 transport medium	Electrolysis	Conversion	Shipping	Reconversion into H_2	Energy delivered
IEA 2024	LH_2	27.780	16.910	2.090	0.010	53.210
	NH_3	30.440	12.530	3.910	16.260	36.860
	LOHC	33.190	0.840	10.100	21.850	34.020
Staiß 2022	LH_2	35.000	12.350	3.686	0.000	48.965
	NH_3	35.000	11.050	1.619	3.663	48.668
	LOHC	35.000	0.650	3.861	16.332	44.157
Hank 2020 (optimistic)	LH_2	29.162	11.561	1.338	0.000	57.938
	LOHC	32.619	0.000	1.777	16.401	49.203
Hank 2020 (base)	LH_2	32.731	13.653	1.211	0.000	52.405
	LOHC	37.528	0.000	1.648	18.247	42.577

Table A.2: Energy delivered in form of the corresponding transport medium when no reconversion into gaseous hydrogen (H_2) is considered (lower heating value). Losses are included from the production and import chain of liquid hydrogen (LH_2), ammonia (NH_3), synthetic liquid methane (LCH_4), methanol (MeOH), and Fischer-Tropsch products when using 100 kWh of electrical energy from renewable sources. IEA and Staiß et al. assumed a distance of 10 000 km for shipping, while Hank et al. considered 4 000 km. Hank et al. assumed a base case for 2020 and an optimistic case for $\sim$ 2030. Data based on [48, 52, 69].

Source	H_2 transport medium	Electrolysis	Conversion	Shipping	Energy delivered
IEA 2024	LH_2	27.780	16.910	2.090	53.220
	NH_3	30.440	12.530	3.910	53.120
Staiß 2022	NH_3	35.000	11.050	1.619	52.332
	LH_2	35.000	12.350	3.686	48.965
	MeOH	35.000	22.750	0.845	41.405
	Fischer-Tropsch	35.000	27.950	0.371	36.680
Hank 2020 (optimistic)	LH_2	29.162	11.561	1.338	57.938
	NH_3	29.794	17.177	0.657	52.372
Hank 2020 (optimistic with heat)	LCH_4	29.777	21.022	0.369	48.832
	MeOH	25.421	30.138	0.316	44.126
Hank 2020 (optimistic without heat)	LCH_4	26.789	28.948	0.332	43.932
	MeOH	25.227	30.669	0.309	43.795
Hank 2020 (base)	LH_2	32.731	13.653	1.211	52.405
	NH_3	33.691	17.986	0.599	47.725
Hank 2020 (base with heat)	LCH_4	33.195	22.605	0.331	43.869
	MeOH	28.757	30.733	0.288	40.222
Hank 2020 (base without heat)	LCH_4	30.171	29.654	0.301	39.873
	MeOH	28.557	31.875	0.281	39.286

Table A.3: Comparison of technology readiness level (TRL) of the components for terminals handling liquid hydrogen (LH_2), liquefied natural gas (LNG), ammonia (NH_3), methanol (MeOH), liquid organic hydrogen carriers (LOHC), dimethyl ether (DME), and synthetic liquid methane (LCH_4). Data adapted from [85]. Cells with * indicate corrected values from: section 5.3.10 (regasification) and appendix C (ship).

Component	Target parameters LH_2	LNG	LH_2	NH_3	MeOH	LOHC	DME	LCH_4
Jetty system, loading arms		TRL9	TRL9	TRL9	TRL9	TRL8	TRL9	TRL9
Storage tank sphere	160 000 m^3	TRL9	TRL9	TRL9	x	TRL8	x	TRL9
Storage tank flat bottom design	160 000 m^3	TRL9	TRL5	TRL9	TRL9	TRL8	TRL9	TRL9
Submerged transfer pumps		TRL9	TRL9	TRL9	TRL9	TRL8	x	TRL9
Regasification		TRL9	TRL6*	TRL9	x	x	x	TRL9
Submerged evaporizer		TRL9	TRL6	x	x	x	x	TRL9
Cold utilization system	300 MW_e	TRL9	TRL5	x	x	x	x	TRL9
Compressors if required		TRL9	TRL9	TRL9	TRL9	TRL9	TRL9	TRL9
Boil-off-gas management	Some t_{H2} d^{-1}	TRL9	TRL9	TRL9	x	x	TRL9	TRL9
Road trailer		TRL9	TRL9	TRL9	TRL9	TRL8	TRL9	TRL9
Ship		TRL9	TRL5*	TRL9	TRL9	TRL8	TRL7	TRL9
Dehydrogenation		x	x	x	x	TRL7	x	x
Hydrogenation		x	x	x	x	TRL7	x	x
Steam reforming		x	x	x	x	x	TRL9	x
Cracking		x	x	TRL6–7	x	x	x	x

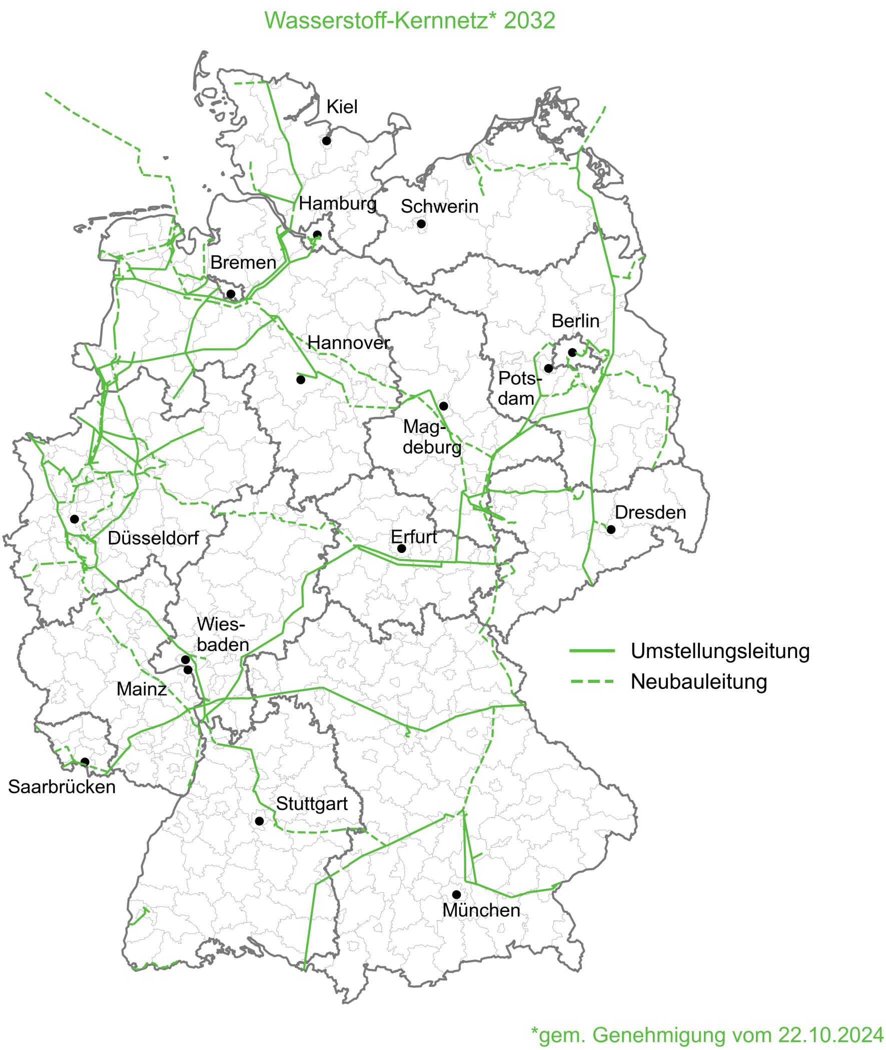

Figure A.1: Approved hydrogen core network, with a length of 9 040 km, for the year 2032 including repurposed pipelines (*"Umstellungsleitung"*) and new pipelines (*"Neubauleitung"*) as of October 22, 2024. Depiction from FNB Gas e.V. [386].

Figure A.2: German natural gas transmission network with a length of approximately 40 000 km divided into a H-Gas network (high calorific gas), an L-Gas network (low calorific gas), pipes not yet in operation (*"Leitungen noch nicht in Betrieb"*), storage connections abroad (*"Speicheranschlüsse Ausland"*), storage on transmission H-Gas pipes (*"Speicher an Fernleitungsnetzen H-Gas"*), and storage on transmission L-Gas (*"Speicher an Fernleitungsnetzen L-Gas"*) as of January 1, 2022. Depiction from FNB Gas e.V. [387].

B Appendix: Material Properties of the Cable

This appendix includes the material properties used for the cable design in section 4.2. Figure B.1 (a) presents the assumed resistivities of copper ϱ_{cu} [263], silver ϱ_{ag} [388], and Hastelloy® ϱ_{hy} [389] on dependence of temperature T between 10 and 300 K. For YBCO, the assumed resistivity ϱ_{hts} is presented from 93 to 300 K in figure B.1 (b) [390]. A critical temperature T_c of 93 K is assumed, as it is defined by Y. Iwasa for $YBa_2Cu_3O_{7\text{-}x}$ [214]. Below the critical temperature T_c, the resistivity of YBCO is described using power law (see section 4.2.4).

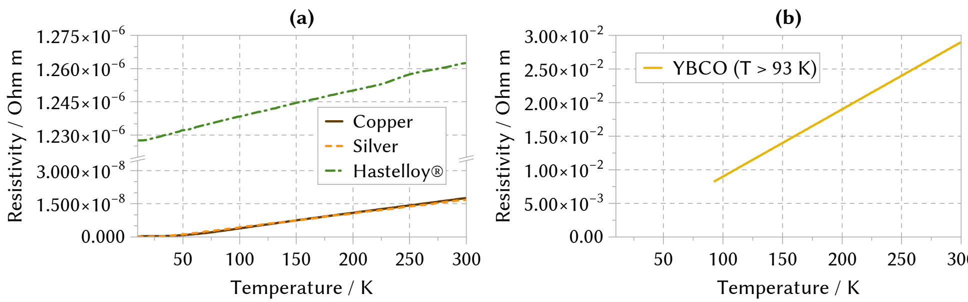

Figure B.1: (a) Resistivity of copper, silver, and Hastelloy® based on [263], [388], and [389], respectively. (b) Resistivity of YBCO from 93 to 300 K based on [390]. Below the critical temperature T_c of 93 K, the resistivity of YBCO is described using power law.

The specific heat capacities of copper $c_{p,\mathrm{cu}}$ [391], silver $c_{p,\mathrm{ag}}$ [388], Hastelloy® $c_{p,\mathrm{hy}}$ [389], and YBCO $c_{p,\mathrm{hts}}$ [392] were used to simulate the temperature variation in each layer of the cable. These temperature dependent parameters are shown in figure B.2. The product of the specific heat capacity, the volume and the mass of each material are their heat capacities, which are used for the model. Table B.1 presents the assumed mass densities for this procedure.

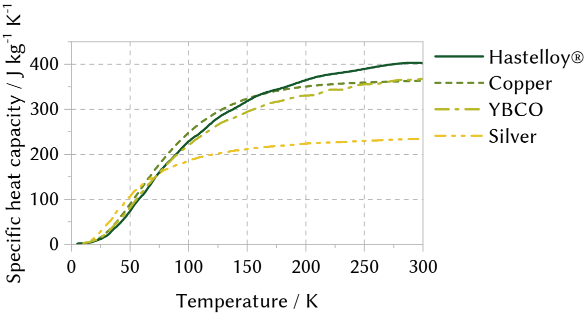

Figure B.2: Specific heat capacities of Hastelloy®, copper, YBCO, and silver based on [389], [391], [392], and [388], respectively.

Table B.1: Mass densities of the materials for the cable simulation.

Material	Symbol	Density
Copper	ρ_{cu}	8 940 kg m^{-3} [236]
Silver	ρ_{ag}	10 492 kg m^{-3} [388]
YBCO	ρ_{hts}	6 380 kg m^{-3} [393]
Hastelloy®	ρ_{hy}	8 890 kg m^{-3} [389]

C Appendix: Techno-economic Assessment

Liquid Hydrogen Carriers

In 2020, Kawasaki Heavy Industries (Japan) built the world's first ship for transporting liquid hydrogen [394]. With a capacity of 1 250 m^3, the vessel sailed 9 000 km to deliver liquid hydrogen from Australia to Japan [395]. Since then, several concepts have received the approval in principle for large carriers of 80 000–160 000 m^3 that are expected to be commercial before 2030 (see table C.1). Three additional projects have obtained an approval in principle for carriers of 20 000 m^3 and one for 37 500 m^3 [396].

Table C.1: Large liquid hydrogen carrier concepts with approval in principle.

Company	Storage type	Volume (m^3)	Approval in principle	Country
Kawasaki Heavy Industries (KHI)	Spherical	160 000	Nippon Kaiji Kyokai [358]	Japan
Samsung Heavy Industries	Membrane	160 000	Lloyd's Register [397]	South Korea
TotalEnergies, GTT, LMG Marin, Bureau Veritas	Membrane	150 000	Bureau Veritas [398]	France
Woodside Energy, MOL, HD KSOE, Hyundai Glovis	-	80 000	DNV [399]	South Korea, Australia, Japan
CB&I, Hanwha Ocean	Spherical	80 000	DNV [400]	USA, South Korea

To estimate the annual delivery of a large liquid hydrogen carrier with a capacity of 160 000 m^3, the following assumptions are made. The vessel is equipped with four spherical tanks of 40 000 m^3 each [358]. Its energy consumption is 970 $kWh_t\ km^{-1}$ when fully loaded and 70% of this value on the empty return segment [401]. The storage boil-off rate is 0.3% d^{-1} [402] and the boil-off gas is used as fuel for propulsion. A journey from Canada to Germany spans approximately 6 000 km and requires at least seven days at a speed of 20 nodes [401]. Consequently, a delivery of 154 640 m^3 arrives in Germany every 14 days, corresponding to roughly 289 249 t_{H2} a^{-1} (≈1.1 GW_t).

Liquid Hydrogen Terminal

Figure C.1 shows a schematic of a liquid hydrogen terminal. The concept builds on the terminal designs presented by [85] and [403]. A pump located inside the vessel transfers the liquid hydrogen through an unloading unit into a flat-bottom storage tank. The unloading unit comprises several flexible transfer arms equipped with vacuum-insulated pipes. Boil-off gas is generated both by the unloading process and by heat transfer into the insulated tank.

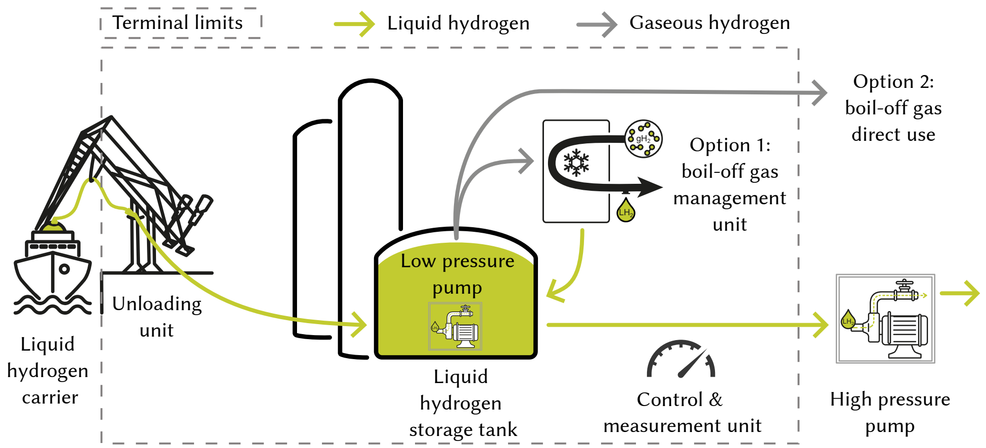

Figure C.1: Schematic of a liquid hydrogen terminal.

In option 1, the boil-off gas is fed into an active boil-off gas management system, which is the standard approach for LNG terminals. A flare system can be added for emergency situations to avoid the indirect green-house effect of released hydrogen, or the hydrogen may be oxidized to water before venting [85]. In option 2, the boil-off gas is used directly at the site, eliminating the need for re-liquefaction and reducing capital and operating costs [403].

A low pressure pump inside the storage tank extracts the liquid hydrogen and feeds it into a high pressure pump that raises the pressure for long-distance transmission. A control and measurement unit monitors the entire process. It comprises pressure-safety and control valves, fire and gas detection systems, flow and temperature sensors, and metering devices [403].

Economic Parameters

Table C.2: Inflation-adjustment factors with consumer price index of 2023 as reference year (base = 1.0) [404].

From	To	EUR	USD	CHF	GBP	NOK
1998	**2023**	1.7266	1.8693	1.1649	2.1225	1.8120
1999	**2023**	1.7067	1.8289	1.1556	2.0903	1.7701
2000	**2023**	1.6702	1.7695	1.1379	2.0303	1.7171
2001	**2023**	1.6308	1.7205	1.1267	1.9949	1.6671
2002	**2023**	1.5946	1.6937	1.1195	1.9622	1.6459
2003	**2023**	1.5615	1.6560	1.1124	1.9071	1.6059
2004	**2023**	1.5283	1.6130	1.1036	1.8519	1.5987
2005	**2023**	1.4954	1.5602	1.0908	1.8011	1.5745
2006	**2023**	1.4631	1.5114	1.0794	1.7453	1.5387
2007	**2023**	1.4321	1.4696	1.0715	1.6735	1.5278
2008	**2023**	1.3858	1.4152	1.0461	1.6094	1.4725
2009	**2023**	1.3814	1.4203	1.0512	1.6180	1.4409
2010	**2023**	1.3595	1.3974	1.0440	1.5466	1.4068
2011	**2023**	1.3234	1.3546	1.0416	1.4701	1.3890
2012	**2023**	1.2912	1.3271	1.0489	1.4243	1.3794
2013	**2023**	1.2740	1.3080	1.0511	1.3823	1.3507
2014	**2023**	1.2685	1.2871	1.0513	1.3504	1.3237
2015	**2023**	1.2681	1.2856	1.0634	1.3372	1.2956
2016	**2023**	1.2650	1.2696	1.0681	1.3144	1.2512
2017	**2023**	1.2437	1.2431	1.0624	1.2689	1.2281
2018	**2023**	1.2206	1.2128	1.0526	1.2355	1.1951
2019	**2023**	1.2029	1.1918	1.0488	1.2054	1.1697
2020	**2023**	1.1941	1.1773	1.0564	1.1841	1.1549

Continued on next page

Table C.2: Inflation-adjustment factors with consumer price index of 2023 as reference year (base = 1.0) [404]. (Continued)

From	To	EUR	USD	CHF	GBP	NOK
2021	**2023**	1.1604	1.1245	1.0503	1.1553	1.1160
2022	**2023**	1.0628	1.0412	1.0214	1.0707	1.0552
2023	**2023**	1.0000	1.0000	1.0000	1.0000	1.0000
2024	**2023**	0.9788	0.9719	0.9895	0.9684	0.9695
2025	**2023**	0.9551	0.9491	0.9880	0.9379	0.9408
2026	**2023**	0.9490	0.9401	0.9828	0.9292	0.9132

Table C.3: Exchange rates expressed in euros (EUR) with a base of 1.0 based on data from [405].

From	To	Date	Rate
USD_{2023}	EUR_{2023}	12/31/2023	0.924224
CHF_{2023}	EUR_{2023}	12/31/2023	1.028955
GBP_{2023}	EUR_{2023}	12/31/2023	1.149226
NOK_{2023}	EUR_{2023}	12/31/2023	0.087568

Cost Assumptions for Hybrid Pipeline

Table C.4 summarizes the material and fabrication costs of the hybrid pipeline. The layer dimensions determine the required material quantities. For copper, Invar, and carbon steel, the required mass is calculated from their respective densities: copper (8 940 kg m^{-3}, see table B.1), Invar (8 100 kg m^{-3} [406]), and carbon steel (7 850 kg m^{-3} [407]). The copper price is based on the trading value, i.e., the raw-material/base price plus processing costs [408].

Table C.4: Material and fabrication costs of the hybrid pipeline.

Description	Original unit	Used unit	Source
	HTS REBCO tape		
Low range (12 mm width)	20 EUR_{2025} m_l^{-1}	1.59 EUR_{2023} m_l^{-1} mm_{width}^{-1}	[232]
High range (12 mm width)	40 EUR_{2025} m_l^{-1}	3.18 EUR_{2023} m_l^{-1} mm_{width}^{-1}	[232]
Total HTS optimistic costs		41.53 $MEUR_{2023}$	
Total HTS mean costs		62.29 $MEUR_{2023}$	
Total HTS pessimistic costs		83.06 $MEUR_{2023}$	
	Copper: material plus workmanship		
Low range (06/21/2023)	917.76 EUR_{2023} 100 kg^{-1}	9 177.60 EUR_{2023} t^{-1}	[409]
Middle range (07/15/2024)	1 036.36 EUR_{2024} 100 kg^{-1}	10 143.89 EUR_{2023} t^{-1}	[410]
High range (02/10/2026)	1 254.98 EUR_{2026} 100 kg^{-1}	11 909.76 EUR_{2023} t^{-1}	[411]
Total copper optimistic costs		8.98 $MEUR_{2023}$	
Total copper mean costs		10.19 $MEUR_{2023}$	
Total copper pessimistic costs		11.66 $MEUR_{2023}$	
	Electrical insulator		
Kapton® 300FN 929/021: 30 mm · 76.2 μm	1.74 EUR_{2025} m^{-1}	72 541 EUR_{2023} m^{-3}	[412]
Kapton® 500HN: 127 cm (50 in) · 127 μm (5 mil)	85.63 USD_{2026} m^{-1} (26.10 USD_{2026} ft^{-1})	461 285 EUR_{2023} m^{-3}	[413]
Total electrical insulator optimistic costs		21.26 $MEUR_{2023}$	
Total electrical insulator mean costs		78.22 $MEUR_{2023}$	
Total electrical insulator pessimistic costs		135.18 $MEUR_{2023}$	
	Invar 36, austenitic		
Low range	20.00 EUR_{2023} kg^{-1}	20.00 EUR_{2023} m^{-3}	[414]
High range	55.00 USD_{2025} kg^{-1}	48.24 EUR_{2023} m^{-3}	[415]
Total Invar optimistic costs		92.56 $MEUR_{2023}$	
Total Invar mean costs		157.92 $MEUR_{2023}$	

Continued on next page

Table C.4: Material and fabrication costs of the hybrid pipeline. (Continued)

Description	Original unit	Used unit	Source
Total Invar pessimistic costs		223.29 $MEUR_{2023}$	
	Carbon steel		
Low range	0.83 EUR_{2023} kg^{-1}	0.83 EUR_{2023} m^{-3}	[416]
High range	1.00 EUR_{2023} kg^{-1}	1.00 EUR_{2023} m^{-3}	[414]
Total carbon steel optimistic costs		9.47 $MEUR_{2023}$	
Total carbon steel mean costs		10.44 $MEUR_{2023}$	
Total carbon steel pessimistic costs		11.41 $MEUR_{2023}$	
	Thermal MLI		
40 layers: 106 000 m^2, COOLCAT 2 NW (3-layer narrow rolls 0.1 m · 370 m)	6.915 $MEUR_{2024}$	1.60 EUR_{2023} m^{-2} $layer^{-1}$	[417]
40 layers: 106 000 m^2, COOLCAT 2 NW (Standard roll 1.5 m · 50 m)	5.840 $MEUR_{2024}$	1.35 EUR_{2023} m^{-2} $layer^{-1}$	[417]
12 layers: 50 m · 1.5 m	4 500 EUR_{2023}	5.00 EUR_{2023} m^{-2} $layer^{-1}$	[418]
40 layers: 106 000 m^2, COOLCAT 2 NW (10-layer standard roll 1.5 m · 45 m)	31.299 $MEUR_{2024}$	7.23 EUR_{2023} m^{-2} $layer^{-1}$	[417]
Total MLI optimistic costs		6.23 $MEUR_{2023}$	
Total MLI mean costs		17.51 $MEUR_{2023}$	
Total MLI pessimistic costs		33.37 $MEUR_{2023}$	
	TOTAL MATERIAL COSTS		
Optimistic costs		180.03 $MEUR_{2023}$	
Mean costs		336.58 $MEUR_{2023}$	
Pessimistic costs		497.96 $MEUR_{2023}$	
	FABRICATION COSTS		
Low range		10% of material costs	[251]

Continued on next page

Table C.4: Material and fabrication costs of the hybrid pipeline. (Continued)

Description	Original unit	Used unit	Source
High range		15% of material costs	[251]
Total fabrication optimistic costs		18.00 $MEUR_{2023}$	
Total fabrication mean costs		42.07 $MEUR_{2023}$	
Total fabrication pessimistic costs		74.69 $MEUR_{2023}$	

Table C.5: Investment costs caused by the pipeline laying in Germany.

Description	Original unit	Used unit	Source
40–120 cm inner diameter, 70–100 bar	850.00 EUR_{2022} m^{-1}	903.38 EUR_{2023} m^{-1}	[335]
Low range, 50 cm, 16–30 bar	618.00 EUR_{2012} m^{-1}	797.96 EUR_{2023} m^{-1}	[419]
Middle range, 50 cm, 16–30 bar	730.00 EUR_{2012} m^{-1}	942.58 EUR_{2023} m^{-1}	[419]
High range, 50 cm, 16–30 bar	839.00 EUR_{2012} m^{-1}	1 083.32 EUR_{2023} m^{-1}	[419]
Total pipe laying optimistic costs		59.85 $MEUR_{2023}$	
Total pipe laying mean costs		69.89 $MEUR_{2023}$	
Total pipe laying pessimistic costs		81.25 $MEUR_{2023}$	

Table C.6: Indirect costs as a percentage of the total system costs of the hybrid pipeline, which include material, fabrication, terminations, and pipe laying costs. Values based on [299, 300].

Description	Value
Site preparation: e.g., land acquisition, site preparation activities, essential electrical infrastructure, internal roads, walkways	5%
Engineering and design: salaries, overhead for engineering and project management personnel	10%
Unforeseen events: risks, uncertainties, potential delays, e.g., owing to storms, strikes, minor design modifications, and unexpected price increases	10%
Permitting costs: necessary approvals for designing and installing control equipment, specific to each site	3%
Owner's costs: owner's engineering, potential construction debt origination, closure costs, and due diligence studies	12%
Sum of indirect costs	40%
Total optimistic indirect costs	104.08 MEUR_{2023}
Total mean indirect costs	180.35 MEUR_{2023}
Total pessimistic indirect costs	262.49 MEUR_{2023}

Sensitivity Analysis on Length

Table C.7 lists the designs of the 50 km and 150 km long hybrid pipelines evaluated in the length-sensitivity analysis in section 5.5.1. The 150 km long hybrid pipeline uses one intermediate cooling station at 75 km to return the temperature and pressure to the inlet conditions.

Table C.7: Designs of the 50 km and 150 km long hybrid pipelines for the sensitivity analysis.

Parameters	Symbol	50 km	150 km
Cable rated parameters			
Rated power	P_0	4.0 $\mathrm{GW_e}$	
Rated voltage	U_0	± 100.0 kV	
Rated current	I_0	20.0 kA	
Required minimum self-field critical current	$I_{c,\min}$	25.0 kA	
Cable layout			

Continued on next page

Table C.7: Designs of the 50 km and 150 km long hybrid pipelines for the sensitivity analysis. (Continued)

Parameters	Symbol	50 km	150 km
HTS tape width	a_{tape}	4.0 mm	
HTS tape thickness	s_{tape}	0.1 mm	
Outer radius of inner copper stabilizer	$r_{1,\text{cu}}$	13.9 mm	18.6 mm
Outer radius of inner HTS tape	$r_{1,\text{hts}}$	14.0 mm	18.7 mm
Outer radius of electrical insulator	$r_{1,\text{ins}}$	28.6 mm	31.9 mm
Outer radius of outer HTS tape	$r_{2,\text{hts}}$	28.7 mm	32.0 mm
Outer radius of outer copper stabilizer	$r_{2,\text{cu}}$	30.7 mm	35.1 mm
Cable cross-section of one monopole	A_{cable}	2 951.6 mm^2	3 873.4 mm^2
Number of tapes in inner phase	$N_{1,\text{tapes}}$	21	28
Gap between tapes inner phase	$g_{1,\text{tapes}}$	0.018 mm	0.033 mm
Number of layers in inner phase	$N_{1,\text{layers}}$	1	1
Lay angle in inner phase	θ_1	15.0°	
Calculated critical current inner phase	$I_{c,1}$	25.6 kA	34.1 kA
Outer phase layout	–	Type III	
Number of tapes in outer phase	$N_{2,\text{tapes}}$	21	28
Gap between tapes outer phase	$g_{2,\text{tapes}}$	4.42 mm	3.02 mm
Number of layers in outer phase	$N_{2,\text{layers}}$	1	
Lay angle in outer phase	θ_2	15.0°	
Calculated critical current outer phase	$I_{c,2}$	−25.2 kA	−33.6 kA
Superconductor length per monopole	–	2 174 km	8 696 km
Total superconductor length	–	4 348 km	17 393 km
Pipeline rated parameters			
Inlet temperature	T_{in}	20.4 K	
Inlet pressure	p_{in}	600 kPa	
Total heat load per unit length	q_{l}	3.857 W m^{-1}	
Surface roughness	ϵ	0.046 mm	
Pipe inner diameter	$D_{\text{LH2,i}}$	33.0 cm	37.0 cm
Liquid hydrogen mass flow	$\dot{m}_{\text{LH2}}$	4.0–10.1 kg$_{\text{H2}}$ s^{-1}	4.7–10.0 kg$_{\text{H2}}$ s^{-1}

Continued on next page

Table C.7: Designs of the 50 km and 150 km long hybrid pipelines for the sensitivity analysis. (Continued)

Parameters	Symbol	50 km	150 km
Chemical power	P_t	0.50–1.20 GW_t	0.56–1.20 GW_t
Outlet temperature	T_{out}	24.5–22.4 K	26.0–23.4 K
Outlet pressure	p_{out}	540–234 kPa	529–293 kPa
	Pipeline layout		
Inner radius of inner pipe	$r_{LH2,i}$	165.0 mm	185.0 mm
Outer radius of inner pipe	$r_{LH2,o}$	170.0 mm	190.0 mm
Outer radius of multi-layer insulation	$r_{MLI,o}$	190.0 mm	210.0 mm
Inner radius of outer pipe	$r_{pipe,i}$	200.0 mm	220.0 mm
Outer radius of outer pipe	$r_{pipe,o}$	208.0 mm	229.0 mm

Power and Electrical Energy Consumption of Cryocooler

For the sensitivity analysis in section 5.5.1, the cooling power of the cryocooler was determined using the following methodology. The cryocooler power $P_{t,cryocool}$ comprises the process load $P_{t,process}$ and the environmental heat leak $P_{t,heat\ leak}$:

$$P_{t,cryocool} = f_{safety} \cdot \left(P_{t,process} + P_{t,heat\ leak}\right) , \tag{C.1}$$

where f_{safety} is a safety factor defined as 1.3 to include an overcapacity margin. The environmental heat leak $P_{t,heat\ leak}$ is assumed to be the empirical value of 20 W, as noted in [251]. The process load $P_{t,process}$ depends on [252]:

$$P_{t,process} = \dot{m}_{LH2} \cdot (h_{in} - h_{out}) , \tag{C.2}$$

where $\dot{m}_{LH2}$ is the mass flow rate, and h_{in} and h_{out} are the inlet and outlet specific enthalpies of the liquid hydrogen. The inlet and outlet temperatures, pressures, and enthalpies depend on the mass flow rate $\dot{m}_{LH2}$, which has a range of 4.6–9.7 $kg_{H2}\ s^{-1}$ (i.e., 16.6–34.9 $t_{H2}\ h^{-1}$, see table 4.4). The enthalpy values for the corresponding inlet and outlet conditions were obtained using REFPROP [50]. A summary of the inlet and outlet conditions of the liquid hydrogen for the cryocooler, the process loads, and the cryocooler powers is listed for both lower and upper mass flow rates in table C.8.

Table C.8: Inlet and outlet conditions of liquid hydrogen for the cryocooler, process load, and cryocooler power for the lower and upper liquid hydrogen mass flow rates $\dot{m}_{\mathrm{LH2}}$.

Parameter	Symbol	$\dot{m}_{\mathrm{LH2}} = 4.6\ \mathrm{kg_{H2}\ s^{-1}}$	$\dot{m}_{\mathrm{LH2}} = 9.7\ \mathrm{kg_{H2}\ s^{-1}}$
Inlet temperature	T_{in}	25.9 K	23.5 K
Inlet pressure	p_{in}	527.5 kPa	293.9 kPa
Inlet specific enthalpy	h_{in}	$69.2\ \mathrm{kJ\ kg_{H2}^{-1}}$	$36.4\ \mathrm{kJ\ kg_{H2}^{-1}}$
Outlet temperature	T_{out}	20.4 K	20.4 K
Outlet pressure	p_{out}	527.5 kPa	293.9 kPa
Outlet specific enthalpy	h_{out}	$5.2\ \mathrm{kJ\ kg_{H2}^{-1}}$	$3.1\ \mathrm{kJ\ kg_{H2}^{-1}}$
Process load	$P_{\mathrm{t,process}}$	$294.1\ \mathrm{kW_t}$	$323.9\ \mathrm{kW_t}$
Cryocooler power	$P_{\mathrm{t,cryocool}}$	$382.4\ \mathrm{kW_t}$	$421.1\ \mathrm{kW_t}$

To calculate the investment costs of the cryocooler $\mathrm{CAPEX_{cryocool}}$, the higher cryocooler power of $P_{\mathrm{t,cryocool}} = 421.1\ \mathrm{kW_t}$ was used in a cost model for large-scale refrigerators based on [252]:

$$\mathrm{CAPEX_{cryocool}} = 2.2\ \mathrm{MCHF_{1998}} \cdot \left(\frac{P_{\mathrm{t,cryo,4.5\ K}}}{1\ \mathrm{kW}}\right)^{0.6} \cdot f_{\mathrm{cryocool}}^{\mathrm{loss}} \cdot f_{\mathrm{cryocool}}^{\mathrm{availability}}, \tag{C.3}$$

where $P_{\mathrm{t,cryo,4.5\ K}}$ is the equivalent cryocooler power at 4.5 K and $f_{\mathrm{cryocool}}^{\mathrm{loss}} \cdot f_{\mathrm{cryocool}}^{\mathrm{availability}}$ is the product of the inverse loss and availability factors, defined as 1.5 based on [252] (see table 5.22). The conversion of the cryocooler power from higher temperatures to 4.5 K is carried out using the following equation [252]:

$$P_{\mathrm{t,cryo,4.5\ K}} = P_{\mathrm{t,cryocool}} \cdot \frac{\mathrm{COP}\,(4.5\ \mathrm{K})}{\mathrm{COP}\left(\bar{T}\right)}, \tag{C.4}$$

where $\mathrm{COP}\,(4.5\ \mathrm{K})$ is the theoretical coefficient of performance at 4.5 K and $\mathrm{COP}\left(\bar{T}\right)$ is the corresponding coefficient at the average temperature $\bar{T}$. The coefficients of performance are determined according to [420]:

$$\begin{aligned} \mathrm{COP}\,(4.5\ \mathrm{K}) &= \frac{4.5\ \mathrm{K}}{300\ \mathrm{K} - 4.5\ \mathrm{K}}, \\ \mathrm{COP}\left(\bar{T}\right) &= \frac{\bar{T}}{300\ \mathrm{K} - \bar{T}}. \end{aligned} \tag{C.5}$$

Here, 300 K is assumed to be the ambient temperature. The mean temperature $\bar{T}$ is derived from the inlet and outlet temperatures at the corresponding mass flow rate (see table C.8) using the following expression, which is obtained by integrating the exergy of a heat flow across a temperature range [252]:

$$\bar{T} = \frac{T_{\text{out}} - T_{\text{in}}}{\ln\left(\frac{T_{\text{out}}}{T_{\text{in}}}\right)}. \tag{C.6}$$

Considering the upper mass flow rate $\dot{m}_{\text{LH2}}$ = 9.7 kg_{H2} s^{-1} and using equation C.4, the equivalent cooling power at 4.5 K is 81.37 kW_{t}. For the lower mass flow rate $\dot{m}_{\text{LH2}}$ = 4.6 kg_{H2} s^{-1}, the equivalent cooling power at 4.5 K is 69.99 kW_{t}.

To calculate the electrical energy consumption of the cryocooler, the nominal electrical power must be determined. Assuming that the cryocooler operates at a constant mass flow rate $\dot{m}_{\text{LH2}}$, the nominal capacity of the cryocooler is given by:

$$w_{\text{e,cryocool}} = \frac{P_{\text{e,cryocool}}}{\dot{m}_{\text{LH2}}}, \tag{C.7}$$

where $P_{\text{e,cryocool}}$ is the electrical power of the cryocooler. This is obtained using the following equation [420]:

$$P_{\text{e,cryocool}} = \frac{P_{\text{t,cryocool}}}{\eta_{\text{exergetic}} \cdot \text{COP}\left(\bar{T}\right)}, \tag{C.8}$$

where $P_{\text{t,cryocool}}$ is the cryocooler power, $\eta_{\text{exergetic}}$ is the exergetic efficiency, and COP $\left(\bar{T}\right)$ is the theoretical coefficient of performance at the mean temperature $\bar{T}$. The exergetic efficiency is assumed to be 27.5%, based on the range of 25–30%, reported in [252]. A summary of the nominal electrical power and energy consumption for the lower and upper mass flow rates is presented in table C.9.

Table C.9: Nominal electrical power and electrical energy consumption of the cryocooler for the lower and upper liquid hydrogen mass flow rates $\dot{m}_{\text{LH2}}$.

Parameter	**Symbol**	$\dot{m}_{\text{LH2}}$ = 4.6 kg_{H2} s^{-1}	$\dot{m}_{\text{LH2}}$ = 9.7 kg_{H2} s^{-1}
Nominal electrical power	$P_{\text{e,cryocool}}$	16.7 MW_{e}	19.4 MW_{e}
Electrical energy consumption	$w_{\text{e,cryocool}}$	1 009.2 kWh_{e} $\text{t}_{\text{H2}}^{-1}$	556.4 kWh_{e} $\text{t}_{\text{H2}}^{-1}$

D Appendix: Use of Artificial Intelligence (AI) Tools

AI Usage Card

PROJECT DETAILS

PROJECT NAME

Techno-economic Assessment of a Hybrid Pipeline for the Synergetic Transmission of Liquid Hydrogen and Electrical Energy by High-temperature Superconductivity

KEY AI APPLICATIONS

Writing: grammar and spelling; style in sections 1.1, 1.2, 2.4.1, & chapter 6
Methodology: partially in sections 5.2, 5.3.1, 5.3.5, 5.3.9, & appendix C
Literature review: partially in chapters 1, 5, & appendix C

CONTACT

NAME	AFFILIATION
Juan Sebastian Palacios Vera	Karlsruhe Institute of Technology (KIT)

MODELS

MODEL NAMES, VERSION, DATE USED

a. Microsoft 365 Copilot Chat, GPT-4 and GPT-5, February–May 2026.
b. KIT's Standard-local Model, GPT-OSS-120b, February–May 2026.

WRITING

GENERATING NEW TEXT BASED ON INSTRUCTIONS

The author used Microsoft 365 Copilot Chat (also known as Copilot Chat) with an institutional account to outline the structure of chapters 1 and 6. The proposed structure was reviewed, compared with other sources, and about 50% was approved. The two introductory sentences before each section 1.1 and 6.1 were AI-generated. Subsequently, these four sentences were rephrased by the author. KIT's Standard-local Model was employed to generate a basis for the Spanish abstract, based on the English version without numerical values. The proposed text was checked for consistency and improved for fluency. About 60% of the translation was adopted.

ASSISTING IN IMPROVING OWN CONTENT OR PARAPHRASING RELATED WORK

Microsoft 365 Copilot Chat with an institutional account was used to enhance the readability and to adopt a more idiomatic style in approximately 40%–50% of the own text in sections 1.1 and 1.2. The author entered mostly single sentences (occasionally paragraphs) and examined each suggestion before agreeing or refusing it. The tool did not produce new content or scientific claims.

Microsoft 365 Copilot Chat was used to rephrase less than 10% of the cited text in sections 2.4.1 and 5.2. The procedure was the same as in the previous case.

In chapter 6 and 6.3, KIT's Standard-local Model was employed for improvement of readability and fluency of about 60% of the own text. Variables were submitted instead of numbers to protect the findings. Microsoft Pilot was not used for these sections to not expose unpublished data outside from KIT infrastructure.

KIT's Standard-local Model was used for a final grammar and spelling check of chapters 2–5. Minor corrections to hyphenation and word order were accepted where appropriate.

METHODOLOGY

PROPOSING NEW SOLUTIONS TO PROBLEMS

Microsoft 365 Copilot Chat was used in few specific cases of this work to develop appropriate methodology:

In section 5.2, the AI tool was asked to propose methods and provide supporting scientific sources to consider component replacement costs during total system lifetime. The suggested methodology was checked against the original sources and tested for several examples. The author adopted the methodology after verifying the validity of the sources and results.

In section 5.3.1, Copilot Chat suggested methods and corresponding references for cost allocation of shared infrastructure delivering multiple energy vectors. The author selected the most adequate methodology based on the characteristics of the present work and on the proposed sources.

In section 5.3.5, the author asked Copilot Chat to suggest methodologies to determine the electrical power rating and energy consumption of the hydrogen compressor. The answers revealed that the simulations developed by the author for the liquid hydrogen pipeline could be adapted for that task. No AI-generated code was involved in this process. The author knew already most of the required references to support this procedure. Additional literature was searched without using AI tools.

FINDING ITERATIVE OPTIMIZATIONS

For section 5.3.9, the author wanted to improve the way electrical energy consumption is determined for liquid hydrogen pumps considering the differential pressure of each design and the compressibility of liquid hydrogen. Copilot Chat was used to enhance previous approaches that did not consider these aspects. The AI tool proposed multiple methodologies but the author rejected several of them based on the results obtained through own simulations. Copilot chat provided approximately 15% of the code used for the numerical integration. The selected methodology was validated through several examples. The AI tool presented the literature on which the method was based and the author verified the validity of the assumptions in the original sources.

COMPARING RELATED SOLUTIONS

For appendix C, Copilot Chat was employed to determine an appropriate methodology to calculate the required cooling power for the case study in this work, based on the methodology presented in [252]. The author asked the AI tool to clarify some of the intermediate steps assumed in that previous work. The results were produced with own calculations and validated comparing them with those of the cited reference.

LITERATURE REVIEW

ADDING LITERATURE FOR EXISTING STATEMENTS

The author asked Microsoft 365 Copilot Chat to find IPCC studies for similar statements to those presented in the first paragraph of section 1.1. For sections 5.2 and 5.3.3, Microsoft 365 Copilot Chat supported finding regulatory data regarding the WACC in Germany, and technical sources reporting the yearly availability and lifetime of underground HVDC cables, respectively. Similarly, Copilot Chat was asked to find technical reports for hydrogen losses in gaseous hydrogen pipelines for section 5.3.4. The same tool proposed data sources for the hydrogen losses and yearly availability of transfer liquid hydrogen pumps in section 5.3.9, and commercial cost estimates of Invar for appendix C.

The references suggested by the AI tool were independently searched and checked to ensure accuracy. Inadequate sources were discarded. When required, the author adapted the text to correspond the used sources. At the beginning of the project in 2022, Litmaps provided approximately 5% of the overview of specific topics, such as hydrogen for road transportation. All other references cited in this work were searched without the use of AI tools.

COMPARING LITERATURE

Microsoft 365 Copilot Chat with an institutional account was used to summarize the published papers in section 1.2. The author verified statements made by Copilot Chat in the original sources. Wrong interpretations made by the AI tool were rejected.

ETHICS

WHAT ARE THE IMPLICATIONS OF USING AI FOR THIS PROJECT AND WHAT STEPS ARE TAKEN TO MITIGATE ERRORS OF AI?

The author acknowledges that using AI services for writing may produce delicate changes in tone or focus. Therefore, AI-enhanced texts were rephrased considering this.

Sensitive data may be exposed when submitted to external AI services, so any research data or unpublished findings were sent to an AI tools outside KIT. The papers summarized by AI services in this work are published and publicly available. Only separate, non-sensitive pieces of draft text were submitted to external AI services.

AI tools may generate wrong results based on incorrect interpretations. The author reviewed the methodologies suggested by AI services comparing them with the original sources and validating the results using own calculations.

AI services may suggest references that disproportionately represent English language sources and the models may omit outcomes from smaller institutions or works that expressed same concepts with different terms. The author employed mainly searching methods that do not use AI but also these methods can miss relevant works.

THE CORRESPONDING AUTHOR REVIEWED AND AGREED WITH THE MODIFICATIONS OR GENERATIONS OF HIS USED AI-GENERATED CONTENT.

AI Usage Card v2.6 https://ai-cards.org [421]

Acronyms and Symbols

Acronyms

ACER	Agency for the Cooperation of Energy Regulators
ANL	Argonne National Laboratory
BSSCO	bismuth strontium calcium copper oxide
CEPCI	Chemical Engineering Plant Cost Index
CIGRE	Conseil International des Grands Réseaux Électriques
DC	direct current
DBS	dynamic braking system
DLR	German Aerospace Center
DOE	Department of Energy
EHB	European Hydrogen Backbone
EPRI	Electric Power Research Institute
HTS	high-temperature superconductor
HVDC	high-voltage direct current
IATA	International Air Transport Association
IEA	International Energy Agency
IET	Institution of Engineering and Technology
IRENA	International Renewable Energy Agency
ITEP	Institute for Technical Physics
KIT	Karlsruhe Institute of Technology
LCC	line-commutated converters
LNG	liquefied natural gas
LOHC	liquid organic hydrogen carriers
$\mathbf{MgB_2}$	magnesium diboride

MLI multi-layer insulation
MRI magnetic resonance imaging
NEP Network Development Plan
NLR Netherlands Aerospace Center
PEM proton-exchange membrane
PPLP polypropylene laminated paper
REBCO rare-earth barium copper oxide
RRR residual resistivity ratio
SNL Sandia National Laboratory
TSO transmission system operator
TRL technology readiness level
TYNDP Ten-Year Network Development Plan
USA United States of America
VSC voltage-source converters
YBCO yttrium barium copper oxide

Constants

π	pi: 3.14159 . . .
g	gravitational acceleration: 9.80665 . . . m s^{-2}
μ_0	vacuum permeability: $4 \cdot \pi \cdot 10^{-7}$ H m^{-1}
LHV_{paraH2}	lower heating value of para-hydrogen (20 K, 100 kPa): 32.9 kWh_t kg_{H2}^{-1}
LHV_{normH2}	lower heating value of normal-hydrogen (293.15 K, 100 kPa): 33.3 kWh_t kg_{H2}^{-1}
ρ_{paraH2}	mass density of para-hydrogen (20 K, 100 kPa): 71.144 kg_{H2} m^{-3}
R	universal gas constant 8.314 J mol^{-1} K^{-1}

Latin Symbols and Variables

A	area
AF	annuity factor
B	magnetic flux density
B_c	critical magnetic flux density

$B_{c,1}$	lower critical magnetic flux density
$B_{c,2}$	higher critical magnetic flux density
C	heat capacity
CAPEX	investment costs
COP	theroetical coefficient of performance
Cost	cost value
D	Diameter
D_h	hydraulic diameter
E	electric field
E_c	electric-field criterion
F	correlated to friction factor
H	head
I	current
I_c	critical current
J	current density
J_c	critical current density
L	inductance
M	molar mass
N	number
O&M	operation and maintenance cost rate as percentage of capital costs
P	power
R	resistance
Re	Reynolds number
S	size
T	temperature
T_c	critical temperature
TOTEX	total costs
U	voltage
V	volume
W	energy
WACC	weighted average cost of capital

Z	compressibility factor
a	width
c	specific heat capacity
c_p	specific heat capacity at constant pressure
d	discount factor
$\dot{m}$	mass flow rate
f	dimensionless factor (e.g., loss or availability)
fixOPEX	fix operational costs
g	gap
h	specific enthalpy
k	fitting parameter
l_w	wetted perimeter
ℓ	pipeline length
n	power-law exponent
n_{poly}	polytropic coefficient
p	pressure
q_{l}	total heat load per unit length
$q_{\text{l,0}}$	off set heat load per unit length
q_{A}	heat flux
r	radius
s	thickness
t	time
varOPEX	variable operational costs
w	specific energy
z	relative elevation

Greek Symbols and Variables

α	thermal expansivity factor
β	fitting parameter
ϵ	surface roughness
η	efficiency

κ_e	electricity cost
μ	viscosity
ν	velocity
θ	angle
τ	lifetime
ϱ	electrical resistivity
ρ	mass density
Φ	kinetic energy correction factor
ζ	friction factor

Operators and Math Symbols

$\vec{a}$	vector
$\perp$	perpendicular
$\|\|$	parallel

General Indices

0	rated
1	inner cable phase
2	outer cable phase
4.5K	at a temperature of 4.5 K
a	area
ag	silver
aghycu	silver, Hastelloy®, and copper
annual	annual
availability	availability
b	break down
cable	superconducting cable
cu	copper
compres	gaseous hydrogen compressor
core	copper stabilizer

converter	converter stations
cryocool	cryocooler
des	design
discharge	discharge
effective	effective
ellip	elliptical model
e	electric
exergetic	exergetic
fill	fill
friction	friction
GH2	gaseous hydrogen
GH2pipe	gaseous hydrogen pipeline
GH2stor	gaseous hydrogen storage
H2	hydrogen
high	high
hts	high-temperature superconductor
hy	Hastelloy®
heatleak	heat leak
HyPipe	hybrid pipeline
HVDCcable	conventional high-voltage underground cable system
i	inner
in	inlet
ins	insulation
initial	initial
J	Joule
Kim	Kim model
L	inductance
l	length
lim	limit
layers	layers
LH2	liquid hydrogen

LH2pump	liquid hydrogen pump
LH2stor	liquid hydrogen storage
liquefi	liquefier
loss	loss
low	low
max	maximum
mech	mechanical
mid	mid
min	minimum
MLI	multi-layer insulation
motor	motor
nodes	nodes
normH2	normal-hydrogen
nominal	nominal
op	operation
o	outer
out	outlet
paraH2	para-hydrogen
pipe	pipe
poly	polytropic
present	present-value
process	process
pump	pump
ref	reference
r	rated operating conditions
rel	relative
safety	safety
sat	saturation
sc	short circuit
sh	shaft
specific	specific

sys	system
T	testing
t	thermal
tapes	REBCO tapes
w	wetted
width	width

List of Figures

List of Tables

List of Publications

Journal Articles

[1] S. Palacios, M. J. Wolf, M. Noe, M. Wehr, and T. Arndt, “Design of a 75 km GW-class Hybrid Pipeline for the Synergetic Transmission of Liquid Hydrogen and Electrical Energy by High-Temperature Superconductivity,” *Superconductor Science and Technology*, 2025. [Online]. Available: https://doi.org/10.1088/1361-6668/ae2cf7

[2] M. Noe, T. Puig, D. C. van der Laan, R. Bach, S. Ishmael, E. Nilsson, C. Räch, N. Chikumoto, A. Allais, B. Song, K. Allweins, F. Herzog, F. Dioguardi, T. Arndt, A. Marian, L. Xiao, J. Cho, S. Palacios, M. Wehr, and M. J. Wolf, “Superconducting high-power cables and lines – Development status and technology roadmap,” *Superconductor Science and Technology*, 2025. [Online]. Available: https://doi.org/10.1088/1361-6668/ae15c2

Conference Contributions

[1] S. Palacios, “Techno-economic Assessment of a Hybrid Pipeline: Synergetic Energy Transmission by LH2 and HTS,” in *TransHyDE-Abschlusskonferenz*, Berlin, 2025.

[2] ——, “Techno-economic Assessment of a Hybrid Pipeline: Synergetic Energy Transmission by LH2 and HTS,” in *Applied Superconductivity Conference (ASC)*, Salt Lake City, 2024. [Online]. Available: https://publikationen.bibliothek.kit.edu/1000179812

[3] S. Palacios and M. Wehr, “AppLHy! und TransHyDE - Hybride Pipeline: Synergetische Energieübertragung mittels HTS und LH2,” in *ZIEHL IX*, Berlin, 2024. [Online]. Available: https://publikationen.bibliothek.kit.edu/1000173137

[4] S. Palacios, M. Wehr, M. J. Wolf, M. Noe, and T. Arndt, “Combined Energy Transmission by LH_2 and HTS: Study of a Hybrid Pipeline,” in *European Conference on Applied Superconductivity (EUCAS)*, Bologna, 2023. [Online]. Available: https://doi.org/10.13140/RG.2.2.10355.75046

[5] S. Palacios, “How Hybrid Pipelines Tackle Multiple Challenges in the Energy Transition,” in *TransHyDE-Konferenz*, Berlin, 2022.

Technical Reports

[1] A. Alekseev, T. Arndt, C. Haberstroh, T. Jordan, D. Lindackers, S. Palacios, A. Pundt, P. Saß, C. Schulz, K.-P. Weiss, C. Wolf, M. J. Wolf, and C. Wu, “Hydrogen liquefaction, storage, transport and application of liquid hydrogen: Flagship Project TransHyDE.” [Online]. Available: https://doi.org/10.5445/IR/1000168281

[2] ——, “Wasserstoff-Verflüssigung, Speicherung, Transport und Anwendung von flüssigem Wasserstoff: Wasserstoff-Leitprojekt TransHyDE.” [Online]. Available: https://doi.org/10.5445/IR/1000155199

Bibliography

[1] IPCC, “Summary for Policymakers,” in *Climate Change: Impacts, Adaptation, and Vulnerability. Contribution of Working Group II to the Sixth Assessment Report of the Intergovernmental Panel on Climate Change*, IPCC, Ed. Cambridge, UK and New York, NY, USA: Cambridge University Press, 2022, pp. 3–33. [Online]. Available: https://doi.org/10.1017/9781009325844.001

[2] ——, “Summary for Policymakers,” in *Climate Change: Mitigation of Climate Change. Contribution of Working Group III to the Sixth Assessment Report of the Intergovernmental Panel on Climate Change*, IPCC, Ed. Cambridge, UK and New York, NY, USA: Cambridge University Press, 2022, pp. 3–48. [Online]. Available: https://doi.org/10.1017/9781009157926.001

[3] Bundestag, “Federal Climate Action Act of 12 December 2019 (Federal Law Gazette I, p. 2513), as last amended by Article 1 of the Act of 15 July 2024 (Federal Law Gazette I No. 235): KSG,” 12.12.2019. [Online]. Available: https://www.gesetze-im-internet.de/englisch_ksg/englisch_ksg.html

[4] Bundesverband der Energie- und Wasserwirtschaft e.V., “Die Energieversorgung 2025 - Jahresbericht -: Aktualisierte Fassung.” [Online]. Available: https://www.bdew.de/media/documents/Die_Energieversorgung_2025_Update_FINAL.pdf

[5] Agora Think Tanks, “Klimaneutrales Deutschland: Von der Zielsetzung zur Umsetzung,” Berlin. [Online]. Available: https://www.agora-energiewende.de/publikationen/klimaneutrales-deutschland-studie#downloads

[6] Fraunhofer Institut für System- und Innovationsforschung (Fraunhofer ISI), Consentec. GmbH, ifeu, and TU Berlin, “Langfristszenarien für die Transformation des Energiesystems in Deutschland: Treibhausgasneutrale Szenarien T45: Webinar zum Energieangebot 22.11.2022.” [Online]. Available: https://www.langfristszenarien.de/enertile-explorer-wAssets/docs/LFS3_T45_Webinar_Angebot_Nov_2022_final_webinarversion.pdf

[7] Kopernikus-Projekt Ariadne, “Vergleich der ”Big 5” Klimaneutralitätsszenarien,” Berlin, 2022. [Online]. Available: https://ariadneprojekt.de/news-de/big5-szenarienvergleich/

[8] E. W. Lemmon, I. H. Bell, M. L. Huber, and M. O. McLinden, “REFPROP Documentation: Release 10.0,” Boulder, CO. [Online]. Available: https://www.nist.gov/system/files/documents/2018/05/23/refprop10a.pdf

[9] Bundesnetzagentur, “Netzausbau Strom: Bedarfsermittlung 2023-2037/2045: Bestätigung Netzentwicklungsplan Strom,” Bonn. [Online]. Available: https://www.netzentwicklungsplan.de/sites/default/files/2024-03/NEP_2037_2045_Bestaetigung.pdf

[10] Vereinigung der Fernleitungsbetreiber Gas e.V., “Netzentwicklungsplan Gas 2022–2032,” Berlin. [Online]. Available: https://fnb-gas.de/wp-content/uploads/2024/03/2024_03_20_NEP-2022_Gas_FINAL_DE.pdf

[11] Federal Ministry of Research, Technology and Space, “Flagship Projects: How the hydrogen flagship projects are supporting Germany’s entry into the hydrogen economy.” [Online]. Available: https://www.wasserstoff-leitprojekte.de/projects

[12] ——, “TransHyDE: How TransHyDE aims to develop a hydrogen infrastructure.” [Online]. Available: https://www.wasserstoff-leitprojekte.de/projects/transhyde

[13] P. Mangin, *Superconductivity: An introduction.* Cham: Springer International Publishing, 2017. [Online]. Available: https://doi.org/10.1007/978-3-319-50527-5

[14] T. Moore, “SuperGrid Concept Sparks Interest,” 2002. [Online]. Available: https://phe.rockefeller.edu/PDF_FILES/SuperGridSummary.pdf

[15] P. M. Grant, “The SuperCable: Dual Delivery of Hydrogen and Electric Power,” *IEEE PES Power Systems Conference and Exposition*, 2004. [Online]. Available: https://doi.org/10.1109/PSCE.2004.1397675

[16] ——, “The SuperCable: Dual Delivery of Chemical and Electric Power,” *IEEE Transactions on Applied Superconductivity*, vol. 15, no. 2, pp. 1810–1813, 2005. [Online]. Available: https://doi.org/10.1109/tasc.2005.849298

[17] L. Trevisani, “Design and simulation of a large scale energy storage and power transmission system for remote renewable energy sources exploitation,” Dissertation, University of Bologna, Bologna, 2006. [Online]. Available: http://die.ing.unibo.it/dottorato_it/Trevisani/Trevisani_PhD-thesis.pdf

[18] L. Trevisani, M. Fabbri, and F. Negrini, “Long distance renewable-energy-sources power transmission using hydrogen-cooled MgB2 superconducting line,” *Cryogenics (Cryogenics)*, vol. 47, no. 2, pp. 113–120, 2007. [Online]. Available: https://doi.org/10.1016/j.cryogenics.2006.10.002

[19] S. Yamada, Y. Hishinuma, T. Uede, K. Schippl, and O. Motojima, “Study on 1 GW class hybrid energy transfer line of hydrogen and electricity,” *Journal of Physics: Conference Series*, vol. 97, p. 012167, 2008. [Online]. Available: https://doi.org/10.1088/1742-6596/97/1/012167

[20] S. Yamada, Y. Hishinuma, T. Uede, K. Schippl, N. Yanagi, T. Mito, and M. Sato, “Conceptual design of 1 GW class hybrid energy transfer line of hydrogen and electricity,” *Journal of Physics: Conference Series*, vol. 234, no. 3, p. 032064, 2010. [Online]. Available: https://doi.org/10.1088/1742-6596/234/3/032064

[21] V. V. Kostyuk, I. V. Antyukhov, E. V. Blagov, V. S. Vysotsky, B. I. Katorgin, A. A. Nosov, S. S. Fetisov, and V. P. Firsov, “Experimental hybrid power transmission line with liquid hydrogen and MgB2-based superconducting cable,” *Technical Physics Letters*, vol. 38, no. 3, pp. 279–282, 2012. [Online]. Available: https://doi.org/10.1134/s106378501203025x

[22] V. V. Kostyuk, E. V. Blagov, I. V. Antyukhov, V. P. Firsov, V. S. Vysotsky, A. A. Nosov, S. S. Fetisov, S. Zanegin, G. G. Svalov, V. S. Rachuk, and B. I. Katorgin, “Cryogenic design and test results of 30-m flexible hybrid energy transfer line with liquid hydrogen and superconducting MgB2 cable,” *Cryogenics (Cryogenics)*, vol. 66, pp. 34–42, 2015. [Online]. Available: https://doi.org/10.1016/j.cryogenics.2014.11.010

[23] V. S. Vysotsky, A. A. Nosov, S. S. Fetisov, G. G. Svalov, V. V. Kostyuk, E. V. Blagov, I. V. Antyukhov, V. P. Firsov, B. I. Katorgin, and A. L. Rakhmanov, “Hybrid Energy Transfer Line With Liquid Hydrogen and Superconducting MgB2 Cable—First Experimental Proof of Concept,” *IEEE Transactions on Applied Superconductivity*, vol. 23, no. 3, p. 5400906, 2013. [Online]. Available: https://doi.org/10.1109/tasc.2013.2238574

[24] V. S. Vysotsky, I. V. Antyukhov, V. P. Firsov, E. V. Blagov, V. V. Kostyuk, A. A. Nosov, S. S. Fetisov, S. Y. Zanegin, V. S. Rachuk, and B. I. Katorgin, “Cryogenic Tests of 30 m Flexible Hybrid Energy Transfer Line with Liquid Hydrogen and Superconducting MgB2 Cable,” *Physics Procedia*, vol. 67, pp. 189–194, 2015. [Online]. Available: https://doi.org/10.1016/j.phpro.2015.06.033

[25] ——, “Energy Transfer with Hydrogen and Superconductivity – The Review of the First Experimental Results,” *Physics Procedia*, vol. 65, pp. 299–302, 2015. [Online]. Available: https://doi.org/10.1016/j.phpro.2015.05.158

[26] V. S. Vysotsky, E. V. Blagov, V. V. Kostyuk, A. A. Nosov, S. S. Fetisov, S. Y. Zanegin, I. V. Antyukhov, V. P. Firsov, G. G. Svalov, B. I. Katorgin, and V. S. Rachuk, “New 30-m Flexible Hybrid Energy Transfer Line With Liquid Hydrogen and Superconducting MgB2

Cable—Development and Test Results," *IEEE Transactions on Applied Superconductivity*, vol. 25, no. 3, pp. 1–5, 2015. [Online]. Available: https://doi.org/10.1109/tasc.2014.2361635

[27] Institute for Technical Physics, "Liquid hydrogen made in Karlsruhe," 2026. [Online]. Available: https://www.itep.kit.edu/english/Liquid_hydrogen_made_in_Karlsruhe.php

[28] Karlsruhe Institute of Technology, "Hydrogen Integration Platform (HIP): AppLHy: Validating the entire liquid hydrogen supply chain." [Online]. Available: https://www.hip.kit.edu/AppLHy.php

[29] B. Qin, H. Wang, Y. Liao, D. Liu, Z. Wang, and F. Li, "Liquid hydrogen superconducting transmission based super energy pipeline for Pacific Rim in the context of global energy sustainable development," *International Journal of Hydrogen Energy*, vol. 56, pp. 1391–1396, 2024. [Online]. Available: https://doi.org/10.1016/j.ijhydene.2023.12.289

[30] L. Fu, X. Chen, Y. Chen, S. Jiang, and B. Shen, "Hydrogen-electricity hybrid energy pipelines for railway transportation: Design and economic evaluation," *International Journal of Hydrogen Energy*, vol. 61, pp. 251–264, 2024. [Online]. Available: https://doi.org/10.1016/j.ijhydene.2024.02.299

[31] L. Cavallucci, A. Musso, G. Angeli, L. Martini, M. Bocchi, A. Macchiagodena, and M. Breschi, "Optimization Procedure to Design a DC Transmission Line with MgB 2 Wires in Liquid Hydrogen," *IEEE Transactions on Applied Superconductivity*, vol. 35, no. 5, pp. 1–5, 2025. [Online]. Available: https://doi.org/10.1109/TASC.2024.3513946

[32] G. Mangiulli, M. Bracco, M. Breschi, L. Cavallucci, S. Farinon, A. Macchiagodena, R. Musenich, and L. Savoldi, "Sizing and Economic Assessment for Auxiliar Components and Grid Connection of a MgB 2 -LH 2 Hybrid Power Cable," *IEEE Transactions on Applied Superconductivity*, vol. 36, no. 5, pp. 1–6, 2026. [Online]. Available: https://doi.org/10.1109/TASC.2026.3651232

[33] M. Cais, M. Nicoli, M. Gandiglio, M. Bracco, M. Breschi, L. Cavallucci, S. Farinon, A. Macchiagodena, G. Mangiulli, R. Musenich, and L. Savoldi, "Hybrid superconducting energy pipelines: key cost thresholds and system implications for Italy," *International Journal of Hydrogen Energy*, vol. 210, p. 153627, 2026. [Online]. Available: https://doi.org/10.1016/j.ijhydene.2026.153627

[34] M. Wehr, M. J. Wolf, and T. Arndt, "Experimental studies on indirect cooling for a hybrid power transfer line (LH2 and HTS)," *Cryogenics (Cryogenics)*, vol. 152, p. 104206, 2025. [Online]. Available: https://doi.org/10.1016/j.cryogenics.2025.104206

[35] M. Wehr, J. S. Palacios Vera, and M. J. Wolf, "Experimental Studies on an HTS DC Cable Prototype for Combined Energy Transmission with LH2," in *Applied Superconductivity Conference (ASC)*, Salt Lake City, 2024. [Online]. Available: https://publikationen.bibliothek.kit.edu/1000191620

[36] ——, "High Current HTS Cable Development for Combined Energy Transmission with LH2," in *European Conference on Applied Superconductivity (EUCAS)*, Bologna, 2023. [Online]. Available: https://publikationen.bibliothek.kit.edu/1000191622

[37] M. J. Wolf, "AppLHy! - Transport and Application of Liquid Hydrogen," 28.03.2023. [Online]. Available: https://indico.gsi.de/event/15856/contributions/69744/attachments/43302/60747/20230327-1700-mjw-PR%C3%84S_ECD-Hydrogen-AppLHy-Wolf.pdf

[38] S. R. Frank, T. Stroebele, P. Swoboda, R. Schwendemann, and M. Hiller, "A Cryogenic Gallium Nitride Full Bridge for Use in a Thermally Insulating Dual Active Bridge," in *2024 IEEE Energy Conversion Congress and Exposition (ECCE)*. Piscataway, NJ: IEEE, 2024, pp. 6798–6805. [Online]. Available: https://doi.org/10.1109/ECCE55643.2024.10861612

[39] C. Schulz, M. Maarouf, Z. Abbasi, E. Gaisina, A. Pundt, and K.-P. Weiss, "Long-Term Exposure in Liquid Hydrogen: Mechanical Properties and Microstructural Investigation of 304 Austenitic Steel After 30 Years of Service," *Hydrogen*, vol. 7, no. 2, p. 69, 2026. [Online]. Available: https://doi.org/10.3390/hydrogen7020069

[40] Bundesnetzagentur, "Ausbau Erneuerbarer Energien 2025," Bonn, 08.01.2026. [Online]. Available: https://www.bundesnetzagentur.de/SharedDocs/Pressemitteilungen/DE/2026/20260108_EEG.html

[41] C. Pape and D. Geiger, "Regionalisierung des Ausbaus der Erneuerbaren Energien," Kassel. [Online]. Available: https://www.netzentwicklungsplan.de/sites/default/files/2023-06/Studie_Regionalisierung_EE_IEE.pdf

[42] Bundesamt für Seeschifffahrt und Hydrographie, "Flächenentwicklungsplan 2023 für die deutsche Nordsee und Ostsee," Hamburg. [Online]. Available: https://www.bsh.de/DE/THEMEN/Offshore/Meeresfachplanung/Flaechenentwicklungsplan/_Anlagen/Downloads/FEP_2023_1/Flaechenentwicklungsplan_2023.pdf?__blob=publicationFile&v=1

[43] Übertragungsnetzbetreiber, "NEP kompakt: Netzentwicklungsplan Strom 2037 mit Ausblick 2045, Version 2025, zweiter Entwurf." [Online]. Available: https://www.netzentwicklungsplan.de/sites/default/files/2026-04/NEP-kompakt_2037_2045_V2025_2_Entwurf_1.pdf

[44] Die Bundesregierung, "Fortschreibung der Nationalen Wasserstoffstrategie: NWS 2023," Berlin. [Online]. Available: https://www.bundeswirtschaftsministerium.de/Redaktion/DE/Wasserstoff/Downloads/Fortschreibung.pdf?__blob=publicationFile&v=4

[45] Die Gas- und Wasserstoffwirtschaft e.V., "Gasbilanz 2025: Erdgas, Wasserstoff und Biogas in Deutschland," Berlin. [Online]. Available: https://gas-h2.de/fileadmin/Public/PDF-Download/gasbilanz-2025-gas-wasserstoffwirtschaft.pdf

[46] Die Bundesregierung, "Importstrategie für Wasserstoff und Wasserstoffderivate," Berlin. [Online]. Available: https://www.bundeswirtschaftsministerium.de/Redaktion/DE/Publikationen/Energie/importstrategie-wasserstoff.pdf?__blob=publicationFile&v=18

[47] A. Odenweller and F. Ueckerdt, "The green hydrogen ambition and implementation gap," *Nature Energy*, vol. 10, no. 1, pp. 110–123, 2025. [Online]. Available: https://doi.org/10.1038/s41560-024-01684-7

[48] IEA, "Global Hydrogen Review 2024." [Online]. Available: https://iea.blob.core.windows.net/assets/89c1e382-dc59-46ca-aa47-9f7d41531ab5/GlobalHydrogenReview2024.pdf

[49] J. Rongé, "Confirmed by IEA - Green hydrogen still growing faster than PV did," 2025. [Online]. Available: https://www.linkedin.com/posts/janronge_electrolyser-hydrogen-pv-activity-7378291260282871808-xAZL

[50] M. Huber, A. Harvey, E. Lemmon, G. Hardin, I. Bell, and M. McLinden, "Reference Fluid Thermodynamic and Transport Properties (REFPROP) Version 10.0 - SRD 23," 2018. [Online]. Available: https://doi.org/10.18434/T4/1502528

[51] Joint Research Centre, "Assessment of Hydrogen Delivery Options." [Online]. Available: https://joint-research-centre.ec.europa.eu/system/files/2021-06/jrc124206_assessment_of_hydrogen_delivery_options.pdf

[52] F. Staiß, J. Adolf, F. Ausfelder, C. Erdmann, M. Fischedick, C. Hebling, T. Jordan, G. Klepper, T. Müller, R. Palkovits, W.-R. Poganietz, W.-P. Schill, M. Schmidt, C. Stephanos, P. Stöcker, U. Wagner, K. Westphal, and S. Wurbs, *Options for importing green hydrogen into Germany by 2030: Transportation routes, country assessments and implementation requirements (Analysis)*, ser. Series on "Energy Systems of the Future" (ESYS). Munich: acatech – National Academy of Science and Engineering, 2024. [Online]. Available: https://doi.org/10.48669/esys_2024-4

[53] A. Wang, J. Jens, D. Mavins, M. Moultak, M. Schimmel, K. van der Leun, D. Peters, and M. Buseman, "Analysing future demand, supply, and transport of hydrogen: European

Hydrogen Backbone," Utrecht. [Online]. Available: https://ehb.eu/files/downloads/EHB-Analysing-the-future-demand-supply-and-transport-of-hydrogen-June-2021-v3.pdf

[54] Agora Energiewende, Agora Industrie, and Guidehouse, "Wasserstoffimporte Deutschlands – Welchen Beitrag können Pipelineimporte in den 2030er Jahren leisten?" [Online]. Available: https://www.agora-energiewende.de/publikationen/wasserstoffimporte-deutschlands#downloads

[55] T. Fleiter, J. Fragoso, B. Lux, Ş. Alibaş, K. Al-Dabbas, P. Manz, F. Neuner, B. Weißenburger, M. Rehfeldt, and F. Sensfuß, "Hydrogen Infrastructure in the Future CO 2 –Neutral European Energy System—How Does the Demand for Hydrogen Affect the Need for Infrastructure?" *Energy Technology*, vol. 13, no. 2, p. 2300981, 2025. [Online]. Available: https://doi.org/10.1002/ente.202300981

[56] Fraunhofer Institut für System- und Innovationsforschung (Fraunhofer ISI), Consentec GmbH, ifeu – Institut für Energie- und Umweltforschung Heidelberg, and Technische Universität Berlin, "Langfristszenarien für die Transformation des Energiesystems in Deutschland: Treibhausgasneutrale Orientierungsszenarien. Modul Energieangebot," Karlsruhe. [Online]. Available: https://langfristszenarien.de/enertile-explorer-wAssets/docs/LFS3_O45-Energieangebot_final.pdf

[57] S. Kigle, N. Helmer, and T. Schmidt-Achert, "Fast enough? The consequences of delayed renewable energy expansion on european hydrogen import needs," *Applied Energy*, vol. 400, p. 126556, 2025. [Online]. Available: https://doi.org/10.1016/j.apenergy.2025.126556

[58] R. Slowinski, Y. Sagdur, R. van Rossum, A. Kozub, L. Kühnen, M. Overgaag, A. Michelet, S. Kandathiparambil, and P. London, "European Hydrogen Backbone: Implementation Roadmap — Cross Border Projects and Costs Update," Utrecht. [Online]. Available: https://ehb.eu/files/downloads/EHB-2023-Implementation-Roadmap-Part-1.pdf

[59] "Wasserstoff-Kompass – Handlungsoptionen für die Wasserstoffwirtschaft," Frankfurt am Main. [Online]. Available: https://www.wasserstoff-kompass.de/fileadmin/user_upload/img/news-und-media/dokumente/Wasserstoff-Kompass_komplett.pdf

[60] European Network of Transmission System Operators for Gas, Gas Infrastructure Europe, CEDEC, Eurogas, Gas Distributors for Sustainability, and GEODE, "Hydrogen Infrastructure Map," 2026. [Online]. Available: https://www.h2inframap.eu/

[61] Reuters, "Norway's Equinor scraps plans to export blue hydrogen to Germany," *Reuters Media*, 21.09.2024. [Online]. Available: https://www.reuters.com/business/energy/norways-equinor-scraps-plans-export-blue-hydrogen-germany-2024-09-20/

[62] IEA, "Global Hydrogen Review 2025." [Online]. Available: https://www.iea.org/reports/global-hydrogen-review-2025

[63] Bundesnetzagentur, "Genehmigung des Szenariorahmens für den Netzentwicklungsplan Gas und Wasserstoff 2025-2037/2045: Netzentwicklung Wasserstoff-/Gastransportnetze," Bonn. [Online]. Available: https://www.bundesnetzagentur.de/DE/Fachthemen/ElektrizitaetundGas/NEP/DL_Szenariorahmen/Genehm_SR_2025Gas.pdf?__blob=publicationFile&v=2

[64] S. Z. Al Ghafri, S. Munro, U. Cardella, T. Funke, W. Notardonato, J. P. M. Trusler, J. Leachman, R. Span, S. Kamiya, G. Pearce, A. Swanger, E. D. Rodriguez, P. Bajada, F. Jiao, K. Peng, A. Siahvashi, M. L. Johns, and E. F. May, "Hydrogen liquefaction: a review of the fundamental physics, engineering practice and future opportunities," *Energy & Environmental Science*, vol. 15, no. 7, pp. 2690–2731, 2022. [Online]. Available: https://doi.org/10.1039/D2EE00099G

[65] C. Haberstroh, "Wasserstoff: Ortho/Para–Umwandlung und Verflüssigung," *Chemie Ingenieur Technik*, vol. 96, no. 1-2, pp. 43–54, 2024. [Online]. Available: https://doi.org/10.1002/cite.202300128

[66] T. Zhang, J. Uratani, Y. Huang, L. Xu, S. Griffiths, and Y. Ding, "Hydrogen liquefaction and storage: Recent progress and perspectives," *Renewable and Sustainable Energy Reviews*, vol. 176, p. 113204, 2023. [Online]. Available: https://doi.org/10.1016/j.rser.2023.113204

[67] A. Alekseev, T. Arndt, C. Haberstroh, T. Jordan, D. Lindackers, S. Palacios, A. Pundt, P. Saß, C. Schulz, K.-P. Weiss, C. Wolf, M. J. Wolf, and C. Wu, "Hydrogen liquefaction, storage, transport and application of liquid hydrogen: Flagship Project TransHyDE." [Online]. Available: https://doi.org/10.5445/IR/1000168281

[68] K. Stolzenburg and R. Mubbala, "Integrated Design for Demonstration of Efficient Liquefaction of Hydrogen (IDEALHY): Grant Agreement Number 278177," Brussels. [Online]. Available: https://www.idealhy.eu/uploads/documents/IDEALHY_D3-16_Liquefaction_Report_web.pdf

[69] C. Hank, A. Sternberg, N. Köppel, M. Holst, T. Smolinka, A. Schaadt, C. Hebling, and H.-M. Henning, "Energy efficiency and economic assessment of imported energy carriers based on renewable electricity," *Sustainable Energy & Fuels*, vol. 4, no. 5, pp. 2256–2273, 2020. [Online]. Available: https://doi.org/10.1039/D0SE00067A

[70] Z. Chen, Y. Zhao, Y. Jia, X. Zheng, G. Shao, Y. Li, M. Liu, J. Shi, and C. Gu, "The impacts of the hydrogen economy on climate: Current research and future projections

to 2050," *International Journal of Hydrogen Energy*, vol. 119, pp. 204–217, 2025. [Online]. Available: https://doi.org/10.1016/j.ijhydene.2025.03.230

[71] M. Sand, R. B. Skeie, M. Sandstad, S. Krishnan, G. Myhre, H. Bryant, R. Derwent, D. Hauglustaine, F. Paulot, M. Prather, and D. Stevenson, "A multi-model assessment of the Global Warming Potential of hydrogen," *Communications Earth & Environment*, vol. 4, no. 1, p. 203, 2023. [Online]. Available: https://doi.org/10.1038/s43247-023-00857-8

[72] D. Hauglustaine, F. Paulot, W. Collins, R. Derwent, M. Sand, and O. Boucher, "Climate benefit of a future hydrogen economy," *Communications Earth & Environment*, vol. 3, no. 1, p. 295, 2022. [Online]. Available: https://doi.org/10.1038/s43247-022-00626-z

[73] A. Schiaroli, L. Claussner, A. Campari, D. Cirrone, B. Linseisen, A. Friedrich, E. L. Torres de Ritter, M. Kuznetsov, and F. Ustolin, "A comprehensive review on liquid hydrogen transfer operations and safety considerations for mobile applications," *International Journal of Hydrogen Energy*, vol. 107, pp. 164–182, 2025. [Online]. Available: https://doi.org/10.1016/j.ijhydene.2024.12.266

[74] Daimler Truck AG, "Daimler Truck #HydrogenRecordRun: Mercedes-Benz GenH2 Truck cracks 1,000 kilometer mark with one fill of liquid hydrogen," 2023. [Online]. Available: https://www.daimlertruck.com/en/newsroom/pressrelease/daimler-truck-hydrogenrecordrun-mercedes-benz-genh2-truck-cracks-1000-kilometer-mark-with-one-fill-of-liquid-hydrogen-52369346

[75] Hydrogen Energy Supply Chain, "About the Project," 2022. [Online]. Available: https://www.hydrogenenergysupplychain.com/about-hesc/

[76] T. Jordan and J. L. Saw, "Pre-normative REsearch for Safe use of Liquid Hydrogen (PRESHLY): White Paper." [Online]. Available: https://hysafe.info/wp-content/uploads/sites/3/2021/06/PRESLHY_D6_4_WhitePaper_202101505_V2p1.pdf

[77] M. Wietschel, M. Riemer, J. Thomann, B. Breitschopf, J. Fragoso, J. Wachsmuth, B. Weißenburger, V. P. Müller, A. Kantel, L. Karkossa, F. Marscheider-Weidemann, N. Pieton, V. Lenivova, B. Drechsler, M. Ragwitz, O. Ranzmeyer, C. Voglstätter, F. Mendler, M. Holst, C. Hank, R. Kunze, D. Vespermann, S. Thielmann, R. Quitzow, A. Stamm, R. Strohmaier, Z. Thiel, M. Müller, and A. Löschel, "HYPAT Abschlussbericht," Karlsruhe. [Online]. Available: https://hypat.de/hypat-wAssets/docs/new/publikationen/HYPAT-Abschlussbericht.pdf

[78] M. Robinius, P. Markewitz, P. Lopion, F. Kullmann, P.-M. Heuser, K. Syranidis, S. Cerniauskas, T. Schöb, M. Reuß, S. Ryberg, L. Kotzur, D. Caglayan, L. Welder, J. Linßen, T. Grube, H. Heinrichs, P. Stenzel, and D. Stolten, *Wege für die*

Energiewende: kosteneffiziente und klimagerechte Transformationsstrategien für das deutsche Energiesystem bis zum Jahr 2050, ser. Energie & Umwelt / Energy & Environment. Jülich: Forschungszentrum Jülich GmbH Zentralbibliothek, Verlag, 2020. [Online]. Available: https://juser.fz-juelich.de/record/877960/files/Energie_Umwelt_499.pdf

[79] M. Pfennig, N. Gerhardt, C. Pape, and D. Böttger, "Mittel- und langfristige Potenziale von PTL- und H2-Importen aus internationalen EE-Vorzugsregionen: Teilbericht: Auftraggeber: Bundesministerium für Umwelt, Naturschutz, Bau und Reaktorsicherheit, Förderkennzeichen: 16EM3007, Förderprogramm Erneuerbar Mobi," Kassel. [Online]. Available: https://www.erneuerbar-mobil.de/sites/default/files/2019-10/Teilbericht_Potenziale_PtL_H2_Importe_FraunhoferIWES.pdf

[80] E. Jalbout and H. Abdel-Khalek, "Techno-Economic Impacts of Shipping Liquid Hydrogen, Ammonia or Methanol on Exporting Nations: The Case of Morocco," in *2025 21st International Conference on the European Energy Market (EEM)*. IEEE, 5/27/2025 - 5/29/2025, pp. 1–6. [Online]. Available: https://doi.org/10.1109/EEM64765.2025.11050281

[81] H. B. Aditiya, S. R. Panuganti, I. Hsia, T. Mat, T. Mahlia, and Z. Huang, "Hydrogen transport across oceans: A techno-economic assessment of hydrogen carriers," *Applied Energy*, vol. 399, p. 126513, 2025. [Online]. Available: https://doi.org/10.1016/j.apenergy.2025.126513

[82] D. Teichmann, W. Arlt, and P. Wasserscheid, "Liquid Organic Hydrogen Carriers as an efficient vector for the transport and storage of renewable energy," *International Journal of Hydrogen Energy*, vol. 37, no. 23, pp. 18 118–18 132, 2012. [Online]. Available: https://doi.org/10.1016/j.ijhydene.2012.08.066

[83] P. S.-L. Chen, H. Fan, and N. Abdussamie, "Evaluation of hydrogen shipping cost for potential trade routes," *WMU Journal of Maritime Affairs*, vol. 24, no. 2, pp. 315–338, 2025. [Online]. Available: https://doi.org/10.1007/s13437-025-00365-w

[84] L. Genge, F. Scheller, and F. Müsgens, "Supply costs of green chemical energy carriers at the European border: A meta-analysis," *International Journal of Hydrogen Energy*, vol. 48, no. 98, pp. 38 766–38 781, 2023. [Online]. Available: https://doi.org/10.1016/j.ijhydene.2023.06.180

[85] K. Ruske, C. Gätsch, T. Michalski, F. Graf, S. Rothenbacher, S. Malzkuhn, F. Mörs, C. Zeller, M. Heneka, F. Glockner, J. Schwarze, B. Munko, T. Systermans, A. Cox, M. Ragwitz, E. Timofeeva, P. Preuster, J. König, C. Pannek, M. Holst, C. Voglstätter, F. Rümmele, R. E. Ali, C. Hank, A. Wunsch, T. Michler, C. Elsässer, F. Schweizer, P. von Hartrott, P. Wasserscheid, M. Geisselbrecht, T. Schärfe,

N. Brücken, J. Morgenstern, S. Maerten, S. Müller, D. Lindackers, U. Krause, H. Weber, F. Allolio, L. Schulz, T. Arndt, H. Neumann, M. Wolf, K.-P. Weiss, A. Alekseev, F. Gremme, A. Fricke, P. Sass, H.-G. Bischoff, T.-C. Just, C. Haberstroh, D. Krieg, and C. Mechler, "Synthesebericht des TransHyDE-Projekts LNG2Hydrogen: Erarbeitung einer wissenschaftlich fundierten, nachhaltigen Datenbasis und Empfehlung als Entscheidungsbasis für die zukunftsfähige und langfristige Nutzung von LNG-Terminal-Standorten als logistische Knotenpunkte für Wasserstoff und dessen Transportvektoren: Wasserstoff-Leitprojekt TransHyDE." [Online]. Available: https://www.wasserstoff-leitprojekte.de/lw_resource/datapool/systemfiles/elements/files/9842531e-7c28-11f0-9a65-fa163e7d9971/live/document/250813_LNG2Hydrogen_Whitepaper-final_V3.pdf

[86] J. Mendoza, "Oman's liquid hydrogen export project gains traction with feasibility progress," *Zawya*, 18.02.2025. [Online]. Available: https://www.zawya.com/en/special-coverage/zawya-green/omans-liquid-hydrogen-export-project-gains-traction-with-feasibility-progress-qgpe1mwq

[87] C. de Jonge, "Historic Agreement Establishes World's First Liquid Hydrogen Import Corridor Between Oman and Amsterdam," *H2A consortium*, 17.04.2025. [Online]. Available: https://h2amsterdam.com/historic-agreement-establishes-worlds-first-liquid-hydrogen-import-corridor-between-oman-and-amsterdam/

[88] LH2 Europe. Green Energy, "LH2 Europe projects will supply Liquid Hydrogen to North West Europe," 2025. [Online]. Available: https://www.lh2europe.com/en/home/lh2-project/

[89] S. Pekic, "C-Job, LH2 Europe present new liquid hydrogen tanker design," *Offshore Energy*, vol. 2022, 04.05.2022. [Online]. Available: https://www.offshore-energy.biz/c-job-lh2-europe-present-new-liquid-hydrogen-tanker-design/

[90] LH2 Energy Pty Ltd, "Darwin Green LH2 Export Project," 2025. [Online]. Available: https://www.lh2energy.com/

[91] P. Grubnic, "Darwin Green Liquid Hydrogen (LH2) Export Project - HyResource," 2025. [Online]. Available: https://research.csiro.au/hyresource/darwin-green-liquid-hydrogen-lh2-export-project/

[92] Daimler Truck AG, "Daimler Truck and Masdar explore liquid green hydrogen supply options to decarbonize road freight transport in Europe," 2024. [Online]. Available: https://www.daimlertruck.com/en/newsroom/pressrelease/daimler-truck-and-masdar-explore-liquid-green-hydrogen-supply-options-to-decarbonize-road-freight-transport-in-europe-52571860

[93] Übertragungsnetzbetreiber, “Netzentwicklungsplan Strom 2037 mit Ausblick 2045, Version 2025: Zweiter Entwurf der Übertragungsnetzbetreiber.” [Online]. Available: https://www.netzentwicklungsplan.de/sites/default/files/2026-03/NEP_2037_2045_V2025_2_Entwurf_1.pdf

[94] The Compressed Gas Association, Inc., “CGA G-5.3-2024 - Commodity Specification for Hydrogen: 8th Edition,” McLean, 2024. [Online]. Available: https://webstore.ansi.org/standards/cga/cga2024-2548518

[95] Pacific Northwest National Laboratory, “H2tools | Hydrogen Tools: What is the hydrogen purity requirement for hydrogen?” 2023. [Online]. Available: https://h2tools.org/faq/hydrogen-purity-requirements

[96] K. T. Møller, T. R. Jensen, E. Akiba, and H.-W. Li, “Hydrogen - A sustainable energy carrier,” *Progress in Natural Science: Materials International*, vol. 27, no. 1, pp. 34–40, 2017. [Online]. Available: https://doi.org/10.1016/j.pnsc.2016.12.014

[97] Airbus, “Hydrogen: An important decarbonisation pathway,” 2024. [Online]. Available: https://www.airbus.com/en/innovation/energy-transition/hydrogen

[98] Boeing, “Hydrogen and Sustainable Aviation: Fact Sheet,” 2025. [Online]. Available: https://www.boeing.com/content/dam/boeing/boeingdotcom/principles/sustainability/assets/pdf/Hydrogen_Factsheet.pdf

[99] Airports Council International and Aerospace Technology Institute, “Integration of hydrogen aircraft into the air transport system: An Airport Operations and Infrastructure Review.” [Online]. Available: https://www.ati.org.uk/wp-content/uploads/2021/08/aci-ati-hydrogen-report-1.pdf

[100] IATA, “Hydrogen for aviation: A future decarbonization solution for air travel? V2.0-February 2025.” [Online]. Available: https://www.iata.org/globalassets/iata/publications/sustainability/h2-for-aviation-facts.pdf

[101] McKinsey & Company, “Hydrogen-powered aviation: A fact-based study of hydrogen technology, economics, and climate impact by 2050,” Luxembourg. [Online]. Available: https://cleansky.paddlecms.net/sites/default/files/2021-10/20200507_Hydrogen-Powered-Aviation-report.pdf

[102] R. Miller, E. Whittington, S. Gabra, P. Hodgson, J. Green, J. Wei Kho, J. Smith, and D. Singh, “Five Years to Chart a New Future for Aviation: The 2030 Sustainable Aviation Goals.” [Online]. Available: https://report.aiazero.org/

[103] S. Tiwari, M. J. Pekris, and J. J. Doherty, "A review of liquid hydrogen aircraft and propulsion technologies," *International Journal of Hydrogen Energy*, vol. 57, pp. 1174–1196, 2024. [Online]. Available: https://doi.org/10.1016/j.ijhydene.2023.12.263

[104] M. İ. Kılıçalp and U. Demir, "Performance, emission, vibration and noise characteristics of gasoline-based fuel blends with JP-8, Jet A-1, and nitromethane mixtures in a single-cylinder gasoline engine," *Fuel*, vol. 393, p. 135034, 2025. [Online]. Available: https://doi.org/10.1016/j.fuel.2025.135034

[105] D. Debney, S. Beddoes, M. Foster, D. James, E. Kay, O. Kay, K. Shawki, E. Stubbs, D. Thomas, K. Weider, and R. Wilson, "Zero-Carbon Emission Aircraft Concepts: FlyZero." [Online]. Available: https://www.ati.org.uk/wp-content/uploads/2022/03/FZO-AIN-REP-0007-FlyZero-Zero-Carbon-Emission-Aircraft-Concepts.pdf

[106] B. Barker, P. Hodgson, D. Hyde, R. Miller, and M. Rapeanu, "Target True Zero: Unlocking Sustainable Battery and Hydrogen-Powered Flight." [Online]. Available: https://www.weforum.org/publications/target-true-zero-unlocking-sustainable-battery-and-hydrogen-powered-flight/

[107] T. Busch, T. Groß, J. Linßen, and D. Stolten, "The role of liquid hydrogen in integrated energy systems–A case study for Germany," *International Journal of Hydrogen Energy*, vol. 48, no. 99, pp. 39 408–39 424, 2023. [Online]. Available: https://doi.org/10.1016/j.ijhydene.2023.05.308

[108] K. Oesingmann, W. Grimme, and J. Scheelhaase, "Hydrogen in aviation: A simulation of demand, price dynamics, and CO2 emission reduction potentials," *International Journal of Hydrogen Energy*, vol. 64, pp. 633–642, 2024. [Online]. Available: https://doi.org/10.1016/j.ijhydene.2024.03.241

[109] W. Grimme and M. Braun, "Estimation of potential hydrogen demand and CO2 mitigation in global passenger air transport by the year 2050," *Transportation Research Procedia*, vol. 65, pp. 24–33, 2022. [Online]. Available: https://doi.org/10.1016/j.trpro.2022.11.004

[110] European Commission: Directorate-General for Research and Innovation, "Market uptake and impact of key green aviation technologies: final report." [Online]. Available: https://data.europa.eu/doi/10.2777/72358

[111] NLR, "Novel propulsion and alternative fuels for aviation towards 2050: Promising options and steps to take (TRANSCEND Deliverable D3.2): A report for Clean Sky 2 Joint Undertaking (NLR-CR 2022-094)."

[112] Steer, "Analysing the costs of hydrogen aircraft: Final Report: For Transport & Environment (ref: 24135101)." [Online]. Available: https://uploads.transportenvironment.org/production/files/Study-Analysing-the-costs-of-hydrogen-aircraft_2024-04-29-204622_wucu.pdf?dm=1714423582

[113] Eurocontrol, "European Aviation Overview 2024." [Online]. Available: https://www.eurocontrol.int/sites/default/files/2025-01/eurocontrol-european-aviation-overview-20250123-2024-review.pdf

[114] L. Dray, A. W. Schäfer, C. Grobler, C. Falter, F. Allroggen, M. E. J. Stettler, and S. R. H. Barrett, "Cost and emissions pathways towards net-zero climate impacts in aviation," *Nature Climate Change*, vol. 12, no. 10, pp. 956–962, 2022. [Online]. Available: https://doi.org/10.1038/s41558-022-01485-4

[115] P. J. Ansell, "Review of sustainable energy carriers for aviation: Benefits, challenges, and future viability," *Progress in Aerospace Sciences*, vol. 141, p. 100919, 2023. [Online]. Available: https://doi.org/10.1016/j.paerosci.2023.100919

[116] I. Purnama, A. Mutamima, M. Aziz, K. Wijaya, I. D. Maulida, J. Junaidi, K. Sari, I. Effendi, and I. R. Dini, "Environmental Impacts and the Food vs. Fuel Debate: A Critical Review of Palm Oil as Biodiesel," *GCB Bioenergy*, vol. 17, no. 6, p. e70043, 2025. [Online]. Available: https://doi.org/10.1111/gcbb.70043

[117] R. Borup, T. Krause, and J. Brouwer, "Hydrogen is Essential for Industry and Transportation Decarbonization," *The Electrochemical Society Interface*, vol. 30, no. 4, pp. 79–84, 2021. [Online]. Available: https://doi.org/10.1149/2.F18214IF

[118] Y. Ruf, M. Baum, T. Zorn, A. Menzel, and J. Rehberger, "Fuel Cells Hydrogen Trucks: Heavy-Duty's High Performance Green Solution: Study Summary," Luxembourg. [Online]. Available: https://www.rolandberger.com/publications/publication_pdf/roland_berger_fuel_cells_hydrogen_trucks.pdf

[119] R. K. Ahluwalia, H.-S. Roh, J.-K. Peng, D. Papadias, A. R. Baird, E. S. Hecht, B. D. Ehrhart, A. Muna, J. A. Ronevich, C. Houchins, N. J. Killingsworth, and S. M. Aceves, "Liquid hydrogen storage system for heavy duty trucks: Configuration, performance, cost, and safety," *International Journal of Hydrogen Energy*, vol. 48, no. 35, pp. 13 308–13 323, 2023. [Online]. Available: https://doi.org/10.1016/j.ijhydene.2022.12.152

[120] Daimler Truck AG, "Safe, Fast and Simple: Daimler Truck and Linde Set New Standard for Liquid Hydrogen Refueling Technology," 2023. [Online]. Available: https://www.daimlertruck.com/en/newsroom/pressrelease/safe-fast-and-simple-daimler-truck-and-linde-set-new-standard-for-liquid-hydrogen-refueling-technology-52581266

[121] IEA, "Global EV Outlook 2025: Expanding sales in diverse markets." [Online]. Available: https://www.iea.org/reports/global-ev-outlook-2025

[122] P. Plötz, "Hydrogen technology is unlikely to play a major role in sustainable road transport," *Nature Electronics*, vol. 5, no. 1, pp. 8–10, 2022. [Online]. Available: https://doi.org/10.1038/s41928-021-00706-6

[123] D. A. Cullen, K. C. Neyerlin, R. K. Ahluwalia, R. Mukundan, K. L. More, R. L. Borup, A. Z. Weber, D. J. Myers, and A. Kusoglu, "New roads and challenges for fuel cells in heavy-duty transportation," *Nature Energy*, vol. 6, no. 5, pp. 462–474, 2021. [Online]. Available: https://doi.org/10.1038/s41560-021-00775-z

[124] N. Johnson, M. Liebreich, D. M. Kammen, P. Ekins, R. McKenna, and I. Staffell, "Realistic roles for hydrogen in the future energy transition," *Nature Reviews Clean Technology*, vol. 1, no. 5, pp. 351–371, 2025. [Online]. Available: https://doi.org/10.1038/s44359-025-00050-4

[125] J. Löfving, S. Brynolf, and M. Grahn, "Geospatial distribution of hydrogen demand and refueling infrastructure for long-haul trucks in Europe," *International Journal of Hydrogen Energy*, vol. 128, pp. 544–558, 2025. [Online]. Available: https://doi.org/10.1016/j.ijhydene.2025.04.257

[126] A. Elgowainy, M. Mintz, U. Lee, T. Stephens, P. Sun, K. Reddi, Y. Zhou, G. Zang, M. Ruth, P. Jadun, E. Connelly, and R. Boardman, "Assessment of Potential Future Demands for Hydrogen in the United States." [Online]. Available: https://doi.org/10.2172/1710201

[127] D. Bonilla, "Road Freight Transport and Energy Use: The USA, China, the EU, Japan and Germany," in *Air Power and Freight : The View from the European Union and China*, D. Bonilla, Ed. Cham: Springer International Publishing, 2020, pp. 5–32. [Online]. Available: https://doi.org/10.1007/978-3-030-27783-3_2

[128] IEA, "Net Zero Roadmap: A Global Pathway to Keep the 1.5 °C Goal in Reach: 2023 Update." [Online]. Available: https://www.iea.org/reports/net-zero-roadmap-a-global-pathway-to-keep-the-15-0c-goal-in-reach

[129] R. Laursen, H. Patel, M. Dowling, D. Sofiadi, C. Ji, D. Nelissen, J. Király, and R. van der Veen, "Potential of Hydrogen as Fuel for Shipping," Lisbon. [Online]. Available: https://emsa.europa.eu/component/flexicontent/download/7646/5062/23.html

[130] P. Balcombe, J. Brierley, C. Lewis, L. Skatvedt, J. Speirs, A. Hawkes, and I. Staffell, "How to decarbonise international shipping: Options for fuels, technologies and

policies," *Energy Conversion and Management*, vol. 182, pp. 72–88, 2019. [Online]. Available: https://doi.org/10.1016/j.enconman.2018.12.080

[131] L. van Hoecke, L. Laffineur, R. Campe, P. Perreault, S. W. Verbruggen, and S. Lenaerts, "Challenges in the use of hydrogen for maritime applications," *Energy & Environmental Science*, vol. 14, no. 2, pp. 815–843, 2021. [Online]. Available: https://doi.org/10.1039/D0EE01545H

[132] DNV AS, "Handbook for Hydrogen-Fuelled Vessels: MarHySafe JDP Phase 1." [Online]. Available: https://www.dnv.com/maritime/publications/handbook-for-hydrogen-fuelled-vessels-download.html

[133] Shell International B.V., "Decarbonising Shipping: Setting Shell's Course." [Online]. Available: https://globalmaritimehub.com/wp-content/uploads/2020/11/decarbonising-shipping-setting-shells-course.pdf

[134] A. G. Elkafas, M. Rivarolo, E. Gadducci, L. Magistri, and A. F. Massardo, "Fuel Cell Systems for Maritime: A Review of Research Development, Commercial Products, Applications, and Perspectives," *Processes*, vol. 11, no. 1, p. 97, 2023. [Online]. Available: https://doi.org/10.3390/pr11010097

[135] Nordic Investment Bank, "Norled operates first hydrogen ferry and pioneers express boat battery swaps," 2024. [Online]. Available: https://www.nib.int/articles/norled-operates-first-hydrogen-ferry-and-pioneers-express-boat-battery-swaps

[136] Norled, "MF "Hydra" the world's first." [Online]. Available: https://www.norled.no/en/nyhet/mf-hydra-the-worlds-first/

[137] N. Gray, S. McDonagh, R. O'Shea, B. Smyth, and J. D. Murphy, "Decarbonising ships, planes and trucks: An analysis of suitable low-carbon fuels for the maritime, aviation and haulage sectors," *Advances in Applied Energy*, vol. 1, p. 100008, 2021. [Online]. Available: https://doi.org/10.1016/j.adapen.2021.100008

[138] Shell International B.V. and Deloitte Consulting and Advisory, "Decarbonising Shipping: All Hands on Deck 2.0: Industry Perspectives." [Online]. Available: https://www.shell.com/business-customers/shell-low-carbon-solutions/_jcr_content/root/main/section_489901290_co_48639111/promo_526075953/links/item0.stream/1685556533872/b8cfc522e207d5e92a19b9f5943f9eb1f73a9d10/all-hands-on-deck-digital-thirty-first-may.pdf

[139] F. Urban, A. Nurdiawati, F. Harahap, and K. Morozovska, "Decarbonizing maritime shipping and aviation: Disruption, regime resistance and breaking through carbon

lock-in and path dependency in hard-to-abate transport sectors," *Environmental Innovation and Societal Transitions*, vol. 52, p. 100854, 2024. [Online]. Available: https://doi.org/10.1016/j.eist.2024.100854

[140] IRENA, "A Pathway to Decarbonise the Shipping Sector by 2050," Abu Dhabi. [Online]. Available: https://www.irena.org/-/media/Files/IRENA/Agency/Publication/2021/Oct/IRENA_Decarbonising_Shipping_2021.pdf

[141] R. Ortiz-Imedio, D. G. Caglayan, A. Ortiz, H. Heinrichs, M. Robinius, D. Stolten, and I. Ortiz, "Power-to-Ships: Future electricity and hydrogen demands for shipping on the Atlantic coast of Europe in 2050," *Energy*, vol. 228, p. 120660, 2021. [Online]. Available: https://doi.org/10.1016/j.energy.2021.120660

[142] Y. Zhang, J. R. G. Evans, and S. Yang, "Corrected Values for Boiling Points and Enthalpies of Vaporization of Elements in Handbooks," *Journal of Chemical & Engineering Data*, vol. 56, no. 2, pp. 328–337, 2011. [Online]. Available: https://doi.org/10.1021/je1011086

[143] X. Zhang, X. Qian, C. Xiao, X. Yin, X. Wang, Z. Wang, H. Yu, Z. Han, and L. Lin, "Advancements in purification and holistic utilization of industrial by-product hydrogen: Progress, challenges, and prospects," *Green Energy and Resources*, vol. 2, no. 4, p. 100098, 2024. [Online]. Available: https://doi.org/10.1016/j.gerr.2024.100098

[144] C. G. van de Walle and J. Neugebauer, "Hydrogen in Semiconductors," *Annual Review of Materials Research*, vol. 36, no. 1, pp. 179–198, 2006. [Online]. Available: https://doi.org/10.1146/annurev.matsci.36.010705.155428

[145] L. Rochlitz, M. Steinberger, R. Oechsner, A. Weber, S. Schmitz, K. Schillinger, M. Wolff, and A. Bayler, "Second use or recycling of hydrogen waste gas from the semiconductor industry - Economic analysis and technical demonstration of possible pathways," *International Journal of Hydrogen Energy*, vol. 44, no. 31, pp. 17 168–17 184, 2019. [Online]. Available: https://doi.org/10.1016/j.ijhydene.2019.05.009

[146] T. Skoczylas, "Securing high-purity hydrogen," *Compound Semiconductor*, vol. 24, no. 8, 2018. [Online]. Available: https://nelhydrogen.com/wp-content/uploads/2020/03/Securing-High-Purity-Hydrogen.pdf

[147] Y. Zhao, Y. Mao, W. Zhang, Y. Tang, and P. Wang, "Reviews on the effects of contaminations and research methodologies for PEMFC," *International Journal of Hydrogen Energy*, vol. 45, no. 43, pp. 23 174–23 200, 2020. [Online]. Available: https://doi.org/10.1016/j.ijhydene.2020.06.145

[148] ISO International Organization for Standardization, "ISO 14687:2025: Hydrogen fuel quality — Product specification," 2025. [Online]. Available: https://www.iso.org/standard/82660.html

[149] Siemens Energy, "Siemens Energy's Electrolyzer Awarded to Decarbonize Semiconductor Sector in Japan," Tokyo, 2025. [Online]. Available: https://www.siemens-energy.com/global/en/home/press-releases/siemens-energy-s-electrolyzer-awarded-to-decarbonize-semiconduct.html

[150] Infineon Technologies AG, "Sustainable hydrogen supply for Infineon Austria," 2025. [Online]. Available: https://www.infineon.com/regional/austria/press-release/2025/nachhaltige-wasserstoffversorgung

[151] D. Trapani, P. Marocco, M. Gandiglio, and M. Santarelli, "Decarbonizing semiconductor manufacturing: cost-competitiveness of PV-based green hydrogen production," *Smart Energy*, vol. 19, p. 100192, 2025. [Online]. Available: https://doi.org/10.1016/j.segy.2025.100192

[152] D. Willén, M. Sedén, M. Pitzer, V. Roudriges-Zermeno, C. Thidemann, J. Kunert, D. D. Tjahjanto, C. Frohne, O. Holte, C. Wolff, W. Prusseit, C. Hintze, R. Bach, P. Mansheim, W. T. B. de Sousa, M. Noe, A. Alekseev, P. Michalek, and R. Prinz, "Development of the Superlink HTS Cable System for Implementation in Munich," *IEEE Transactions on Applied Superconductivity*, vol. 35, no. 5, pp. 1–8, 2025. [Online]. Available: https://doi.org/10.1109/TASC.2025.3553829

[153] W. T. B. de Sousa, F. Boehm, S. Grohmann, M. Noe, D. Willén, A. Alekseev, P. Mansheim, R. Bach, W. Prusseit, C. Hintze, R. Prinz, and P. Michalek, "SuperLink: Development and Impacts of a Superconducting Power Cable in a 110-kV Distribution Network," *IEEE Transactions on Applied Superconductivity*, vol. 35, no. 7, pp. 1–11, 2025. [Online]. Available: https://doi.org/10.1109/TASC.2025.3585422

[154] A. Allais, J.-M. Saugrain, B. West, N. Lallouet, H. Caron, D. Ferandelle, L. Terrien, G. Bouvier, G. Hajiri, K. Berger, and L. Quéval, "SuperRail–World-First HTS Cable to be Installed on a Railway Network in France," *IEEE Transactions on Applied Superconductivity*, vol. 34, no. 3, pp. 1–7, 2024. [Online]. Available: https://doi.org/10.1109/TASC.2024.3356450

[155] R. A. H. de Oliveira, O. Taalibi, and T. Arndt, "Compact HTS Motor Designs Especially Useful to Be Cooled by Liquid Hydrogen," *IEEE Transactions on Applied Superconductivity*, vol. 34, no. 6, pp. 1–5, 2024. [Online]. Available: https://doi.org/10.1109/TASC.2024.3392961

[156] Ludovic Ybanez, Souhaib Boukayoua, Nilsson Emelie, Tassisto Matteo, Kharche Swapnil, Rouquette Jean-François, Jacob Timin, Ravi-Kiran Surapaneni, Gowtham Galla, and Berg Frederick, “Cryogenic electric propulsion system: ASCEND main results and perspectives,” in *International conference proceedings*, International Conference on More Electric Aircraft, Ed., Toulouse, 2024. [Online]. Available: https://openscience.isae-supaero.fr/Default/doc/SYRACUSE/15952/cryogenic-electric-propulsion-system-ascend-main-results-and-perspectives

[157] F. Grilli, T. Benkel, J. Hänisch, M. Lao, T. Reis, E. Berberich, S. Wolfstädter, C. Schneider, P. Miller, C. Palmer, B. Glowacki, V. Climente-Alarcon, A. Smara, L. Tomkow, J. Teigelkötter, A. Stock, J. Büdel, L. Jeunesse, M. Staempflin, G. Delautre, B. Zimmermann, R. van der Woude, A. Perez, S. Samoilenkov, A. Molodyk, E. Pardo, M. Kapolka, S. Li, and A. Dadhich, “Superconducting motors for aircraft propulsion: the Advanced Superconducting Motor Experimental Demonstrator project,” *Journal of Physics: Conference Series*, vol. 1590, no. 1, p. 012051, 2020. [Online]. Available: https://doi.org/10.1088/1742-6596/1590/1/012051

[158] W. Nick, M. Frank, G. Klaus, J. Frauenhofer, and H.-W. Neumuller, “Operational Experience With the World’s First 3600 rpm 4 MVA Generator at Siemens,” *IEEE Transactions on Applied Superconductivity*, vol. 17, no. 2, pp. 2030–2033, 2007. [Online]. Available: https://doi.org/10.1109/TASC.2007.899996

[159] G.-D. Nam, H.-J. Sung, C. Kim, M. Park, and I.-K. Yu, “Design and Characteristic Analysis of a 1 MW Superconducting Motor for Ship Propulsions,” *IEEE Transactions on Applied Superconductivity*, vol. 29, no. 5, pp. 1–5, 2019. [Online]. Available: https://doi.org/10.1109/TASC.2019.2902872

[160] T. Arndt, M. Eisele, M. Kläser, A. Binder, R. Köster, A. Jöckel, R. Zeichfüßl, and J. Krämer, “Speedy_HTS – An HTS Rotor for an Uprated Mid-Speed Wind Power Generator,” *IEEE Transactions on Applied Superconductivity*, vol. 36, no. 3, pp. 1–4, 2026. [Online]. Available: https://doi.org/10.1109/TASC.2025.3619467

[161] G. Majkic, R. Pratap, A. Xu, E. Galstyan, H. C. Higley, S. O. Prestemon, X. Wang, D. Abraimov, J. Jaroszynski, and V. Selvamanickam, “Engineering current density over 5 kA mm −2 at 4.2 K, 14 T in thick film REBCO tapes,” *Superconductor Science and Technology*, vol. 31, no. 10, p. 10LT01, 2018. [Online]. Available: https://doi.org/10.1088/1361-6668/aad844

[162] H. Mun, S. Park, and I. Lee, “Liquid hydrogen cold energy recovery to enhance sustainability: Optimal design of dual-stage power generation cycles,” *Energy*, vol. 284, p. 129229, 2023. [Online]. Available: https://doi.org/10.1016/j.energy.2023.129229

[163] S. Estrada-Flores, “Novel cryogenic technologies for the freezing of food products,” *The Official Journal of Airah*, vol. 1, pp. 16–21, 2002. [Online]. Available: https://www.researchgate.net/publication/262011071_Novel_cryogenic_technologies_for_the_freezing_of_food_products

[164] B. Zohuri, *Hydrogen Energy: Challenges and Solutions for a Cleaner Future*, ser. SpringerLink Springer eBook Collection. Springer, 2019.

[165] Bundesnetzagentur, “Anbindungsleitungen in der Nordsee,” Bonn, 2025. [Online]. Available: https://www.netzausbau.de/Vorhaben/ansicht/de.html?nummer=1001&gruppe=offshore

[166] TenneT TSO GmbH, “Die West-küstenleitung: Das Projekt auf einen Blick,” Bayreuth, 2023. [Online]. Available: https://tennet-drupal.s3.eu-central-1.amazonaws.com/default/2023-11/Westk%C3%BCstenleitung%20Doppelparallelfalz.pdf

[167] Bundesnetzagentur, “Heide West – Polsum (Korridor B),” Bonn, 2024. [Online]. Available: https://www.netzausbau.de/Vorhaben/ansicht/de.html?nummer=48&gruppe=bbplg

[168] TenneT TSO GmbH, “Netzverstärkung NordElbe,” 2024. [Online]. Available: https://www.tennet.eu/de/projekte/netzverstaerkung-nordelbe

[169] Deutsche Energy Terminal GmbH, “Standort Brunsbüttel,” 2024. [Online]. Available: https://energy-terminal.de/terminals/brunsbuettel

[170] D. Karres, “Versorgung mit Flüssigerdgas LNG: Energiesicherheit,” 20.05.2025. [Online]. Available: https://www.kfw.de/stories/energiesicherheit_film.html

[171] Statistisches Bundesamt, “Größte Seehäfen in Deutschland in den Jahren von 2019 bis 2024 nach Güterversand: (in 1.000 Tonnen),” 2025. [Online]. Available: https://de.statista.com/statistik/daten/studie/239219/umfrage/groesste-haefen-in-deutschland-nach-gueterversand/

[172] Flughafen Hamburg GmbH, “Corporate: All about Hamburg Airport.” [Online]. Available: https://www.hamburg-airport.de/en/corporate

[173] Hamburger Hafen und Logistik Aktiengesellschaft, “The Power of Networks.” [Online]. Available: https://hhla.de/en/the-power-of-networks

[174] ArcelorMittal Germany Holding GmbH, “ArcelorMittal Hamburg.” [Online]. Available: https://barsandrods.arcelormittal.com/mill-hamburg

[175] A. Färber, “Das Luftfahrtcluster der Metropolregion Hamburg.” [Online]. Available: https://metropolregion.hamburg.de/wirtschaft-wissenschaft/branchen/luftfahrt-12722

[176] Airbus, “Airbus in Germany.” [Online]. Available: https://www.airbus.com/en/our-worldwide-presence/airbus-in-germany

[177] NXP Semiconductors, “NXP in Germany.” [Online]. Available: https://www.nxp.com/company/about-nxp/worldwide-locations/germany:GERMANY

[178] A. Färber, “Metropolregion Hamburg - Stark in der Chemieindustrie.” [Online]. Available: https://metropolregion.hamburg.de/wirtschaft-wissenschaft/branchen/chemie-12708

[179] Statistisches Amt für Hamburg und Schleswig-Holstein, “Metropolregion Hamburg,” 2025. [Online]. Available: https://www.statistik-nord.de/zahlen-fakten/regionalstatistik-datenbanken-und-karten/metropolregion-hamburg

[180] Hamburg Behörde für Wirtschaft und Innovation, “Green Hydrogen Hub Europe: Hamburg als Drehkreuz für Wasserstoffimporte nach Deutschland und Europa: Ein wirtschaftspolitisches Konzept der Behörde für Wirtschaft und Innovation,” Hamburg. [Online]. Available: https://www.hamburg.de/resource/blob/202902/8dcebfaf86f577e3562696c19de3db53/wasserstoff-importstategie-data.pdf

[181] Institut der deutschen Wirtschaft Köln Consult GmbH, “Potenziale der Wasserstoffwirtschaft in der Freien und Hansestadt Hamburg: Studie für HIW Hamburg Invest Wirtschaftsförderungsgesellschaft mbH,” Köln. [Online]. Available: https://suche.transparenz.hamburg.de/dataset/tp-veroeffentlichung-h2-studie-hamburg-hiw-iwc

[182] Hamburger Senat, “Fragenkatalog Wasserstoffstrategie für Industrie & Hafen: Energiewendebeirat Hamburg,” Hamburg, 2024. [Online]. Available: https://www.hamburg.de/resource/blob/963698/fd4e237f945e210c4bf1775bb56152d6/d-fragenkatalog-wasserstoffstrategie-ewb-data.pdf

[183] Bundesministerium für Wirtschaft und Energie, “Rahmenbedingungen für den Netzausbau.” [Online]. Available: https://www.bundeswirtschaftsministerium.de/Redaktion/DE/Artikel/Energie/stromnetze-und-netzausbau-regulierung-rahmenbedingungen.html

[184] Übertragungsnetzbetreiber, “Übertragungstechniken | Network Development Plan,” 01.09.2025. [Online]. Available: https://www.netzentwicklungsplan.de/en/node/2657

[185] Bundesnetzagentur, “Bundesfachplanung für Gleichstrom-Vorhaben mit gesetzlichem Erdkabelvorrang: Positionspapier der Bundesnetzagentur für die Unterlagen nach § 8

NABEG," Bonn. [Online]. Available: https://www.netzausbau.de/SharedDocs/Downloads/DE/Methodik/Positionspapier_Erdkabel-Methodik_2017.pdf?__blob=publicationFile

[186] Tagesspiegel Background Energie & Klima, "Bundesbedarfsplangesetz: Kabinett beschließt eingeschränktes Freileitungsgebot," 2026. [Online]. Available: https://background.tagesspiegel.de/energie-und-klima/briefing/kabinett-beschliesst-eingeschraenktes-freileitungsgebot

[187] TenneT TSO GmbH and TransnetBW GmbH, "SuedLink verstehen: Alles Wichtige zu Kabeln, Bauwerken und Genehmigungsverfahren." [Online]. Available: https://suedlink.com/cms/media/SuedLink_verstehen.pdf

[188] 50Hertz Transmission GmbH, "SuedOstLink: Informationen zum Projekt. Gleichstromverbindung zwischen Sachsen-Anhalt und Bayern," 2024. [Online]. Available: https://www.50hertz.com/xspProxy/api/staticfiles/50hertz-client/dokumente/netz/suedostlink/240408_50hertz_fl_suedostlink.pdf

[189] TenneT TSO GmbH, "SuedLink Oberirdische Bauwerke: Technische Anlagen für den fehlerfreien Betrieb von SuedLink," Bayreuth. [Online]. Available: https://www.tennet.eu/de/projekte/suedlink-oberirdische-bauwerke

[190] S. Pöhler, "Streustrombeeinflussung von Rohrsystemen: TenneT TSO GmbH."

[191] Bundesnetzagentur, "Hydrogen core network," 2025. [Online]. Available: https://www.bundesnetzagentur.de/EN/Areas/Energy/HydrogenCoreNetwork/start.html

[192] ——, "Genehmigung eines Wasserstoff-Kernnetzes: Gemäß § 28q Abs. 8 S. 1 i. V. m. § 28q Abs. 1, 2, 4, 5, 6 Satz 1 sowie des Abs. 7 EnWG," Bonn. [Online]. Available: https://www.bundesnetzagentur.de/DE/Fachthemen/ElektrizitaetundGas/Wasserstoff/_DL/Genehmigung.pdf

[193] W. Peschka, *Liquid Hydrogen: Fuel of the Future.* Vienna: Springer Vienna, 1992.

[194] W. Notardonato, "Ground Operations Demonstration Unit for Liquid Hydrogen (GODU LH2)," Jeju, 2013. [Online]. Available: https://ntrs.nasa.gov/citations/20130011589

[195] Butting CryoTech GmbH, "Vaccum-Insulated Pipelines," 12.11.2025. [Online]. Available: https://www.butting.com/en/products/cryogenic-systems/vacuum-insulated-pipelines/

[196] ITP Interpipe, "Cryogenic Pipelines," 17.07.2025. [Online]. Available: https://www.itp-interpipe.com/efficient-pipeline-solutions-for-extreme-temperature-fluids/cryogenic-pipelines/

[197] G. Markowz, A. Dylla, and T. Elliger, "icefuel® - An Infrastructure System for Cryogenic Hydrogen Storage, Distribution and Decentral Use," in *Proceedings / 18th World Hydrogen Energy Conference 2010 - WHEC 2010: Proceedings*, ser. Schriften des Forschungszentrums Jülich : Reihe Energie & Umwelt, D. Stolten, Ed. Jülich: Forschungszentrum Jülich, Zentralbibliothek, 2010, pp. 365–371. [Online]. Available: https://juser.fz-juelich.de/record/135363/files/HI1_6_Markowz.pdf

[198] P. Grant, "The energy supergrid," in *2004 IEEE Power Engineering Society general meeting: Denver, CO, 6 - 10 June 2004*. Piscataway, NJ: IEEE Service Center, 2004, p. 2276. [Online]. Available: https://doi.org/10.1109/pes.2004.1373284

[199] L. Wang, G. Bai, R. Zhang, and J. Liang, "Concept Design of 1 GW LH2-LNG-Superconducting Energy Pipeline," *IEEE Transactions on Applied Superconductivity*, vol. 29, no. 2, pp. 1–2, 2019. [Online]. Available: https://doi.org/10.1109/TASC.2019.2895461

[200] J. Jin, L. Wang, R. Yang, T. Zhang, S. Mu, and Q. Zhou, "A composite superconducting energy pipeline and its characteristics," *Energy Reports*, vol. 8, pp. 2072–2084, 2022. [Online]. Available: https://doi.org/10.1016/j.egyr.2022.01.126

[201] L. Savoldi, A. Balbo, C. E. Bruzek, G. Grasso, M. Patti, and M. Tropeano, "Conceptual Design of a SuperConducting Energy Pipeline for LH2 and Power Transmission Over Long Distances," *IEEE Transactions on Applied Superconductivity*, vol. 34, no. 3, pp. 1–5, 2024. [Online]. Available: https://doi.org/10.1109/TASC.2024.3370123

[202] M. Bracco, A. Balbo, C.-E. Bruzek, M. Breschi, L. Cavallucci, S. Farinon, A. Macchiagodena, G. Mangiulli, R. Musenich, L. Soldati, and L. Savoldi, "Design of a Submarine 30-km MgB2 Cable for the Combined Transfer of 0.3 GWe and LH2 from Offshore Plants to the Ravenna Port," *IEEE Transactions on Applied Superconductivity*, vol. 35, no. 5, pp. 1–6, 2025. [Online]. Available: https://doi.org/10.1109/TASC.2025.3528923

[203] L. Savoldi, M. Bracco, M. Breschi, L. Cavallucci, S. Farinon, N. Gallino, A. Macchiagodena, G. Mangiulli, and R. Musenich, "Analysis of the Evolution of Accidental Transients in the Cooling of a MgB 2 -LH 2 Hybrid Power Cable," *IEEE Transactions on Applied Superconductivity*, vol. 36, no. 5, pp. 1–6, 2026. [Online]. Available: https://doi.org/10.1109/TASC.2026.3651230

[204] L. Cavallucci, M. Breschi, A. Macchiagodena, G. Mangiulli, M. Bracco, S. Farinon, R. Musenich, and L. Savoldi, "Analysis of Electric Fault in a MV DC MgB 2 Transmission

Line Cooled by Liquid Hydrogen," *IEEE Transactions on Applied Superconductivity*, pp. 1–6, 2026. [Online]. Available: https://doi.org/10.1109/TASC.2026.3655642

[205] C. E. Bruzek, T. Spina, U. Melaccio, M. Tropeano, A. Marian, A. Morandi, F. Gömöry, P. Kováč, W. Reiser, S. Holé, N. Lallouet, T. Iannaccone, J. Roudaut, and N. Magnusson, "MgB2-Based MVDC Superconducting Power Cable in Liquid Hydrogen for Hybrid Energy Distribution," *IEEE Transactions on Applied Superconductivity*, vol. 34, no. 3, pp. 1–5, 2024. [Online]. Available: https://doi.org/10.1109/TASC.2023.3347216

[206] F. Mimmi, E. Guerra, M. Simonazzi, A. Morandi, U. Melaccio, and C.-E. Bruzek, "Comparative Analysis of MgB 2 Cable Layouts for 1 GW Superconducting Transmission-Insights From the SCARLET Project," *IEEE Transactions on Applied Superconductivity*, vol. 35, no. 5, pp. 1–12, 2025. [Online]. Available: https://doi.org/10.1109/TASC.2024.3520535

[207] J. Chen, G. Zhang, Q. Qiu, X. Chen, Y. Teng, L. Jing, and N. Song, "Simulation and experiment on superconducting DC energy pipeline cooled by LNG," *Cryogenics (Cryogenics)*, vol. 112, p. 103128, 2020. [Online]. Available: https://doi.org/10.1016/j.cryogenics.2020.103128

[208] L. Xiao, "The Prospect of Carbon-Neutrality-Driven Energy & Power and the Possible Application of Superconductor: Institute of Electrical Engineering Chinese Academy of Sciences," Aix-en-Provence, 12.09.2023. [Online]. Available: https://snf.ieeecsc.org/files/ieeecsc/slides/Xiao%20plenary%20presentation.pdf

[209] J. J. Harrison, "New infrared absorption cross sections for the infrared limb sounding of carbon tetrafluoride (CF4)," *Journal of Quantitative Spectroscopy and Radiative Transfer*, vol. 260, p. 107432, 2021. [Online]. Available: https://doi.org/10.1016/j.jqsrt.2020.107432

[210] F. Fuhry, H. Neumann, K.-P. Weiss, and M. J. Wolf, "Transport und Nutzung von flüssigem Wasserstoff: Leitprojekt TransHyDE – Projekt AppLHy!" *Chemie Ingenieur Technik*, 2025. [Online]. Available: https://doi.org/10.1002/cite.202400075

[211] A. Preuß, *Development of high-temperature superconductor cables for high direct current applications.* Karlsruhe: KIT Scientific Publishing, 2021, vol. Band 31. [Online]. Available: https://doi.org/10.5445/KSP/1000122861

[212] A. Koblischka-Veneva, M. R. Koblischka, K. Berger, Q. Nouailhetas, B. Douine, M. Muralidhar, and M. Murakami, "Comparison of Temperature and Field Dependencies of the Critical Current Densities of Bulk YBCO, MgB2, and Iron-Based Superconductors," *IEEE Transactions on Applied Superconductivity*, vol. 29, no. 5, pp. 1–5, 2019. [Online]. Available: https://doi.org/10.1109/TASC.2019.2900932

[213] M. E. Reuß, "Techno-ökonomische Analyse alternativer Wasserstoffinfrastruktur," Dissertation / PhD ThesisBook, University, RWTH Aachen, Jülich, 2019. [Online]. Available: https://doi.org/10.18154/rwth-2019-07432

[214] Y. Iwasa, *Case Studies in Superconducting Magnets: Design and Operational Issues*, 2nd ed., ser. Springer eBook Collection Engineering. Boston, MA: Springer US, 2009. [Online]. Available: https://doi.org/10.1007/b112047

[215] M. J. Wolf, W. H. Fietz, M. Heiduk, S. Huwer, A. Kienzler, S. I. Schlachter, and T. Vogel, "200 kA DC Busbar Demonstrator DEMO 200 – Conceptual Design of Superconducting 20 kA Busbar Modules Made of HTS CroCo Strands," *IEEE Transactions on Applied Superconductivity*, vol. 32, no. 4, pp. 1–7, 2022. [Online]. Available: https://doi.org/10.1109/TASC.2022.3152130

[216] A. Kuhnert, "Einfluss von Materialeigenschaften auf die Stromtragfähigkeit von technischen Supraleitern," Dissertation, Friedrich-Alexander-Universität Erlangen-Nürnberg, Erlangen, 2012. [Online]. Available: https://d-nb.info/102392675X

[217] J. G. Bednorz and K. A. Müller, "Possible high Tc superconductivity in the Ba-La-Cu-O system," *Zeitschrift für Physik B Condensed Matter*, vol. 64, no. 2, pp. 189–193, 1986. [Online]. Available: https://doi.org/10.1007/BF01303701

[218] Y. Zhang, "REBCO HTS Wire Manufacturing and Continuous Development at SuperPower," in *IAS-HEP Mini-Workshop on High Temperature Superconducting Materials and Magnets*, Hong Kong, 2018. [Online]. Available: https://zenodo.org/records/3271531/files/HEP_20180118_1430_Yifei_Zhang.pdf

[219] W. Zhang, M. W. Rupich, U. Schoop, D. T. Verebelyi, C. Thieme, X. Li, T. Kodenkandath, Y. Huang, E. Siegal, D. Buczek, W. Carter, N. Nguyen, J. Schreiber, M. Prasova, J. Lynch, D. Tucker, and S. Fleshler, "Progress in AMSC scale-up of second generation HTS wire," *Physica C-Superconductivity and Its Applications*, vol. 463-465, pp. 505–509, 2007. [Online]. Available: https://doi.org/10.1016/j.physc.2007.04.239

[220] T. Puig, "Overview on progress, challenges and frontier research of coated conductors for application," Bologna, 06.09.2023. [Online]. Available: https://snf.ieeecsc.org/files/ieeecsc/slides/Puig%20plenary%20presentation.pdf

[221] Faraday Factory Japan, "About us," 31.05.2026. [Online]. Available: https://www.faradaygroup.com/en/company/

[222] A. Molodyk, "Production of 2G HTS tape at Faraday Factory Japan," Geneva, 24.07.2024. [Online]. Available: https://indico.cern.ch/event/1296489/contributions/5881530/attachments/2902968/5091645/Molodyk-Wed-Or12.pdf

[223] Fujikura Ltd., "Fujikura's Superconductor Development History." [Online]. Available: https://www.fujikura.co.jp/en/products/superconductors/history/

[224] Industry Research, "High Temperature Superconductor Market | Global Industry Analysis 2034," 2025. [Online]. Available: https://www.industryresearch.biz/market-reports/high-temperature-superconductor-market-100736

[225] Shanghai Creative Superconductor Technologies Co., Ltd., "About: Company Introduction," 31.05.2026. [Online]. Available: http://www.shscsc.com/HomeEN/AboutEN

[226] Shanghai Superconductor Technology Co., Ltd, "About us: Company Vision: Creating product, Igniting progress, Unleashing energy, A future to exchange," 22.05.2026. [Online]. Available: https://www.shsctec.com/en/company/dream

[227] J. Zhu, "Mass Production and Performance of SST REBCO Tape: Shanghai Superconductor Technology Co. Ltd." Porto, 23.09.2025. [Online]. Available: https://eucas2025.abstractserver.com/program/#/details/presentations/679

[228] Trade Korea, "SuNAM Co,. Ltd. - Company Introduction," 31.05.2026. [Online]. Available: https://sunam2004.tradekorea.com/company.do

[229] Y. Zhang, "REBCO tape production at SuperPower: state of the art and prospects: SuperPower Inc./Furukawa Electric Co. Ltd." 09.03.2023. [Online]. Available: https://indico.cern.ch/event/1220254/contributions/5270410/attachments/2607656/4508214/2023%20HiTAT%20SuperPower_Yifei_Zhang.pdf

[230] THEVA, "Unternehmen: Profil," 28.11.2025. [Online]. Available: https://www.theva.de/unternehmen/#profil

[231] A. Smara, C. Hintze, and W. Prusseit, "REBCO Wire Production at THEVA: State of the Art and Prospects: THEVA Dünnschichttechnik GmbH," Germany, 18.10.2023. [Online]. Available: https://indico.gsi.de/event/17548/contributions/74970/attachments/45362/64330/ReBCO%20Wire%20Production%20at%20THEVA%20GSI%20workshop%20Smara%20Anis.pdf

[232] M. Noe, "Current costs of REBCO tapes: Private communication," 26.11.2025.

[233] A. Pantoja and N. Strickland, “Critical current characterisation of Shanghai Creative Superconductor Technologies SCST-W12 2G HTS superconducting wire,” 2023. [Online]. Available: https://doi.org/10.6084/m9.figshare.5309947.v2

[234] ——, “Critical current characterisation of Eastsuper MF 2G HTS superconducting wire,” 2025. [Online]. Available: https://doi.org/10.6084/m9.figshare.30338536.v1

[235] A. Pantoja, S. Wimbush, and N. Strickland, “Critical current characterisation of Faraday Factory Japan YBCO 2G HTS superconducting wire,” 2023. [Online]. Available: https://doi.org/10.6084/m9.figshare.23536374.v4

[236] M. Skonieczny, N. Izdebska, M. Królikowska, and M. Marczewski, “Corrosion behaviour of aluminum and copper in dimethyl- and diethyl phosphate ionic liquids,” *Electrochimica Acta*, vol. 500, p. 144770, 2024. [Online]. Available: https://doi.org/10.1016/j.electacta.2024.144770

[237] boerse.de, “Kupfer EUR | Euro Kupferpreis aktuell | Euro Kupferkurs heute - boerse.de,” 2025. [Online]. Available: https://www.boerse.de/rohstoffe/Kupferpreis/XC0005705501

[238] B. J. Parkinson, R. Slade, M. J. D. Mallett, and V. Chamritski, “Development of a Cryogen Free 1.5 T YBCO HTS Magnet for MRI,” *IEEE Transactions on Applied Superconductivity*, vol. 23, no. 3, p. 4400405, 2013. [Online]. Available: https://doi.org/10.1109/TASC.2012.2235893

[239] M. Parizh, Y. Lvovsky, and M. Sumption, “Conductors for commercial MRI magnets beyond NbTi: requirements and challenges,” *Superconductor Science and Technology*, vol. 30, no. 1, p. 014007, 2017. [Online]. Available: https://doi.org/10.1088/0953-2048/30/1/014007

[240] Y. Zhao, Y. Wu, A. Goyal, H. Huhtinen, P. Paturi, and Y. Tsuchiya, “Commercial compact fusion triggered REBCO tape industry: Pulsed laser deposition technology opportunities and challenges,” *Superconductivity*, vol. 15, p. 100188, 2025. [Online]. Available: https://doi.org/10.1016/j.supcon.2025.100188

[241] S. Palacios, M. J. Wolf, M. Noe, M. Wehr, and T. Arndt, “Design of a 75 km GW-class Hybrid Pipeline for the Synergetic Transmission of Liquid Hydrogen and Electrical Energy by High-Temperature Superconductivity,” *Superconductor Science and Technology*, 2025. [Online]. Available: https://doi.org/10.1088/1361-6668/ae2cf7

[242] C. Hagart-Alexander, “Chapter 21 - Temperature Measurement,” in *Instrumentation Reference Book (Fourth Edition)*, W. Boyes, Ed. Boston: Butterworth-Heinemann, 2010, pp. 269–326. [Online]. Available: https://doi.org/10.1016/B978-0-7506-8308-1.00021-8

[243] C. Geertsen, A. Damour, W. Grobbelaar, and A. Sainz Torrent, "Cryogenic Pipelines for Industrial Applications. Feedback from LNG Projects and Applications to Liquid Hydrogen," PTC 2024. [Online]. Available: https://www.pipeline-conference.com/abstracts/cryogenic-pipelines-industrial-applications-feedback-lng-projects-and-applications-liquid

[244] E. Aldalur, A. Suárez, and F. Veiga, "Thermal expansion behaviour of Invar 36 alloy parts fabricated by wire-arc additive manufacturing," *Journal of Materials Research and Technology*, vol. 19, pp. 3634–3645, 2022. [Online]. Available: https://doi.org/10.1016/j.jmrt.2022.06.114

[245] T. Michler, "Influence of gaseous hydrogen on the tensile properties of Fe−36Ni INVAR alloy," *International Journal of Hydrogen Energy*, vol. 39, no. 22, pp. 11 807–11 809, 2014. [Online]. Available: https://doi.org/10.1016/j.ijhydene.2014.05.133

[246] R. L. Mills and F. J. Edeskuty, "Hydrogen embrittlement tests of cryogenic metals," Los Alamos, 1965. [Online]. Available: https://www.osti.gov/servlets/purl/4583616

[247] VDE Verband der Elektrotechnik Elektronik Informationstechnik e.V., "Technische Anschlussregel Mittelspannung (VDE-AR-N 4110)," 2023. [Online]. Available: https://www.vde.com/de/fnn/themen/tar/tar-mittelspannung-vde-ar-n-4110

[248] G. Kuhn, "MVDC PLUS® Introduction: Siemens Energy Transmission Solutions," Erfurt, 12.11.2020. [Online]. Available: https://www.vde-thueringen.de/resource/blob/2012804/fd02c72ddf7e5dfcadc24581be3e666f/verteilernetzverbund-mittels-gleichstromuebertragungs-technologie-data.pdf

[249] A. Morandi, "HTS dc transmission and distribution: concepts, applications and benefits," *Superconductor Science and Technology*, vol. 28, no. 12, p. 123001, 2015. [Online]. Available: https://doi.org/10.1088/0953-2048/28/12/123001

[250] S. S. Kalsi, *Applications of high temperature superconductors to electric power equipment.* Piscataway, NJ: IEEE Press, 2011. [Online]. Available: https://doi.org/10.1002/9780470877890

[251] D. Kottonau, E. Shabagin, W. de Sousa, J. Geisbüsch, M. Noe, H. Staggo, S. Fechner, H. Woiton, and T. Küsters, *Evaluation of the Use of Superconducting 380 kV Cable.* Karlsruhe: KIT Scientific Publishing, 2020, vol. Band 30. [Online]. Available: https://doi.org/10.5445/ksp/1000117918

[252] S. Klöppel, A. Marian, C. Haberstroh, and C.-E. Bruzek, "Thermo-hydraulic and economic aspects of long-length high-power MgB2 superconducting cables,"

Cryogenics (Cryogenics), vol. 113, p. 103211, 2021. [Online]. Available: https://doi.org/10.1016/j.cryogenics.2020.103211

[253] International Electrotechnical Commission, *IEC 62895:2017. High voltage direct current (HVDC) power transmission - cables with extruded insulation and their accessories for rated voltages up to 320 kV for land applications - test methods and requirements*, 1st ed., ser. Norme internationale / Commission Electronique Internationale, CEI. Geneva: International Electrotechnical Commission, 2017-05, vol. 62895. [Online]. Available: https://permalink.obvsg.at/AC15222169

[254] M. J. Jefferies and K. N. Mathes, "Dielectric Loss and Voltage Breakdown in Liquid Nitrogen and Hydrogen," *IEEE Transactions on Electrical Insulation*, vol. EI 5, no. 3, pp. 83–91, 1970. [Online]. Available: https://doi.org/10.1109/tei.1970.299101

[255] N. Inoue, N. Chikumoto, H. Watanabe, Y. Ivanov, T. Hino, A. Sato, T. Sawamura, H. Yamamoto, K. Sumi, K. Okuno, and O. Motojima, "Test operation of 500 m /100 MW Ishikari high-temperature superconducting DC transmission line to demonstrate the required cost reduction and robustness," *Journal of Physics: Conference Series*, vol. 2545, no. 1, p. 012024, 2023. [Online]. Available: https://doi.org/10.1088/1742-6596/2545/1/012024

[256] A. V. Naumov, D. N. Diev, A. N. Dinisilov, O. P. Anashkin, V. E. Keilin, I. A. Kovalev, V. V. Lobyntsev, V. I. Scherbakov, D. I. Shutova, and V. E. Sytnykov, "Current leads and joints for HTS DC cable of 2.5 kA 20 kV," in *AIP Conference Proceedings*, ser. AIP Conference Proceedings. AIP Publishing LLC, 2014, pp. 1694–1699. [Online]. Available: https://doi.org/10.1063/1.4860911

[257] J.-M. Saugrain, "Three years operation experience of the AmpaCity system installation in Essen, Germany," Geneva, 20.09.2017. [Online]. Available: https://indico.cern.ch/event/659554/contributions/2709480/attachments/1527270/2388461/3LO4-05_Jean-Maxime_Saugrain_Room_1.pdf

[258] M. Ross, "Utility applications and experience with resilient electric grid systems utilizing high temperature superconductor wires in Chicago," *Physica C-Superconductivity and Its Applications*, vol. 614, p. 1354374, 2023. [Online]. Available: https://doi.org/10.1016/j.physc.2023.1354374

[259] B. Yang, J. Kang, S. Lee, C. Choi, and Y. Moon, "Qualification Test of a 80 kV 500 MW HTS DC Cable for Applying Into Real Grid," *IEEE Transactions on Applied Superconductivity*, vol. 25, no. 3, pp. 1–5, 2015. [Online]. Available: https://doi.org/10.1109/TASC.2015.2396683

[260] M. Wolf, M. Wehr, S. Palacios, and T. Arndt, "Opportunities and Challenges of Using HTS REBCO in Liquid Hydrogen (LH2)," Matsue, Japan, 23.10.2024. [Online]. Available: https://publikationen.bibliothek.kit.edu/1000177644

[261] Manufacturer of superconducting cable terminations, "Terminations: Oral communication," 2024.

[262] G. Didier, C. H. Bonnard, T. Lubin, and J. Lévêque, "Comparison between inductive and resistive SFCL in terms of current limitation and power system transient stability," *Electric Power Systems Research*, vol. 125, pp. 150–158, 2015. [Online]. Available: https://doi.org/10.1016/j.epsr.2015.04.002

[263] J. G. Hust and A. B. Lankford, "Thermal Conductivity of Aluminium, Copper, Iron, and Tungsten for Temperatures from 1 K to the Melting Point: NBSIR 84-3007," Boulder (Colorado). [Online]. Available: https://ia800400.us.archive.org/34/items/thermalconducti8430hust_0/thermalconducti8430hust_0.pdf

[264] J. A. Lee and S. Woods, "Hydrogen Embrittlement," Huntsville. [Online]. Available: https://ntrs.nasa.gov/citations/20160005654

[265] A. Rosskopf and C. Brunner, "Enhancing Litz Wire Power Loss Calculations by Combining a Sparse Strand Element Equivalent Circuit Method With a Voronoi-Based Geometry Model," *IEEE Transactions on Power Electronics*, vol. 37, no. 9, pp. 11 450–11 456, 2022. [Online]. Available: https://doi.org/10.1109/TPEL.2022.3169992

[266] W. T. B. de Sousa, "Transient Simulations of Superconducting Fault Current Limiters," Tese (doutorado), Universidade Federal do Rio de Janeiro, Rio de Janeiro, 2015. [Online]. Available: https://www.researchgate.net/publication/274511690_Transient_Simulations_of_Superconducting_Fault_Current_Limiters

[267] J. C. Butcher, *Numerical methods for ordinary differential equations.* Hoboken, N.J: Wiley, 2008. [Online]. Available: https://doi.org/10.1002/9780470753767

[268] T. H. Glisson, "Circuit Elements, Circuit Diagrams, and Kirchhoff's Laws," in *Introduction to Circuit Analysis and Design.* Springer, Dordrecht, 2011, pp. 49–81. [Online]. Available: https://doi.org/10.1007/978-90-481-9443-8_3

[269] A. Khonya, *System-Level Modeling of the Powertrain for an Electric Aircraft with Superconducting Components*, ser. Karlsruher Schriftenreihe zur Supraleitung. Karlsruhe: KIT Scientific Publishing, 2025. [Online]. Available: https://doi.org/10.5445/KSP/1000181030

[270] S. Ruck, *Thermofluiddynamik: Grundlagen, Theorie und Beispiele der konvektiven Wärmeübertragung bei laminaren und turbulenten Strömungen.* Wiesbaden: Springer Vieweg and Springer Fachmedien Wiesbaden GmbH, 2025. [Online]. Available: https://doi.org/10.1007/978-3-658-48882-6

[271] T. M. Flynn, *Cryogenic engineering*, 2nd ed. New York: Dekker, 2005.

[272] P. F. Herrmann, C. Cottevieille, G. Duperray, A. Leriche, T. Verhaege, C. Albrecht, and J. Bock, "Cryogenic load calculation of high Tc current lead," *Cryogenics (Cryogenics)*, vol. 33, no. 5, pp. 555–562, 1993. [Online]. Available: https://doi.org/10.1016/0011-2275(93)90253-K

[273] R. Heller, W. H. Fietz, M. Heiduk, M. Hollik, A. Kienzler, C. Lange, R. Lietzow, I. Meyer, T. Richter, and T. Vogel, "Overview of JT-60SA HTS Current Lead Manufacture and Testing," *IEEE Transactions on Applied Superconductivity*, vol. 28, no. 3, pp. 1–5, 2018. [Online]. Available: https://doi.org/10.1109/TASC.2017.2768166

[274] H. Belyadi, E. Fathi, and F. Belyadi, "Chapter Eight - Hydraulic Fracturing Chemical Selection and Design," in *Hydraulic Fracturing in Unconventional Reservoirs*, H. Belyadi, E. Fathi, and F. Belyadi, Eds. Boston: Gulf Professional Publishing, 2017, pp. 107–120. [Online]. Available: https://doi.org/10.1016/B978-0-12-849871-2.00008-3

[275] A. Hussein, "Chapter 2 - Flow Assurance," in *Essentials of Flow Assurance Solids in Oil and Gas Operations*, A. Hussein, Ed. Gulf Professional Publishing, 2023, pp. 53–103. [Online]. Available: https://doi.org/10.1016/B978-0-323-99118-6.00015-0

[276] D. A. Simpson, "Chapter Four - Surface Engineering Concepts," in *Practical Onshore Gas Field Engineering*, D. A. Simpson, Ed. Gulf Professional Publishing, 2017, pp. 221–272. [Online]. Available: https://doi.org/10.1016/B978-0-12-813022-3.00004-3

[277] C. E. Bruzek, A. Allais, K. Allweins, D. Dickson, N. Lallouet, and E. Marzahn, "6 - Using superconducting DC cables to improve the efficiency of electricity transmission and distribution (T&D) networks: An overview," in *Superconductors in the power grid*, ser. Woodhead Publishing series in energy, C. Rey, Ed. Cambridge: Woodhead Publ, 2014, pp. 189–224. [Online]. Available: https://doi.org/10.1016/B978-1-78242-029-3.00006-6

[278] Demaco Holland B.V., "Vacuum insulation: 10 benefits of vacuum insulated systems," 14.02.2024. [Online]. Available: https://demaco-cryogenics.com/blog/vacuum-insulation-10-benefits-of-vacuum-insulated-systems/

[279] K. Krempetz, J. Grimson, and P. Kelly, “A Design Chart for Long Vacuum Pipes and Shells: TM-1378,” Batavia, Illinois. [Online]. Available: https://lss.fnal.gov/archive/test-tm/1000/fermilab-tm-1378.pdf

[280] TenneT, “HelWin1.” [Online]. Available: https://www.tennet.eu/de/projekte/helwin1

[281] ——, “HelWin2.” [Online]. Available: https://www.tennet.eu/de/projekte/helwin2

[282] ——, “SylWin1.” [Online]. Available: https://www.tennet.eu/de/projekte/sylwin1

[283] ——, “BorWin6.” [Online]. Available: https://www.tennet.eu/de/projekte/borwin6

[284] C. Wu, “BOG und BOG-Management für LH2-Systeme: Linde GmbH,” 08.05.2024.

[285] Chicago Bridge & Iron Company, “Liquid Hydrogen Storage Technologies.” [Online]. Available: https://www.energy.gov/sites/default/files/2022-03/Liquid%20H2%20Workshop-CBandI.pdf

[286] FNB Gas e.V., “Das deutsche Fernleitungsnetz,” 02.06.2026. [Online]. Available: https://fnb-gas.de/pressematerialien/karte_das-deutsche-fernleitungsnetz/

[287] Y. Sandeep, B. Rangan, and S. Srinivas, “Thermodynamic Analysis of LNG Regasification Process,” *Chemical Engineering Transactions*, vol. 94, pp. 919–924, 2022. [Online]. Available: https://doi.org/10.3303/CET2294153

[288] X. Hong, V. B. Thaore, I. A. Karimi, S. Farooq, X. Wang, A. K. Usadi, B. R. Chapman, and R. A. Johnson, “Techno-enviro-economic analyses of hydrogen supply chains with an ASEAN case study,” *International Journal of Hydrogen Energy*, vol. 46, no. 65, pp. 32 914–32 928, 2021. [Online]. Available: https://doi.org/10.1016/j.ijhydene.2021.07.138

[289] Ø. Sekkesæter, “Evaluation of Concepts and Systems for Marine Transportation of Hydrogen,” Master’s thesis in Mechanical Engineering, Norwegian University of Science and Technology, Trondheim, 2019. [Online]. Available: https://hdl.handle.net/11250/2623195

[290] M. Reuß, T. Grube, M. Robinius, P. Preuster, P. Wasserscheid, and D. Stolten, “Seasonal storage and alternative carriers: A flexible hydrogen supply chain model,” *Applied Energy*, vol. 200, pp. 290–302, 2017. [Online]. Available: https://doi.org/10.1016/j.apenergy.2017.05.050

[291] W. Sullivan, E. Wicks, and C. Koelling, *Engineering Economy, Global Edition*, 17th ed. Harlow: Pearson Education Limited, 2019. [Online]. Available: https://elibrary.pearson.de/book/99.150005/9781292264967

[292] K. E. Lonergan, F. Egli, S. Osorio, G. Sansavini, M. Pahle, T. S. Schmidt, and B. Steffen, "Improving the representation of cost of capital in energy system models," *Joule*, vol. 7, no. 3, pp. 469–483, 2023. [Online]. Available: https://doi.org/10.1016/j.joule.2023.02.004

[293] Bundesnetzagentur, "Regulatory Factsheet: Return on Equity, Cost of Debt and WACC," Bonn, 2026. [Online]. Available: https://www.bundesnetzagentur.de/DE/Beschlusskammern/GBK/Kosten_ErloesReg/Regulatory_Fact_Sheets/start.html

[294] A. Rapoport, "Netzinvestitionen: EK-Zinssatz könnte durch NEST auf sieben Prozent steigen," *Tagesspiegel Background Energie & Klima*, 16.12.2025. [Online]. Available: https://background.tagesspiegel.de/energie-und-klima/briefing/ek-zinssatz-koennte-durch-nest-auf-sieben-prozent-steigen

[295] L. Hatton, I. Staffell, M. Jansen, G. Oluleye, and A. Hawkes, "Historical and future projected costs of capital for ten energy technologies across 176 countries," *Scientific Data*, vol. 12, no. 1, p. 1912, 2025. [Online]. Available: https://doi.org/10.1038/s41597-025-06177-0

[296] R. Sota and S. Venghaus, "Empirical estimates of cost of capital for industrial-scale green hydrogen projects in Germany," 2026. [Online]. Available: https://doi.org/10.22541/essoar.176763137.75228369/v1

[297] B. Lux, J. Gegenheimer, K. Franke, F. Sensfuß, and B. Pfluger, "Supply curves of electricity-based gaseous fuels in the MENA region," *Computers & Industrial Engineering*, vol. 162, p. 107647, 2021. [Online]. Available: https://doi.org/10.1016/j.cie.2021.107647

[298] Bundesverband der Energie- und Wasserwirtschaft e.V., "BDEW-Strompreisanalyse April 2026: Haushalte und Industrie," 2026. [Online]. Available: https://www.bdew.de/media/documents/BDEW_Strompreisanalyse_042026.pdf

[299] M. D. Solomon, W. Heineken, M. Scheffler, and T. Birth-Reichert, "Cost Optimization of Compressed Hydrogen Gas Transport via Trucks and Pipelines," *Energy Technology*, vol. 12, no. 1, 2024.

[300] University of Chicago, "Hydrogen Delivery Scenario Analysis Model (HDSAM): Microsoft Excel 2010," Argonne, IL. [Online]. Available: https://hdsam.es.anl.gov/index.php?content=hdsam

[301] D. Gromoll, R. Schumacher, and C. Humpert, "Dielectric strength of insulating material in LN 2 with thermally induced bubbles," *Journal of Physics: Conference Series*, vol. 1559, no. 1, p. 012087, 2020. [Online]. Available: https://doi.org/10.1088/1742-6596/1559/1/012087

[302] A. Sen, T. Jamasb, and C. Brandstätt, “Cross-border Allocation of Costs and Benefits of Shared Energy Infrastructure in the EU: An Organisational Perspective,” 2024. [Online]. Available: https://research.cbs.dk/en/publications/cross-border-allocation-of-costs-and-benefits-of-shared-energy-in/

[303] T.-P. Chen, Air Liquide, Chevron Technology Venture, Gas Technology Institute, National Renewable Energy Laboratory, Tiax, and Argonne National Laboratory, “Final Report: Hydrogen Delivery Infrastructure Options Analysis.” [Online]. Available: https://www1.eere.energy.gov/hydrogenandfuelcells/pdfs/delivery_infrastructure_analysis.pdf

[304] F. Grilli, E. Pardo, A. Stenvall, D. N. Nguyen, W. Yuan, and F. Gomory, “Computation of Losses in HTS Under the Action of Varying Magnetic Fields and Currents,” *IEEE Transactions on Applied Superconductivity*, vol. 24, no. 1, pp. 78–110, 2014. [Online]. Available: https://doi.org/10.1109/TASC.2013.2259827

[305] A. Arrigoni and L. Bravo Diaz, “Hydrogen emissions from a hydrogen economy and their potential global warming impact: Summary report of the Clean Hydrogen Joint Undertaking expert workshop on the Environmental Impacts of Hydrogen.” [Online]. Available: https://data.europa.eu/doi/10.2760/065589

[306] Frazer-Nash Consultancy, “Fugitive Hydrogen Emissions in a Future Hydrogen Economy.” [Online]. Available: https://www.gov.uk/government/publications/fugitive-hydrogen-emissions-in-a-future-hydrogen-economy

[307] R. van Rossum, J. Jens, G. La Guardia, A. Wang, L. Kühnen, and M. Overgaag, “European Hydrogen Backbone: A European Hydrogen Infrastructure Vision Covering 28 Countries,” Utrecht. [Online]. Available: https://ehb.eu/files/downloads/ehb-report-220428-17h00-interactive-1.pdf

[308] IEA, “IEA G20 Hydrogen report: Assumptions,” Paris. [Online]. Available: https://iea.blob.core.windows.net/assets/29b027e5-fefc-47df-aed0-456b1bb38844/IEA-The-Future-of-Hydrogen-Assumptions-Annex_CORR.pdf

[309] Mott MacDonald Limited and The Institution of Engineering and Technology, “A comparison of electricity transmission technologies: costs and characteristics: An independent report by Mott MacDonald in conjunction with the IET,” Brighton. [Online]. Available: https://www.theiet.org/media/axwkktkb/100110238_001-rev-j-electricity-transmission-costs-and-characteristics_final-full.pdf

[310] Ea Energy Analyses A / S, Energynautics, J. van Uden, N. Ebersbach, J. Reijntjes, P. Ayivor, and A. Campagne, "Pathway 2.0 Techno-economic data," 2024. [Online]. Available: https://doi.org/10.5281/zenodo.13382786

[311] A. Vafeas, T. Pagano, and E. Peirano, "e-HIGHWAY 2050. Modular Development Plan of the Pan-European Transmission System 2050. D3.1. Technology assessment from 2030 to 2050." [Online]. Available: https://docs.entsoe.eu/baltic-conf/bites/www.e-highway2050.eu/fileadmin/documents/Results/D3_1_Technology_assessment_from_2030_to_2050.pdf

[312] I. Walker, B. Madden, and F. Tahir, "Hydrogen supply chain evidence base." [Online]. Available: https://assets.publishing.service.gov.uk/media/5c00053d40f0b65b09a3a827/H2_supply_chain_evidence_-_publication_version.pdf

[313] Übertragungsnetzbetreiber, "Kostenschätzungen (zu Kapitel 5.2.1 und 5.2.6): NEP 2037/2045 (2023), 2. Entwurf." [Online]. Available: https://www.netzentwicklungsplan.de/kostenschaetzungen-zu-kapitel-521-und-526-0

[314] ——, "Netzentwicklungsplan Strom 2035, Version 2021, 1. Entwurf, Kostenschätzungen." [Online]. Available: https://www.netzentwicklungsplan.de/sites/default/files/2023-02/NEP_2035_2021_1_Entwurf_Kostenschaetzungen_0.pdf

[315] European Network of Transmission System Operators for Electricity and European Network of Transmission System Operators for Gas, "TYNDP // 2024 Scenarios Methodology Report." [Online]. Available: https://2024.entsos-tyndp-scenarios.eu/#download

[316] PricewaterhouseCoopers Advisory s.r.o., "Unit Investment Cost Indicators - Project Support to ACER. Final Report." [Online]. Available: https://www.acer.europa.eu/sites/default/files/documents/Publications/UIC_report_2023.pdf

[317] Conseil International des Grands Réseaux Électriques, "Global Interconnected and sustainable electricity system. WG C1.44." [Online]. Available: https://www.e-cigre.org/publications/detail/938-global-interconnected-and-sustainable-electricity-system-effects-of-storage-demand-response-and-trading-rules.html

[318] W. Reiser, "Austausch zum aktuellen Stand der Supraleitertechnologie: Supraleitung: Zukunftsmusik oder Schnelligkeit und Effizienz für die Energiewende von heute?" 13.11.2024. [Online]. Available: https://www.energiedialog2050.de/wp-content/uploads/2025/01/Dr.-Wolfgang-Reiser-ivSupra_Energiepolitisches-Fruehstueck-13.11.2024.pdf

[319] M. G. Bennett and L. Crowe, “A survey of the reliability of HVDC systems throughout the world during 2017-2018 | CSE: Cigre Science & Engineering,” 2021. [Online]. Available: https://cse.cigre.org/cse-n023/a-survey-of-the-reliability-of-hvdc-systems-throughout-the-world-during-2017-2018.html

[320] L. Hofmann, “Einsatz von Erdkabeln und Freileitungen in Hochspannungs-Drehstrom- und -Gleichstrom-Übertragungssystemen,” Hannover, 05.05.2015. [Online]. Available: https://www.netzausbau.de/SharedDocs/Downloads/DE/Veranstaltungen/2015/Infotage/Hannover_Freileitung_Erdkabel.pdf?__blob=publicationFile

[321] C. Davidson, “Comparison of HVDC Converters,” in *High voltage DC transmission systems*, ser. CIGRE Green Books, B. R. Andersen and S. L. Nilsson, Eds. Cham: Springer, 2025, pp. 247–262. [Online]. Available: https://doi.org/10.1007/978-3-031-27353-7_8

[322] D. Westermann, D. van Hertem, G. Real, M. Meisingset, T. Rauhala, M. Kurra, B. Deppe, R. Atmuri, A. Küster, D. Soerangr, G. Asplund, M. Takasaki, B. Klöckl, M. Bennett, and K. Friedrich, “Voltage Source Converter (VSC) HVDC for Power Transmission – Economic Aspects and Comparison with other AC and DC Technologies: Working Group B4.46.” [Online]. Available: https://www.e-cigre.org/publications/detail/492-voltage-source-converter-vsc-hvdc-for-power-transmission-economic-aspects-and-comparison-with-other-ac-and-dc-technologies.html

[323] J. Cabañas Ramos, I. Jahn, M. Moritz, and Moore, John, Kjaer, Christian, “Ready DC. WG4: Long-term View for HVDC Technology.” [Online]. Available: https://ec.europa.eu/research/participants/documents/downloadPublic?documentIds=080166e505208432&appId=PPGMS

[324] Amprion GmbH, “Anlage 1 Erläuterungsbericht: Vorhaben Nr. 92 BBPLG: Höchstspannungsleitung Walsum-Beeck, Drehstrom Nennspannung 380 kV.” [Online]. Available: https://www.ihk.de/blueprint/servlet/resource/blob/6421028/5989dfcf5a15b615e6b9d3e0674783cc/anlage-01-erlaeuterungsbericht-data.pdf

[325] H. Seidl and R. Heuke, “Technologieübersicht. Das deutsche Höchstspannungsnetz: Technologien und Rahmenbedingungen.” Berlin. [Online]. Available: https://www.bundeswirtschaftsministerium.de/Redaktion/DE/Publikationen/Energie/technologieuebersicht.pdf?__blob=publicationFile&v=1

[326] T. K. Vrana and P. Härtel, “Estimation of investment model cost parameters for VSC HVDC transmission infrastructure,” *Electric Power Systems Research*, vol. 160, pp. 99–108, 2018. [Online]. Available: https://doi.org/10.1016/j.epsr.2018.02.007

[327] Prysmian Group, “525 kV New Cable Systems for the Energy Transition: Linking the Future,” Milano. [Online]. Available: https://www.prysmian.com/staticres/525-kV-HVDC/

[328] S. Nishikawa, T. Shimizu, N. Nakajima, O. Saito, T. Sato, and S. Tomioka, “Expansion of HVDC Cable Application in Response to Growing Demand for Renewable Energy Transmission,” 2022. [Online]. Available: https://sumitomoelectric.com/sites/default/files/2022-04/download_documents/E94-07.pdf

[329] Powerlink: A Brand of Prysmian Group, “SuedLink.” [Online]. Available: https://www.prysmian.com/sites/default/files/20210826_PG_GermanCorridors_Sheets_Suedlink_ENG.pdf

[330] C. Gatermann, “Entwurf eines Verfahrens zur Allokation von thermischen Betriebsmittelreserven eines HGÜ-Systems für den AC-DC-Systemschutz,” Diplomarbeit, Technische Universität Ilmenau, Ilmenau, 2023. [Online]. Available: https://www.db-thueringen.de/servlets/MCRFileNodeServlet/dbt_derivate_00061968/ilm1-2023100055.pdf

[331] Bundesnetzagentur, “Hydrogen core network: Annexes: Amended application: amended Annex 3,” Bonn. [Online]. Available: https://www.bundesnetzagentur.de/DE/Fachthemen/ElektrizitaetundGas/Wasserstoff/Kernnetz/start.html

[332] Department of Energy (DOE) United States of America, “Multi-Year Research, Development, and Demonstration Plan – 3.2 Hydrogen Delivery.” [Online]. Available: https://www.energy.gov/sites/prod/files/2015/08/f25/fcto_myrdd_delivery.pdf

[333] F. H. Saadi, N. S. Lewis, and E. W. McFarland, “Relative costs of transporting electrical and chemical energy,” *Energy & Environmental Science*, vol. 11, no. 3, pp. 469–475, 2018. [Online]. Available: https://doi.org/10.1039/C7EE01987D

[334] Carbon Limits AS and DNV AS, “Re-Stream: Study on the reuse of oil and gas infrastructure for hydrogen and CCS in Europe.” [Online]. Available: https://www.concawe.eu/wp-content/uploads/Re-stream-final-report_Oct2021.pdf

[335] F. Staiß, M. Schmidt, C. Stephanos, P. Stöcker, and S. Wurbs, “Optionen für den Import grünen Wasserstoffs nach Deutschland bis zum Jahr 2030, Materialband,” München. [Online]. Available: https://doi.org/10.48669/esys_2022-8

[336] The Danish Energy Agency, “Energy Transport: Technology descriptions and projections for long-term energy system planning.” Copenhagen. [Online]. Available: https://ens.dk/en/analyses-and-statistics/technology-data-transport-energy

[337] B. Thawani, R. Hazael, and R. Critchley, “Assessing the pressure losses during hydrogen transport in the current natural gas infrastructure using numerical modelling,” *International Journal of Hydrogen Energy*, vol. 48, no. 88, pp. 34 463–34 475, 2023. [Online]. Available: https://doi.org/10.1016/j.ijhydene.2023.05.208

[338] M.-R. Tahan, “Recent advances in hydrogen compressors for use in large-scale renewable energy integration,” *International Journal of Hydrogen Energy*, vol. 47, no. 83, pp. 35 275–35 292, 2022. [Online]. Available: https://doi.org/10.1016/j.ijhydene.2022.08.128

[339] A. Escamilla, D. Sánchez, and L. García-Rodríguez, “Assessment of power-to-power renewable energy storage based on the smart integration of hydrogen and micro gas turbine technologies,” *International Journal of Hydrogen Energy*, vol. 47, no. 40, pp. 17 505–17 525, 2022. [Online]. Available: https://doi.org/10.1016/j.ijhydene.2022.03.238

[340] Q.-h. Luo, B.-g. Sun, and H.-y. Tian, “The characteristic of polytropic coefficient of compression stroke in hydrogen internal combustion engine,” *International Journal of Hydrogen Energy*, vol. 39, no. 25, pp. 13 787–13 792, 2014. [Online]. Available: https://doi.org/10.1016/j.ijhydene.2014.04.035

[341] S. Mokhatab, W. A. Poe, and J. Y. Mak, *Handbook of natural gas transmission and processing: Principles and practices*, 3rd ed. Amsterdam and Boston and Cambridge: Gulf Professional Publishing an imprint of Elsevier, 2015. [Online]. Available: https://doi.org/10.1016/C2013-0-15625-5

[342] F. Stöckl, W.-P. Schill, and A. Zerrahn, “Optimal supply chains and power sector benefits of green hydrogen,” *Scientific Reports*, vol. 11, no. 1, 2021. [Online]. Available: https://doi.org/10.1038/s41598-021-92511-6

[343] Z. Abdin, C. Tang, Y. Liu, and K. Catchpole, “Large-scale stationary hydrogen storage via liquid organic hydrogen carriers,” *iScience*, vol. 24, no. 9, p. 102966, 2021. [Online]. Available: https://doi.org/10.1016/j.isci.2021.102966

[344] S. Song, H. Lin, P. Sherman, X. Yang, C. P. Nielsen, X. Chen, and M. B. McElroy, “Production of hydrogen from offshore wind in China and cost-competitive supply to Japan,” *Nature Communications*, vol. 12, no. 1, p. 6953, 2021. [Online]. Available: https://doi.org/10.1038/s41467-021-27214-7

[345] R. K. Ahluwalia, D. D. Papadias, J.-K. Peng, and H. S. Roh, “System Level Analysis of Hydrogen Storage Options,” Washington, D.C. [Online]. Available: https://www.hydrogen.energy.gov/docs/hydrogenprogramlibraries/pdfs/review19/st001_ahluwalia_2019_o.pdf

[346] M. Wieliczko, "Hydrogen Liquefaction Capacity in the United States: DOE Hydrogen Program Record," 2024. [Online]. Available: https://www.hydrogen.energy.gov/docs/hydrogenprogramlibraries/pdfs/24003-hydrogen-liquefaction-capacity-united-states.pdf

[347] SK Innovation E&S, "Business. Hydrogen Energy: Build the world's largest liquefaction plant," 2024. [Online]. Available: https://www.skens.com/en/sk/content/view.do?cate=energy&m1=h2

[348] H.-k. Kim, "SK E&S builds world's largest hydrogen liquefaction plant," *KED Global*, 09.05.2024. [Online]. Available: https://www.kedglobal.com/hydrogen-economy/newsView/ked202405080013

[349] E. Connelly, M. Penev, A. Elgowainy, and C. Hunter, "Current Status of Hydrogen Liquefaction Costs: DOE Hydrogen and Fuel Cells Program Record: Record #: 19001." [Online]. Available: https://www.hydrogen.energy.gov/pdfs/19001_hydrogen_liquefaction_costs.pdf

[350] R. d'Amore Domenech, T. J. Leo, and B. G. Pollet, "Bulk power transmission at sea: Life cycle cost comparison of electricity and hydrogen as energy vectors," *Applied Energy*, vol. 288, p. 116625, 2021. [Online]. Available: https://doi.org/10.1016/j.apenergy.2021.116625

[351] S. Bruce, M. Temminghoff, J. Hayward, E. Schmidt, C. Munnings, D. Palfreyman, and P. Hartley, "National Hydrogen Roadmap." Australia. [Online]. Available: https://research.csiro.au/hydrogenfsp/wp-content/uploads/sites/247/2018/08/18-00314_EN_NationalHydrogenRoadmap_WEB_180815.pdf

[352] IEA, "Technology Roadmap: Hydrogen and Fuel Cells." [Online]. Available: https://iea.blob.core.windows.net/assets/e669e0b6-148c-4d5c-816b-a7661301fa96/TechnologyRoadmapHydrogenandFuelCells.pdf

[353] DNV GL, "Study on the Import of Liquid Renewable Energy: Technology Cost Assessment." [Online]. Available: https://www.gie.eu/wp-content/uploads/filr/2598/DNV-GL_Study-GLE-Technologies-and-costs-analysis-on-imports-of-liquid-renewable-energy.pdf

[354] Air Liquide, "Technology Handbook." [Online]. Available: https://engineering.airliquide.com/sites/engineering/files/2022-09/technohandbook11oct.pdf

[355] D. Sadler, H. S. Anderson, M. Sperrink, A. Cargill, M. Sjøvoll, K. I. Åsen, J. E. Finnesand, T. Melien, R. Thorsen, L. Hagesæther, P. Ringrose, B. Nazarian, and H. H. Kvadsheim, "H21 North of England. H21 NoE Report/2018." [Online].

Available: https://web.archive.org/web/20231015102406/https://www.h21.green/app/uploads/2019/01/H21-NoE-PRINT-PDF-FINAL-1.pdf

[356] IRENA, "Global Hydrogen Trade to Meet the 1.5°C Climate Goal: Part II - Technology Review of Hydrogen Carriers," Abu Dhabi. [Online]. Available: https://www.irena.org/-/media/Files/IRENA/Agency/Publication/2022/Apr/IRENA_Global_Trade_Hydrogen_2022.pdf?rev=3d707c37462842ac89246f48add670ba

[357] Linde, "Liquefied Hydrogen Tank Solutions," 02.03.2026. [Online]. Available: https://www.linde-engineering.com/products-and-services/plant-components/liquefied-hydrogen-tank-solutions

[358] Kawasaki Heavy Industries, Ltd., "Kawasaki Obtains AIP for Large, 160,000 m3 Liquefied Hydrogen Carrier," 2022. [Online]. Available: https://global.kawasaki.com/en/corp/newsroom/news/detail/?f=20220422_3378

[359] Chicago Bridge & Iron Company, "CB&I and Shell Demonstrate First Commercial-Scale Liquid Hydrogen Storage Tank Design for International Trade Applications at NASA," The Woodlands, Texas, 2025. [Online]. Available: https://www.cbi.com/cbi-and-shell-demonstrate-first-commercial-scale-liquid-hydrogen-storage-tank-design-for-international-trade-applications-at-nasa/

[360] K. Zhang, "First Demonstration of a Commercial Scale Liquid Hydrogen Storage Tank Design for International Trade Applications: Shell International Exploration and Production, Inc." 07.04.2023. [Online]. Available: https://www.hydrogen.energy.gov/docs/hydrogenprogramlibraries/pdfs/review23/st241_holgate_2023_o-pdf.pdf

[361] J. W. Pratt and L. E. Klebanoff, "Feasibility of the SF-BREEZE: a Zero-Emission, Hydrogen Fuel Cell, High-Speed Passenger Ferry: Sandia Report: SAND2016-9719," Albuquerque. [Online]. Available: https://rosap.ntl.bts.gov/view/dot/51783

[362] M. Raab, S. Maier, and R.-U. Dietrich, "Comparative techno-economic assessment of a large-scale hydrogen transport via liquid transport media," *International Journal of Hydrogen Energy*, vol. 46, no. 21, pp. 11 956–11 968, 2021. [Online]. Available: https://doi.org/10.1016/j.ijhydene.2020.12.213

[363] J. Wang, P. A. Webley, and T. J. Hughes, "Thermodynamic modelling of low fill levels in cryogenic storage tanks for application to liquid hydrogen maritime transport," *Applied Thermal Engineering*, vol. 256, p. 124054, 2024. [Online]. Available: https://doi.org/10.1016/j.applthermaleng.2024.124054

[364] Mitsubishi Heavy Industries, Ltd., “FirstElement Fuel Inc. and Mitsubishi Heavy Industries, Ltd. Complete the Reliability Testing of MHI’s 90 MPa Class Liquid Hydrogen Pump (LH2 Pump) through the Long-Term Durability Test, Launching the LH2 Pump into the Markets,” 2023. [Online]. Available: https://www.mhi.com/news/23091101.html

[365] S. Schäfer and S. Maus, “Technology Pitch: Subcooled Liquid Hydrogen (sLH2),” 21.04.2021. [Online]. Available: https://www.now-gmbh.de/wp-content/uploads/2021/05/Heavy-Duty-Event-Subcooled-Liquid-Hydrogen-sLH2-Schaefer-Linde-Maus-Daimler.pdf

[366] Cryostar, “Hydrogen Expanders and Pumps: Equipment and expertise for Industrial Gas, Natural Gas, Hydrocarbons and Clean Energy.” [Online]. Available: https://www.sintef.no/globalassets/project/hyper/presentations-day-2/day2_1005_hautdidier_cryostar.pdf

[367] H. A. Krog and D. Berstad, “Strategies for zero boil-off liquid hydrogen transfer: an export terminal case-study.” [Online]. Available: https://arxiv.org/pdf/2512.04609

[368] Torishima Pump Mfg. Co., Ltd., “Torishima Wins Order for World’s First Superconducting Hydrogen Pumps: Revolutionary Technology Enables Commercial-Scale Liquid Hydrogen Terminal,” Osaka, Japan, 2026. [Online]. Available: https://www.torishima.co.jp/common/uploads/sites/2/2026/01/20260127a_en.pdf

[369] Nexant, Air Liquide, Argonne National Laboratory, Chevron Technology Venture, Gas Technology Institute, National Renewable Energy Laboratory, Pacific Northwest National Laboratory, and T. LLC, “H2A Hydrogen Delivery Infrastructure Analysis Models and Conventional Pathway Options Analysis Results.” [Online]. Available: https://www1.eere.energy.gov/hydrogenandfuelcells/pdfs/nexant_h2a.pdf

[370] Manufacturer of liquid hydrogen pumps, “Costs of liquid hydrogen pumps: E-Mail,” 2024.

[371] Cryostar, “Liquid Hydrogen Transfer Pumps,” Mulhouse. [Online]. Available: https://cryostar-hydrogen-solutions.com/liquid-hydrogen-transfer-pumps/

[372] G. Hupp and D. Chalk, “Ultra-Cryopump for High-Demand Transportation Fueling: Rotoflow - An Air Products Business,” 07.11.2021. [Online]. Available: https://www.hydrogen.energy.gov/docs/hydrogenprogramlibraries/pdfs/review21/in019_gross_2021_o-pdf.pdf

[373] F. M. White, *Fluid mechanics*, 7th ed. Singapore: McGraw-Hill, 2011.

[374] A. Laouir, "Performance analysis of open-loop cycles for LH2 regasification," *International Journal of Hydrogen Energy*, vol. 44, no. 39, pp. 22 425–22 436, 2019. [Online]. Available: https://doi.org/10.1016/j.ijhydene.2018.12.204

[375] Shuai Chen and Zhixuan Zhang, "Energy-saving operation of ORV under low seawater temperatures at LNG terminals," *Natural Gas Industry*, vol. 36, no. 05, 2016. [Online]. Available: https://doi.org/10.3787/j.issn.1000-0976.2016.05.016

[376] R. Agarwal, T. J. Rainey, S. M. A. Rahman, T. Steinberg, R. K. Perrons, and R. J. Brown, "LNG Regasification Terminals: The Role of Geography and Meteorology on Technology Choices," *Energies*, vol. 10, no. 12, p. 2152, 2017. [Online]. Available: https://doi.org/10.3390/en10122152

[377] World sea temperature, "Neufeld Sea Temperature," 2026. [Online]. Available: https://www.seatemperature.org/europe/germany/neufeld.htm

[378] A. Atienza-Márquez, J. C. Bruno, and A. Coronas, "Regasification of liquefied natural gas in satellite terminals: Techno-economic potential of cold recovery for boosting the efficiency of refrigerated facilities," *Energy Conversion and Management*, vol. 248, p. 114783, 2021. [Online]. Available: https://doi.org/10.1016/j.enconman.2021.114783

[379] A. T. Wijayanta, T. Oda, C. W. Purnomo, T. Kashiwagi, and M. Aziz, "Liquid hydrogen, methylcyclohexane, and ammonia as potential hydrogen storage: Comparison review," *International Journal of Hydrogen Energy*, vol. 44, no. 29, pp. 15 026–15 044, 2019. [Online]. Available: https://doi.org/10.1016/j.ijhydene.2019.04.112

[380] Bundesnetzagentur, "SMARD - Maßnahmenvolumen im Gesamtjahr stabil: Netzengpassmanagement im Q4 und Gesamtjahr 2025," 2026. [Online]. Available: https://www.smard.de/page/home/topic-article/444/219906/massnahmenvolumen-im-gesamtjahr-stabil

[381] Deutsche Presse-Agentur GmbH, "Stromnetz: Kostenersparnis durch Freileitungen laut BNetzA bei 35 Milliarden," *Tagesspiegel Background Energie & Klima*, 2024. [Online]. Available: https://background.tagesspiegel.de/energie-und-klima/briefing/kostenersparnis-durch-freileitungen-laut-bnetza-bei-35-milliarden

[382] K. Wiedemann and A. Rapoport, "Gesetzentwurf: Hochspannungstrassen sollen künftig pauschal als Freileitung gebaut werden," *Tagesspiegel Background Energie & Klima*, 2026. [Online]. Available: https://background.tagesspiegel.de/energie-und-klima/briefing/hochspannungstrassen-sollen-kuenftig-pauschal-als-freileitung-gebaut-werden

[383] Übertragungsnetzbetreiber, "Hintergrundsmaterial. Kostenschätzungen (zu Kapitel 4.2)," 2015. [Online]. Available: https://www.netzentwicklungsplan.de/kostenschaetzungen-zu-kapitel-42-0

[384] S. Eckroad, "Superconducting DC Cables for High Power Transport over Long Distances," Potsdam, 12.-13.05.2011. [Online]. Available: https://www.w2agz.com/Library/IASS/IASS%20Workshop%20(May%202011)/Content/7%20Eckroad_presentation.pdf

[385] X. Chen, S. Jiang, Y. Chen, Z. Zou, B. Shen, Y. Lei, D. Zhang, M. Zhang, and H. Gou, "Energy-saving superconducting power delivery from renewable energy source to a 100-MW-class data center," *Applied Energy*, vol. 310, p. 118602, 2022. [Online]. Available: https://doi.org/10.1016/j.apenergy.2022.118602

[386] FNB Gas e.V., "Pressematerial: Genehmigtes Wasserstoff-Kernnetz 2032," 2025. [Online]. Available: https://fnb-gas.de/pressematerialien/genehmigtes-wasserstoff-kernnetz-2032/

[387] ——, "Pressematerial: Das deutsche Fernleitungsnetz," 2025. [Online]. Available: https://fnb-gas.de/pressematerial/

[388] D. R. Smith and F. R. Fickett, "Low-Temperature Properties of Silver," *Journal of Research of the National Institute of Standards and Technology*, vol. 100, no. 2, pp. 119–171, 1995. [Online]. Available: https://doi.org/10.6028/jres.100.012

[389] J. Lu, E. S. Choi, and H. D. Zhou, "Physical properties of Hastelloy® C-276™ at cryogenic temperatures," *Journal of Applied Physics*, vol. 103, no. 6, p. 064908, 2008. [Online]. Available: https://doi.org/10.1063/1.2899058

[390] O. Mäder, "Simulationen und Experimente zum Stabilitätsverhalten von HTSL-Bandleitern," Dissertation, Karlsruher Institut für Technologie, Karlsruhe, 2012. [Online]. Available: https://doi.org/10.5445/KSP/1000028713

[391] N. J. Simon, Drexler E. S., and R. P. Reed, "Properties of Copper and Copper Alloys at Cryogenic Temperatures: NIST Monograph 177," Washington D. C., 1992. [Online]. Available: https://nvlpubs.nist.gov/nistpubs/Legacy/MONO/nistmonograph177.pdf

[392] T. Naito, H. Fujishiro, Y. Yamamura, K. Saito, H. Okamoto, H. Hayashi, N. Fujiwara, Y. Gosho, and Y. Shiohara, "Thermal Conductivity of YBCO Coated Conductors Reinforced by Metal Tape," *IEEE Transactions on Applied Superconductivity*, 2011. [Online]. Available: https://doi.org/10.1109/TASC.2010.2089481

[393] W. Dirahoui, H. Menana, M. Hinaje, and J. Lévêque, "Magnetothermal modeling of multilayer HTS tapes for quality control at room temperature," *Physica C-Superconductivity and Its Applications*, vol. 600, p. 1354101, 2022. [Online]. Available: https://doi.org/10.1016/j.physc.2022.1354101

[394] Hydrogen Energy Supply Chain, "The Suiso Frontier," 2026. [Online]. Available: https://www.hydrogenenergysupplychain.com/about-the-pilot/supply-chain/the-suiso-frontier/

[395] HySTRA, "HySTRA: CO2-free Hydrogen Energy Supply-chain Technology Research Association," 2023. [Online]. Available: https://www.hystra.or.jp/dist/pdf/pamphlet-en.pdf

[396] IEA, "Global Hydrogen Review 2023," Paris. [Online]. Available: https://iea.blob.core.windows.net/assets/8d434960-a85c-4c02-ad96-77794aaa175d/GlobalHydrogenReview2023.pdf

[397] Lloyd's Register, "AIP for SHI's liquefied hydrogen carrier," 2021. [Online]. Available: https://www.lr.org/en/knowledge/press-room/press-listing/press-release/2021/approval-in-principle-for-shi-liquefied-hydrogen-carrier/

[398] The Maritime Executive, "BV Approves Concept for a Full-Size Liquid Hydrogen Carrier," 2024. [Online]. Available: https://maritime-executive.com/article/french-consortium-develops-concept-for-full-size-liquid-hydrogen-carrier

[399] DNV GL, "DNV awards AiP to HD KSOE's hydrogen system for liquefied hydrogen carrier," 2023. [Online]. Available: https://www.dnv.com/news/dnv-awards-aip-to-hd-ksoe-s-hydrogen-system-for-liquefied-hydrogen-carrier-247109

[400] McDermott, "CB&I and Hanwha Ocean Receive Approval for Cargo Containment System and Ship Design for Liquid Hydrogen Carriers from DNV," 2024. [Online]. Available: https://www.mcdermott.com/press-release-detail/123021/cbi-and-hanwha-ocean-receive-approval-cargo-containment-system-and-ship-design-liquid-hydrogen

[401] C. Staudt, C. Hofsäß, B. von Lewinski, and F. Mörs, "Kurzstudie zu Transportoptionen von Wasserstoff: Aktualisierte Version 26. Juni 2023." [Online]. Available: https://www.dvgw.de/medien/dvgw/forschung/berichte/g202224-h2-import-abschlussfolien-akt20230626.pdf

[402] "Kawasaki Proves Excellent Thermal-insulation Performance for Liquefied Hydrogen Storage Tanks," 11.12.2023. [Online]. Available: https://global.kawasaki.com/en/corp/newsroom/news/detail/?f=20231211_8742

[403] M. Riemer, F. Schreiner, and J. Wachsmuth, "Conversion of LNG Terminals for Liquid Hydrogen or Ammonia: Analysis of Technical Feasibility und Economic Considerations," Karlsruhe. [Online]. Available: https://www.isi.fraunhofer.de/content/dam/isi/dokumente/cce/2022/Report_Conversion_of_LNG_Terminals_for_Liquid_Hydrogen_or_Ammonia.pdf

[404] I. Webster, "CPI Inflation Calculator: U.S. Inflation Calculator: 1635→2026, Department of Labor data," 11.03.2026. [Online]. Available: https://www.officialdata.org/

[405] OFX, "Historical exchange rates - OFX (UK)," 26.06.2025. [Online]. Available: https://www.ofx.com/en-gb/forex-news/historical-exchange-rates/

[406] Nikon SLM Solutions AG, "Invar® 36. Material Data Sheet: ASTM F1684 / DIN 1715-1," Lübeck. [Online]. Available: https://nikon-slm-solutions.com/wp-content/uploads/2024/07/MDS_InvarR36_2026-02.1_EN.pdf

[407] MatWeb: Material Property Data, "Overview of materials for Medium Carbon Steel." [Online]. Available: https://www.matweb.com/search/datasheet_print.aspx?matguid=098700ed63b24b14bd3bfdbec937489f

[408] Südmetall Otto Leonhard GmbH, "Metallbörse: Fachbegriffe." [Online]. Available: https://www.suedmetall.de/article/metallboerse

[409] Helu kabel GmbH, "Metallnotierung," 2023. [Online]. Available: https://shop.helukabel.com/de-de/metal-stock-price

[410] ——, "Metallnotierung," 2024. [Online]. Available: https://shop.helukabel.com/de-de/metal-stock-price

[411] ——, "Metallnotierung," 2026. [Online]. Available: https://shop.helukabel.com/de-de/metal-stock-price

[412] Krempel GmbH, "KAPTON® 300 FN 929 / KAPTON® 300 FN 021: E-Mail," 27.05.2025.

[413] Insulectro Printed Electronics, "QNITY Kapton® 500HN. Item number: KPHN5000000013Y5000001000," 2026. [Online]. Available: https://insulectro-pe.com/products/dupont%E2%84%A2-kapton%C2%AE-500hn

[414] Manufacturer of cryogenic pipelines, "Carbon steel and invar prices: E-Mail," 09.07.2024.

[415] NC Alloys, "Invar Price Per Kg," 2025. [Online]. Available: https://www.ncalloys.com/blog/invar-price-per-kg/

[416] MEPS International, "Europe Carbon Steel Prices, Indices & Forecasts. Europe Steel Prices," 2024. [Online]. Available: https://mepsinternational.com/gb/en/products/europe-steel-prices

[417] Beyond Gravity Austria GmbH, "Private e-mail communication regarding cryogenic superinsulation costs," 22.07.2024.

[418] R. Lietzow and H. Neumann, "Multi-layer insulation costs: Oral," 2023.

[419] D. Krieg, *Konzept und Kosten eines Pipelinesystems zur Versorgung des deutschen Straßenverkehrs mit Wasserstoff*, ser. Schriften des Forschungszentrums Jülich: Reihe Energie & Umwelt. Jülich: Forschungszentrum, Zentralbibliothek, 2012, vol. Bd. 144.

[420] Y. A. Çengel and M. A. Boles, *Thermodynamics: An engineering approach*, 8th ed. New York: McGraw Hill Education, 2015.

[421] J. Wahle, T. Ruas, S. M. Mohammad, N. Meuschke, and B. Gipp, "Ai usage cards: Responsibly reporting ai-generated content," in *2023 ACM/IEEE Joint Conference on Digital Libraries (JCDL)*. Los Alamitos, CA, USA: IEEE Computer Society, jun 2023, pp. 282–284. [Online]. Available: https://doi.ieeecomputersociety.org/10.1109/JCDL57899.2023.00060